Mechanisms underlying $P2Y_1$ receptor-mediated excitation of the inspiratory network in vitro; and NPY-induced stress resilience in vitro and in vivo.

by

Ana Miranda Tapia

A thesis submitted in partial fulfillment of the requirements for the degree of

Doctor of Philosophy

Neuroscience
University of Alberta

Abstract

The present thesis will discuss the cellular and molecular mechanisms by which neurochemical systems modulate the activity of CNS networks underlying breathing and anxiety. The thesis is divided into two parts. The first part examines the mechanisms by which the neuromodulator/neurotransmitter ATP excites the brainstem network that is responsible for generating inspiratory rhythm, the preBötzinger Complex (preBötC). The biphasic hypoxic ventilatory response (HVR) is an adaptive response in which a fall of arterial oxygen is detected by peripheral chemoreceptors which trigger a rapid increase in breathing that is followed by a centrally-mediated secondary hypoxic respiratory depression (HRD). This HRD is more pronounced in premature mammals and it can be life threatening, bringing breathing below the initial baseline. The dogma that has reigned for the last 30 years holds that the initial increase in ventilation is mediated by peripheral carotid body chemoreceptors, and the secondary depression is mediated through central depressive mechanisms. It is believed that the only role of the CNS in this response is to depress breathing, i.e., there is no mechanism whereby central hypoxia stimulates breathing. Recent data from our laboratory challenge this dogma. These data suggest that during hypoxia, astrocytes within the preBötC release ATP, which then activates $P2Y_1$ receptors ($P2Y_1Rs$) on inspiratory preBötC neurons to excite the inspiratory network and increase ventilation. This uncovered a novel mechanism by which hypoxia excites breathing. The purpose of this part of the thesis is to determine the mechanisms by which ATP acts via $P2Y_1Rs$ in the preBötC to increase inspiratory frequency.

The second part of this thesis examines the mechanisms by which neuropeptide Y (NPY) modulates behaviour of amygdala circuits that control anxiety-related behaviour. NPY is a potent anxiolytic that acts on a variety of receptor subtypes. The basolateral amygdala (BLA) is the neural substrate of fear and anxiety, and its activation is associated with high fear and anxiety states. When administered acutely into the BLA, NPY reduces anxiety via activation of Y_1 receptors (Y_1Rs), in part by reducing the excitability of a subpopulation of excitatory BLA principal neurons. Moreover, repeated injection of NPY into the BLA results in a sustained state of anxiolysis, called stress resilience, that long outlasts the period of NPY injection. Recently, NPY-induced stress resilience was attributed to downregulation of the hyperpolarization activated inward current, I_h, and dendritic remodeling (hypotrophy). However, the receptor responsible for this long-term effect is unknown. The purpose of this part of the thesis is to determine the receptor mechanism by which NPY induces a less anxious phenotype and the neural pathways underlying NPY-induced stress resilience.

The two components of the thesis are each preceded by an independent literature review to cover the background information necessary to understand their rational and significance. The first chapter begins with a review of relevant topics in central respiratory control including: the organization of the central networks underlying the neural control of breathing; the organization of the brainstem respiratory network; afferent control of breathing; respiratory rhythm generation, and; the role of purinergic signalling in the homeostatic regulation of breathing. This is followed by a brief introduction, and the methods, results and discussion for the initial study that explores the mechanisms underlying the $P2Y_1$R-mediated excitation of the inspiratory network in vitro.

This is followed by a review of literature relevant to the second study which examines amygdala networks and their modulation by NPY in relation to understanding the control of anxiety-related behaviors. The literature review is followed by the methods, results and the discussion of the second chapter that examines mechanisms underlying NPY-induced stress resilience in vitro and *in vivo*.

Preface

This thesis is an original work by Ana Pamela Miranda Tapia. The research project, of which this thesis is a part, received research ethics approval from the University of Alberta Research Ethics Board, Project Name "Neuromodulation of inspiratory network activity in vitro", No. AUP00000255, 2007 (renewed through to 2020) and "Mechanisms underlying stress resilience" supported by the National Institutes of Health (NIH) (grant R01MH090297; Dr. Janice H. Urban, PI). This research received ethics approval from the University of Alberta Research Ethics Board, approval No. 056/02/08 (2008 – 2013) and AUP0000240 (2014 – 2016).

Collaborations

All the experiments were designed and completed in Dr. Funk's laboratory or in Dr. Colmers's laboratory at the University of Alberta. I was the primary researcher in these studies and was involved in all aspects of experimental design, data analysis, figure preparation and manuscript preparation. I also generated the majority of the data independently, but an MSc student (V. Jalubula), a Research Associate (V. Rancic) and histology lab technician (Wei Zhang) contributed to specific components of the study, as detailed below:

- The experiments that evaluated the effects of paxilline on the MRS 2365-induced frequency increase were done in collaboration with Venkatesh Jalubula (50/50) (Chapter 1, Figure 2A). I performed ~50% of the experiments independently and Mr. Jalubula did the same.

- The experiments that evaluated the effects of MRS 2365 on intracellular calcium signals in inspiratory neurons from vGLUT2+ mice were done in collaboration with Dr. Vladimir Rancic (Chapter 1, Figure 14). We were both present for all experiments, but I performed all the data analysis.

- The immunohistochemistry experiments that characterized the expression of $P2Y_1$ receptors throughout the medulla on vGLUT2+ and GLYT2+ neurons in mice were done

in collaboration with Ms. Wei Zhang (Chapter 1, Figures 11 and 12). My role was in experimental design, tissue harvesting and all data analysis.

- The experiments that tested the effect of NPY Y_5 receptor agonist *in vivo* were done in collaboration with Dr. Sheldon Michaelson (Chapter 2, Figure 12). I performed all the data analysis.

All data analysis, interpretation and discussion of these experiments represent my original work.

Acknowledgments

First and foremost, I would like to thank my supervisor Dr. Gregory Funk for his support. As a graduate student who was in need of a new laboratory to complete my degree, Dr. Funk became a fundamental pilar in my personal and professional development. Despite my crash-landing at his lab, which occurred halfway through my PhD, Dr. Funk managed to beat me back up to shape and lead me to a stage in which I am proud of the work I have done and excited of the work I want to do in the future. Greg, thank you for making me recover my enthusiasm and esteem for science, my work, people and myself.

I would also like to thank the members of my supervisory committee; Dr. Silvia Pagliardini and Dr. Peter Smith for their guidance throughout my PhD, as well as external examining members, Dr. Richard Wilson and Dr Bradley Kerr for their role in the examination process.

I would like to thank my colleagues and friends for their help throughout my PhD study including Robert Reklow, Alexander Toohey, Dr. Vladimir Rancic, Dr. Ren Jun, Wei Zhang, Dr. Daniel Zoccal and Tucaauê Alvares. Special thanks to Dr.Vivian Biancardi for her support, advice and for always being that warm and happy ray of sunshine that we sometimes need.

I would also like to thank members of my previous laboratory for their support: Miss Amanda Mackinty, Dr. Heika Silveira, Dr. Barbora Doslikova, Dr. James MacKay, Dr. Sheldon Michaelson and Dr. Colmers.

I would also like to thank to my Mom, sister and brother for their unbelievable encouragement and love. Finally, thank you, Danny, for your constant support and encouragements. And most of all for all the patience and love through this crazy adventure very far away from home.

This research has been funded by the generous support of: CIHR, AIHS, NSERC, CFI, NIH and the Stollery Children's Hospital Foundation through the Women and Children’s Health Research Institute (WCHRI).

Table of Contents

I. Chapter 1: Cellular and molecular mechanisms of the $P2Y_1R$- mediated excitation of the preBötC inspiratory network.

List of figures

Figure 16: Effect of blocking inhibition with low concentrations of BIC and STRYC on the MRS 2365-induced excitation of the preBötC network.

Figure 17: Effect of blocking inhibition with high concentrations of BIC and STRYC on the MRS 2365-induced excitation of the preBötC network.

List of abbreviations

Abbreviation	Definition
aCSF	Artificial spinal fluid
ADO	Adenosine
ADP	Adenosine diphosphate
AMP	Adenosine monophosphate
AMPA	α-amino-3-hydroxy-5-methyl-4-isoxazolepropionic acid
ATP	Adenosine triphosphate
BIC	Bicuculline
BK_{Ca}	Big conductance Ca^{2+}-dependent K^+ channel
BötC	Bötzinger complex
CHE	Chelerythrine chloride
CNS	Central nervous system
CO_2	Carbon dioxide
CSE	Cystathionine-Y-lyase
CSN	Carotid sinus nerve
CNS	Central nervous system
CPA	cyclopiazonic acid
DAG	Diacylglycerol
DBX1	Developing brain homeobox protein 1
DMSO	Dimethyl sulfoxide
EGFP	Enhanced green fluorescent protein
EGTA	Ethylene glycol-bis(β-aminoethyl ether)-N,N,N′,N′-tetraacetic acid

ENT	Equilibrative nucleoside transporter
EPSC	Excitatory post synaptic current
EPSP	Excitatory post synaptic potential
EYFP	Enhanced Yellow Fluorescent Protein
FFA	Flufenamic acid
GABA	Gamma aminobutyric acid
$GABA_AR$	Gamma aminobutyric acid type A receptor
$GABA_BR$	Gamma aminobutyric acid type B receptor
GABAR	Gamma aminobutyric acid receptor
GAD	Glutamic acid decarboxylase
GFAP	Glial fibrillatory acidic protein
GFP	Green fluorescent protein
GIRK	G-protein coupled inward rectifying K channel
GLUR	Glutamate receptor
GLUT	Glutamate
GLY	Glycine
GLYR	Glycine receptor
GLYT2	Glycine transporter type 2
GPCR	G-protein coupled receptor
GPR4	proton-activated receptor
GTP	guanosine triphosphate
HRD	hypoxic respiratory depression
HRP	horse radish peroxidase

HVR	hypoxic ventilatory response
I_{CAN}	calcium-activated, nonselective cationic current
I_h	hyperpolarization activated inward current
I_{NaP}	Persistent sodium current
IEI	Interevent interval
IP_3	inositol trisphosphate
IPSC	inhibitory post synaptic current
KF	Kölliker-Fuse
LTD	Long-term depression
LTP	Long-term potentiation
mAHP	Medium afterhyperpolarization
MOR	μ opioid receptors
NA	Nucleus Ambiguus
NMDA	N-Methyl-D-aspartate
NTS	Nucleus of the solitary tract
P1R	P1 receptor
P2R	P2 receptor
$P2Y_1R$	$P2Y_1$ receptor
PBS	Phosphate buffered saline
PFA	Paraformaldehyde
PIP	Phosphatidyl inositol 4, 5-biphosphate
PKC	Protein kinase C
pF	Parafacial nucleus

pF_L	Lateral parafacial nucleus
pF_v	Ventral parafacial nucleus
PLC	Phospholipase C
PPADS	Pyridoxallphosphate-6-azophenyl-2',4'-disulfonic acid
preBötC	preBötzinger complex
PRG	Pontine respiratory group
PTX	Pertussis toxin
rCPG	Respiratory central pattern generator
rVRG	Rostral ventral respiratory group
RGP	Regulator G-protein signaling
RMP	Resting membrane potential
R_N	Input resistance
ROI	Region of interest
ROS	Reactive oxygen species
RTN	retrotrapezoid nucleus
RVLM	Rostroventral medulla
SCG	Superior cervical ganglion
SERCA	Sarco/endoplasmic reticulum Ca^{2+}-ATPase
SK_{Ca}	Small conductance Ca^{2+} dependent K^+ channel
SP	Substance P
SSC	Saline sodium citrate
SST	Somatostatin
STRYC	Strychnine

TASK	Tandem pore domain acid-sensitive K^+ channel
TNB	Tris NaCl Blocking Reagent-Tween
TNT	Tris NaCl Tween
TRP	Transient receptor potential
TRS	Target retrieval solution
TSA	Tyramide signal amplification
TTX	Tetrodotoxin
VLM	Ventrolateral medulla
vGAT	Vesicular GABA transporter
VGCC	Voltage gated Ca^{2+} channels
vGLUT2	Vesicular glutamate transporter type 2
VNUT	Vesicular nucleotide transporter
VRC	Ventral respiratory column
VRG	Ventral respiratory group
XII	Hypoglossal nucleus

1. Literature Review

1.1 Organization of the central networks underlying the neural control of breathing

1.1.2 Breathing Behavior

The breathing cycle comprises three main phases of activity: an inspiratory phase, a post-inspiratory phase and an expiratory phase. During inspiration, the diaphragm contracts and descends while the external intercostal muscles contract, expanding the ribcage. This expansion increases the volume of the thoracic cavity, which in turn decreases intrapulmonary pressure (below atmospheric pressure), causing the flow of air into the lungs. The flow rate at which air flows into the lungs depends on the force generated by the pump muscles and the airway resistance, which is modulated by skeletal muscles in the nose, mouth (including the tongue and glottis) and throat, as well as bronchial smooth muscles. After inspiration, expiration begins with a post-inspiratory phase when laryngeal adduction and diaphragm contraction slows expiratory airflow, facilitating gas exchange. At rest, expiration occurs passively due to the elastic recoil of the chest wall and diaphragm. This recoil reduces the thoracic cavity volume, decreasing the intrapulmonary volume which in turn increases intrapulmonary pressure (above atmospheric pressure) causing flow of air out of the lungs. However, during periods of increased ventilatory drive, as occurs at altitude or during exercise, abdominal and internal intercostals expiratory muscles are recruited and their contraction drives active expiration. This contraction potentiates expiratory airflow, causing a reduction in lung volume below functional residual capacity (FRC) resulting in a larger volume breath on the subsequent inspiration. This, along with an increased rate of ventilation that is accomplished in part by faster expiration, results in increased ventilation (Feldman and Del Negro, 2006; Del Negro et al., 2018).

Breathing behaviour is governed by a neural network located in the ventrolateral brainstem extending from the caudal medulla to the pons in what is referred as the Ventral Respiratory Column (VRC). The VRC is subdivided into multiple subregions, each with its own distinct function that will be discussed in detail below. Breathing in mammals is dominated by inspiration, which is generated within an oscillatory network in the preBötzinger Complex (preBötC). The preBötC is coupled with a second, more rostral oscillator in the lateral parafacial region (pF_L) that generates active expiration when respiratory drive is increased as described above. There may also be a third oscillator that underlies postinspiration (PI), referred to as PiCO. The precise spatial relationships of these different regions of the VRC and current theories of rhythm generation are discussed below. I will provide a brief review of the pF_L and PiCO but my discussion focuses on the preBötC because it is within this region that ATP is released during hypoxia to increase breathing and the objective of my study is to determine the mechanisms by which ATP excites the preBötC network.

1.2 Organization of the brainstem respiratory network.

1.2.1 Anatomical organization of brainstem respiratory network.

The VRC extends along the rostrocaudal axis of the brainstem and comprises a series of functionally and anatomically distinct structures (Fig. 1). At the rostral end, in the dorsolateral pons, the pontine respiratory group (PRG) comprises several nuclei, including the Kölliker-Fuse (KF) and parabrachialis medialis (PB). This area participates in the transition from the inspiratory to expiratory phase and in the control of the upper airway patency during breathing. The trigeminal motor nucleus (Vn) and the masticatory trigeminal principal sensory nucleus (NVsnpr) are located

caudal to the PRG. Ventrocaudal to the Vn is the VIIn, the ventrolateral margin of which demarcates the parafacial nucleus (pF). The pF is comprised by two functionally distinct subnuclei. The lateral parafacial nucleus (pF_L), located lateral to the VIIn, is inactive at rest and is associated with active expiration. The pF_V, located ventral to the VIIn, has chemosensitive properties. Caudal to VIIn, and dorsal to nucleus ambiguus (NA) is the recently described Post Inspiratory Complex (PiCo) which is hypothesized to generate PI activity. Ventral to NA and caudal to VIIn is the Bötzinger complex (BötC) which harbors inhibitory, expiratory-related neurons. Posterior to BötC is the kernel for inspiratory rhythm generation, and a core focus of the work in this dissertation, the preBötC. Dorsal to the preBötC bordering the IVth ventricle is the hypoglossal motor nucleus (XIIn), which innervates the genioglossus muscle of the tongue and is under direct control of the preBötC and other brain regions involved in oromotor control. Caudal to the preBötC are the rostral and caudal Ventral Respiratory Groups (rVRG; cVRG), which primarily contain inspiratory and expiratory premotor neurons, respectively (Fig. 1)

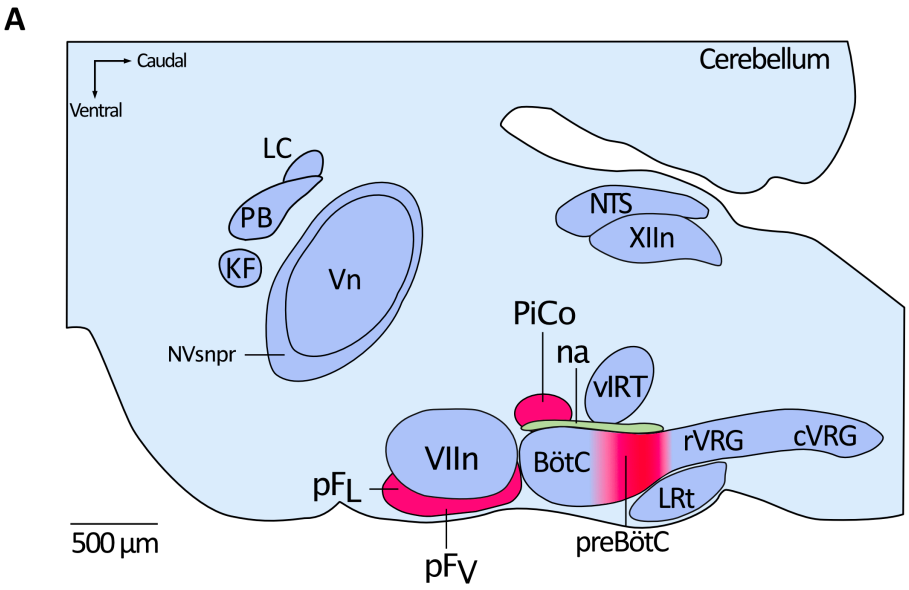

Figure 1: Anatomical organization of the brainstem respiratory network. Sagittal view of the rodent brainstem. LC, Locus coeruleus; PB, parabrachialis medialis; KF, Kölliker-Fuse; Vn; trigeminal motor nucleus; NVsnpr, masticatory trigeminal principal sensory nucleus; VIIn; facial motor nucleous; pF_L, lateral parafacial nucleus; pF_V, ventral parafacial nucleus; PiCo, Postinspiratory Complex; NA, nucleus ambiguous; BötC, Bötzinger Complex; preBötC, preBötzinger Complex; vIRT, ventral Intermediate Reticular Formation; rVRG, rostral Ventral Respiratory Group; cVRG, caudal Ventral Respiratory Group; LRt, lateral reticular nucleus; XIIn, hypoglossal motor nucleus; NTS, nucleus of the solitary tract.

1.2.2 preBötC; critical region for inspiratory rhythm generation

A discrete ensemble of rhythmically active neurons essential for the generation of inspiration was first described by Smith et al (Smith et al., 1991). Located at the rostroventrolateral medulla (rVLM), the preBötC is considered the core of the inspiratory rhythm generating network (Fig. 1).

The respiratory central pattern generator (rCPG) has two very distinct and anatomically segregated functions: (i) rhythm generation, which is the basic oscillation generated in the preBötC, and (ii) pattern formation where the basic rhythm is translated into the activity patterns that are necessary for the inspiratory muscles to control airflow resistance and move air in and out of the lungs to meet the metabolic demands in order to maintain homeostasis. First, the preBötC generates the basic inspiratory rhythm and then drives inspiration through projections to the rVRG, which in turn projects monosynaptically to phrenic motoneurons in the C4-6 spinal cord that innervate the main inspiratory pump muscle, the diaphragm. Polysynaptic projections to thoracic motoneurons provide inspiratory drive to external intercostals muscles. Projections to XII motoneurons and other cranial motoneurons (IX, X, XI) provide inspiratory drive to the tongue, laryngeal and accessory respiratory muscles, respectively (Feldman et al., 2013).

The preBötC comprises a heterogeneous group of inspiratory-active neurons that, through processes to be discussed below, generate the inspiratory rhythm. Substantial effort has been devoted over the last two decades to define the specific types of preBötC inspiratory neurons based on developmental origin, transcription factor expression patterns as well as transmitter and receptor expression patterns in order to define the specific function of each. Although the preBötC is bilaterally distributed, it presents extensive contralateral connectivity between left and right

preBötC (Wang et al., 2001; Stornetta et al., 2003; Bouvier et al., 2010; Picardo et al., 2013; Wu et al., 2017). The preBötC contains glutamatergic, GABAergic, Glycinergic and peptidergic neurons (Kuwana et al., 2006; Winter et al., 2009; Koizumi et al., 2013), but the generation of rhythm depends on excitatory AMPA receptor-mediated transmission in the preBötC (Greer et al., 1991; Funk et al., 1993; Wallén-Mackenzie et al., 2006; Smith et al., 2013; Koizumi et al., 2016). These rhythmically active glutamatergic neurons are derived from V0 progenitor cells (Wu et al., 2017). Several types of inspiratory neurons have been described based on their receptors, peptide or transcription factor expression. Activation of neurokinin type 1 receptors (NK1Rs) with substance P (SP) accelerates inspiratory-related activity by depolarizing preBötC inspiratory neurons (Gray et al., 1999). These preBötC neurons express NK1R receptors and project to the contralateral preBötC (Wang et al., 2001). Nearly all NK1R-expressing neurons are inspiratory-modulated while a fraction has pacemaker properties (Pagliardini et al., 2005). Ablation of NK1R-expressing preBötC neurons produces ataxic breathing and abnormal hypoxic and hypercapnic responses (Gray et al., 2001). preBötC neurons also express μ-opioid receptors (MORs) and activation of MOR slows breathing (Gray et al., 1999; Montandon et al., 2011). Moreover, putative rhythmogenic neurons co-express NK1R and MORs (Gray et al., 1999). Somatostatin (SST) has also been described in preBötC neurons (Stornetta et al., 2003). Administration of SST slows inspiratory activity *in vitro* (Gray et al., 1999), while silencing SST preBötC neurons *in vivo* stops breathing (Tan et al., 2008). A subpopulation of preBötC neurons express the homeodomain transcription factor Developing Brain Homeobox 1 (DBX1) and is rhythmically active with bursts in phase with inspiratory activity (Bouvier et al., 2010; Gray et al., 2010; Picardo et al., 2013). The importance of DBX1-expressing preBötC neurons in the generation of breathing is based on studies showing that preBötC DBX1 neurons are essential for the generation of inspiration. DBX1

KO mice do not generate respiratory output and die at birth (Bouvier et al., 2010; Gray et al., 2010). Photoinhibition (Vann et al., 2018) or laser ablation (Wang et al., 2014) of DBX1 preBötC neurons stops breathing. On the other hand, photoactivation of these neurons accelerates breathing (Vann et al., 2018) and triggers premature inspiratory-related activity (Cui et al., 2016). Of particular importance are NK1R/ DBX1/Vglut2 neurons, which are considered the rhythmogenic core of the preBötC while SST neurons are considered premotor pattern generating neurons (Cui et al., 2016).

Recently, mRNA for the bombesin-like neuropeptide neuromedin B (NMB) receptor and the gastrin-releasing peptide (GRP) receptor has been identified in the preBötC. Activation of preBötC NMB receptors induces sighs without affecting respiratory rate while ablation of NMB or GRP receptors abolishes basal and hypoxia-induced sighs (Li et al., 2016).

1.2.3 Lateral region of the parafacial nucleus (pF_L): generation of active expiratory rhythm

The idea of a second oscillator is based on the existence of neurons located in the lateral region of the parafacial nucleus (pF_L) that generate spontaneous late-expiratory bursts during late embryonic-early postnatal period. Onimaru et al (2003b) found in brainstem-spinal cord preparation of P0-P1 rats that neurons located in the superficial region of the rVLM show bursts of activity that precede C4 inspiratory bursts (Onimaru and Homma, 2003b). Later, an embryonic population of rhythmically bursting neurons was characterized in embryonic E14.5 mice. Thoby-Brisson et al (2009) showed that silencing this neuronal group disrupts respiratory rhythm (Thoby-Brisson et al., 2009). These neurons lose their pre-inspiratory spontaneous activity near birth, and the mechanisms underlying this phenomenon remains unknown (Fortuna et al., 2008).

The pF is located adjacent to the ventral and lateral margins of the facial nucleus (VIIn) and comprises two functionally distinct regions. The pF_V contains chemosensory neurons that express the transcription factor paired-like homeobox 2B (PHOX2B), NK1R (Onimaru et al., 2008) and the Atonal BHLH Transcription Factor 1 (ATOH1) (Ruffault et al., 2015). This region has been historically referred to as the retrotrapezoid nucleus (RTN) and is hypothesized as the most important region involved in central respiratory chemoreception; i.e., the region most important for the homeostatic reflex that controls arterial PCO_2, the hypercapnic ventilatory response.

The pF_L appears not only to be anatomically but functional distinct from the pFv. The pF_L is the hypothesized site responsible for generating the active expiratory rhythm observed during periods of high respiratory drive and also occasionally during REM sleep. The pF_L is normally silent at rest but contains rhythmic neurons that discharge rhythmically in phase with active expiration. This region is hypothesized to be the source of active expiration based on a number of observations. In juvenile rats, transections rostral to the pF_L have no effect on active expiration, however, transections at the level, or just caudal, to the pF_L eliminate abdominal burst activity (Janczewski and Feldman, 2006). Pharmacological disinhibition or excitation of pF_L neurons induces late-expiratory activity associated with active expiration (Pagliardini et al., 2011; Huckstepp et al., 2015). Chemogenetic activation of pF_L evokes abdominal activity at rest (Huckstepp et al., 2016). Additionally, blocking pF_L glutamatergic activity reduces hypercapnia-induced late-expiratory activity (Zoccal et al., 2018). More recently, Pisansky et al (2020) demonstrated that chemogenetic inhibition of the pF_L reduces the number of REM episodes associated with abdominal muscle activity, whereas their chemogenetic activation increases the number of REM events associated with abdominal muscle activity (Pisanski et al., 2020).

1.2.4 Post Inspiratory complex (PiCo): putative postinspiratory oscillator

For decades, it has been hypothesized that the postinspiratory phase of the respiratory cycle derives from synaptic interactions, primarily inhibitory, between different types of respiratory neurons located along the VRC with a predominant role attributed to the PRG (Fig. 1). This view was challenged recently with the identification of a third respiratory oscillator, PiCo, that was hypothesized as responsible for PI. Located caudally to VIIn and dorsomedial to NA, PiCo is comprised of excitatory glutamatergic-cholinergic neurons that are more sensitive to the inhibitory actions of opioids than preBötC neurons. The suggestion that another oscillator is responsible for PI is based on a study by Anderson et al (2016). The authors reported excitatory glutamatergic-cholinergic rhythmically active neurons that burst during PI. Additionally, photostimulation of cholinergic PiCo neurons evokes PI-related bursts and delays the following inspiratory burst. Noradrenaline accelerates PiCo network activity while MORs activation and SST inhibit PiCo network activity *in vitro* and shorten burst duration *in vivo* (Anderson et al., 2016). However, PiCo has only been described by a single research group in a single paper. Also problematic is that others have not yet been able to identify a cholinergic group of neurons in the proposed location of PiCo (Biancardi et al., 2020).

The existence of three functionally different brainstem regions (Fig. 1), each one associated with one of the three phases of the respiratory cycle, suggests that the generation of respiratory rhythm is driven by three distinct coupled oscillators. At rest, the preBötC and the recently discovered PiCo alternate their activity to drive inspiration and PI respectively, while expiration remains a passive process. Photostimulation of preBötC DBX1 neurons inhibits PiCo activity while

photoactivation of PiCo delays inspiratory activity (Anderson et al., 2016), suggesting that the preBötC-PiCo coupling is mutually inhibitory. However, photostimulation of DBX1 preBötC neurons while blocking GABAR, excites PiCo (Anderson et al., 2016), suggesting that PiCo also receives excitatory drive from preBötC DBX1 neurons. During high metabolic demand, the pF_L is incorporated to drive active expiration, coupling to preBötC-PiCo to establish a three-phase rhythm (Anderson and Ramirez, 2017). It is hypothesised that, in embryonic and early postnatal stages, pF_L provides direct excitatory projections to the preBötC (Anderson and Ramirez, 2017; Oniparu et al., 2007; Thoby-Brisson et al., 2009; Huckstepp et al., 2016). In adult stages, pF_L was found to sends inputs to SST and glycinergic preBötC neurons (Yang et al., 2020) and it is believed that inhibitory connections from pF_L to preBötC are indirect (Huckstepp et al., 2016). On the other hand, the preBötC provides excitatory and inhibitory drive to the pF_L (Anderson and Ramirez, 2017; Yang and Feldman, 2018; Biancardi et al., 2020).

1.3 Afferent control

Breathing requires the precise spatiotemporal pattern of activation of multiple muscles groups to achieve efficient, non-stop, rhythmic movement of air into and out of the lungs. The physiological function of breathing is to provide O_2 to support metabolism and remove waste produces, including CO_2. Thus, breathing is unique among motor behaviours in that its overall activity has the additional constraint of having to match metabolic rate. Achieving efficient motor behaviour that matches metabolic demand is dependent on the modulation of breathing by two main types of afferent feedback, mechanoreceptive and chemoreceptive.

Like any motor control system, efficient breathing depends on constant, rapid mechanoreceptive feedback from the respiratory apparatus that includes the lungs, respiratory muscles, chest wall, and airways. The most important mechanoreceptive feedback controlling basic breathing rhythm and pattern comes from slow adapting pulmonary stretch receptors that travel via the vagus nerve to synapse in the NTS, the BötC and ultimately the preBötC. They underlie a series of reflexes called the Breuer-Herring Reflexes, that allow for volume-dependent modulation of breathing. The best characterized of these reflexes is the inspiratory burst terminating reflex that terminates inspiration when lung volume reaches a specific level. There are a variety of sensory irritant receptors in the airways including transient receptor potential (TRP) channels TRPV1, TRPV4, TRPA1 and the antitussive TRM8 (Benemei et al., 2015), that underlie protective reflexes including cough and sneezing. Details can be found in more comprehensive reviews by Bolser and Pitts (Bolser and Davenport, 2002; Pitts et al., 2012; Pitts, 2014).

Most relevant to this thesis is the chemosensory feedback because the purpose is to understand how ATP, which is released into the preBötC during hypoxia, contributes to the homeostatic HVR. There are two main classes of chemoreceptors, peripheral and central. The carotid bodies (CBs) are the primary peripheral chemoreceptors. They predominantly respond to hypoxia triggering an initial increase in ventilation and only contribute to ~ 30% of the response to the CO_2/pH response. Multiple brain regions act in concert to contribute to central chemoreception, including the pF_V, raphe nucleus, NTS and locus coeruleus. The main site for central chemoreception is the ventral parafacial nucleus (pF_V) (Mulkey et al., 2004a; Stornetta et al., 2006). Neurons of the pF_V detect changes in levels of CO_2 and pH and relay that information to VRC nuclei, including the preBötC, KF nucleus, lateral PB region and NTS (Guyenet and Bayliss, 2015; Guyenet et al., 2019) to

increase breathing rate, inspiratory amplitude, active expiration and the opening of airways (Guyenet and Bayliss, 2015). In parallel, ATP is released by pF_V astrocytes in response to hypercapnia to excite chemosensory neurons (Gourine et al., 2005a; 2010). Whether the medullary raphe responds directly to increased CO_2 remains controversial. However, its activation potentiates the CO_2-induced increase of ventilation (DePuy et al., 2011). Unlike the pF_V, ATP has no effect on baseline breathing when administered in the raphe or NTS (Sobrinho et al., 2014).

I will review in more detail peripheral and central chemoreception in a later section when discussing the role of ATP signaling in the homeostatic control of ventilation as it seems to play important roles in both CO_2 and O_2 sensing.

1.4 Respiratory rhythm generation

1.4.1 Historical review

Our understanding of the mechanisms underlying respiratory rhythm generation have evolved enormously over the last 50 years. A detailed account of this evolution is available elsewhere (Feldman & Del Negro, 2006; Feldman et al., 2013; Anderson & Ramirez, 2017; Ramirez & Baertsch, 2017; Del Negro et al., 2018). The main purpose of this section is to provide a brief historical overview, starting in the 1970's, of the various theories of rhythm generation and the main experimental observations that have precipitated revised views. Most attention will focus on the most recent models since knowledge of these concepts is most relevant to understanding the cellular and synaptic mechanisms by which ATP, when released during hypoxia, might bring about an increase in inspiratory frequency.

A single theory of respiratory rhythm generation, termed the Three-Phase Network Model, dominated the field of Central Respiratory Control from the early 1970's to the early '90's. This model, initially proposed by Richter (Richter et al., 1986), described breathing as a three-phase behaviour comprising inspiration, PI (or Stage I expiration) and stage II expiration. Indeed, breathing is still considered a three-phase behaviour – just the proposed mechanisms responsible for the various phases have changed. The Three-Phase Network Model resembles a half-centre oscillator as proposed by Brown (1914) for locomotion in which rhythm results from the interaction of two reciprocally-inhibitory half centres that, in the respiratory field, were responsible for inspiratory and PI phases. Additional complex network interactions between other components of the VRC were proposed to underlie stage two expiration.

As mentioned above, the Three-Phase Network Model dominated for more than two decades, not necessarily because everyone in the field was a firm "believer", but because there simply were no good alternatives. This began to change in the late '80's with the development of a powerful new *in vitro* approach for studying the respiratory network in which the brainstem of neonatal rodents, isolated in a dish, continues to generate an inspiratory-related rhythm (Suzue, 1984; Smith and Feldman, 1987; Feldman and Smith, 1989). The ability that the *in vitro* preparation offers to precisely control the neurochemical environment led to the first direct challenge of the Three-Phase Network Model. The fundamental organizational principle of the Three-Phase Network Model is that it depends on synaptic inhibition. However, block of synaptic inhibition by removing extracellular Cl^- and or addition of $GABA_A$, $GABA_B$ and GLY receptor antagonists in the brainstem spinal cord preparation increased the duration of inspiratory bursts recorded from the

nerves driving the diaphragm but had no effect on rhythm (Feldman and Smith, 1989). This finding has been repeated several times *in vitro* (Feldman and Smith, 1989; Brockhaus and Ballanyi, 2001) and even *in vivo* (Janczewski et al., 2013; Sherman et al., 2015; Marchenko et al., 2016), strongly suggesting that post-synaptic inhibition is not essential for respiratory rhythm generation.

While the inhibition block experiments were a significant challenge to the Three-Phase Network Model, they did not offer an alternative hypothesis. Shortly thereafter, however, came the landmark study published by Smith et al. (1991) in Science that identified a novel brainstem region, the preBötC, that was not only necessary for inspiratory rhythm generation, when isolated in a thin medullary slice it was sufficient for rhythm generation. Smith et al. (1991) also recorded for the first time preBötC inspiratory neurons with voltage-dependent pacemaker properties, which gave rise to the Conditional Pacemaker-Network hypothesis of inspiratory rhythm generation (Smith et al., 1991).

These preBötC pacemaker neurons make up ~20-30% of inspiratory neurons in the area, are voltage dependent (meaning that their frequency of oscillation increases with membrane depolarization) (Smith et al., 1991; Koshiya and Smith, 1999; Picardo et al., 2013), remain rhythmic when the network itself is silenced by blocking excitatory synaptic transmission (Johnson et al., 1994; Koshiya and Smith, 1999), and were hypothesized to be bilaterally connected with each other (Smith et al., 1991; Robert J Butera et al., 1999). Two types of pacemaker neurons were ultimately characterized. One, found in rats and mice, is dependent on the interaction of a persistent Na^+ (I_{NaP}) and leak-type K^+ (I_{Leak}) currents. These neurons were referred to as persistent Na-dependent pacemaker neurons, whose pacing activity could be blocked with blockers of I_{NaP} such

as riluzol and low concentrations of TTX (Del Negro et al., 2002). A second type, identified primarily in mice older than 5 days of age, shows pacemaker activity that is dependent on a calcium-activated, nonspecific and voltage-insensitive cationic current (I_{CAN}) (Del Negro et al., 2005). Block of I_{CAN} with flufenamic acid and cadmium indeed blocks pacemaker activity of this type of neurons (Del Negro et al., 2005).

Importantly, evidence of preBötC pacemaker neurons is not evidence that the pacemaker properties are actually responsible for rhythm generation. This question, i.e., The importance of pacemaker properties in inspiratory rhythm generation, was elegantly addressed by Del Negro et al (2005) with the demonstration that concentrations of riluzol acid that completely blocked pacemaker activity in every pacemaker neuron they recorded had no effect on inspiratory rhythm (Del Negro et al., 2005). Del Negro's paper generated enormous controversy and precipitated several papers where high concentrations of riluzol would eventually disrupt rhythm but only after long incubations at drug concentrations associated with significant off-target actions (Doble, 1996; Guinamard et al., 2013).

This left two important questions. What is the function of the pacemaker properties, and if the pacemaker network hypothesis is not correct, what is responsible for inspiratory rhythm generation?

The next hypothesis to emerge was the Network Pacemaker, or Group Pacemaker, hypothesis. This model proposes that the formation of inspiratory burst results from recurrent excitation in combination with intrinsic membrane properties. Here, a single group-pacemaker neuron is

incapable of intrinsic bursting. However, a small number of group-pacemaker neurons through recurrent excitation stimulate each other to elicit a burst. First, excitatory transmission between a small fraction of spontaneously active preBötC neurons initiate a positive feedback which results in the recruitment of more interneurons. Intrinsic I_{NaP} and I_{CAN} conductances amplify membrane depolarizations to generate the inspiratory burst (Fig. 2A) (Feldman and Del Negro, 2006). A variation on this theory referred to as the Burstlet hypothesis has emerged recently. This model posits that bursts; and bursting neurons; are important for a robust output but are not required for rhythm generation. Instead, the fundamental inspiratory behavior relies on the synchronized discharge of a small fraction, rather than on a large population of inspiratory rhythm generating preBötC neurons. Here, a small group of spontaneously active inspiratory preBötC neurons recruit more preBötC interneurons through recurrent synaptic excitation. This generates a low-amplitude pre-inspiratory potential that percolates throughout the rhythmogenic population which constitutes a burstlet. Finally, the burstlet triggers a full burst of activity which then propagates to pattern-related preBötC neurons, pre-motor neurons and motor neurons generating motor output. Thus, the underlying basal rhythmogenic mechanism is a burstlet that, once it reaches a threshold, becomes a full burst of activity in pre-motoneurons and motoneurons. The nature of the mechanism that underlies this threshold remains to be determined (Fig. 2B) (Del Negro et al., 2018).

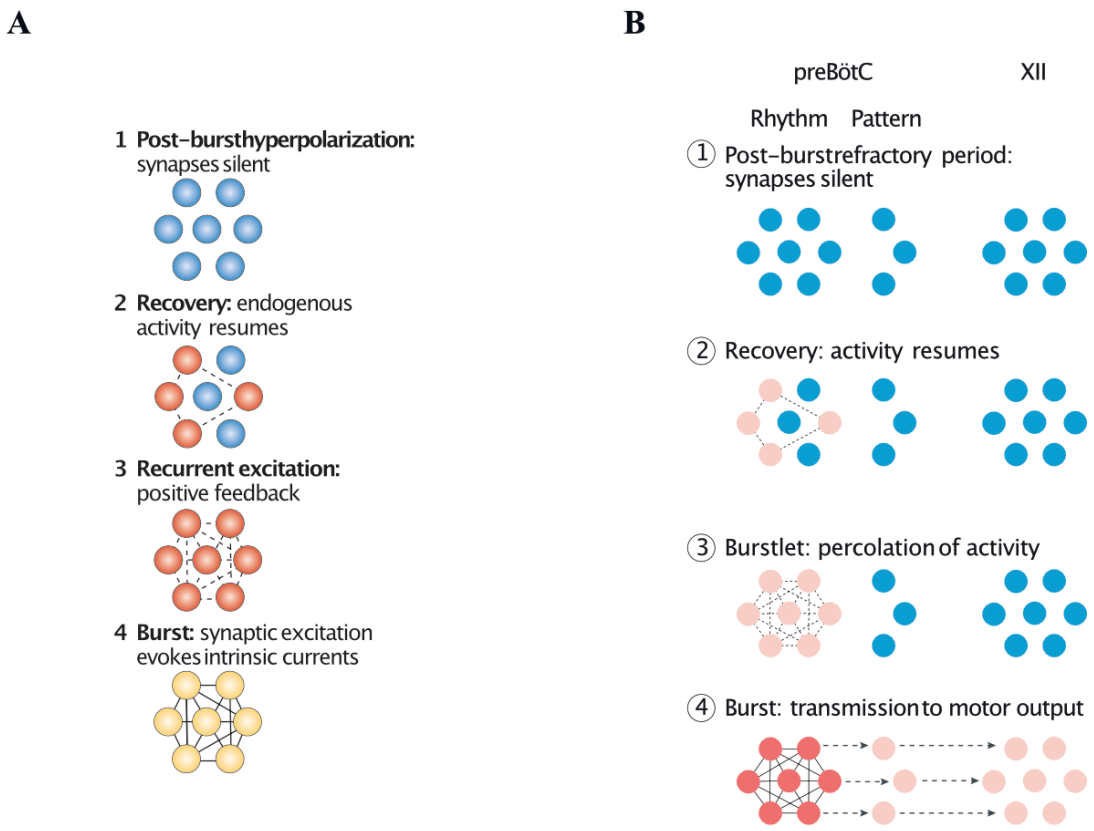

Figure 2: Network-pacemaker (A) and emergent burstlet theory (B) of rhythm generation. A. Schematic of network activity underlying group pacemaker showing neuronal activity at different stages of the rhythmogenic cycle. Followed inspiration a refractory stage (1). During stage (2), highly excitable neurons begin to spike. On stage (3) more interneurons are recruited through recurrent excitation to finally reach a minimum number of neurons necessary to elicit a full burst during stage (4). B. Schematic of network activity underlying burstlet showing. Followed a refractory period (1) neurons begin to spontaneously fire (2). A small group of neurons is recruited through recurrent synaptic excitation eliciting low-amplitude pre-inspiratory activity (3) which percolates throughout the network evoking a burstlet. In the final stage (4) the burstlet, once it reaches a "threshold", produces a full burst. Adapted with permission from (Feldman and Del Negro, 2006; Del Negro et al., 2018).

1.5 Role of ATP in the homeostatic control of ventilation

1.5.1 Purinergic signalling

Biological responses to ATP (and other nucleoside tri and diphosphates) are mediated by the activation of purinergic ionotropic P2X and metabotropic P2Y receptors. Seven P2X canonical ligand-gated cation channels had been identified in neural cells (Burnstock, 2018). Assembled from seven distinct subunits ($P2X_1$-$P2X_7$), P2X receptors show different kinetics and pharmacological sensitivity to modulators and contribute to fast excitatory synaptic transmission in several CNS regions (Pankratov et al., 2009). Two distinct subgroups of P2Y receptors have been identified. The first subgroup principally couples to G_q/G_{11}-proteins which activate phospholipase C/inositol triphosphate (InsP3) endoplasmic reticulum Ca^{2+}-release signaling pathway and consists of $P2Y_1$, $P2Y_4$, $P2Y_6$, $P2Y_{11}$ receptors The second subgroup is coupled preferentially to G_i/G_o-proteins to inhibit adenylyl cyclase-dependent pathway and consist of $P2Y_{12}$, $P2Y_{13}$ and $P2Y_{14}$ receptors (Abbracchio et al., 2006).

ATP is transported into synaptic vesicles via the Cl^--dependent vesicular nucleotide transporter (VNUT). Once released, ATP is quickly broken down to ADP and AMP and finally to adenosine (ADO) by ectonucleotidases (Abbracchio et al., 2009). Biological functions of ADO are mediated by activation of G-protein coupled P1 receptors, A1, A2A, A2B and A3 (Burnstock, 2018; Reklow et al., 2019). ADO is transported bidirectionally across membranes down its concentration gradient by equilibrative nucleoside transporters (ENTs) or against its concentration gradient by concentrative (CNTs) nucleoside transporters (King et al., 2006; E Parkinson et al., 2011). ADO levels are also modulated by the enzyme adenosine kinase, a phosphotransferase that phosphorylates adenosine into AMP (Boison and Alexander, 2013; Reklow et al., 2019). ADO has

long been proposed to be the mechanism responsible for the HRD; possibly via the activation of A1 receptors. ADO depresses breathing in a variety of species including piglets, rabbits, cats, lambs and rats (Eldridge et al., 1984; Lagercrantz et al., 1984; Burr and Sinclair, 1988; Koos and Matsuda, 1990; Herlenius et al., 1997; Wilson et al., 2004). Blockade of P1Rs, via intravenous injections of a P1R antagonist, increases respiratory activity, suggesting that breathing is under tonic adenosine inhibition (Eldridge et al., 1985). More importantly, systemic administration of P1 receptors antagonists can abolish the HRD (Runold et al., 1989; Bissonnette et al., 1990; Koos et al., 2005).

In this thesis I will focus on the actions of ATP through P2YR, especially ATP and $P2Y_1$ receptors ($P2Y_1R$), because this mechanism has been recently implicated in shaping the HVR, counteracting the HRD.

1.5.2 P2 receptor signaling in the regulation of breathing by O_2

1.5.2.1 Peripheral chemoreceptors

Changes in arterial PO_2, PCO_2, and pH are constantly being monitored by peripheral chemoreceptors. The carotid bodies (CB), which receive the highest relative blood flow rate of any organ in the body, are located bilaterally at the bifurcation of the common carotid artery (Fig. 3A, B) and are comprised of clusters of glomus, or Type I, neuronal-like cells engulfed by glial-like sustentacular, or Type II, cells (Fig. 3C). Glomus cells are synaptically coupled to sensory nerve endings of petrosal neurons of the carotid sinus nerve (CSN), which relay information to the brainstem via the glossopharyngeal nerve (cranial nerve IX) (Fig. 3C) (Tse et al., 2012; Prabhakar,

2013; 2016). CB activation, either by hypoxia or CO_2/pH, increases discharge of CSN axons,. From here, excitatory sensory information is transmitted to the NTS via the solitary tract. Neurons from the NTS project to the pontine respiratory group and chemosensory neurons of the pF_V. From the pF_V, neurons send excitatory inputs to the preBötC to increase ventilation (Fig. 3D) (Bochorishvili et al., 2012; Funk, 2013; Guyenet et al., 2018).

Two main hypotheses have been proposed to explain the mechanism of O_2 sensing by the CB. The "membrane hypothesis" postulates a K^+ channel as the O_2 sensor. During hypoxia a K^+ conductance, possibly carried by the "tandem of pore domains in a weak inward rectifying K^+" (TWIK)-related acid-sensitive K^+ (TASK), and a large Ca^{2+}-activated K^+ conductance are inhibited, causing the CB glomus cells to depolarize. This depolarization triggers Ca^{2+} entry via voltage-gated Ca^{2+} channels (VGCC) and Ca^{2+}-dependent release of multiple neurotransmitters. The "metabolic or mitochondrial hypothesis" suggest that hypoxia reduces a specialized mitochondrial cytochrome in CB glomus cells which acts as the O_2 sensing mechanism. This results in mitochondrial depolarization, inhibition of mitochondrial function, K^+ channel inactivation, glomus cell depolarization, increase of intracellular Ca^{2+} to finally trigger neurotransmitter release (Prabhakar, 2016). Both hypotheses culminate in the release of a variety of neurotransmitters to increase CSN activity, but ATP, acting at $P2X_2$ and $P2X_3$ receptors on CSN afferents, appears primarily responsible for transmission of the hypoxic information, since mice lacking $P2X_2$ and $P2X_{2\text{-}3}$ receptors show reduced CSN activity in response to hypoxia and essentially lack the initial phase (or Phase I) of the HVR (Fig. 3C) (Rong et al., 2003).

More recently, hydrogen sulfide (H_2S) has been implicated in O_2 sensing in the CB. This suggestion is based on evidence showing that hypoxia increase the levels of H_2S in the CB and that cystathionine-Y-lyase (CSE), an enzyme involved in the generation of H_2S, is present in glomus cells (Peng et al., 2010; 2019). Additionally, genetic deletion of CSE in mice, or the pharmacological block of CSE on mice and rats, reduces CSN activity and the ventilatory response to hypoxia (Peng et al., 2010; 2019). Under basal conditions, H_2S production is downregulated by the carbon monoxide (CO)-generating enzyme hemeoxigenase-2 (HO-2). When O_2 levels fall, HO-2 is inhibited and CO production is decreased, allowing the accumulation of H_2S inside glomus cells (Peng et al., 2010; Prabhakar, 2016), suggesting that H_2S acts as an hypoxia mediator rather that a sensor. CO, which is increased during normoxia, activates of a voltage-dependent K^+ channel while H_2S, which is suppressed during normoxia, inhibits a Ca^{2+}-dependent K^+ conductance in glomus cells (Prabhakar, 2016). Thus, during hypoxia, reduction of CO and accumulation of H_2S would act in concert to depolarize carotid body glomus cells. During hypercapnia, it his suggested that CO_2, which is converted to H_2CO_3 in type I cells by the enzyme carbonic anhydrase, acts through Na^+/H^+ exchangers, Na^+/HCO_3 symporters or Cl^-/HCO_3 antiporters to change intracellular pH (Prabhakar, 2016). This change on intracellular pH depolarizes type I glomus cells, promoting the release of neurotransmitters, primarily ATP (Rong et al., 2003; Prabhakar, 2016), acetylcholine and peptides (Prabhakar, 2016).

In addition to its role as the main excitatory transmitter communicating between glomus cells and CSN sensory axons, ATP and P2R signaling have additional roles in controlling CB excitability through communication between type II cells and glomus cells and in the efferent control of CB excitability (Leonard et al., 2018). While ATP released from CBs is excitatory on CSN axons,

purinergic signaling has multiple actions in the CB, including ATP activation of $P2Y_1Rs$ on glomus cells. Activation of glomus cell $P2Y_1Rs$ leads to a decrease in glomus cells excitability, which suppresses the hypoxia-dependent $[Ca^{2+}]_i$ increase (Xu et al., 2005) and attenuates the ventilatory response. Thus, ATP may also provide negative feedback modulation of hypoxia-induced glomus cells excitation. ATP can also trigger $[Ca^{2+}]_i$ increases in sustentacular cells through the activation of $P2Y_2Rs$ (Xu et al., 2003; Piskuric and Nurse, 2012), which could modulate glomus cell excitability and the magnitude of the ventilatory responses (Fig. 3C).

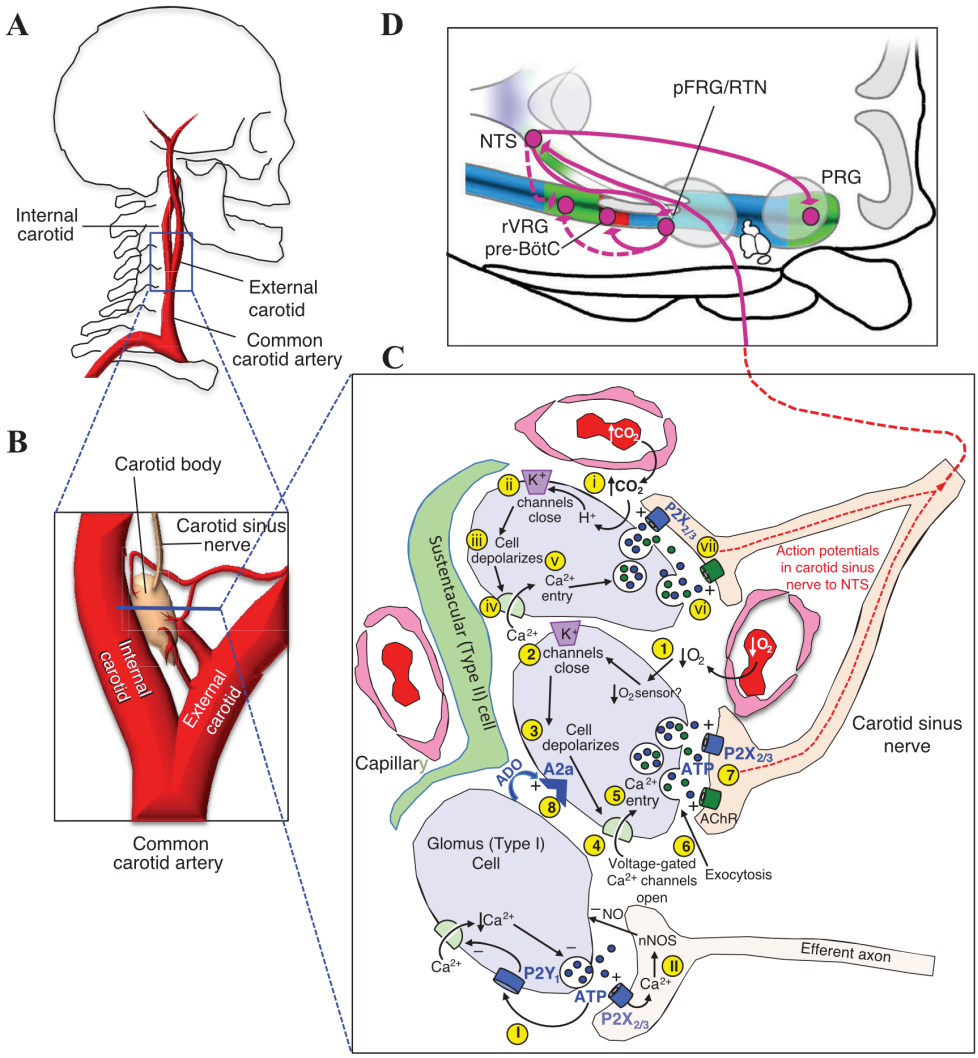

Figure 3: Carotid body function. A, B. The carotid bodies are located bilaterally in the bifurcation of the carotid artery. C. Illustration of the structure and signalling of the carotid body showing glomus (Type I cells) and sustentacular cells (Type II cells), capillaries and CSN endings and the signalling pathways initiated by decreased O_2 and increased CO_2. D. Sagittal section of the ventrolateral medulla illustrating the brainstem targets of the carotid bodies. From (Funk, 2013).

1.5.2.3 Central chemoreception, ATP and P2Rs.

Central chemoreception refers to process by which the CNS stimulates breathing in response to increased CO_2 (Guyenet et al., 2010). CO_2 sensing by the brain relies on specialized cells, located at the brainstem, that can detect changes in CO_2 and signal for an increase in breathing. Multiple brain regions have been involved in mediating chemoreception including the pF_V, NTS, preBötC, raphe nucleus and locus coeruleus (Nattie and Li, 2009; Guyenet and Bayliss, 2015). However, glutamatergic neurons located in the pF_V seem to play a predominant role (Fig. 4). Mulkey et al (2004) showed that increases in CO_2 activate glutamatergic pF_V neurons that are normally silent (Mulkey et al., 2004b). These neurons in the pF_V detect $PaCO_2$ in a pH-dependent manner (Guyenet et al., 2005), possibly through inhibition of the H^+-sensitive TASK-2 background K^+ channel (Gestreau et al., 2010; Wang et al., 2013; Kumar et al., 2015) and activation of the proton-activated receptor GPR4 (Kumar et al., 2015). As described earlier, pF_V neurons express PHOX2B (Onimaru et al., 2008) and the photoactivation of these PHOX2B-expressing neurons stimulates breathing in manner similar to that of CO_2 (Abbott et al., 2011). Ruffault et al. (2015) demonstrated that PHOX2B-expressing and ATOH1-expressing neurons of the pF_V are necessary for an appropriated response to hypercapnia. The authors, using intersectional genetics, selectively inactivated ATOH1 on PHOX2B-expressing neurons and PHOX2B on ATOH1-expressing neurons. They found that, in both cases, the ventilatory response to CO_2 was abolished (Ruffault et al., 2015). In addition, patients with congenital central hypoventilation syndrome, a condition attributed to a mutation in the Phox2B gene, have diminished responses to CO_2 (Weese-Mayer et al., 2010). All this evidence suggests that PHOX2B-expressing pF_V neurons are be the principal CO_2 chemoreceptor.

Neural networks are metabolically and structurally supported by astrocytes and they act as an interface between vasculature and neurons. Thus, astrocytes are uniquely positioned to act as chemoreceptors. In fact, astrocytes located on the ventral surface of the medulla, at the level of the pF_V, are highly sensitive to changes in $PaCO_2$/pH. Work done by Gourine et al (2005a) demonstrated that the increase in $PaCO_2$ produces an increase in extracellular ATP on the ventral surface of the medulla at the level of the pF_V *in vivo*. In addition, they found that antagonizing P2 receptors in this area reduces the CO_2 sensitivity (i.e the threshold CO_2 level required to stimulate breathing is increased in the presence of P2R antagonists). They also showed that the application of ATP, or a P2YR agonist, increases respiratory activity in a similar way to CO_2 excites (Gourine et al., 2005a). In a later study, Gourine et al (2010) demonstrated that the acidification of the ventral surface of the medulla, at the level of the pF_V, triggers an increase of intracellular Ca^{2+} in cells expressing the glial fibrillatory acidic protein (GFAP) *in vivo* and *in vitro* (Gourine et al., 2010), suggesting that astrocytes are excited when pH decreases (Fig. 4). This increase in astrocytic intracellular Ca^{2+} is accompanied by an increase of extracellular ATP (Gourine et al., 2010), suggesting that astrocytes respond to a decrease in pH by releasing ATP (Fig. 4). In the same study, they demonstrated that acidification of slices from adult rats depolarized and increased intracellular Ca^{2+} of pF_V neurons that express PHOX2B (Gourine et al., 2010). They also showed that photoactivation of astrocytes in the ventral surface of the medulla induces the release of ATP and depolarizes pF_V neurons in organotypic brainstem slices. This depolarization and increase in intracellular Ca^{2+} was blocked by a $P2Y_1R$ antagonist. More importantly, photoactivation of astrocytes of the ventral surface of the medulla induced a robust increase in phrenic nerve activity *in vivo* on anesthetized, artificially ventilated rats and this was also blocked by a $P2Y_1R$ antagonist locally applied to the ventral surface of the medulla (Gourine et al., 2010). In parallel, Huckstepp

et al (2010) reported a gap junction-mediated mechanism of CO_2-induced ATP release in the ventral surface of the medulla (Huckstepp et al., 2010). The studies described above suggest that, CO_2 induces the release of ATP from pF_V astrocytes, which in turn depolarizes PHOX2B neurons to excite breathing (Fig. 4).

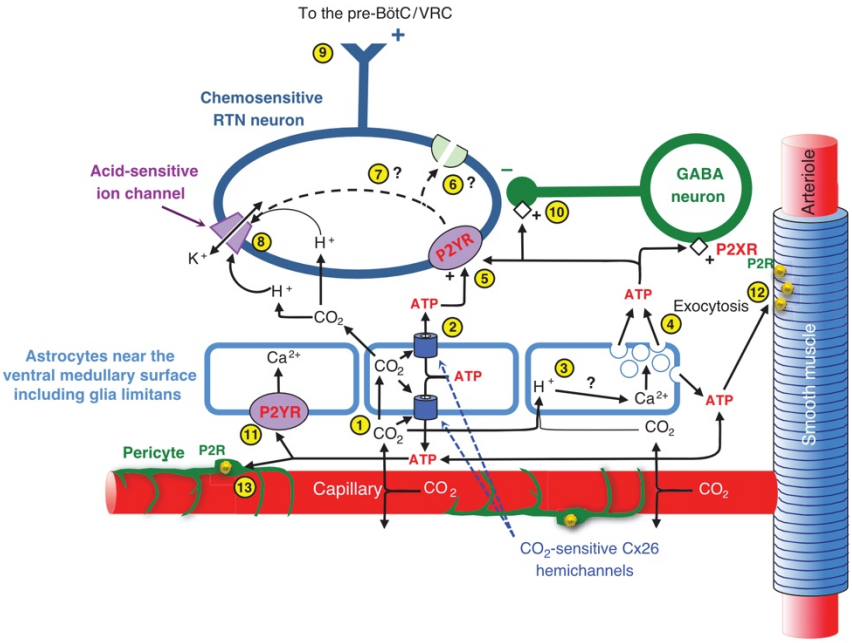

Figure 4. Schematic illustrating the role of P2 signaling in central chemoreception on the pF_V. Increases in CO_2 elicit ATP release form astrocytes. ATP then activates P2Y receptors on pF_V which excited them. pF_V also respond directly to acidification. This acidification blocks a K^+ conductance, depolarizing pF_V neurons. As a result, pF_V stimulates the preBötC to increase ventilation. From (Funk, 2013).

1.5.3 P2 receptor signaling in the hypoxic ventilatory response

1.5.3.1 Hypoxic ventilatory response.

The HVR is an adaptive response characterized by an initial increase in ventilation followed by a secondary depression (Moss, 2000). When arterial O_2 levels fall, peripheral chemoreceptors, the CBs, trigger a rapid increase in ventilation. The initial peripheral-mediated response to hypoxia is followed by a slower, secondary HRD that is largely mediated by the CNS (although CB desensitization may contribute), in which ventilation decreases to a new baseline. In adults, this new ventilation baseline remains elevated and above pre-hypoxia levels (Fig. 5A). However, in prematurity, the HRD is most pronounced and in infants born with apnea of prematurity it can be life-threatening since it brings ventilation below pre-hypoxia baseline levels (Fig. 5A) (Moss, 2000; Martin et al., 2005) About 80% of infants with apnea of rematurity are succesfully treated with caffeine, an adenosine antagonist, which increases ventilation (Aranda et al., 1983; Abdel-Hady, 2015; Schmidt et al., 2006). However, for the remaining 20% of infants there is no treatment available and they are at greater risk of suffering bronchopulmonary dysplasia due to the positive airway pressure of artificial ventilation. This ventilation-induced lung damage, as well as the hypoxia induced by apneas can also promote cognitive delay and cerebral palsy (Schmidt et al., 2009; 2012).

1.5.3.2 Mechanisms that shape the secondary hypoxic respiratory depression.

The secondary HRD has been mainly attributed to the inhibitory actions of adenosine through activation of P1 receptors (Reklow et al., 2019; Martin et al., 2005). However, recent studies suggest that the central nervous system also exert excitatory actions that help shape the secondary HRD.

In a series of studies, Gourine et al (2003, 2005b) showed, first, that exogenous ATP excites inspiratory-related ventrolateral medulla neurons via activation of P2Rs in neonatal medullary slices, and that this effect is blocked by suramin, a P2R antagonist (Gourine et al., 2003). Second, using an ATP-specific biosensor Gourine et al (2005b) later showed that ATP is released in the ventrolateral medulla during systemic hypoxia *in vivo* (Gourine et al., 2005b). This hypoxia-induced ATP release is delayed, starting ~25 seconds after the initial increase in ventilation, and peaks during the secondary HRD (Fig 5B). Additionally, antagonizing P2 receptors in the preBötC with PPADS, a nonselective P2R antagonist, exacerbates the secondary HRD (Gourine et al., 2005b) (Fig 5C). This suggests that, under hypoxia, ATP is released in the ventrolateral medulla, and that this ATP counteracts the secondary depression via P2Rs.

Studies from our laboratory showed that ATP, via activation of $P2Y_1$Rs, depolarizes inspiratory preBötC neurons to increase inspiration in vitro, and suggest that preBötC glial cells are the source of ATP release in vivo. First, it was demonstrated that $P2Y_1$Rs are expressed in NK1R-expressing preBötC neurons (Lorier et al., 2007) and that local microinjections of ATP specifically into the preBötC of rhythmically active medullary slices from neonatal rats (Lorier et al., 2007) and mice (Zwicker et al., 2011) increase inspiratory motor output. Moreover, the increase in inspiratory-related activity was induced by local administration of $P2Y_1$R agonists into the preBötC of medullary slices from rats and mice; the ATP-evoked excitation was also blocked by pre-administration of a $P2Y_1$R antagonist (Lorier et al., 2007; Huxtable et al., 2009; Zwicker et al., 2011). This $P2Y_1$R-induced inspiratory-related activity was observed as early as embryonic day 17 in rats (Huxtable et al., 2009), which coincides with the developmental age when respiratory

activity first emerges (Pagliardini et al., 2003). Later, Lorier et al (2008) demonstrated that local microinjections of ATP, and a $P2Y_1R$-preffering agonist, into the preBötC evokes depolarizing inward currents in inspiratory, expiratory and non-respiratory neurons in isolated rhythmically active medullary slices from neonatal rats. This ATP-induced inward current on inspiratory neurons is attenuated by a $P2Y_1R$ antagonist (Lorier et al., 2008). Finally, Huxtable et al (2010) showed that bath co-applications of two different glial toxins, methionine sulfoximine and glutamine, attenuate the ATP-induced increase in inspiratory motor output in rhythmically active medullary slices from neonatal rats (Huxtable et al., 2010). Together, these studies suggest that ATP, which is released by preBötC glial cells under hypoxia, activates $P2Y_1R$ to excite inspiratory neurons to increase ventilation and counterbalance the secondary HVD.

Recently, Angelova et al (2015) showed that hypoxia evokes an increase in intracellular Ca^{2+} in cortical astrocytes *in vivo*, in astrocytes from organotypic brainstem slices and dissociated cell cultures *in vitro*, suggesting that astrocytes are sensitive to low oxygen levels (Angelova et al., 2015), and they proposed that the astrocytic oxygen sensor resides in the mitochondria. They showed that, in cultured astrocytes, the increase of Ca^{2+} inside the mitochondria precedes the cytosolic Ca^{2+} increase during hypoxia. This mitochondrial Ca^{2+} elevation is abolished by a mitochondrial uncoupler in cultured astrocytes as well as in cortical astrocytes of anesthetized rats. Moreover, hypoxia fails to increase intracellular Ca^{2+} in astrocytes cultured from mice with impaired mitochondrial function. Angelova et al (2015) also reported that hypoxia increases mitochondrial reactive oxygen species, phospholipase C activation, IP3-induced calcium release which leads to the release of ATP (Angelova et al., 2015). In the same study, by monitoring the mobility of VNUT-expressing vesicles using total internal reflection microscopy, they showed that

hypoxia induces a calcium-dependent release of ATP-containing vesicles in cultured brainstem astrocytes (Angelova et al., 2015). Additionally, blocking astrocytic vesicular release by expressing the light chain of tetanus toxin (TeLC) under the astroglial promoter GFAP inhibits vesicular fusion in cultured astrocytes. Most importantly, the expression of TeLC in preBötC astrocytes blunted the hypoxia-induced increase in respiratory rate, *in vivo* (Angelova et al., 2015).

Recent data from our laboratory also showed that transfecting preBötC astrocytes with TeLC attenuates the hypoxia-induced increase of ventilatory output in anesthetized rats during the initial during the secondary HRD (Rajani et al., 2018). Additionally, microinjections of a $P2Y_1R$ agonist into the preBötC increases respiratory frequency in anesthetized rats at rest, while microinjections of a $P2Y_1R$ antagonist had no effect on the initial phase of the HVR but potentiate the secondary depression *in vivo* (Fig. 5D) (Rajani et al., 2018). Finally, activation of $P2Y_1Rs$ induce an increase in intracellular Ca^{2+} on inspiratory preBötC neurons (Rajani et al., 2018). The evidence described above suggests that hypoxia triggers the release of ATP from astrocytes. ATP then activates postsynaptic $P2Y_1Rs$ on inspiratory preBötC neurons, which induces the release of calcium from intracellular stores exciting inspiratory neurons to finally increase ventilation.

Adenosine, via P1 receptors, also contributes to shaping the hypoxic ventilatory response. During hypoxia, the concentration of extracellular adenosine increases in respiratory-associated brainstem regions of fetal sheep (Koos et al., 1994), anesthetized juvenile piglets (Yan et al., 1995) and adult cats (Richter et al., 1999). The peak of hypoxia-induced release of adenosine coincides with the depression of breathing (Koos et al., 1994; Richter et al., 1999). Hypoxia depresses fetal sheep breathing movements and this effect is mimicked by systemic administration of adenosine during

normoxia. Moreover, the hypoxia-induced depression in breathing is attenuated by systemic perfusion of an adenosine antagonist (Koos and Matsuda, 1990). Similarly, in neonatal rabbits and piglets, adenosine analogs depress ventilation and the pre-administration of an adenosine antagonist prevents this respiratory depression (Lagercrantz et al., 1984; Elnazir et al., 1996). Additionally, in neonatal rabbits, the secondary HRD is potentiated by adenosine agonists and adenosine uptake inhibitors, and is attenuated by adenosine antagonists (Fig. 5F) (Runold et al., 1989; Lopes et al., 1994). Similar effects of adenosine antagonists on the hypoxia-induced respiratory depression were found in isolated brainstem-spinal cord from neonatal rats (Kawai et al., 1995), and in anesthetized and awake adult cats (Long and Anthonisen, 1994; Schmidt et al., 1995). In humans, augmenting endogenous extracellular adenosine via intravenous injection of an adenosine uptake inhibitor potentiates the secondary HRD, and this effect is prevented by an adenosine antagonist (Yamamoto et al., 1994). As previously reviewed by Funk et al (2013) and, later by Reklow et al (2019), *in vivo* and *in vitro* evidence support the participation of A1 and A2a receptors in secondary HRD (Funk, 2013; Reklow et al., 2019).

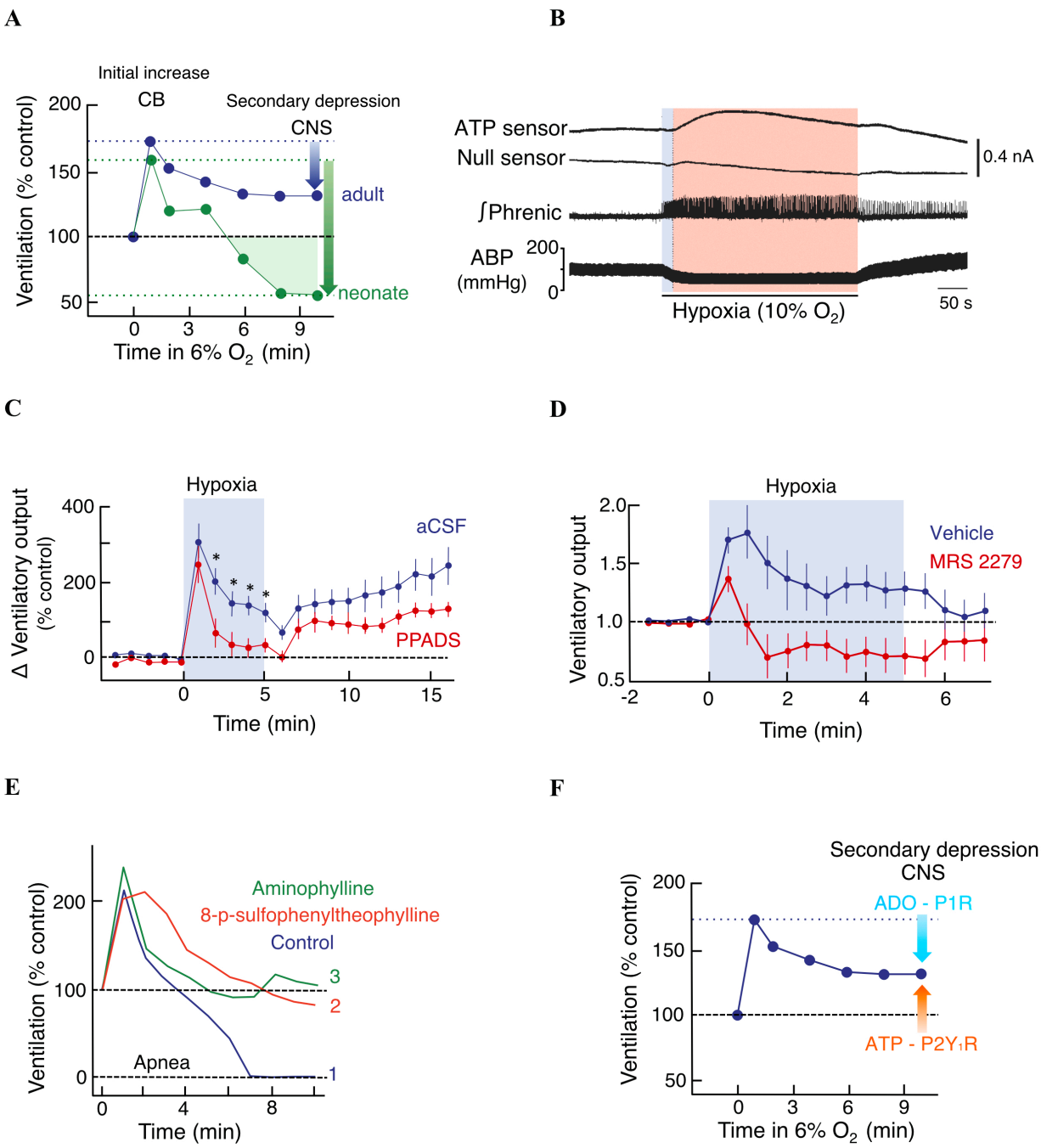
A
Initial increase
CB
Secondary depression
CNS
adult
neonate
Ventilation (% control)
200
150
100
50
0
3
6
9
Time in 6% O2 (min)
B
ATP sensor
Null sensor
∫Phrenic
ABP
(mmHg)
200
0
0.4 nA
Hypoxia (10% O2)
50 s
C
Hypoxia
aCSF
PPADS
Δ Ventilatory output
(% control)
400
200
0
0
5
10
15
Time (min)
D
Hypoxia
Vehicle
MRS 2279
Ventilatory output
2.0
1.5
1.0
0.5
-2
0
2
4
6
Time (min)
E
Aminophylline
8-p-sulfophenyltheophylline
Control
3
2
1
Apnea
Ventilation (% control)
200
100
0
0
4
8
Time (min)
F
Secondary depression
CNS
ADO - P1R
ATP - P2Y1R
Ventilation (% control)
200
150
100
50
0
3
6
9
Time in 6% O2 (min)

Figure 5: Mechanisms that underlie the hypoxic ventilatory response. A. Hypoxic ventilatory response (HVR) of adult (blue) and neonatal (green) pigs exposed to 6% O_2 showing a biphasic response. The initial increase in ventilation mediated by the carotid bodies is followed by a secondary depression. In neonates, the secondary depression is more pronounced than in adults and falls below baseline to life threatening levels. Adapted with permission from (Moss, 2000). B, During hypoxia, ATP is released in the ventral respiratory column to counterbalance the secondary respiratory depression. In B, null and ATP sensor currents recorded on the ventral medullary surface are illustrated. Below is the integrated phrenic nerve discharge and in the bottom is the arterial blood pressure during hypoxia. ATP release occurs after the increase in the phrenic nerve inspiratory activity. C. Blockade of P2Rs of the ventral medulla potentiates the secondary respiratory depression in adult rats. Adapted with permission from (Gourine et al., 2005b). D. Blockade of $P2Y_1R$ of the preBötC potentiates the secondary depression on adult rats. Adapted with permission from (Rajani et al., 2018). E. During hypoxia, adenosine (ADO) contributes to the secondary depression of breathing. The scheme illustrates the ventilatory response of rabbit pups after an infusion of saline (control) or after infusion of two ADO antagonists (aminophylline, 25 mg kg−1; or 8-p-sulfophenyltheophylline, 5 mg kg−1) Adapted with permission from (Runold et al., 1989). F. Schematic illustrating the opposing actions of ATP and ADO on ventilation. Adapted with permission from (Moss, 2000)

1.5.4. $P2Y_1R$ signaling and its role in the CNS.

$P2Y_1R$ are widely expressed in the CNS. They preferentially couple to G_q/G_{11}-proteins to activate the phospholipase C (PLC)/inositol triphosphate (InsP3) endoplasmic reticulum Ca^{2+}-release signaling pathway. $G_{\alpha q}/G_{11}$ signaling pathway starts with the dissociation of alpha subunit of the $G_{\alpha q}$-protein (αq) from the beta/gamma ($\beta\gamma$) subunit (Fig. 6). The dissociation of the αq subunit activates PLC which triggers the hydrolysis of phosphatidyl inositol 4, 5-biphosphate (PIP_2) to inositol triphosphate (IP_3) and diacylglycerol (DAG). IP_3 binds to IP_3 receptors located in the intracellular Ca^{2+} stores and promotes the release of Ca^{2+} from the endoplasmic reticulum. This intracellular Ca^{2+} mobilization promotes the activation of several Ca^{2+}-dependent kinases, including protein kinase C (PKC). DAG on the other hand, also activates PKC (Fig. 6). The $\beta\gamma$ subunit can directly modulate the activity of ion channels (Abbracchio et al., 2009), as can the loss of PIP2.

1.5.4.1 $P2Y_1R$ modulation of synaptic drive

In layer V pyramidal neurons of the rat prefrontal and parietal cortex, $P2Y_1R$ activation with a $P2Y_1$-preffering agonist reduces the amplitude of evoked excitatory postsynaptic currents (eEPSCs), decreases NMDA-induced depolarization and inhibits NMDA currents. This reduction of NMDA currents is abolished by a $P2Y_1R$ antagonist (Luthardt et al., 2003). The perfusion of a $P2Y_1R$ antagonist reduces the magnitude sEPSCs and promotes the development of long term depression (LTD) (Guzman et al., 2005), suggesting that $P2Y_1Rs$ can modulate NMDA receptor activity and attenuate the strength and plasticity of glutamatergic synapses *in vitro*, which may interfere with memory formation. In cerebellar Purkinje neurons, $P2Y_1Rs$ potentiate GABA release. Application of a P2YR agonist increases the excitability of GABAergic Lugaro neurons

of the cerebellum, eliciting an increase in frequency and amplitude of spontaneous and evoked inhibitory postsynaptic currents (sIPSCs and eIPSCs). The increase in sIPSCs was abolished by a $P2Y_1R$ antagonist (Saitow et al., 2005). In the same study, the activation of $P2Y_1Rs$ induced an increase in intracellular calcium in Purkinje neurons promoting LTP (Saitow et al., 2005). Thus, $P2Y_1R$ can potentiate synaptic inhibitory drive onto Purkinje neurons but also induce LTP via elevations of intracellular calcium to regulate information processing in the cerebellum.

1.5.4.2 $P2Y_1R$ modulation of Voltage-gated Ca^{2+} channels

G-protein coupled receptors (GPCR) can modulate the activity on a wide range type of ion channels. In rat superior cervical ganglion (SCG) and dorsal root ganglion neurons, $P2Y_1Rs$ inhibit N-type Ca^{2+} channels via the $\beta\gamma$ subunits (Filippov et al., 2000; Borvendeg et al., 2003; Gerevich et al., 2004). In the NTS, $P2Y_1Rs$ inhibit N-, P/Q- and L-type Ca^{2+}channels via $\beta\gamma$ subunits of a $G\alpha_i$ protein (Aoki et al., 2004). Thus, $P2Y_1Rs$ can modulate neurotransmission, neuronal excitability, dendritic integration and synaptic plasticity via modulation of voltage-gated Ca^{2+} channels (VGCCs). Inhibition of VGCCs has been associated with a decrease in inspiratory activity. N-, P/Q- and L-type Ca^{2+} channels have been described in neurons of the preBötC. In neonatal rats, blocking N- and P/Q-type VGCCs reduces inspiratory frequency while a cocktail of L-, N- and P/Q-type VGCC blockers abolishes rhythm *in vitro* (Onimaru et al., 2003a). Others have found that blocking P/Q-type VGCCs can slow, and even abolish, inspiratory rhythm *in vitro,* while blocking N- or L-type VGCC has no effect on rhythm (Lieske and Ramirez, 2006). On the other hand, it was reported that hypoxia can potentiate the activity of L-type VGCC *in vitro*, via activation of metabotropic glutamate receptors mGlu1/5 (Mironov and Richter, 2000). More recently, Koch et al (2013) showed that genetic ablation of the pore-forming subunit of the P/Q-

type VGCCs results in breathing abnormalities and ultimately death (Koch et al., 2013). In addition, inhibition of N-type VGCC slows rhythm from control mice, but completely abolishes activity in slices from mice lacking the pore-forming subunit of the P/Q-type VGCC (Koch et al., 2013). In summary, $P2Y_1Rs$ can modulate VGCCs but the nature of this interaction appears to be inhibitory. Thus, the possibility that $P2Y_1Rs$ excite inspiratory preBötC neurons via potentiation of VGCC is unlikely.

1.5.4.3 $P2Y_1R$ modulation of KCNQ channels

M-type or KCNQ channels are low-threshold voltage-gated K^+ channels and have a predominant role in controlling neuronal hyperexcitability. KCNQ channel opening requires the binding of phosphatidylinositol-4,5-bisphospate (PIP_2). Thus, they are typically inhibited by $G_{\alpha q}$-mediated activation of PLC and PKC (Vigil et al., 2020). M-currents of SCG sympathetic neurons can be supressed by P2YR-induced intracellular Ca^{2+} release, which requires IP_3 accumulation and functional Ca^{2+}/calmodulin binding to the M-channel (Zaika et al., 2007). On the same type of neurons (Brown et al., 2000), and on rat primary hippocampal culture neurons (Filippov et al., 2006), KCNQ2/3 channels are inhibited by $P2Y_1Rs$. In rat slices containing the RTN, blocking KCNQ channels increases basal firing rate and potentiates the response to CO_2 of RTN chemoreceptors. On the other hand, the activation of KCNQ channels inhibits RTN chemosensitive neurons (Hawryluk et al., 2012). In the preBötC, KCNQ channel openers decrease inspiratory burst frequency, an effect that is similar to the activation of MORs. Inhibitors of KCNQ channels reversed MOR-induced depression of inspiratory burst frequency (Wei and Ramirez, 2019). Thus, $P2Y_1Rs$ could potentially increase neuronal excitability by suppressing KCNQ channel activity on inspiratory preBötC neurons.

1.5.4.4 $P2Y_1R$ modulation of GIRK channels

G-protein coupled inward rectifying K^+ (GIRK) channels are K^+ channels that are modulated by direct interaction with the $\beta\gamma$ subunits of G proteins, and their activation results in membrane hyperpolarization. Montandon et al. (2016a) reported that the GIRK2 subunit is expressed in the preBötC and that pharmacological activation of GIRK channels with flupirtine in rats and mice reduces respiratory rate (diaphragm muscle frequency) *in vivo*. This effect was absent in $GIRK2^{-/-}$ mice (Montandon et al., 2016a). In the same study, they showed that the inhibitory effect of MOR activation on breathing is dependent on the activation of GIRK channels (Montandon et al., 2016a). In a later study, Montandon et al (2016b) showed that GIRK2 subunits are co-expressed with NK1R on preBötC neurons and that the activation of GIRK channels with flupirtine and with the selective GIRK channel opener ML297 decreases breathing rate and genioglossus muscle amplitude in anesthetized rats (Montandon et al., 2016b). On the other hand, perfusion of a NK1 receptor agonist in the preBötC of wild type mice stimulates breathing and increases genioglossus muscle amplitude. This effect is absent in mice lacking GIRK2 subunits (Montandon et al., 2016b), suggesting that GIRK channels contribute to the stimulatory effects of NK1 receptors on breathing and position GIRK channels as an important modulator inspiratory rhythm. Contrary, Wei et al (2019) found that the activation of preBötC GIRK channels does not reduces inspiratory frequency in vitro. They also showed that blocking GIRK channels does not reverses the opioid-induced decrease of inspiratory rhythm *in vitro*. Finally, they evaluated the effects of activating GIRK channels in vivo and they found a modest (10%) decrease on respiratory rate (Wei and Ramirez, 2019).

Activation of $P2Y_1Rs$ on rat sympathetic neurons produces a rapid but transient activation of I_{GIRK}, followed by inactivation. The activation of I_{GIRK} was sensitive to pertussis toxin (PTX) and was reduced by co-expression of a G$\beta\gamma$-scavenging protein. Thus, activation of $P2Y_1Rs$ activates GIRK channels via the $\beta\gamma$ subunit, suggesting an interaction of $P2Y_1Rs$ with the $\beta\gamma$ subunit from Gi/o proteins. The inactivation of GIRK channels by $P2Y_1R$ is reduced by the regulator G-protein signaling 2 (RGP2), a protein with GTPase activity that is known to interact with $G\alpha_{q/11}$, and not by the RGP11, which interacts with $G\beta_q$. Thus, the inhibition of I_{GIRK} by $P2Y_1R$ activation is dependent on $G\alpha_{q/11}$ (Filippov et al., 2004). Similar results were found with bath application of ATP on Chinese hamster ovary cells transfected with $P2Y_1Rs$ and GIRK1/GIRK4 heterodimers. Here, ATP produced a rapid transient activation of I_{GIRK}, that was PTX sensitive, followed by inactivation, which was attenuated by RGP2 (Wu et al., 2012).

The contribution of GIRK channels to the $P2Y_1$-induced increase in respiratory frequency was examined previously in our lab using rhythmically active medullary slices containing the preBötC. Inhibiting GIRK channels with bath application of barium chloride ($BaCl_2$) reduced baseline XII nerve inspiratory-related frequency progressively with increasing concentrations of $BaCl_2$. However, the absolute peak increase on inspiratory frequency induced by local activation of $P2Y_1Rs$ with the selective agonist MRS 2365 in the preBötC was unaffected by $BaCl_2$ (Zhang et al., 2016a; 2016b). Thus, GIRK channels do not seem to contribute to the $P2Y_1R$-induced inspiratory excitation of the preBötC inspiratory network.

1.5.4.5 $P2Y_1R$ modulation of TASK channels

TASK channels belong to the two-pore domain K^+ channel family. TASK channels contribute to leak K^+ currents that maintain resting membrane potential and also help to control membrane excitability. TASK-1, TASK-2 and TASK-3 channels are sensitive to extracellular H^+ concentrations and have been proposed as sensors for central chemoreception. TASK-1 and TASK-3 can form homo- or heterodimers and they are activated at a pH range from 6.7 to 7.4, depending on the subunit composition. TASK-2 channels have a broader range of pH sensitivity, and they are activated from pH values from 7.0 to 10 (Bayliss et al., 2015). Both, TASK-1 and TASK-3 channels are present in brainstem respiratory regions, including in preBötC inspiratory neurons, rVRG neurons, and respiratory motoneurons of the brainstem and spinal cord (Bayliss et al., 2015). TASK-2 is present in RTN neurons that also express PHOX2B. In an *in situ* preparation from $TASK^{-/-}$ mice, pH sensitivity of RTN neurons is reduced and the respiratory chemoreflex is blunted (Wang et al., 2013). TASK-1 and TASK-3 channels were also identified on neurons from upstream chemoreceptor-related areas such as the dorsal raphe nuclei and locus coeruleus (Bayliss et al., 2015). Deletion of TASK-1 and/or TASK-3 channels on the dorsal raphe, but not on the RTN, abolishes the increase in excitability induced by a decrease on pH (Mulkey et al., 2007). The above evidence suggest that, at the level of the RTN, TASK-2 rather than TASK1-3 channels, are responsible for chemosensitivity properties of RTN neurons More recently, it was demonstrated that astrocytes release ATP which activates $P2Y_1Rs$ on cholecystokinin hippocampal interneurons, increasing their excitability by inhibiting the two-pore domain K^+ channel, TASK-3, in a $G_{q/11}$-dependend but PLC-independent pathway. This increase in excitability was abolished by a $P2Y_1R$ antagonist and was absent in a $P2Y_1R$ K.O mice (Tan et al., 2017). Thus, it is possible that $P2Y_1Rs$ excite inspiratory neurons of the preBötC by inhibiting TASK channels.

1.5.4.6 $P2Y_1R$ modulation of SK_{Ca}, IK_{Ca}, BK_{Ca} channels

Calcium-activated potassium channels (K_{Ca}) are expressed in all cell types on the CNS. They are unique in their ability to couple intracellular Ca^{2+} increases to membrane hyperpolarization which confers K_{Ca} channels an important role in regulating neuronal excitability. Thus, is no surprise that they are located in close proximity of Ca^{2+} entry sources such as VGCC, TRPV1 channels and to NMDA receptors (Kshatri et al., 2018). K_{Ca} channels can be divided into three subfamilies, depending on their single channel conductance: small (SK_{Ca}, ~1–20 pS), intermediate (IK_{Ca}, ~20–80 pS) and big conductance (BK_{Ca}, ~100–280 pS) calcium-activated K^+ channels. They can also be distinguished by their Ca^{2+} sensitivity, voltage-dependence and pharmacology. SK_{Ca} and IK_{Ca} channels are voltage-insensitive, require low (50–900 nM) intracellular Ca^{2+} concentration to be activated, which binds to the channel calmodulin (CaM) binding domain. SK_{Ca} and IK_{Ca} channels are commonly blocked by the bee venom apamin and the antifungal clotrimazole, respectively (Kshatri et al., 2018). SK_{Ca} channels are expressed throughout the CNS (Stocker and Pedarzani, 2000) and underlie the medium afterhyperpolarization (mAHP) in various neuronal types (Schulz et al., 2012; Ferreira-Neto et al., 2017; Matschke et al., 2018). Additionally, activation of SK_{Ca} channels shunts excitatory postsynaptic potentials (EPSPs) on lateral amygdala and hippocampal pyramidal neurons providing feedback regulation of neuronal excitability (Faber et al., 2005; Ngo-Anh et al., 2005; Bloodgood and Sabatini, 2007). IK_{Ca} are most abundant in non-excitable cells types but they have been found in enteric neurons where they seem to modulate the slow afterhyperpolarization (sAHP) (Neylon et al., 2004).

Administration of a SK_{Ca} channel opener to rhythmically active medullary slices from P6-8 neonatal mice depresses basal preBötC inspiratory activity, and this effect is reversed by apamin. Blocking SK_{Ca} channels with apamin causes an increase in frequency and amplitude of preBötC inspiratory bursts and increases irregularity of respiratory activity (Zavala-Tecuapetla et al., 2008). Additionally, the activation of SK_{Ca} channels seems to abolish bursting of pacemaker preBötC neurons and this is reversed by apamin. Apamin also promotes bursting on non-pacemaker preBötC neurons. Zavala-Tecuapleta el at (2008) showed that activating SK_{Ca} channels depresses breathing in neonatal mice, *in vivo*, resulting in death. On the other hand, blocking SK_{Ca} increases respiratory rate (Zavala-Tecuapetla et al., 2008). However, in a later study conducted by Onimaru et al (2003a) using neonatal P0-4 brainstem-spinal cord preparations from rats, apamin failed to produce any effects on inspiratory rhythm or burst amplitude, measured at the ventral roots of the spinal cervical C4-C5 nerves (Onimaru et al., 2003a).

In the enteric nervous system, ATP is released from inhibitory motoneurons causing afterhyperpolarization and relaxation of the human smooth muscle, via $P2Y_1Rs$. This is apamin-sensitive suggesting that, in this system, $P2Y_1Rs$ act through modulation of SK_{Ca} channels (Gallego et al., 2006). In the rat ileum smooth muscle, the activation of $P2Y_1Rs$ induces IP_3-dependent Ca^{2+} increase, activating SK_{Ca} channels and causing muscle relaxation (Mader et al., 2016). In PC12 cells and hippocampal neurons, ADP activates of SK_{Ca}-mediated currents via $P2Y_1Rs$ (Schicker et al., 2010). In neonatal striatal neurons from rats, $P2Y_1Rs$ activation evokes SK_{Ca}-mediated currents (Coppi et al., 2012). Thus, SK_{Ca} channels are a potential mechanism by which $P2Y_1R$ excite the respiratory network. The contribution of SK_{Ca} channels to the $P2Y_1$-induced excitation of the preBötC has been examined in our laboratory. Local application of

apamin into the preBötC has no effect on the $P2Y_1R$-evoked increase on inspiratory frequency (Zhang et al., 2016a; 2016b). Thus, SK_{Ca} channels do not seem to contribute to the $P2Y_1R$-induced inspiratory excitation of the preBötC inspiratory network.

Unlike SK_{Ca} and IK_{Ca}, BK_{Ca} channels are voltage sensitive and require high (1–10 mM) intracellular Ca^{2+} concentration to be activated (Kshatri et al., 2018), acting as coincident detectors of intracellular calcium increase and membrane depolarization. BK_{Ca} channels are ubiquitously expressed throughout the CNS and the pore forming unite expression has been detected in several brain regions including the cortex, hippocampus, thalamus, habenula, basal ganglia, cerebellum, spinal cord and preBötC (Zhang et al., 2010; Contet et al., 2016; Kshatri et al., 2018). BK_{Ca} channels are located in dendrites, soma, axons and synaptic terminals of neurons where they regulate action potential shape, propagation, firing frequency and neurotransmitter release, but they are also expressed in the mitochondria, where they attenuate ROS production and promote cell viability (Kshatri et al., 2018). BK_{Ca} channels can be further classified into type I and type II depending on their activation and inactivation kinetics, subcellular trafficking and pharmacology, which depends on the associated auxiliary subunit. Type I BK_{Ca} channels have faster gating kinetics and are iberiotoxin (IbXT)-sensitive. Type II BK_{Ca} channels have slower gating kinetic and are IbXT -insensitive (Contet et al., 2016).

The role of BK_{Ca} channels in modulating respiratory rhythm is unclear. Onimaru et al (2003a) reported that bath application of the non-selective K^+ blocker tetraethylammonium, at a concentration in which also blocks BK_{Ca} channels, decreases respiratory frequency in brainstem-spinal cord preparations from neonatal P0-4 rats, without affecting the burst amplitude of the

ventral roots of the spinal cervical C4-C5 nerves (Onimaru et al., 2003a). Zao et al (2006) showed that blocking type I BK_{Ca} channels with iberiotoxin decreases preBötC burst frequency in rhythmically active slices from P8-P20 control mice and that in mutant oscillator mice, where glycinergic inhibition is lost, iberiotoxin abolishes preBötC burst frequency (Zhao et al., 2006). Similar results were found earlier by Büsselberg et al (2003) where blockade of BK_{Ca} channels with charybdotoxin terminated phrenic burst activity when glycinergic transmission was pharmacologically or genetically eliminated (Büsselberg et al., 2003). Later, Zavala-Tecuapleta et al (2008) reported that BK_{Ca} channels have mild effects on basal inspiratory activity *in vitro*. Activation of BK_{Ca} channels with NS 1619 on rhythmically active medullary slices from neonatal P6-8 mice had no effect on basal inspiratory preBötC burst amplitude, frequency or irregularity. This contrasted with their *in vivo* results in which intracisternal administration of NS 1619 increased respiratory amplitude, without affecting frequency or irregularity on P8 mice. In the same study, Zavala-Tecuapleta et al (2008) showed that blocking type I BK_{Ca} channels with IbXT has no effect on preBötC inspiratory frequency but increased burst amplitude *in vitro*, while *in vivo* IbXT decreases inspiratory amplitude without affecting frequency. They also reported that blocking type I and type II BK_{Ca} channels with the mycotoxin paxilline increases preBötC inspiratory burst frequency while decreasing burst amplitude in a dose-dependent manner *in vitro.* However, they found that intracisternal administration of paxilline increased respiratory amplitude, without affecting frequency or irregularity, *in vivo*. (Zavala-Tecuapetla et al., 2008). More recently, Zhang et al. (2010) showed that the pore-forming subunit of BK_{Ca} channels is expressed in neurons of the preBötC and that bath application of paxilline on rhythmically active medullary slices from neonatal P0-P3 rats increases the frequency of inspiratory hypoglossal discharge while reducing burst amplitude (Zhang et al., 2010).

In neonatal striatal neurons from rats, $P2Y_1R$ activation induced BK_{Ca}-mediated currents (Coppi et al., 2012). Due to its Ca^{2+}-dependence, BK_{Ca} channels present an attractive mechanism to mediate the excitatory actions of $P2Y_1R$ on preBötC inspiratory neurons. The participation of BK_{Ca} channels in the $P2Y_1R$-evoked increase in inspiratory frequency has also been studied in our laboratory. Blocking preBötC type I BK_{Ca} channels in rhythmically active medullary slices from rats with IbTX has no effect on the $P2Y_1R$-induced increase in XII inspiratory frequency, suggesting that type I BK_{Ca} channels are not involved in the $P2Y_1R$ excitation of the preBötC. On the other hand, blocking type I and type II BK_{Ca} channels with local application of paxilline into the preBötC presented confounding results. While paxilline reduced the $P2Y_1R$-induced increase of XII inspiratory frequency on a subpopulation of preparations, when grouped together, the effect was not statistically significant (Zhang et al., 2016a; 2016b).

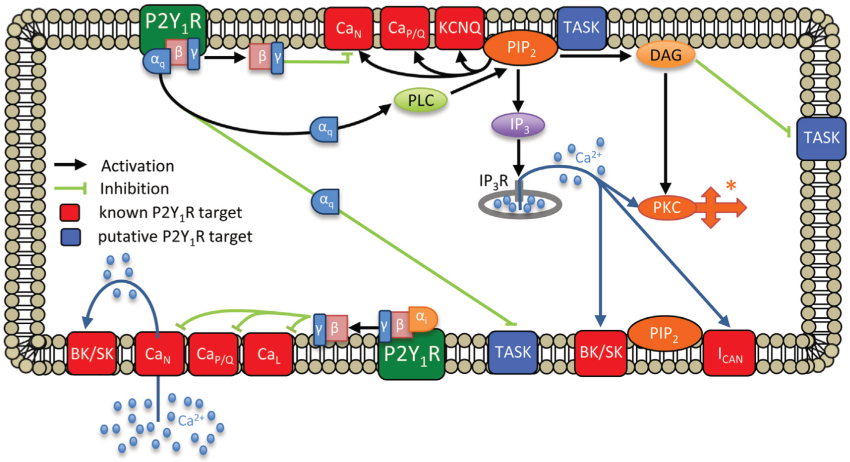

Figure 6: Schematic of a preBötC inspiratory neuron of known and putative $P2Y_1$ signaling. Red ion channels are known targets of $P2Y_1R$ signaling and are involved in the modulation of inspiratory rhythm. Blue ion channels are Gq associated and have not being linked to $P2Y_1R$ activation. $P2Y_1R$ activation leads to the dissociation of Gαq and Gαi from $\beta\gamma$ subunits. Gαq inhibits TASK channels directly via PLC. PIP2 modulates KCNQ, TASK, BK_{Ca}/SK_{Ca}, I_{CAN} and Ca^{2+} channels. $P2Y_1R$ activation leads to of IP3-induced Ca^{2+} release. This in turns activates BK_{Ca} and SK_{Ca} channels. From (Rajani et al., 2016).

1.6 Thesis Objectives:

During hypoxia ATP is released form astrocytes in the preBötC. ATP acts on $P2Y_1Rs$ of inspiratory preBötC neurons to increase ventilation and attenuate the HRD (Rajani et al., 2018). $P2Y_1Rs$, which are preferentially coupled to the $G_{\alpha q}$ signaling pathway (Abbracchio et al., 2009), are solely responsible for network frequency increase (Lorier et al., 2007), but they account for only a fraction (~30%) of the total ATP current (Zhang et al., 2016a; 2016b). Whether $P2Y_1Rs$ act on excitatory or inhibitory inspiratory preBötC neurons is unknown. The general objective of this component of the dissertation is to study the cellular and ionic mechanisms that underly the $P2Y_1R$-induced excitation of the preBötC.

The specific objectives of this dissertation are to test the hypotheses that:

a. the depolarizing inward current evoked by the activation of $P2Y_1R$ with the selective agonist MRS 2365 on preBötC inspiratory neurons will be abolished by blocking the activity of PLC and PKC with U71233 and chelerythrine (CHE), respectively.
b. the $P2Y_1R$-evoked depolarizing current in preBötC inspiratory neurons will be abolished by blocking type I and type II BK_{Ca} channels with the mycotoxin, paxilline.
c. the excitatory effect of $P2Y_1Rs$ on the preBötC network is mediated through activation of a subpopulation of excitatory glutamatergic preBötC inspiratory neurons.

2. Methods

2.1 Animals

Male Sprague – Dawley rats aged postnatal day 0 (P0) to 4 (P4) were used for *in vitro* experiments. Pregnant female rats of embryonic day (E9) and 16 (E16) were obtained from Charles River (Wilmington, Massachusetts). They were single housed and given water and food ad libitum. vGLUT2^{TdTomato} and GAD67^{venus} (C57BL/6-Tg(Slc32a1-Venus)39Yyan) mice were kindly provided by Dr. Simon Gogsnach (University of Alberta, AB, Canada). vGLUT2^{TdTomato} mice were obtained by crossing B6J.129S6(FVB)-Slc17a6$^{tm2(cre)Lowl}$/MwarJ) with B6.Cg-Gt(ROSA)26Sor$^{tm9(CAG-tdTomato)Hze}$/J. They were littermate housed and given water and food ad libitum. Fixed brain and brainstem tissue from GLYT2^{EGFP} (Tg(Scl6a5-EGFP)1Uze) mice were generously gifted by Dr. Kaiwen Kam (Dept. of Cell Biology and Anatomy, Chicago Medical School, Rosalind Franklin University, IL, USA). Fixed brain and brainstem tissue from *P2y1r*$^{-/-}$ mice were generously gifted by Dr. Ute Krügel (Rudolf Boehm Institute of Pharmacology and Toxicology, Faculty of Medicine, Leipzig University). The housing room was maintained on a 12 h light/dark cycle (7:00 A.M./7:00 P.M.) and at 22°C. All procedures were in approved by the University of Alberta Animal Ethics Committees and performed in accordance with their guidelines for the care, handling, and treatment of experimental animals.

2.2 Brainstem slice preparation.

Rhythmically active medullary slices were obtained from neonatal (postnatal day 0 to 4) Sprague-Dawley rats, vGLUT2^{TdTomato} and GAD67^{venus} mice as described previously (Smith et al., 1991; Funk et al., 1993; Ruangkittisakul et al., 2006; Lorier et al., 2007; Rajani et al., 2018). Briefly, pups were placed in a small induction chamber and anesthetised by isoflurane inhalation. The

brainstem-spinal cord was quickly isolated and kept in cold (4°C) artificial spinal fluid (aCSF) containing (in mM): 120 NaCl, 3 KCl, 2.0 $MgSO_4$, 26 $NaHCO_3$, 1.25 NaH_2PO_4, 20 D-glucose and bubbled with carbogen (95% O_2-5% CO_2). The brainstem-spinal cord was pinned down to a wax chuck and serial sections (100-200 μm) were cut through the rostro-caudal axis using a vibratome (TV1000S: Leica, Nussloch, Germany). Once the 2nd loop of the inferior olive was identified in the 100-200 μm section, a 700 μm transverse rhythmic slice was obtained. For experiments examining the effects of drugs on network activity assessed via extracellular recording of nerve activity, slices were pinned rostral surface up in a custom-made 5 mL recording chamber coated with Sylgard Resin and constantly perfused with aCSF at a flow rate of 15 mL min^{-1}. For experiments examining the effects of drugs on single neuron activity assessed by intracellular whole-cell recordings and two-photon Ca^{2+} imaging, rhythmically-active medullary slices were placed rostral surface up in a 3 mL recording chamber and held submerged on the glass coverslipped base of the chamber with a U-shaped platinum and nylon fiber "harp". Slices were continuously perfused with carbogenated aCSF at a rate of 2.5-2.7 mL min^{-1}for whole-cell recordings. For two-photon Ca^{2+} imaging recordings slices were perfused at a rate of 10 ml min^{-1}. In all the experiments, the extracellular K^+ concentration was raised from 3 to 9 mM and slices were allowed to stabilize for at least 30 min prior to experimental manipulation (Ruangkittisakul et al., 2006). All recordings were made at room temperature (24-25°C).

2.3 Recordings of nerve activity

In vitro recordings of inspiratory activity were made using suction electrodes (AM Systems, Calrsborg, WA, USA), fitted with glass pipettes (90-120 μm internal diameter), placed on the XII (hypoglossal) nerve rootlets using a four-axis manual manipulator. Nerve signals were amplified

(x10,000), bandpass filtered (300 Hz to 1kHz) using a Model-1700 differential AC amplifier, (AM-Systems, Sequim, WA, USA), rectified, integrated (leaky integrator, τ = 25 or 50 ms) and displayed using Axoscope (Molecular Devices) or LabChart 7 (AD Instruments). All recordings were made using Axoscope 9.2 via a Digidata 1322 A/D interface (Molecular Devices, Sunnydale CA, USA).

For calcium imaging experiments, XII nerve activity was acquired at 10,000 Hz, amplified (x10,000) and band-pass-filtered using a Model-1700 differential AC amplifier (AM-Systems, Sequim, WA, USA) and integrated (leaky integrator, τ = 25 or 50 ms) using a MA-821/RSP module (CWE Inc. Allentown, PA).

2.4 Drugs and their application.

[Sar^9-$Met(O_2)^{11}$]-substance P (1 μM) and MRS 2365 (10, 100 μM), chelerythrine chloride (10 μM) and U71322 (2 μM) were obtained from Tocris Biosicences. (-) Bicuculline (5, 20 μM) and strychnine (1, 20 μM) were obtained from Sigma-Aldrich (St Louis, MO, USA). Paxilline (1, 4 μM) and TTX (0.5 μM) were obtained from Alomone Labs. [Sar^9-$Met(O_2)^{11}$]-substance P and MRS 2365 were prepared as stock solutions in aCSF. Chelerythrine chloride, TTX and strychnine were prepared in MilliQ water (EMD Millipore, Billerica, MA, USA). (-) Bicuculline, paxilline and U73122 were prepared as stock solutions in 100% of dimethyl sulfoxide (DMSO). The stock solutions where diluted to the final concentration of 0.01% DMSO before use. All time controls were treated with matched vehicle concentrations. All drugs were kept at -20°C. Substance P, MRS2365 (100 μM) and paxilline (10 μM) were injected unilaterally into the preBötC via triple-barrel pipettes (4-5 μm outer diameter per barrel) controlled by a programmable stimulator

(Master-8; AMPI, Jerusalem, Israel) connected to a picospritzer (~15 psi Spritzer 4 Pressure Micro-Injector; Bioscience Tools, San Diego CA, USA). Substance P (1 μM) was repeatedly injected at 15 minutes intervals to functionally identify the preBötC in a grid-like manner until a characteristic immediate two- to four-fold increase in inspiratory frequency was obtained (Lorier et al., 2007). Sequential injections MRS 2365 were separated by a minimum of 15 min. Bicuculline (5, 20 μM), strychnine (1, 20 μM) and TTX (0.5 μM) were added directly to the circulating aCSF and at least 15 minutes were allowed for the drugs to wash in.

For calcium imaging experiments in vGLUT2^{TdTomato} mice, the membrane-permeant Ca^{2+} -sensitive dye, Fluo-4-AM (Sigma-Aldrich, Oakville, ON, Canada), was dissolved in 20% DMSO + pluronic acid, further diluted to 0.01 mM in aCSF containing no Ca^{2+}, Mg^{2+} or glucose. The preBötC of the slices was loaded via methods described below. To assess the identity of neurons that responded (with increases in Ca^{2+} fluorescence) to $P2Y_1R$ activation, perfusion solution was changed for 60 s from normal aCSF to aCSF that also contained MRS 2365 (10 μM), at which point the perfusion solution was returned to normal aCSF.

2.5 Whole-cell recording.

Patch pipettes were pulled from filamented borosilicate glass (1.2 mm OD, Harvard Apparatus, Holliston, MA, USA) with a three-stage puller (P-97; shutter Instruments). Pipette resistance was 4.5-6.0 MΩ when backfilled with an internal solution containing the (in mM): 140 K^+ gluconate, 5 NaCl, 1 $MgCl_2$, 0.1 EGTA, 10 HEPES, 1 glucose, 0.2% biocytin (pH 7.3-7.4, 295-300 mOsm). Recordings were made using a MultiClamp 700A amplifier, Digidata 1322 A/D board and AxoScope 9.2 software (Molecular Devices, Union City, CA). Signals were pass filtered at 5 kHz,

digitized at a sampling rate of 20 kHz and stored in a computer for posterior analysis. Voltage-clamp protocols were controlled with a MultiClamp Commander software (Axon Instruments) and data were acquired using pClamp (Version 9.2) software. Hypoglossal nerve activity was simultaneously recorded using and Axoscope (version 9.2) and via a Digidata 1322A interface (all Molecular Devices) as described above. Patch pipettes were positioned near the surface of the slice and introduced into the tissue in a downward and forward direction. Neurons were visualized under infrared-DIC (ir-DIC) optics on an upright microscope (Axioskop2 FS plus, Carl Zeiss, Oberkochen, Germany) and were selected based on their ventrolateral location with respect to the semicompact division of the nucleus ambiguus, the presence of rhythmic inward synaptic current inputs that were synchronized with inspiratory-related bursts recorded from the XII nerve rootlets. Neurons were approached along the electrode axis in a diagonal fashion. GigaOhm seals were established in voltage clamp mode. Once a seal was formed, the patch was ruptured with the cell held near its estimated resting potential (-60 mV). Series resistance and whole-cell capacitance was estimated with short voltage pulses (100 Hz, –10 mV, 3.0 ms). Only experiments where series resistance changes lower than 20% between control and trial conditions were considered. Input resistance was calculated from the inverse of the slope of a linear regression line between –60 to –70 mV, which is the range to examine the effects of modulators on leak conductances, fitted to the I–V curves generated by depolarizing ramps from −90 to −40mV of 1.5 s duration. Once the recordings were concluded, slices were fixed and kept at 4˚C for RNAScope assay.

2.6 Two-photon Ca^{2+} imaging recordings.

Fluo-4-AM (0.01 mM) was backfilled into a broken glass pipette (1.2 mm OD, VWR) to a tip diameter of 2 μm. The pipette was positioned near the surface of the slice and introduced into the

tissue in a downward and forward direction across the axis of the pipette, ventrolateral to NA. Fluo-4-AM was continuously injected on a single site of the preBötC for 10 minutes at 60 – 80 μm depth from the surface via a programmable stimulator (SEC-05L, nbi, Germany) connected to a picospritzer (PDES-02DX, nbi, Germany). The pressure of the dye injection was regulated based on injection and it varied between preparations. Positive pressure was slowly and progressively increased until the dye was visually seen being expelled from the pipette tip and the slice tissue was gently stretched by the pressure. At this point, pressure increase was stopped and held steady for 15 min to ensure maximal diffusion of the dye into the cells. The injection pipette remained in place during the 15 min of dye injection. The stanning area was 200 – 300 μm diameter and imaging was made at a depth of 30 – 60 μm from the surface at scanning rate of 2.5 Hz. Fluorescence excitation was performed via a MaiTai-BBTi:sapphire (10 W Mira/Verdi; Coherent, Santa Clara, CA) femtosecond pulsed laser set to excite at 810 or 895 nm. Fluorescence intensity was measured using an upright Olympus FV1000 MPE multiphoton scanning microscope (Olympus, Markham, Ontario, Canada) fitted with an 20x water immersion objective (NA = aperture 0.95).

2.7. Transcardial perfusion and paraffin sectioning

Mice aged P0-P14 were placed in a custom-made cylindrical glass chamber and anesthetized via cotton embedded with isoflurane. Next, pups were mined facing up on a Styrofoam platform and a 5 mL of freshy made phosphate buffered saline (PBS) solution containing 4% of paraformaldehyde (PFA) was directly injected into the heart using a 26G needle and a 10 mL syringe. Brains and brainstems were carefully extracted and postfixed with a 4% of paraformaldehyde solution over night at 4˚C. Then, slices were rinsed in PBS 0.01 M three times

for 15 min each at RT. The tissue was then dehydrated in a series of ethanol washes as follow: 50% for 30 min, 70% for 1 h, 80% for 1 h, 90% for 1 h, 95% for 1 h and 100 % over night. The next day, slices are transferred to 100 % xylene for 1 h and then transferred to embedding block filled with melted paraffin and keep at 56˚C for 1 h. Finally, blocks were let to cold at RT. Rostrocaudal serial sections of 8 µm thick were obtained using a microtome and immediately mounted on charged superfrost microscope glass slides (Fisher).

2.8. $P2Y_1R$ Imnunohistochemistry

To examine expression of $P2Y_1R$ on the preBötC of $GLUT2^{TdTomato}$ and $GLYT2^{EGFP}$ mice, we used a rabbit polyclonal $P2Y_1R$ antibody (Proteintech) in combination with tyramide signal amplification (TSA) Kit (Perkin Elmer). Paraffin sections were first dewaxed in Xylene three times for 5 min each and then rehydrated through a series of ethanol washes for 5 min each as follow: 100 %, 95 %, 80 %, 70 %, 50 % and double distilled H_2O (ddH_2O). To perform antigen retrieval, sections were immersed in 0.01 M sodium citrate buffer pH 6.0 and microwaved twice for 5 min each. Then, sections were treated with 1 % oxygen peroxide (H_2O_2) in 100 % methanol for 15 min to quench endogenous peroxidase activity and increase antibody penetration. Sections were washed in Tris NaCl Tween (TNT) buffer (0.1 M Tris HCl, pH 7.5, 0.15 M NaCl and 0.05 % Tween 20) 3 times for 10 min each, followed by blocking with 0.3 % Tris NaCl Blocking Reagent-Tween (TNB-T) (0.1 M Tris HCl, pH 7.5, 0.15 M NaCl, 0.5 % Blocking Reagent and 0.3 % Tween 20) for 1 h. After blocking, sections were washed in TNT buffer and then incubated in the following primary antibodies in in 0.3 % TNB-T at 4˚C overnight: rabbit anti-$P2Y_1R$ antibody at dilution of 1:3000, rat monoclonal anti-SST antibody (Abcam) at a dilution of 1:400 and to examine the expression of vGLUT2 on $vGLUT2^{TdTomato}$ mice, we used goat polyclonal anti-m-

cherry antibody (Cedarlane) to label the red fluorescent protein TdTomato at a dilution 1:500. To examine the expression of GLYT2 on GLYT^{EGFP} mice we used a chicken anti-GFP antibody (Abcam) at a dilution 1:500. Next, sections were washed in TNT buffer and then incubated with biotin conjugated donkey anti- IgG secondary antibodies: donkey anti-rat 647 at a dilution 1:200, donkey anti goat Cy3 at a dilution 1:400 and donkey anti-chicken 488 at a dilution 1:500 (all Cedarlane) for 1 h at RT. Sections were washed in TNT buffer, followed by incubation with streptavidin-HRP 1:150 in TNB buffer for 1 h. Sections were washed in TNT buffer. Next, sections were incubated with tyramide conjugated fluorescein 1:75 in amplification diluent for 10 min. Finally, slices were cover slipped with FluorSave reagent (EMD Millipore).

2.9 RNAscope assay and Lucifer Yellow Immunohistochemistry

RNAScope and immunofluorescence protocols were combined to determine the phenotype of MRS 2365 sensitive neurons. Following whole cell recordings, 700 µm thick rat slices were fixed in phosphate buffer saline (PBS) 0.01 M 4% PFA for 12 – 24 h at and kept at 4˚C. Next, slices were washed in PBS 0.01 M three times for 5 minutes each. Slices were then dehydrated in PBS 0.01 M 30% sucrose solution for 48 h at 4˚C. Brain slices were placed in an embedding mold and covered with optimal cutting temperature (OCT) compound (Tissue Tek) and freeze in a container with 100% ethanol and dry ice. Slices were stored at -80˚C until RNAScope assay.

Two days before the RNAscope assay, OCT blocks containing the 700 µm fixed slices were trimmed to a small 10 x 10 x 10 mm block using a razor blade and mounted on a removable cryostat base with the rostral side facing up. Next, the 700 µm slices were re-sectioned completely into 50 µm thick serial sections at -20˚C and transferred to a 48-wheel plate filled with PBS 0.01 M (1

section per wheel). Slices were then mounted on charged superfrost plus microscope glass slides (Fisher), let to air dry for 1 h at room temperature (RT) and stored at -80˚C for two days.

On the day of the assay, the sliced were thawed and pretreated via a modified version of the manufacturer's suggested protocol (Advanced Cell Diagnostics—ACDBio, Newark, CA) that was implemented to improve adhesion of tissue sections thicker than the recommended 15 µm to the slide. First, slices were post fixed in PFA 4% for 1 h at 4˚C. Then, slices were washed in PBS 0.01 M two times for a few seconds each and placed in an oven at 60 ˚C for 15 min. sliced were gradually dehydrated in a series of ethanol washes as follow: 50%, 70% 100% ethanol for 5 min each. Slices were then placed in an oven at 60˚C for 15 min. This was followed by a treatment with a H_2O_2 solution (provided with the kit) for 10 min at RT and then washed in ddH_2O. Slices were placed in an oven at 60˚C for 10 min. Finally, slices were incubated with a target retrieval solution (TRS) containing 50 mL of TRS and 450 mL ddH_2O at 100˚C for 10 min.

Following the pre-treatment, slices were let to air-dry for 30 min and a barrier was made around each slice with a hydrophobic pen (Fisher). Next, slices were incubated in Protease III at 40˚C for 30 min and quicky washed with ddH_2O two times for 2 seconds each. Slices were incubated in RNAScope oligonucleoutide probes for the Vesicular Glutamate Transporter (*Vglut2*, Slc17a6, ACDBio) and the vesicular GABA transporter (*Vgat*, Slc6a5, ACDBio) at 40˚C for 2 h. Slices were washed 2 times in wash buffer (ACDBio) at RM for 2 minutes each and tissue was then incubated in saline sodium citrate (SSC) 0.05 M overnight. The next day, slices were processed using the RNAScope Multiplex Fluorescent Assay kit version 2 (ACDBio) according to the manufacturer instructions, as follow. Slices were washed three times in wash buffer at RT for 2 min each, incubated with AMP-1 reagent at 40˚C for 30 min and washed with wash buffer two

times at RT for 2 min each. Next, slices were incubated in AMP-2 reagent at 40˚C for 30 min and washed with wash buffer two times at RT for 2 min each. Then, slices were incubated in AMP-3 reagent at 40˚C for 30 min and washed with wash buffer two times at RT for 2 min each.

Slices were then incubated in HRP-C1 reagent (ACDBio) at 40˚C for 15 min, washed two times at RT for 2 min each, incubated in Cy2 at a dilution 1:1000 in TSA buffer at 40˚C for 30 min and washed two times at RT for 2 min each. Next, slices were incubated in HRP-blocker reagent (ACDBio) at 40˚C for 15 min, washed two times at RT for 2 min each. Next, slices were incubated with HRP-C2 reagent (ACDBio) at 40˚C for 15 min, washed two times at RT for 2 min each, incubated in Cy5 at a dilution 1:1000 in TSA buffer at 40˚C for 30 min and washed two times at RT for 2 min each. Slices were incubated again in HRP-blocker reagent (ACDBio) at 40˚C for 15 min.

Immediately following the RNAScope protocol we performed the immunofluorescence protocol for lucifer yellow in order to visualize the whole-cell recorded neurons. Briefly, slides were rinsed in PBS 0.01 M and incubated in 10% normal donkey serum in 0.3% triton at RT for 60 min to prevent nonspecific binding. Next, tissue was incubated with a polyclonal rabbit anti-lucifer yellow IgG (Invitrogen) in a dilution 1:800 for 24h at RT. Slides were then rinsed in PBS 0.01 M and incubated for 2 h in Cy3 donkey anti-rabbit IgG antibody (1:200; Jackson ImmunoResearch). Slides were rinsed once more in PBS 0.01M, covered with Fluorosave mounting medium (Millipore Sigma) and coverslipped.

2.10 Confocal Imaging and cell counting

Low (10) and high power (25) analysis and representative images were acquired using a Leica TCS SP8 Laser Scanning Confocal Microscope. To quantify the number of $P2Y_1R$-, vGLUT2-, SST- and GLYT2-expressing neurons in the preBötC we used high power (25X) images and created templates that delimited a region of interest (ROI) ventrolateral to NA and followed the SST expression pattern (preBötC marker) for each slice. On its dorsal part (which is immediately ventral to NA), this ROIs extended 100 µm wide and extended 300 µm ventrolateral from NA towards the surface of the slice. On its ventral part, ROIs extended 200 µm wide. Only cells which somas were completely inside this ROI were included in the analysis. Cells were selected based its uniform somatic labeling (i.e, cells somas completely and evenly labeled) except for the $P2Y_1R$ labelling, which in many preparations showed incomplete labeling of somas. These cells were included in the analysis only if the portion that was labeled perfectly overlapped with shape of the neurons.

2.11 Statistical analysis

XII nerve activity from rhythmic slices was analysed offline using Clampfit, version 9.2 and Excel software. The specific effects of a drug on the frequency response evoked by local injection of MRS2365 into the preBötC, were analyzed by comparing the relative increase in peak frequency evoked by MRS2365 in control conditions, in the presence of specific blocking agents (antagonists of specific proteins in the GPCR signaling pathway) and after periods allowed for washout. Baseline frequency was calculated as the average frequency measured over the 2 min immediately prior to drug application. Peak frequency was calculated as the peak value in the first min of drug application obtained from a moving average calculated based on three consecutive XII bursts.

Prism version 8 (GraphPad Software Inc., La Jolla, CA, USA) was used for statistical analysis and figure creation. Paired, unpaired student t-tests or ANOVA, with either a Tukey or Bonferroni post-hoc multiple comparison test, were used as appropriate. Group data are presented as whiskers box plots detailing the spread of data points, the lowest point, 1st quartile, median, 3rd quartile and highest point are corresponding to open circles, the lower whisker, bottom, middle, and top of box, and top whisker respectively. The mean for each group is denoted by "+"

3. Results

3.1 Mechanisms of $P2Y_1R$ signaling in the preBötC

3.1.1 Contribution of the Gq signaling system to the excitatory actions of $P2Y_1$ receptor on preBötC inspiratory neurons.

Purinergic signalling in the ventrolateral medulla modulates inspiratory rhythm during oxygen deprivation by modulating the activity of preBötC inspiratory neurons. ATP can act on 7 subtypes of ionotropic P2XRs and 8 subtypes of metabotropic P2YRs. However, during hypoxia, astrocytes release ATP, which activates $P2Y_1R$, causing excitation of inspiratory neurons, which in turns increases ventilation *in vivo* (Rajani et al., 2018). Under in vitro conditions in the rhythmic slice preparation, $P2Y_1R$ are responsible for the entire ATP-evoked increase in network frequency (Lorier et al., 2007); i.e., $P2Y_1R$ antagonists completely block the frequency increase evoked by injection of ATP into the preBötC. $P2Y_1R$ are believed to signal almost exclusively through the $G_{q/11}$ second messenger pathway. However, $G_{q/11}$-signalling pathway blockers targeting PLC/InsP3 and the endoplasmic reticulum Ca^{2+}-release signaling pathway either failed or partially attenuated (by 55%) the $P2Y_1R$-induced increase in frequency (Zhang et al., 2016a, 2016b). The incomplete block could reflect that $P2Y_1Rs$ signal through other pathways or that the $G_{q/11}$ inhibitors did not gain complete access to their intracellular sites of action throughout the preBötC. Access of these drugs can be a significant limitation in thick (700 μm) slice preparations like those used here where drugs need to diffuse deep into tissue and cross cell membranes. To distinguish between these two possibilities, Dr. Zhang performed whole-cell recordings from preBötC inspiratory neurons using pipettes that were filled with the $G_{q/11}$ blocking agents. He then compared ATP-evoked currents taken immediately upon rupturing into whole-cell configuration with those evoked 15 minutes after the blocker had time to diffuse into the neuron and take action. This

eliminated concerns that the blocker was not gaining access to the intracellular environment. Assuming that the ATP current, like the ATP frequency effect on the network, was entirely mediated by $P2Y_1Rs$, the expectation was that the $G_{q/11}$ blockers would completely block the ATP current. This was not the case. The $G_{q/11}$ blockers reduced the ATP currents by 20-30%. Further experiments confirmed that while the ATP frequency effect is entirely $P2Y_1R$-mediated, the ATP currents are not. Up to 70% of the ATP current is not blocked by $P2Y_1R$ antagonists but it is blocked by other general P2R antagonists and it does not participate in the ATP-mediated frequency increase. Thus, the goal of the first study was to assess the contribution of the $G_{q/11}$ signaling pathway specifically to the $P2Y_1R$-mediated excitation of preBötC inspiratory neurons. We tested the hypothesis that the $P2Y_1R$ current evoked by local application of the $P2Y_1R$ selective agonist, MRS 2365 (Fig. 7), will be fully blocked by inhibitors of PLC and PKC.

We compared the $P2Y_1R$-induced inward currents evoked by local application of MRS 2365 (30 s, 100 μM) within the first two minutes of obtaining whole-cell configuration (0 min) with the current evoked after 15 minutes (15 min) of intracellular dialysis of the PLC inhibitor, U73122 (2 μM), or the PKC inhibitor CHE (10 μM) (Fig. 7B, D). To control for any time-dependent decrease in the MRS 2365-induced currents, data were compared to a time-matched control group (Time control. Fig 7A, D). The MRS 2365 currents are reported as the percentage of decrease of the peak amplitude of the current evoked by the second, relative to the first MRS 2365 application. In the time-control group, which had an average RN of 281.4 ± 40.3 MOhms and RMP of -43.7 ± 1.4 mV, MRS 2365-induced inward currents decreased by 4.4 ± 3.6 % (n = 6) between the first and second application (Fig. 7A) from -19.4 ± 1.3 pA to 18.5 ± 1.5 pA. The MRS 2365 currents were not associated with any significant change in RN in this control group or any subsequent set of

experiments (Pre-MRS 2365: 257.0 ± 53.1 MOhms, MRS 2365: 232.0 ± 38.4 MOhms, p = 0.43, paired t-test). With U73122 in the pipette, the MRS 2365-evoked currents were significantly reduced by 49.8 ± 7.0% between the first and second application from -24.0 ± 4.3 pA to 12.8 ± 3.3 pA (n = 6), which was significantly greater than the decrease observed in the time controls (p = 0.0002, One-way ANOVA with Tukey's post hoc test) (Fig. 7A, B, D). The neurons tested with U73122 had an average of 281.9 ± 27.2 MOhms.

We next tested the contribution PKC to the MRS 2365-induced inward currents in a group of preBötC inspiratory neurons with an average RN of 279.1 ± 22.4 MOhms. In the presence of CHE (10 μM), the MRS 2365-evoked currents were reduced by 54.8 ± 3.2% (n = 5) between the first and second application from -30.5 ± 7.4 pA to -13.3 ± 2.7 pA, which was significantly greater compared with time-controls (p = 0.0001, One-way ANOVA with Tukey's post hoc test) (Fig. 7A, C, D). These results suggest that $P2Y_1$-induced inward currents are produced in part via activation of PLC and PKC, which typically couple through the $G_{q/11}$ protein.

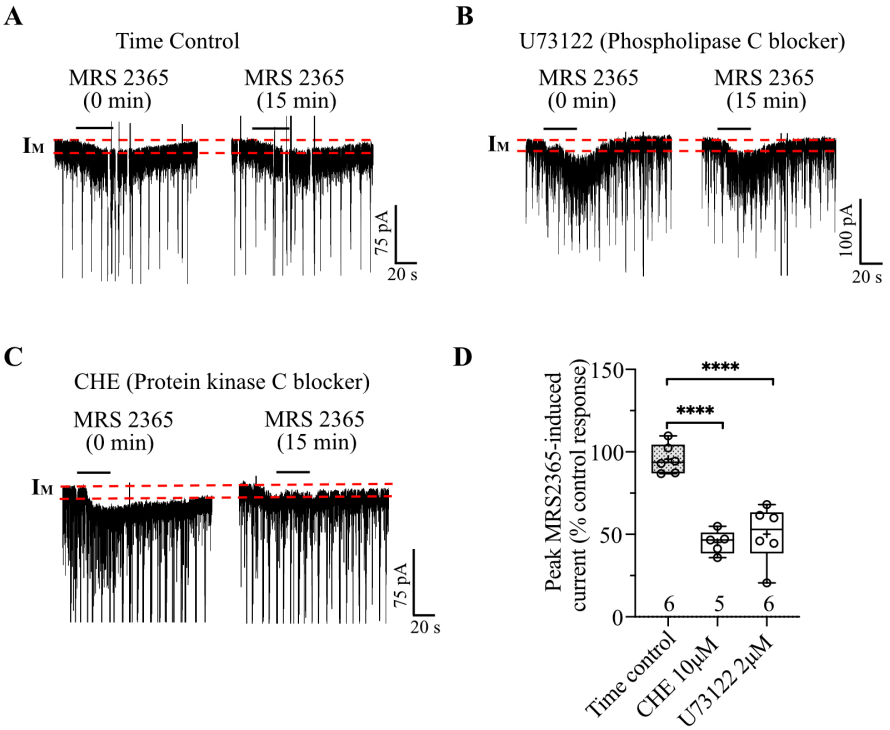

Figure 7: Attenuation of the MRS 2365-induced inward current on preBötC inspiratory neurons by intracellular dialysis of a PKC and PLC blocker. A-C. Representative traces showing a time-matched control (A), the effect of CHE (B) and U73122 (C) on MRS2365-induced inward currents at 0 and after 15 minutes of dialysis. D. Box and whisker plot of the grouped data showing the MRS 2365-induced response after 15 min intracellular dialysis of U73122 and CHE relative to the control response. Data represent the Mean ± SEM. ****$p<0.001$.

3.1.2 Contribution of BKCa channels to the excitatory actions of $P2Y_1$ receptor on the preBötC

Previous studies (Zhang et al., 2016a; 2016b) together with the data described above (Fig. 7) suggest that the $G_{q/11}$ signaling pathway contributes to the $P2Y_1R$-mediated excitation of inspiratory preBötC neurons. $G_{q/11}$ proteins activate the PLC/InsP3 endoplasmic reticulum Ca^{2+}-release signaling pathway. Depleting intracellular calcium stores with a sarco/endoplasmic reticulum Ca^{2+}-ATPase (SERCA) blocker attenuates the $P2Y_1R$-induced increase of intracellular calcium and the $P2Y_1R$-evoked increase in respiratory frequency (Rajani et al., 2018), indicating that the $P2Y_1R$-mediated frequency increase is dependent on Ca^{2+} release from intracellular stores. BK_{Ca} channels are one type of Ca^{2+}-activated K^+ channel and their activation is regulated by both, membrane voltage and intracellular calcium (Yang et al., 2015). Thus, since the $P2Y_1R$-induced increase in inspiratory frequency is attenuated by the SERCA blockers thapsigargin and CPA injected into the preBötC *in vitro*, BK_{Ca} channels are a strong candidate as a mediator of the effects of $P2Y_1R$ in the respiratory network. The role of BK_{Ca} channels in modulating baseline activity of the inspiratory network is not clear, with some studies showing that their inhibition has either no effect, excitatory or inhibitory effects on rhythm (Rajani et al., 2016). However, its role in mediating the actions of $P2Y_1Rs$ signaling has not been examined. Thus, we evaluated the hypothesis that BK_{Ca} channel activation contributes to the $P2Y_1$-induced frequency increase.

We locally applied the BK_{Ca} channel blocker, paxilline (1 μM; injection pulse: 5 s on and 5 s off; injection duration: 30 min) to the preBötC. Paxilline had no effect on the MRS 2365-evoked frequency increase when all the data were pooled (Fig. 8A, n = 10). However, paxilline effects on the MRS 2365 response were highly variable. In 5 of the 10 preparations, paxilline reduced the MRS 2365-induced frequency increase by up to 75% (Fig. 8B for representative traces). In the

remaining 5 preparations, paxilline had no effect. This variability may reflect poor access of paxilline to the network. The easiest approach to address this possibility would be to increase the concentration of paxilline, but the limitation is that at higher concentrations paxilline can also block SERCA with an IC_{50} of 5 μM, which will inhibit the MRS 2365 frequency increase. To assess whether we could increase paxilline concentration without affecting SERCA, we performed whole-cell recording experiments in which paxilline (1 μM or 4 μM) was added to the intracellular solution. The effect of paxilline on the MRS 2365-induced inward currents was assessed by comparing the currents evoked by MRS 2365 2 min after rupture with those evoked 15 min later. When neurons are recorded under voltage-clamp conditions and held a potential of -60 mV, blocking BK_{Ca} should not affect the MRS 2365 current because both depolarization and an increase in intracellular Ca^{2+} are required for BK_{Ca} activation. Any effect of paxilline on the MRS 2365 current would indicate that paxilline inhibited SERCA. Intracellular dialysis of paxilline (1 μM, 15 min) in a group of neurons with had an average RN of 260 ± 64 MΩ (n = 8) had no effect on the MRS 2365 currents (Figs. 8C, D, E). With 1 μM paxilline in the pipette, the peak currents evoked by the second application of MRS 2365 were -26.4 ± 3.7 pA compared to -25.4 ± 3.9 pA in the first (n = 8), an insignificant increase of 7.4 ± 7.3 % (p = 0.62, One-way ANOVA with Tukey's post hoc test) compared to the time-controls (Fig. 8A, E). This was predicted because at this concentration paxilline does not affect SERCA (Bilmen *et al.*, 2002). In contrast, compared to time controls, intracellular dialysis of paxilline at 4 μM in another group of preBötC inspiratory neurons (RN 290 ± 65 MΩ; RMP ± -51.6 mV, n = 7) significantly reduced the amplitude of the MRS 2365-induced inward currents from -26.1 ± 3.7 pA to -13.0 ± 1.1 pA, a reduction of 46.6 ± 5.8 % (n = 7, p = 0.0004, One-way ANOVA with Tukey's post hoc test) (Figs. 8D, E). The IC_{50} of paxilline for SERCA inhibition is in the range of 5 – 50 μM (Bilmen et al., 2002). Our

observation that 4 μM paxilline reduced the MRS 2365 currents strongly suggests that at this concentration paxilline affects SERCA in the recorded preBötC neurons. Due to this potential side effect, we were unable to further increase the concentration of paxilline to conclusively test the role of BK_{Ca} in the MRS 2365-evoked increase in preBötC frequency.

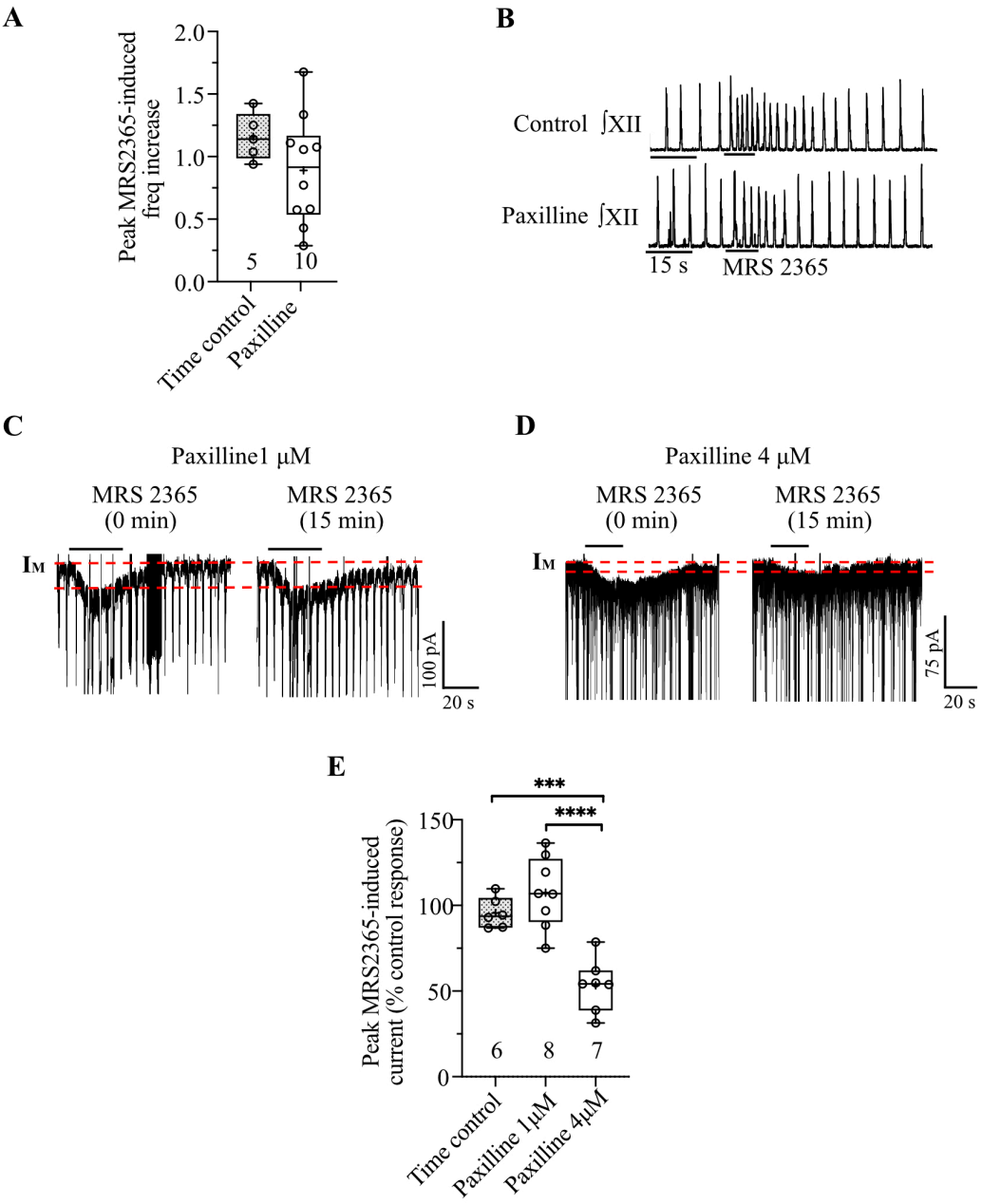
A
Peak MRS2365-induced freq increase
2.0
1.5
1.0
0.5
0.0
5
10
Time control
Paxilline
B
Control ∫XII
Paxilline ∫XII
15 s
MRS 2365
C
Paxilline1 µM
MRS 2365 (0 min)
MRS 2365 (15 min)
IM
100 pA
20 s
D
Paxilline 4 µM
MRS 2365 (0 min)
MRS 2365 (15 min)
IM
75 pA
20 s
E
***
****
Peak MRS2365-induced current (% control response)
150
100
50
0
6
8
7
Time control
Paxilline 1µM
Paxilline 4µM

Figure 8: Contribution of BK_{Ca} channels to the $P2Y_1R$-mediated excitation of the preBötC inspiratory network. A. Effect of paxilline on the MRS 2365-induced increase in inspiratory frequency. Paired student t-test B. Representative traces showing that paxilline attenuates the MRS 2365-induced increase in frequency in some preparations. C, D. Representative traces and group data (E) showing the attenuation of the MRS 2365-evoked inward currents by intracellular dialysis of 4 μM but not 1 μM paxilline. RM one-way ANOVA, Tukey's multiple comparisons test. Data represent the Mean ± SEM. ***p<0.001, ****p<0.001.

3.1.3 $P2Y_1R$ modulation of spontaneous and miniature post-synaptic currents on inspiratory preBötC neurons.

In addition to the slow inward currents produced by MRS 2365, we also recorded in 11 out of 25 inspiratory preBötC neurons, an MRS 2365-evoked increase in spontaneous post-synaptic currents (sPSCs) (Fig. 9), suggesting that $P2Y_1Rs$ potentiate synaptic drive to preBötC inspiratory neurons. We were not able to find any properties that distinguished neurons that responded with an increase in sPSCs. Those that showed the increase in sPSCs had an average RN of 268 ± 42 MΩ and received inspiratory synaptic inputs that averaged -185 ± 27 pA in peak amplitude. The other group had RN that averaged 235 ± 43 MΩ and received inspiratory synaptic inputs that averaged -155 ± 21 pA in peak amplitude.

To quantify the effects of MRS 2365 on synaptic activity, we measured sPSCs for 30 – 60 s before MRS 2365 application and during the 30 s of MRS 2365 application. In average we counted 141 events in control and 426 events during MRS 2365 application per neuron that occurred in between inspiratory bursts. sPSCs were selected using the suggested detection parameters included in the MiniAnalysis software (Synaptosoft. Inc). For every neuron (n=11), we calculated the average sPSC amplitude (Fig. 9C) and inter event interval (IEI) (Fig. 9D) before and during MRS 2365 application. Local application of MRS 2365 produced a small but significant increase in sPSC amplitude (pre-MRS 2365: 33 ± 2 pA, MRS 2365: 37 ± 3 pA, p=0.011, paired t-test. Fig. 2B, C). and markedly decreased the inter event interval (IEI) of sPSCs from 459 ± 58 ms to 103 ± 10 ms (Fig. 9B, D, p=0.0001, paired t-test).

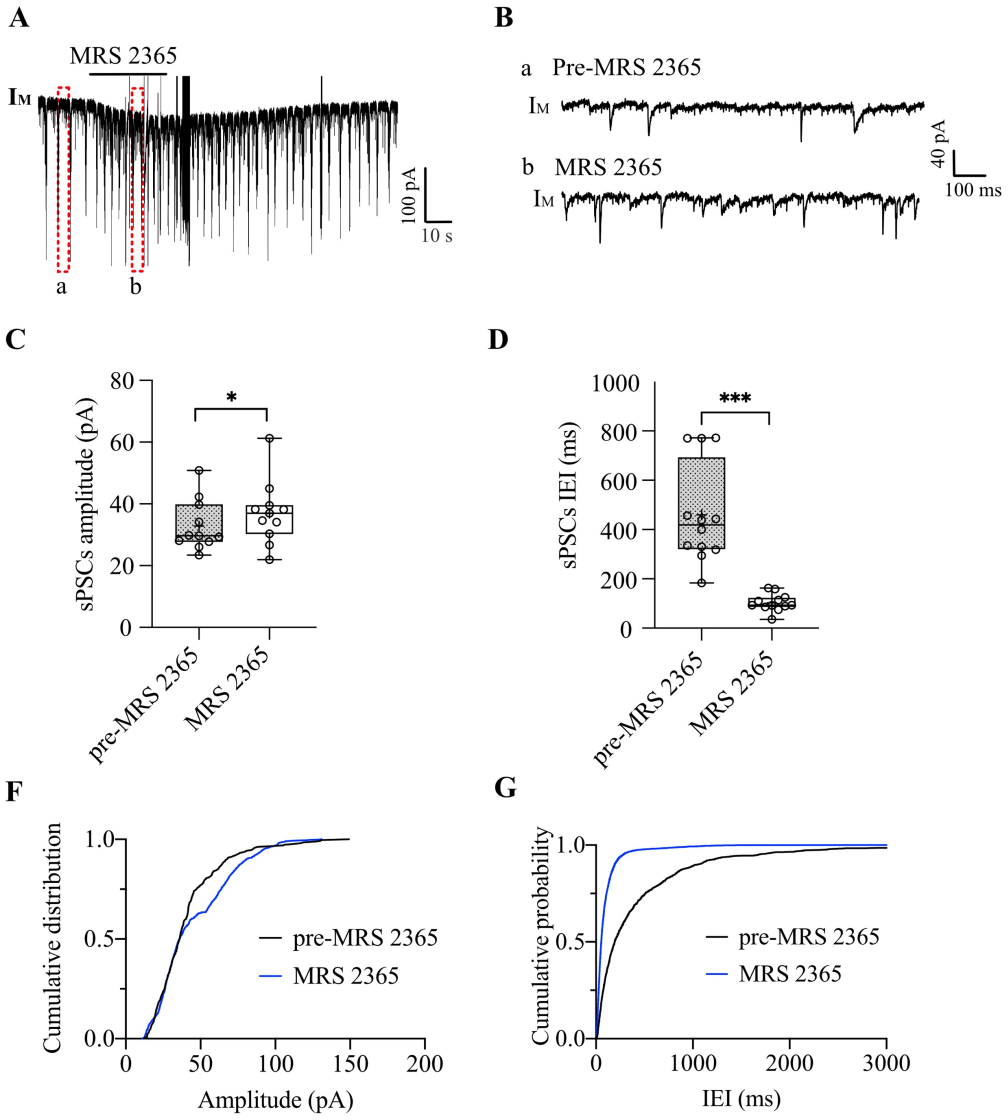

Figure 9: MRS 2365 increases spontaneous post synaptic currents (sPSCs) on inspiratory preBötC neurons. A. Representative trace of an inspiratory preBötC neuron, held at -60 mV showing an MRS 2365-induced inward current and an increase in sPSCs. B. Larger view of boxes in A showing sPSCs before (a) and during (b) MRS 2365 local application. C, D. Group data showing an increase in sPSCs amplitude amplitude (C) and a decrease in inter event interval (IEI) (D). E, F. Cumulative probability plots showing the frequency distribution of sPSC amplitudes (F) and IEI (G). Paired student t-test. Data represent the Mean ± SEM. *p<0.05, ***p<0.001.

To determine whether $P2Y_1Rs$ act pre-synaptically to increase the frequency of spontaneous vesicle release, we bath applied TTX (500 nM) to two of those neurons and evaluated the effect of MRS 2365 on miniature post-synaptic currents (mPSCs) (Fig. 10). mPSCs were selected using the automatic suggested detection parameters included in the MiniAnalysis program (Synaptosoft Inc.). For every neuron we calculated amplitude and IEI of events occurring 30 – 60 s before and after local MRS 2365 application. In those neurons, MRS 2365 had no effect on mPSCs amplitude (Fig. 10C, E) but decreased IEI from 637 ±132 to 132 ± 34 ms (Fig 10C, D). We observed a reduction in the variability in the mPSCs amplitude from 60.4% pre-MRS 2365 to 14.7% during MRS 2365 in those two neurons tested. This suggest that $P2Y_1Rs$ can modulate neurotransmitter release onto preBötC inspiratory neurons.

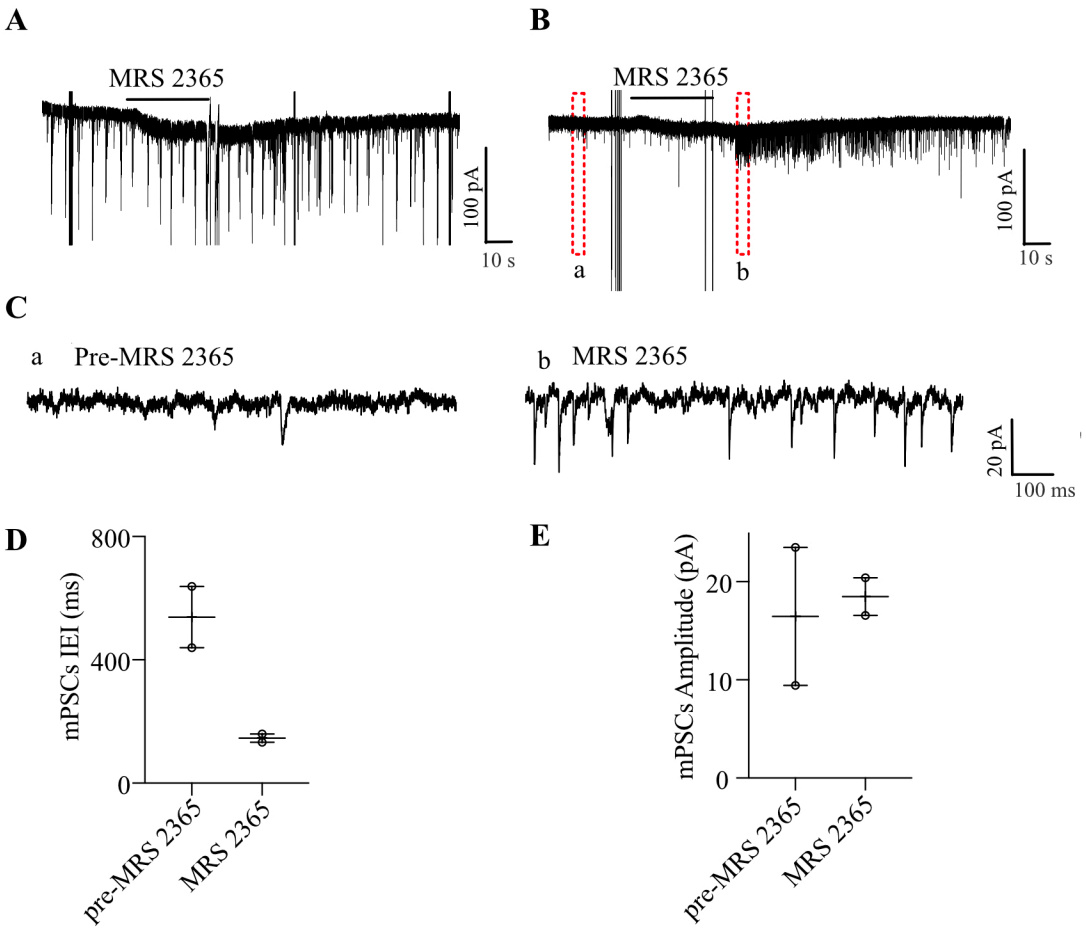

Figure 10: MRS 2365 increases miniature post synaptic currents (mPSCs) on inspiratory preBötC neurons. A. Representative trace of an inspiratory preBötC neuron, held at -60 mV showing an MRS 2365-induced inward current and an increase in PSCs. B. Representative trace of the neuron in A showing an increase in mPSCs in the presence of TTX. C. Larger view of boxes in B showing mPSCs before (a) and during (b) MRS 2365 local application. D, E. Group data showing a decrease in mPSC IEI (D) and no effect on mPSC amplitude (E). Paired student t-test. Data represent the Mean ± SEM. *p<0.05, ***p<0.001.

3.2 Neuronal mediators of the $P2Y_1R$ evoked frequency increase.

Elegant optogenetic experiments that enabled selective expression of ChR2 and photostimulation of excitatory or inhibitory neurons (Baertsch et al., 2018) in the preBötC have clearly demonstrated that excitation of either neuron type can increase inspiratory frequency. This raises the important question of whether the increase in frequency evoked by ATP in the preBötC is produced via $P2Y_1R$ activation of excitatory or inhibitory inspiratory preBötC neurons?

3.2.1 Immunofluorescence

We began by asking if $P2Y_1Rs$ in the preBötC are located on excitatory or inhibitory neurons. We used mice to address this question because rats and mice respond similarly to $P2Y_1R$ activation in the preBötC (Zwicker et al., 2011) and transgenic mouse lines facilitate identification of excitatory and inhibitory neuron populations. We examined the pattern of $P2Y_1R$ immunolabeling in two transgenic reporter mouse lines that express either TdTomato in excitatory (vGLUT2-expressing) neurons or EYFP in glycinergic (GLYT2-expressing) neurons. First, we identify the preBötC area based on the SST labeling which is a marker for preBötC (Fig. 11F-J) and we studied the expression pattern of $P2Y_1Rs$ across the rostrocaudal axis of the VRC of neonatal mice (Fig 11A-E) in relation to SST expression (Fig. 11K-O). $P2Y_1R$ immunolabeling was sparse in the brainstem and VRC (Fig. 11A). However, when moving in the rostral to caudal direction, a relatively dense cluster of $P2Y_1R$ labeled cells appeared in the VRC at the level that SST labeling emerged, i.e., at the rostral margin of the preBötC (Fig. 11B). Anatomical landmarks confirmed the location as the rostral preBötC. Similarly, SST and $P2Y_1R$ immunolabeling was high throughout the preBötC (Fig 11B- D, G-I, L-N) and then diminished greatly at the caudal margin of the preBötC (Fig. 11E, J, O).

Then, to ensure that the labeling of $P2Y_1R$ was specific we tested the $P2Y_1R$ antibody specificity on brainstem tissue from neonatal mice and cerebellar tissue from $P2Y_1R$ KO mice compared to wild type. Fig. 11P-R show lack of $P2Y_1R$ labelling on the preBötC area of a P0 $P2Y_1R$ KO mouse (Fig. P, R) compared to a P3 wild type control mouse (Fig 11T, V). In the wild type and $P2Y_1R$ KO mouse, preBötC was identified based on SST labeling (Fig. 11Q, U). Others have reported expression of $P2Y_1R$ in the cerebellum (Yoshioka et al., 2002; Amadio et al., 2007). Thus, we also used tissue from $P2Y_1R$ KO adult mice to control for antibody specificity (Fig 11S, W). Images show lack of $P2Y_1R$ on cerebellar tissue from KO mice (Fig. 11S) compared to controls (Fig. 11W).

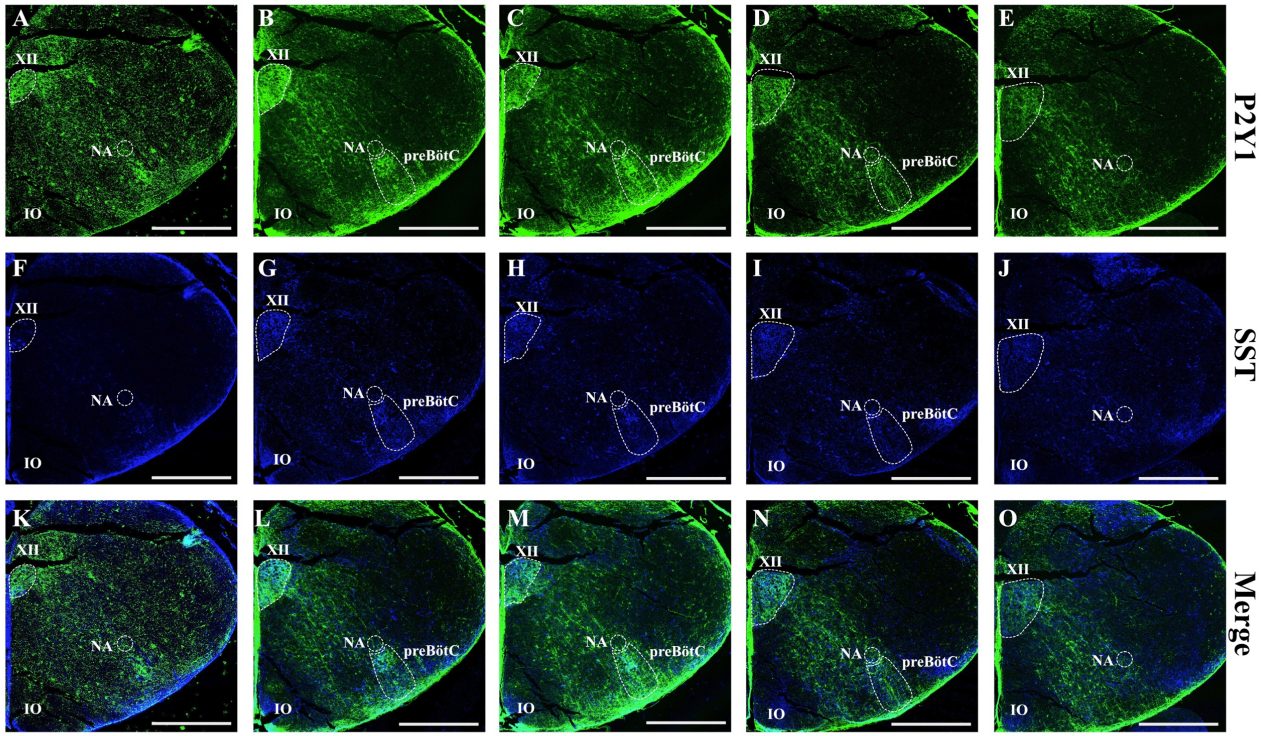
A
B
C
D
E
F
G
H
I
J
K
L
M
N
O
XII
NA
preBötC
IO
P2Y1
SST
Merge

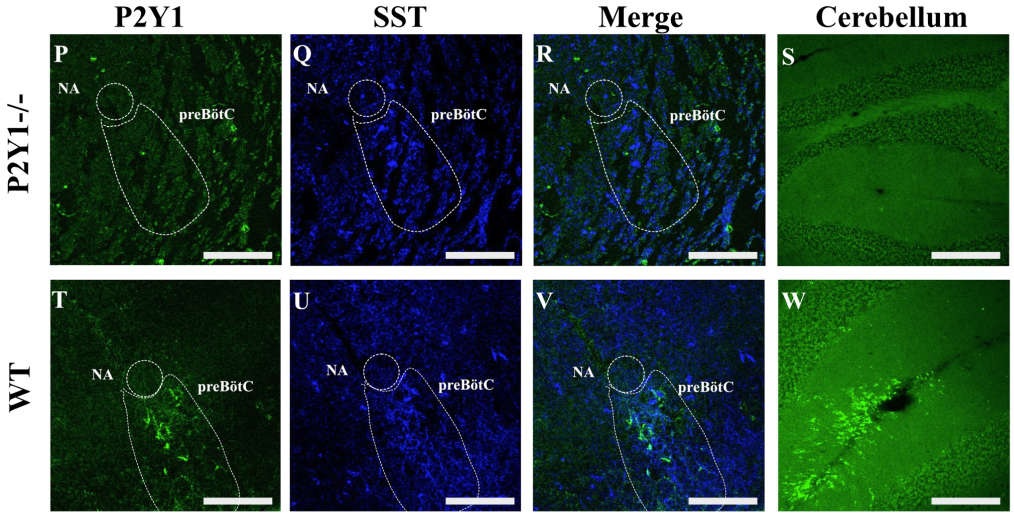
P2Y1
SST
Merge
Cerebellum
P2Y1-/-
WT
P
Q
R
S
T
U
V
W
NA
preBötC

Figure 11: $P2Y_1R$ are expressed differentially across the ventrolateral medulla in the preBötC region. A-O: Low power (10X) confocal images of a series of 8 µm thick medullary slices 100 µm apart illustrating the pattern of immunolabeling of $P2Y_1R$ (A-E, green), SST (F-J, blue) and the merge (K-O) across the rostrocaudal axis of the ventrolateral medulla of a wild type control P0 mouse, highlighting the preBötC, XII, IO and NA. Scale bars represent 500 µm. P-S: Low power (10X) confocal images illustrating pattern of immunolabeling of $P2Y_1R$ (green), SST (blue), and merge on the VRC of P5 $P2Y1R^{-/-}$ (P-R) and P3 wildtype (T-V) mice. S, W: Low power (10X) confocal images illustrating the pattern of immunolabeling of $P2Y_1R$ in the cerebellum from $P2Y_1^{-/-}$ (S) and wild type (W) adult mice. Scale bars represent 200 µm.

Next, we tested the expression of $P2Y_1R$ on $vGLUT2^{TdTomato}$ and $GLYT2^{EGFP}$ mice. Brainstem sections taken from the rostral VRG to the caudal margin of the facial nucleus were processed to reveal immunolabelling for somatostatin (SST, blue), $P2Y_1R$ (green) immunolabeling (Fig. 12 A-H). To better visualize vGLUT2 neurons, which express the red fluorescent protein TdTomato, we immunolabeled with the anti-red fluorescent protein antibody anti-mCherry. Examination of sections from 6 neonatal vGLUT2 mice aged P0-P6 revealed a high density of vGLUT2-expressing neurons that intermingle and was co-expressed with the extent of SST labeling. From a total of 57 SST-expressing neurons, 46 were glutamatergic (9 ± 0.6 neurons/mouse), which correspond to 84 %. (Fig 12A-H, Q). There was also a high concentration of vGLUT2 neurons in the preBötC (Fig 12A-H). We found that from a total of 566 vGLUT2 neurons counted in the preBötC region of 7 mice (94 ± 15 neurons/mouse), only 53 neurons expressed $P2Y_1R$ (8 ± 2 neurons/mouse), which corresponds to 10.3 %. From a total of 53 $P2Y_1R$-expressing cells counted (8 ± 2 neurons/mouse), 50 expressed vGLUT2 (9 ± 2 neurons/mouse), which correspond to 95% (Fig. E-H, white arrow heads show $P2Y_1$-expressing neurons that are vGLUT2 positive and white show $P2Y_1R$-expressing neurons that do not co-express vGLUT2). We also found that none of the 53 $P2Y_1R$-expressing cells co-expressed SST+(Fig. 12Q). We found a total of three $P2Y_1R$-expressing cells (0.5 ± 0.3 cells/mouse), which correspond to 5%, that did not express vGLUT2 (Fig. E-H). However, we cannot say, based on our labeling, if those $P2Y_1R$-labelled cells are GLYcinergic, GABAergic or cholinergic. In fact, the lack of neuronal markers makes it impossible to assess if those cells are neurons or glial cells.

To examine expression of $P2Y_1Rs$ on inhibitory neurons, we evaluated the $P2Y_1R$ labeling on glycinergic GLYT2 neurons because, while GABAergic and glycinergic neurons are both

inhibitory, glycinergic inhibition is dominant in the interactions between respiratory neurons (Richter et al., 1975; Richter, 1982), specifically, the termination of inspiratory activity is particularly influenced by glycinergic inputs that arrive during late inspiration and early expiration. Schmid et al (1996) observed that while the iontophoretic application of the $GABA_A$ antagonist in the VRG of anesthetized cats increased discharge frequency throughout inspiration, the iontophoretic administration the GLYR antagonist, strychnine (STRYC), increased bulbar inspiratory neurons discharge at the end of inspiration. (Schmid et al., 1996). More recently, Morgado-Valle et al, using rhythmically active medullary slices from mice that express the enhanced green fluorescent protein (EGFP) under the GLYT2 promoter combined with whole-cell recordings, found a subpopulation of glycinergic preBötC inspiratory neurons with pacemaker properties (Morgado-Valle et al., 2010).

Brainstem sections of $GLYT2^{EGFP}$ mice (generously supplied by Dr. Kaiwen Kam, Dept. of Cell Biology and Anatomy, Chicago Medical School, Rosalind Franklin University) were taken from the rostral VRG to the caudal margin of the facial nucleus and processed to reveal immunolabelling for somatostatin (SST, blue), a marker of the preBötC, $P2Y_1R$ (red) and green fluorescent protein (GFP) which labels $GLYT2^{EGFP}$ neurons. GLYT2-expressing neurons appear intermingled with SST+ neurons (Fig. 12 I-P). However, GLYT2 labeling did not overlap with $P2Y_1$ cells (Fig M-P). Despite being expressed throughout the preBötC region (Fig. 12J, N), GLYT2 neurons were strikingly absent in areas where $P2Y_1$ immunolabeling was detected (Fig 12P). We found that from a total of 207 GLYT2 neurons counted from 4, P0-P3 mice (52 ± 9 neurons/mouse), none co-expressed $P2Y_1R$. Also, from a total of 25 $P2Y_1R$-expressing cells counted (6 ± 1 neurons/mouse), none co-expressed GLYT2 (Fig 12I-P, arrow heads show $P2Y_1$-espressing cells that do not express GLYT2).

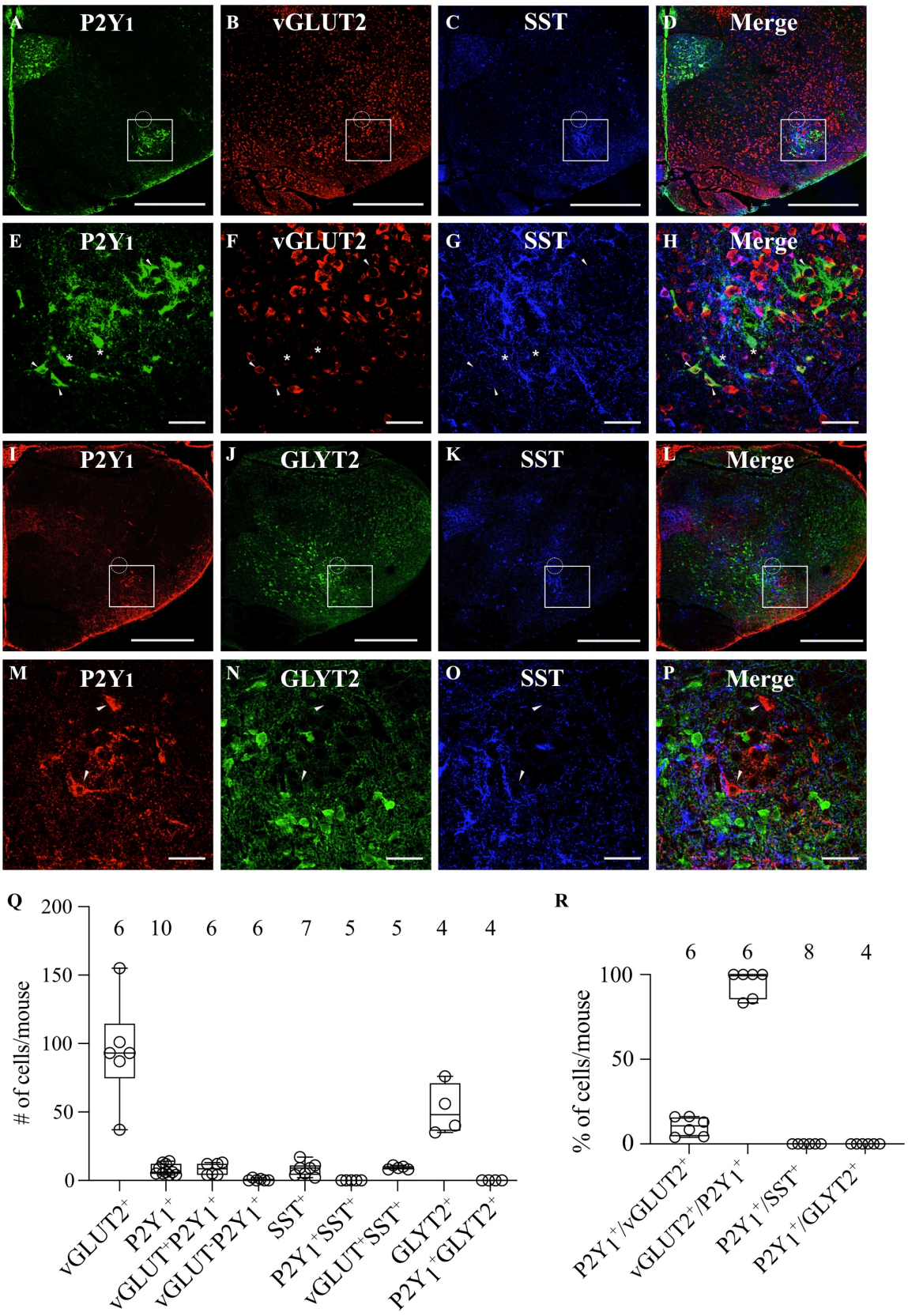
A P2Y1
B vGLUT2
C SST
D Merge
E P2Y1
F vGLUT2
G SST
H Merge
I P2Y1
J GLYT2
K SST
L Merge
M P2Y1
N GLYT2
O SST
P Merge
Q
# of cells/mouse
200
150
100
50
0
6 10 6 6 7 5 5 4 4
vGLUT2+
P2Y1+
vGLUT+P2Y1+
vGLUT-P2Y1+
SST+
P2Y1+SST+
vGLUT+SST+
GLYT2+
P2Y1+GLYT2+
R
% of cells/mouse
100
50
0
6 6 8 4
P2Y1+/vGLUT2+
vGLUT2+/P2Y1+
P2Y1+/SST+
P2Y1+/GLYT2+

Figure 12: Excitatory, glutamatergic, but not inhibitory glycinergic preBötC neurons express P2Y$_1$R. A-D. Low power (10X) confocal images illustrating the expression of P2Y$_1$R (A, green), vGLUT2 (B, red) and SST (C, blue), and thee merge (D) on the preBötC of a P5 vGLUT2 mouse. Squares on A-D correspond to E-H. Scale bars represent 500 μm. E-H: High power (25X) confocal images illustrating the immunolabeling of P2Y$_1$R (E), vGLUT2 (F), SST (G) and the merge (H) from the preBötC area highlighted in A-D. White arrow heads indicate P2Y$_1$R-expressing neurons that co-express vGLUT2. White asterisks are P2Y$_1$R-expressing neurons that do not co-express vGLUT2. Scale bars represent 25 μm. I-L. Low power (10X) confocal images illustrating the expression of P2Y$_1$R (I, red), GLYT2 (J, green), SST (K, blue), and the merge on the preBötC of a P0 GLYT2 mouse. Squares on I-J correspond to M-P. Scale bars represent 500 μm. M-P: High power (25X) confocal images illustrating the immunolabeling of P2Y$_1$R (M, red), GLYT2 (N, green), SST (O, blue) and the merge (H) from the preBötC area highlighted in I-L. White arrow heads indicate P2Y$_1$R-expressing neurons that do not co-express GLYT2. Scale bars represent 25 μm. Q. Group data showing the average number of vGLUT2+, P2Y$_1$R+, vGLUT2+P2Y$_1$R+, vGLUT2-, P2Y$_1$R+, SST+, P2Y$_1$R+SST+, GLYT2+, P2Y$_1$R+GLYT2+ neurons per mouse. Data represent Mean ± SEM. R. Group data showing the percentage of vGLUT2 neurons that co-express P2Y$_1$R, percentage of P2Y$_1$R-expressing cells that co-express vGLUT2, percentage of SST-expressing neurons that also express P2Y$_1$R and the percentage of GLYT2 neurons cells that also express P2Y$_1$R. Data represent Mean ± SEM.

3.2.2 Whole-cell electrophysiology and 2-photon imaging.

To obtain a direct measure of whether vGLUT2+ inspiratory neurons are excited by $P2Y_1R$ activation, we prepared rhythmic slices from neonatal $vGLUT2^{TdTomato}$ mice and targeted vGLUT2+ inspiratory preBötC neurons to test their sensitivity to MRS 2365 using whole-cell recording. Local application of MRS 2365 (10s, 100 μM) induced a small, -12.6 ± 0.6 pA current in 7 of 21 vGLUT2 inspiratory neurons (Fig. 13A-D). These 7 neurons had an average RN of 354 ± 81 MΩ, RMP of -49.8 ± 3.8 mV and inspiratory synaptic currents with an average peak of 131 ± 38 pA and did not differ from the 14 vGLUT2+ inspiratory neurons that did not respond to MRS 2365 (RN 312 ± 50 MΩ p = 0.64, Unpaired t-test; RMP -46.9 ± 2.4 mV p=0.53, Unpaired t-test; peak inspiratory synaptic current 143 ± 15 pA, p=0.63, Unpaired t-test). We attempted a similar approach to test whether GABAergic preBötC inspiratory neurons are also sensitive to $P2Y_1R$ activation by preparing rhythmic slices from a $GAD67^{Venus}$ reporter mice. From 4 slices, we found zero GAD67+ inspiratory neurons from a total of 28 neurons recorded.

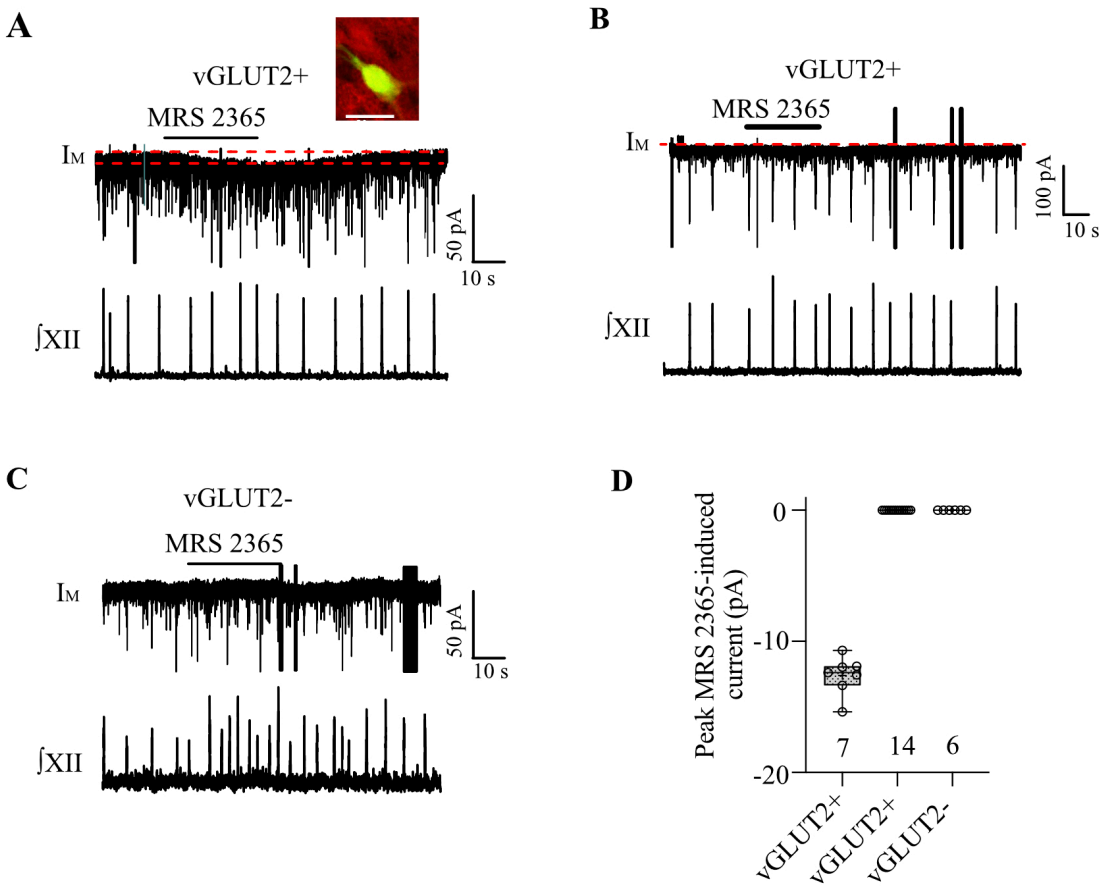

Figure 13: P2Y$_1$R activation excites vGLUT2+ inspiratory preBötC neurons. A. Representative trace of a vGLUT2+ inspiratory neuron held at -75 mV showing an MRS 2365-induced inward current. Insert in A shows the recorded vGLUT2+ neuron (red) filled with biocytin (green). B. Representative trace a different vGLUT2+ inspiratory neuron held at -75 mV that did not respond to MRS 2365. C. Representative trace a different vGLUT2- inspiratory neuron held at -75 mV showing a lack of an MRS 2365-induced inward current. D. Group data of the peak MRS 2365-induced current amplitude of 7 MRS 2365 sensitive vGLUT2+, 14 MRS 2365 insensitive vGLUT2+ and 6 vGLUT2- inspiratory preBötC neurons. Data represent the Mean ± SEM.

While the preceding whole-cell recording data from vGLUT2^{TdTomato} mice slices clearly show that a subpopulation of vGLUT2+ preBötC inspiratory neurons is excited by $P2Y_1R$ activation, an equally important question is whether vGLUT2+ neurons are the only type of inspiratory preBötC neurons that is excited by $P2Y_1R$ activation. To address this question, we loaded the preBötC of rhythmic slices from vGLUT2^{TdTomato} mice via local injection of Fluo-4 AM. Slices were placed on the stage of a multiphoton microscope to facilitate simultaneous recording of inspiratory-related activity from the XII nerve and from the Fluo-4 fluorescence signal of individual preBötC neurons. Slices were kept in the chamber for 20 minutes after the injections of Fluo-4 (Fig. 14A, B). ROI were placed over as many neurons as possible in the field of view and Ca2+ fluorescence of each ROI monitored in reference to the XII nerve recording. Inspiratory neurons were identified by ROIs that showed rhythmic increases in Fluo-4 fluorescence in phase with XII nerve activity (Fig. 14B). In control conditions, we identified a total of 16 glutamatergic (vGLUT2+) and 16 non-glutamatergic (vGLUT2-) inspiratory neurons from 3 slices (Fig. 14D). We then bath applied TTX (500 nM) to block action potential dependent transmitter release to examine postsynaptic sensitivity of preBötC inspiratory neurons to $P2Y_1R$ activation. In the presence of TTX, bath-applied MRS 2365 (60 s, 10 μM) increased Fluo-4 signal in only 5 of the 32 inspiratory neurons by an average of 33.6 ± 9.2 % (Fig. 14A-C). Two of these 5 responding inspiratory neurons were identified as vGLUT2+ while 3 were vGLUT2- (Fig. 14D). Taken together, these results suggest that in mice $P2Y_1R$ activation excites a subset of preBötC inspiratory neurons that includes both glutamatergic and non-glutamatergic, most likely inhibitory neurons.

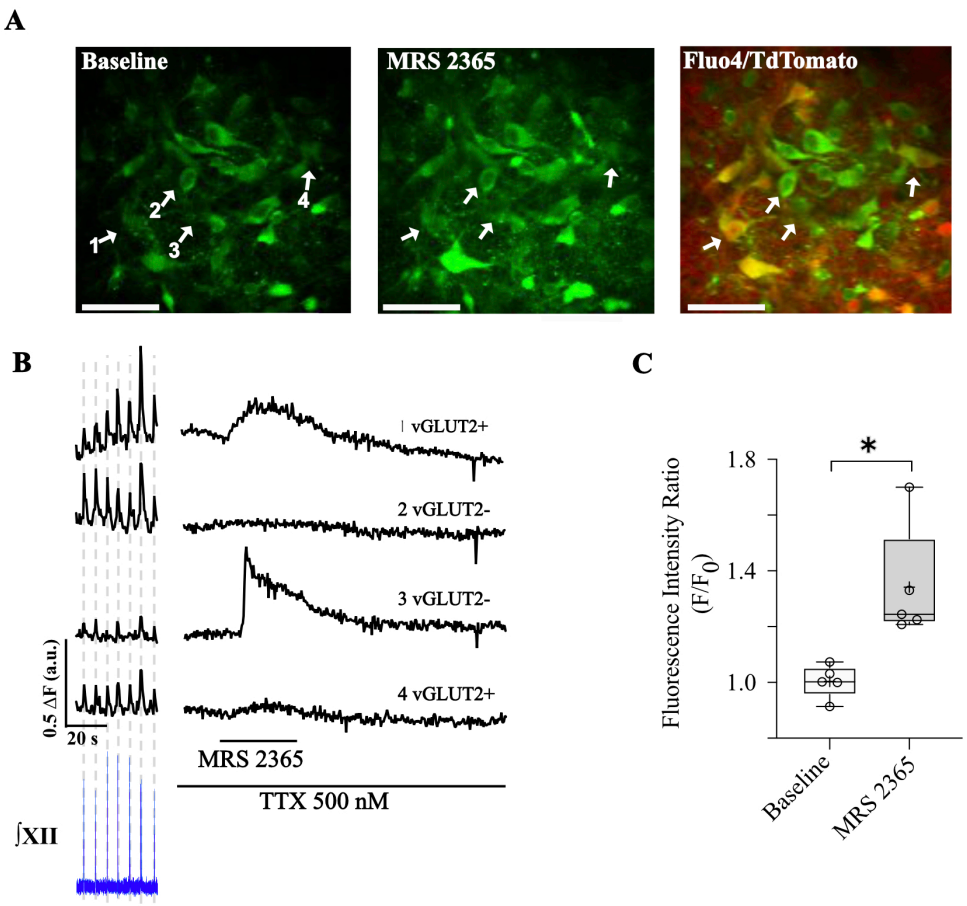
A
Baseline
MRS 2365
Fluo4/TdTomato
1
2
3
4
B
1 vGLUT2+
2 vGLUT2-
3 vGLUT2-
4 vGLUT2+
0.5 ΔF (a.u.)
20 s
MRS 2365
TTX 500 nM
∫XII
C
Fluorescence Intensity Ratio (F/F0)
1.8
1.4
1.0
*
Baseline
MRS 2365
D
2
3
14
13
Inspiratory/vGLUT2+
Inspiratory/vGLUT2-
Inspiratory/vGLUT2+/MRS 2365 sensitive
Inspiratory/vGLUT2-/MRS 2365 sensitive
Total = 32 inspiratory neurons

Figure 14: Effect of MRS 2365 on intracellular calcium signal of vGLUT2xTdTomato mice. A. Confocal images showing Fluo-4 signal at Baseline, during MRS 2365 + TTX and Fluo-4/TdTomato merge. Scale bars represent 20 μm._B. Fluo-4 signal traces of inspiratory preBötC neurons from a vGLUT2xTdTomato mouse showing the inspiratory-associated calcium transients (left) and the effect of MRS 2365 during TTX (right) on cells labeled in A. Blue trace shows inspiratory bursts simultaneously recorded from the XII nerve. C. Effect of MRS 2365 on the fluorescence intensity ratio of vGLUT2+ and vGLUT2- inspiratory neurons. Unpaired student t-test. D. Overall distribution of MRS 2365 sensitivity of vGLUT2+ and vGLUT2- inspiratory neurons across three independent experiments. 2/16 vGLUT2+ inspiratory neurons responded to MRS 2365; 3/16 vGLUT2- neurons responded to MRS 2365. Unpaired student t-test. Data represent the Mean ± SEM. *$p<0.05$.

We next assessed whether this was also the case in rats (i.e., that MRS 2365 excites both excitatory, glutamatergic and non-glutamatergic neurons), and more directly assessed whether MRS 2365 excites inhibitory neurons. Using rhythmic slices from rats, we recorded from preBötC neurons using pipettes that contained 1% of the fluorescent dye Lucifer Yellow. Inspiratory neurons that responded to MRS 2365 with an inward current were later processed to assess whether they expressed vGLUT2 or the vesicular GABA transporter vGAT mRNA using RNAScope-based in situ hybridization (Fig. 15). We found 2 MRS 2365-sensitive, inspiratory preBötC neurons that presented vGLUT2 mRNA (Fig. 15A – G, E); 1 MRS 2365-sensitive, inspiratory neuron positive for vGAT mRNA (Fig. 15H – N, E), and 5 preBötC, MRS 2365-sensitive, inspiratory neurons that were vGLUT2 - and vGAT- (Fig. 15E).

These data are consistent with the imaging data in mouse showing that vGLUT2+ neurons are not the only neurons that are excited by MRS 2365. The in situ data and detection of vGAT mRNA in MRS 2365-sensitive, inspiratory preBötC neurons confirms that inhibitory neurons respond to $P2Y_1R$ activation.

These data do not allow us to comment on the percentage of MRS 2365-sensitive neurons that are vGLUT2 or vGAT+ because the large number of neurons that did not label for either probe suggests that in some recordings there may be significant degradation of mRNA or that cell contents were lost/dialyzed after removal of the whole-cell pipette. The high negative rate was not a function of the RNAScope protocol because in all cases surrounding neurons labeled for vGLUT2 or vGAT.

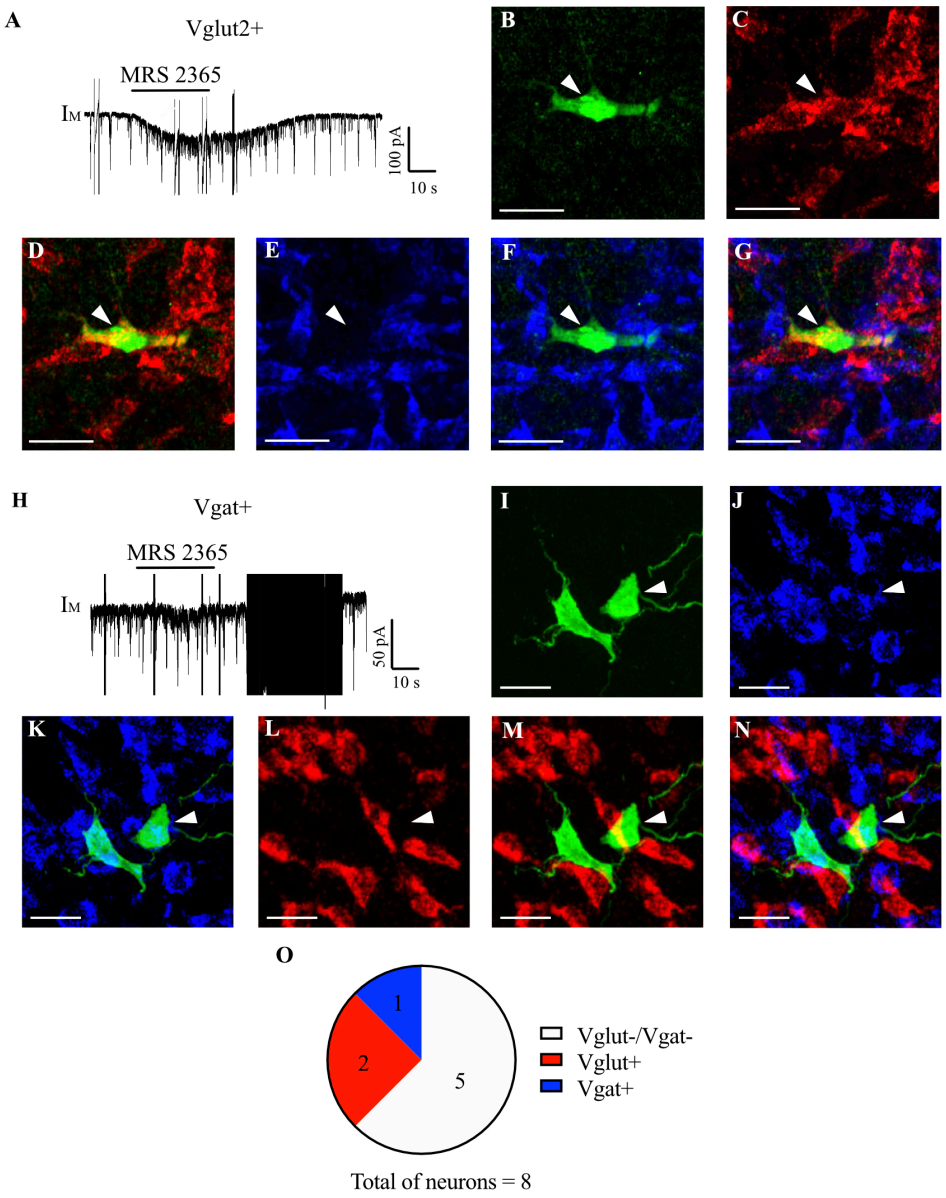
A
Vglut2+
MRS 2365
IM
100 pA
10 s
B
C
D
E
F
G
H
Vgat+
MRS 2365
IM
50 pA
10 s
I
J
K
L
M
N
O
1
2
5
Vglut-/Vgat-
Vglut+
Vgat+
Total of neurons = 8

Figure 15: $P2Y_1R$ activation excites glutamatergic, GABA/GLYcinergic and non-gutamatergic non-GABA/GLYcinergic inspiratory preBötC neurons from rats. A. Representative trace of an MRS 2365-sensitive inspiratory neuron showing an inward current filled with lucifer yellow. B – G. High power (40X) confocal images of neuron in A for lucifer yellow immuolabeling (B, green), mRNA for vGLUT2 (C, red), the merge of lucifer yellow and vGLUT2 (D), mRNA for vGLUT2 (E, blue), the merge of lucifer yellow and vGAT (G) and the merge of lucifer yellow, vGLUT2 and vGAT (G), showing the cell expressing vGLUT2 and no vGAT mRNA. H. Representative trace of a different MRS 2365-sensitive neuron showing an inward current and filled with lucifer yellow. I – N. Hight power (40X) confocal images of neuron in H for lucifer yellow immuolabeling (I, green), mRNA for vGAT (J, blue), the merge of lucifer yellow and vGAT (K), mRNA for vGLUT2 (L, red), the merge of lucifer yellow and vglut2 (M) and the merge of lucifer yellow, vGAT and vGLUT2 (N) showing the cell expressing vGAT and no Vlgut2 mRNA. O. Overall distribution of MRS 2365 sensitivity on vGLUT2+ and vGAT+ and vGLUT2-/ vGAT-. Scales bars represent 25 μm. The solid black section in H is a 100Hz 10 mV pulses applied to monitor Rs after drug application.

3.2.3 Role of inhibitory neurons in the $P2Y_1$-evoked network excitation.

Multiple lines of evidence, described above, strongly suggest that excitatory and inhibitory preBötC inspiratory neurons are excited by $P2Y_1R$ activation. Thus, these data do not help resolve whether the $P2Y_1R$-mediated increase in preBötC frequency is due to the activation of excitatory or inhibitory neurons; both types could contribute. To resolve this question, we tested whether inhibitory synaptic transmission is required for the MRS 2365-evoked increase in preBötC frequency.

We compared the network response evoked by local application MRS 2365 (10s, 100 μM) in the preBötC before and 30 min after bath application of the $GABA_A$ and glycine receptor (GLYRs) antagonists, bicuculline (BIC, 5 μM) and strychnine (STRYC, 1 μM), respectively (Fig. 16). In control conditions, baseline inspiratory frequency (Baseline 1) was 13.4 ± 0.8 breaths per min^{-1} (n = 8). Bath application of 5 μM BIC plus 1 μM STRYC caused an increase in the amount of tonic background activity recorded from the XII nerve, which can be seen as smaller, irregular discharge in the period between inspiratory bursts, but inspiratory rhythm remained easily distinguishable. BIC/STRYC also caused a minor, insignificant (p=0.81, Mixed-effects model, Tukey's multiple comparisons test) increase in the baseline frequency to 15.3 ± 1.7 breaths per min^{-1} (Baseline 2). Under control conditions, local application of MRS 2365 in the preBötC increased frequency significantly from 13.4 ± 0.8 to 38.8 ± 4.8 breaths per min^{-1}, which is an increase of 25.4 cycles per min^{-1} (p=0.006, Mixed-effects model, Tukey's multiple comparisons test, Fig. 16B). In the presence of 5 μM BIC plus 1 μM STRYC, MRS 2365 increased respiratory frequency from 15.3 ± 1.7 to 37.6 ± 2.2 breaths per min^{-1}, which is an increase of 22.3 breaths per min^{-1}, similar to control conditions (p=0.001, Mixed-effects model, Tukey's multiple comparisons test, Fig. 16B).

After 30 min of washing out of BIC plus STRYC, MRS 2365 increased inspiratory frequency from 15.2 ± 2.4 breaths per min^{-1} to 41.4 ± 4.8 breaths per min^{-1}, which is an increase of 26.2 cycles per min^{-1}, similar to control conditions ($p=0.04$, Mixed-effects model, Tukey's multiple comparisons test, not shown). Overall, the effect of MR 2365 on inspiratory frequency was the same in control and BIC/Strychine; MRS 2365 increased inspiratory frequency by 2.9 ± 0.3-fold in control conditions and by 2.7 ± 0.3-fold in presence of 5μM BIC plus 1 μM STRYC ($p=0.513$, Paired t-test, Fig. 16C).

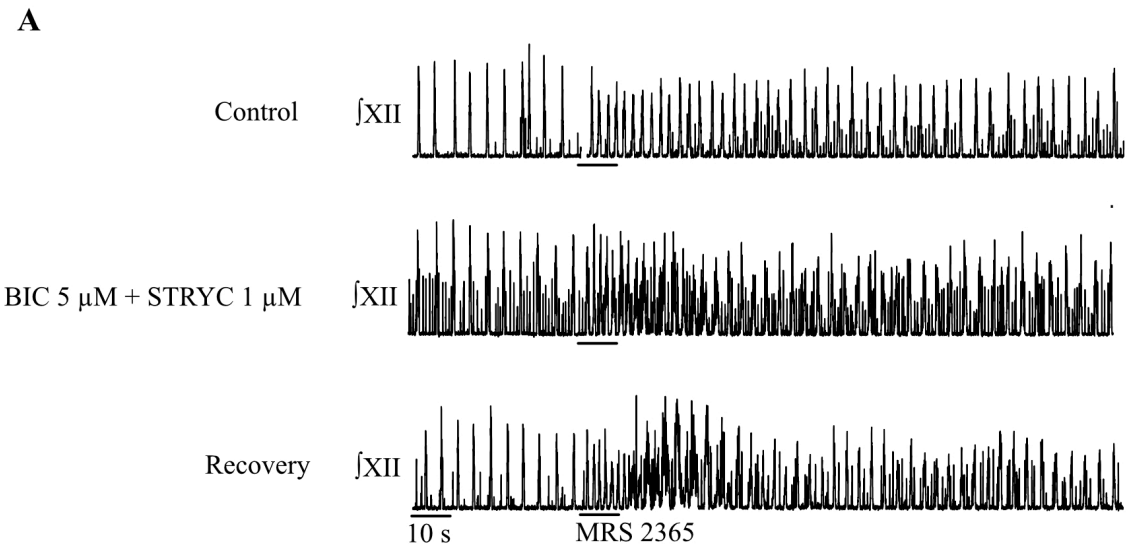
A
Control
∫XII
BIC 5 μM + STRYC 1 μM
∫XII
Recovery
∫XII
10 s
MRS 2365

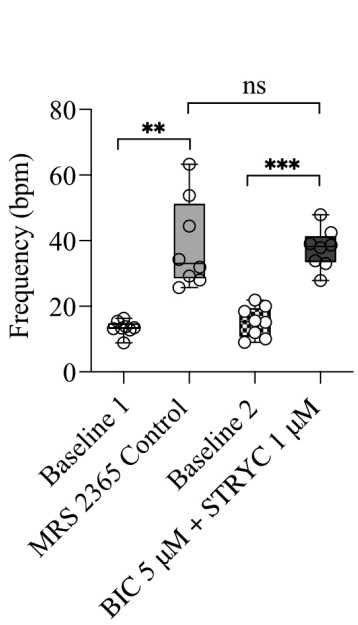
B
ns
**
***
Frequency (bpm)
80
60
40
20
0
Baseline 1
MRS 2365 Control
Baseline 2
BIC 5 μM + STRYC 1 μM

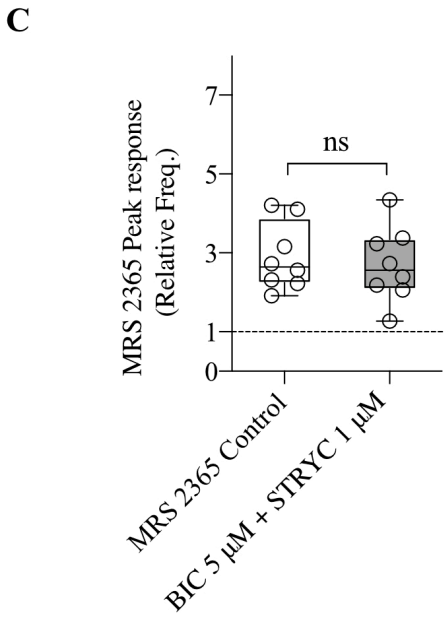
C
ns
MRS 2365 Peak response
(Relative Freq.)
7
5
3
1
0
MRS 2365 Control
BIC 5 μM + STRYC 1 μM

Figure 16: Effect of blocking inhibition with low concentrations of BIC and STRYC on the MRS2365-induced excitation of the preBötC network. A. Representative traces showing the effect of MRS 2365 in XII frequency in control conditions, during bath application of 5 μM Bicuculline + 1 μM Strychnine and during recovery. B. Grouped data showing the effect of 5μM Bicuculline + 1μM Strychnine on the MRS2365-induced increase in XII frequency. RM one-way ANOVA, Tukey's multiple comparisons test. C. Group data showing the relative frequency of MRS 2365-induced increase in frequency in controls and during 5 μM Bicuculline + 1 μM Strychnine. Unpaired student t-test. Data represent the Mean ± SEM. **p<0.01, ***p<0.001.

To ensure a more complete block of inhibitory synaptic transmission, we repeated the above experiments with higher concentrations of BIC (20 μM) and STRYC (20 μM) (Fig. 17) (Shao and Feldman, 1997). In baseline conditions, respiratory frequency (Baseline 1) was 12.6 ± 1.4 breaths per min^{-1} (n = 7). Bath application of 20 μM BIC plus 20 μM STRYC (Baseline 2) caused an even greater increase in tonic discharge compared to 5 and 1 μM and an insignificant decrease in the baseline frequency (p = 0.85, RM one-way ANOVA, Tukey's multiple comparisons test) to 11.8 ± 1.7 breaths per min^{-1} (Fig. 17B). Local application of MRS 2365 (10 s, 100 μM) in the preBötC caused a significant frequency increase from 12.6 ± 1.3 breaths per min^{-1} to 34.3 ± 2.3 breaths per min^{-1} (an increase of 21.73 cycles per min^{-1}, p<0.0001, RM one-way ANOVA, Tukey's multiple comparisons test, Fig. 19B) in control. In the presence of 20 μM BIC plus 20 μM STRYC, MRS 2365 increased respiratory frequency from 11.8 ± 1.7 to 37.1 ± 4.7, an increase of 25.3 breaths per min^{-1}, similar to control conditions (p=0.007, RM one-way ANOVA, Tukey's multiple comparisons test, Fig. 17B). After 15 min of washing out the BIC and STRYC, MRS 2365 increased inspiratory frequency from 9.5 ± 1.4 breaths per min^{-1} to 37.7 ± 4.0 breaths per min^{-1}, an increase of 28.1 cycles per min^{-1} (p=0.0005, RM one-way ANOVA, Tukey's multiple comparisons test, not shown). Overall, the MR 2365-evoked increase in inspiratory frequency was not significantly affected by the higher concentrations of BIC/STRYC; MRS 2365 increased inspiratory frequency by 2.8 ± 0.2-fold in control conditions and by 3.5 ± 0.6-fold in presence of BIC and STRYC, p=0.3, Paired t-test, Fig. 17C). In summary, these results indicate that synaptic inhibition is not necessary frequency increase evoked by $P2Y_1R$ in the preBötC, suggesting that the $P2Y_1R$ -mediated increase in frequency is brought about through excitation of excitatory, glutamatergic inspiratory preBötC neurons.

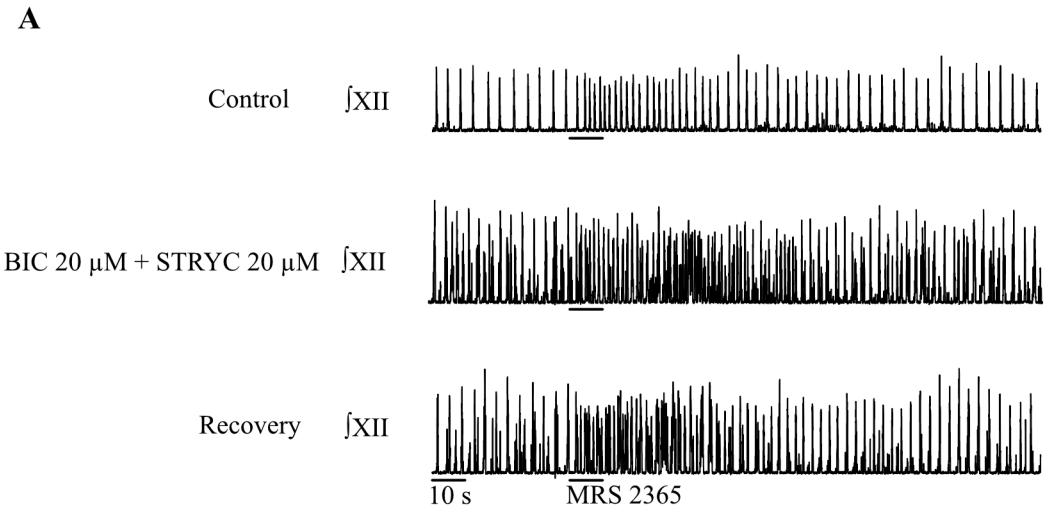
A
Control
∫XII
BIC 20 µM + STRYC 20 µM
∫XII
Recovery
∫XII
10 s
MRS 2365

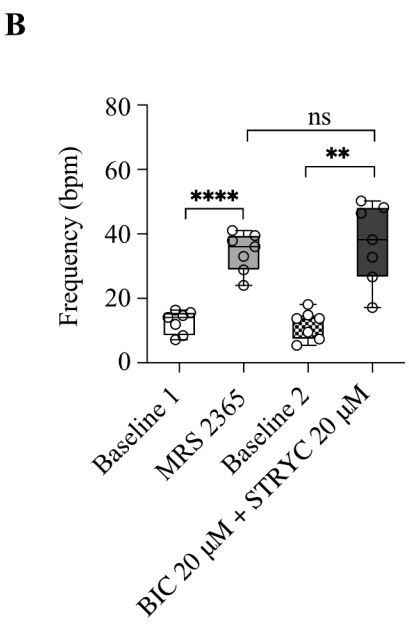
B
Frequency (bpm)
80
60
40
20
0
ns
**
****
Baseline 1
MRS 2365
Baseline 2
BIC 20 µM + STRYC 20 µM

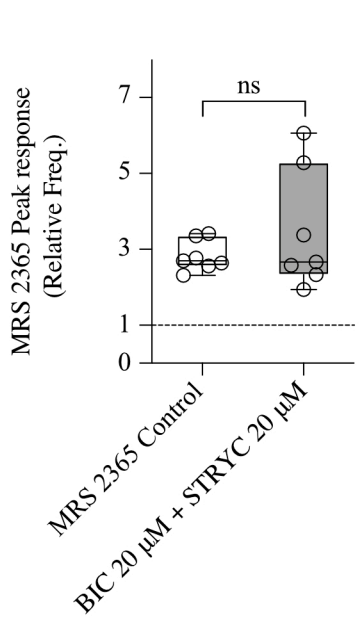
C
MRS 2365 Peak response
(Relative Freq.)
7
5
3
1
0
ns
MRS 2365 Control
BIC 20 µM + STRYC 20 µM

Figure 17: Effect of blocking inhibition with high concentrations of BIC and STRYC on the MRS2365-induced excitation of the preBötC network. A. Representative traces showing the effect of of MRS 2365 in XII frequency in control conditions, during bath application of 20 μM Bicuculline + 20 μM Strychnine and during recovery. B. Grouped data showing the effect of 20μM Bicuculline + 20 μM Strychnine on the MRS2365-induced increase in XII frequency. RM one-way ANOVA, Tukey's multiple comparisons test. C. Group data showing the relative frequency of MRS 2365-induced increase in frequency in controls and during 20 μM Bicuculline + 20 μM Strychnine. Unpaired student t-test. Data represent the Mean ± SEM. **p<0.01, ****p<0.0001.

4. Discussion

During hypoxia, astrocytes in the preBötC detect the reduction in oxygen levels and release ATP, which increases ventilation and counteracts the secondary HRD (Angelova et al., 2015; Rajani et al., 2018). In the preBötC in vitro, the excitatory effects of ATP on inspiratory behaviour are mediated entirely by the activation of $P2Y_1Rs$ (Lorier et al., 2008; Huxtable et al., 2009; 2010). Under *in vivo* conditions during hypoxia, ATP released in the preBötC acts primarily through $P2Y_1Rs$ to counteract the HVD, but the potential contribution of other P2Rs has not been examined (Angelova et al., 2015; Rajani et al., 2018; SheikhBahaei et al., 2018). The cellular and molecular mechanisms that underlie the $P2Y_1R$-mediated excitation of the preBötC inspiratory network are unknown and are the focus of this section of the thesis. We focussed on two key questions in this regard. The first objective was to advance understanding of the second messenger pathways and ion channels through which $P2Y_1Rs$ signal to excite preBötC inspiratory neurons and increase network frequency. First, we have provided evidence that $P2Y_1R$ activation induced excitation of preBötC inspiratory neurons, in part, by activating a $G_{q/11}$-coupled signalling pathway that involves the activation of PLC and PKC. We found that this mechanism contributes to 50% of the total $P2Y_1R$-evoked current, suggesting that $P2Y_1Rs$ also act through an unidentified, non- $G_{q/11}$ signalling pathway. We also provided evidence suggesting that BK_{Ca} channels are unlikely to mediate $P2Y_1$-induced excitation of the preBötC. Additionally, we presented evidence suggest that, in the preBötC, $P2Y_1Rs$ act presynaptically to facilitate neurotransmitter release.

The second objective was to determine whether excitatory or inhibitory preBötC inspiratory neurons are sensitive to $P2Y_1R$ activation, and which of these neuron types underlie the $P2Y_1R$-mediated excitation of inspiratory rhythm. Using a combination of immunohistochemistry,

RNAScope, electrophysiology, Ca^{2+} imaging and pharmacology we have provided evidence that $P2Y_1Rs$ are preferentially expressed in the preBötC, principally on glutamatergic neurons but they are also expressed on nonglutamatergic, most likely non-glycinergic preBötC neurons. Second, activation of $P2Y_1Rs$ depolarized a subpopulation of glutamatergic and nonglutamatergic inhibitory neurons. Third, inhibitory synaptic transmission is not necessary for the $P2Y_1R$-induced network excitation, suggesting that $P2Y_1Rs$ act through glutamatergic preBötC inspiratory neurons to excite the inspiratory network.

4.1 Second messenger signaling cascades that mediate $P2Y_1R$ actions in the preBötC

Canonically, $P2Y_1Rs$ preferentially couple to $G_{q/11}$-proteins to activate the PLC/InsP3 endoplasmic reticulum Ca^{2+}-release signalling pathway. The dissociation of the αq subunit activates PLC triggering the hydrolysis of PIP_2 to InsP3 and DAG. InsP3 binds to IP_3 receptors located on the intracellular stores and promotes the release of Ca^{2+} from the endoplasmic reticulum. This intracellular Ca^{2+} mobilization promotes the activation of several Ca^{2+}-dependent kinases, including PKC (Abbracchio et al., 2009).

Our laboratory is actively exploring the signalling cascades and ion channels via which $P2Y_1Rs$ excite the preBötC inspiratory network and its neurons. Based on the observation that the network effect of ATP to increase frequency is entirely mediated by $P2Y_1Rs$ *in vitro* (Lorier et al., 2007; Huxtable et al., 2009; 2010), initial whole-cell studies were conducted using the full agonist, ATP. The assumption was that the ATP current evoked in inspiratory neurons would also be entirely mediated by $P2Y_1Rs$. These initial experiments (Zhang et al., 2016a; 2016b) revealed that inhibitors of critical steps in the $G_{q/11}$ signalling pathway, PLC and PKC, reduced ATP currents by

25 – 30 % compared to a larger, 40-50% reduction in the ATP-evoked frequency increase. One possible explanation for this difference was that the ATP-evoked currents involved other, non $P2Y_1R$-mediated components. Indeed, when this was tested by comparing the sensitivity of ATP current to the $P2Y_1R$ antagonists, MRS 2279, vs non-selective P2R antagonists PPADS/Suramin revealed that $P2Y_1Rs$ account for only 30-40% of the total ATP current (Zhang et al., 2016a; 2016b). Thus, the main goal of the experiments here was to test the percentage of the $P2Y_1R$-mediated currents that were mediated by pathways involving PLC and PKC. Based on an extensive literature that $P2Y_1Rs$ signal through G_q/G_{11}-proteins, we predicted that $P2Y_1R$ currents would be almost completely blocked by inhibitors of PLC and PKC.

This was not the case. In all inspiratory preBötC neurons tested, intracellular block of PLC with U71322 (4 μM) reduced the peak amplitude of depolarizing current evoked by the local application of the selective $P2Y_1R$ agonist, MRS 2365 (100 μM), by only 50%. Similarly, intracellular block of PKC with CHE (10 μM) also reduced the peak MRS 2365-mediated inward current by only 55%. We propose two possible explanations for this surprising finding. First, unlike receptor antagonists against $P2Y_1Rs$ which reside on the cell membrane, a challenge with blocking second messenger signaling pathways is that the blocking agent has to cross the cellular membrane and accumulate in the intracellular compartment at a sufficient concentration to block the signaling pathway. This has been a challenge for us in the past, especially when trying to block network effects where the blocker has to entire a substantial portion of the neurons that comprise the network. It can also be a problem for whole-cell experiments when blockers are added to the bath and have to diffuse across the cell membrane to their site of action. However, we do not think this is a major factor in our experiments. We overcame the diffusion limitation issue by adding the

intracellular blockers to the intracellular solution. As a result, the blockers had access to the intracellular compartment as soon as the membrane was ruptured to obtain the whole-cell configuration. Fifteen minutes is typically more than sufficient time for the blocker to diffuse throughout the neuron and achieve block. In addition, the concentration of blockers used here have been able to block the majority of PLC- and PKC -mediated currents in neurons from other regions of the brain. Bath application of 1-5 μM U73122 effectively inhibit BDNF-induced cationic currents in pontine neurons from neonatal rats (Li et al., 1999), GIRK currents in isolate pyramidal neurons of rats (Sickmann et al., 2008), TRPV1 currents in magnocellular neurosecretory cells of rats (Bansal and Fisher, 2017), block the $P2Y_1R$ inhibition of GIRK channels (Fillipov et al., 2014), and block the ability of mGLUR7R to inhibit VGCC on cerebellar granule cells (Perroy et al.2000), and intracellular dialysis of U73122 attenuates ATP-mediated currents on inspiratory preBötC neurons from rats (Zhang et al., 2016a; 2016b). In addition, others have demonstrated that U71233, and not the inactive isomer U73343, attenuates M-currents of bullfrog sympathetic neurons (Stemkowski el at., 2002). Bath application of 10 μM of CHE effectively block oxytocin-induced increase action potential firing frequency of amygdala neurons (Hu et al., 2020), bitter taste receptors 2 potentiation of capsaicin-dependent TRPV1 currents on isolated bronchopulmonary sensory neurons of rats (Gu et al., 2017), A-type K^+ currents on striatal culture neurons (Deng et al., 2011) and intracellular dialysis of CHE attenuates ATP-mediated currents on inspiratory preBötC neurons from rats (Zhang et al., 2016a; 2016b). It is possible that our measurements underestimate the magnitude of the block because our measurement of the initial maximum MRS 2365 current is made within the first 2 minutes of membrane rupture. This initial measurement is made as fast as possible but even at 2 min the blockers may have attenuated the maximum MRS 2365 current. Substances of similar molecular weight to CHE and U73122 (380

– 480 g/mol) are able to diffuse form the pipette into the cell with a diffusion coefficient of 48.1 $\mu m^2 s^{-1}$, which will saturate a 2000 μm^2 diameter spherical cell in a few seconds (Pusch and Neher, 1988). Neurons have complex dendritic trees that could affect the diffusion of compounds from the patch pipettes. However, even if we have underestimated the degree of block, it is clear that there was still a substantial component of the MRS 2365 current that was not blocked by U71322 or CHE.

A more likely explanation is that in preBötC inspiratory neurons, $P2Y_1Rs$ signalling is not limited to the $G_{q/11}$ pathway but involves another G-protein coupled receptor, perhaps G_s. There is a single report of $P2Y_1Rs$ signaling through the G_s in cultured hippocampal neurons to promote axonal elongation (del Puerto et al., 2012). Consistent with this possibility is strong evidence from our laboratory showing that a substantial portion of the $P2Y_1R$-mediated excitation of the preBötC network is blocked by the hyperpolarization-activated (I_h) current blocker, ZD7288 (Zhang et al., 2018). The I_h current is carried by hyperpolarization activated, cyclic nucleotide gated (HCN) ion channels that are primarily modulated by Gs through cAMP. Whole-cell data further establish that $P2Y_1R$ activation potentiates the Ih currents in preBötC inspiratory by causing a depolarizing shift in its voltage activation curve (Zhang et al., 2018). Thus, we consider it most likely that excitatory actions of $P2Y_1R$ activation on preBötC neurons and the preBötC network are mediated by the $G_{q/11}$ signaling pathway in combination with another, as yet unidentified GPCR pathway, perhaps Gs.

4.2 Ion channels that might mediate $P2Y_1R$ actions in the preBötC

Additional evidence that the $P2Y_1R$-mediated excitation of the preBötC network involves $G_{q/11}$ and the PLC-IP3 signaling pathway is that the $P2Y_1R$-induced increase in inspiratory activity in the preBötC is dependent in part on Ca^{2+} release from intracellular stores; e.g., the increase is blunted by the SERCA inhibitors CDA and thapsigargin (Rajani et al., 2018). Of course, this is not definitive since a host of signaling pathways converge on SERCA and intracellular Ca^{2+} (Berridge et al., 2003). Nevertheless, the importance of elevated intracellular Ca^{2+} in the actions of $P2Y_1Rs$ on network activity implicated several ion channels of possible effectors. We focussed on BK_{Ca} channels because they act as coincidence detectors of membrane depolarization and intracellular Ca^{2+}, which makes them an attractive downstream effector of $P2Y_1R$ activation. Moreover, BK_{Ca} channels modulate a host of rhythmic behaviours including circadian rhythms and pacemaker neurons activity of the suprachiasmatic nucleus, gait and motor coordination by modulation of Purkinje neurons activity and pituitary activity where BK_{Ca} channels modulate the transitions from spontaneous single spike to bursting behavior of pituitary cells (Sausbier et al., 2004; Meredith et al., 2006; Chen et al., 2010; Shipston, 2018). In the preBötC, reported effects of BK_{Ca} channel blockade on inspiratory frequency include an increase, a decrease or no effect (Rajani et al., 2016). Variability could reflect preparation, developmental and species differences. However, we did not consider that this variability excluded a potential role for BK_{Ca} in the actions of $P2Y_1Rs$ on preBötC rhythm because all of these previous studies involved blocking BK_{Ca} under baseline conditions. We reasoned that if BK_{Ca} was potentiated by $P2Y_1R$ activation, it could play a role. However, our data suggest that BK_{Ca} channels do not contribute to the actions of $P2Y_1Rs$ in the preBötC since the lower concentration of paxilline used (1 μM) should effectively block BK_{Ca} channels.

At a concentration of 1 μM, bath-applied paxilline had no overall effect on the MRS 2365-induced frequency increase evoked by $P2Y_1R$ activation in the preBötC of medullary rhythmic slices. However, substantial variability in the effects of paxilline and substantial inhibition of the frequency increase in some experiments suggest that this conclusion must be made with caution. The most obvious solution to resolve this ambiguity was to increase the concentration of paxilline or use a different antagonist. The limitation with this approach is the dearth of selective antagonists. The best agent and the one used here is paxilline, which effectively blocks BK_{Ca} channels at a concentration is 10 – 100 nM (Alomone Labs). However, paxilline also inhibits SERCA with an IC_{50} of 5 – 10 μM (Bilmen et al., 2002). We have already established that inhibition of SERCA markedly attenuates the $P2Y_1R$-mediated frequency increase (Rajani et al., 2018). Thus, the key feature of our paxilline experiments is that paxilline had to be used at the highest possible concentration where it clearly does not affect SERCA.

Since paxilline inhibits SERCA with an IC_{50} of 5 – 10 μM (Bilmen et al., 2002), we compared the effects of 1 and 4 μM paxilline on MRS 2365-evoked inward currents in whole-cell voltage-clamp recording experiments. Under these conditions, the only way that paxilline could alter these currents was via inhibition of SERCA. As expected, 1 μM paxilline was without effect on MRS 2365 evoked currents. At 4 μM, paxilline reduced the peak amplitude of the MRS 2365-mediated current by 50% in every inspiratory preBötC neuros tested, strongly suggesting that 4 μM paxilline inhibits SERCA.

Thus, while our data suggest that BK_{Ca} channels are not involved in the $P2Y_1$-mediated increase in inspiratory frequency, we cannot definitively exclude a contribution for three reasons. First, in 50% of our preparations, 1 μM paxilline reduced the frequency increase between 26 and 76 percent. Second, failure to obtain a significant effect may reflect that 1 μM paxilline was too low to sufficiently inhibit BK_{Ca}. This is unlikely given that the effective range for paxilline to block BK_{Ca} is 10 – 100 nM (Alomone Labs), but these measurements are typically made in culture systems where drug access to the channel is not a limitation. Higher concentrations are typically required in thick slice preparations. Finally, paxilline is a fungal alkaloid that serves as an allosteric modulator between the open-close state transitions, favouring the stabilization of BK_{Ca} channels in their closed state. It was previously reported that paxilline block of BK_{Ca} channels is reduced when $[Ca^{2+}]_i$ is increased in *Xenopus* oocytes patches expressing BK_{Ca} channels (Sanchez and McManus, 1996). In oocytes patches expressing BK_{Ca} channels, paxilline is less effective in blocking BK_{Ca} when the probability of channel opening (Po) is increased (equilibrated at 0 mV and 300 μM $[Ca^{2+}]_i$), compared to conditions that promote low channel Po (equilibrated at 0 mV and 10 μM $[Ca^{2+}]_i$) where paxilline reaches maximal block, suggesting that $[Ca^{2+}]_i$ elevations reduce paxilline block (Zhou and Lingle, 2014). However, when conditions are changed from 0 mV and 300 μM $[Ca^{2+}]_i$ to -70 mV and 300 μM $[Ca^{2+}]_i$, which increases Po, paxilline block is restored (Zhou and Lingle, 2014), suggesting that paxilline block is a function of Po rather than $[Ca^{2+}]_i$. The activation of $P2Y_1R$ elicits a SERCA-dependent increase of intracellular Ca^{2+}, which might increase BK_{Ca} channel Po, which could reduce the efficacy of paxilline to block BK_{Ca} channels, increasing the chance of our obtaining a false negative result. Overall, our data strongly suggest that $P2Y_1Rs$ act in part via a $G_{q/11}$-coupled pathway. Data also suggest that BK_{Ca} does not contribute to the actions of $P2Y_1Rs$ in the preBötC. Thus, the molecular identity of $G_{q/11}$-sensitive

ion channel(s) responsible for $P2Y_1R$-mediated excitation of the preBötC network remains unknown.

4.3 Presynaptic actions

The possibility that the presynaptic mechanisms could contribute to the excitatory actions of ATP or MRS 2365 on preBötC frequency has received little attention, primarily because presynaptic P2YRs primarily inhibit neurotransmitter release (Gonçalves and Queiroz, 2008). However, there is limited evidence that P2YR signaling facilitates neurotransmitter release by both direct and indirect mechanisms. For example, $P2Y_1Rs$ directly facilitate noradrenaline release from rat sympathetic ganglia neurons in primary culture (Chandaka et al., 2011). Indirectly, presynaptic facilitation of glutamate release occurs in superficial dorsal horn neurons, where inflammation activates microglia, causing them to release ATP, which stimulates astrocytic $P2Y_1R$ and astrocytic release of glutamate. Astrocytic glutamate, in turn, activates presynaptic mGLUR5Rs, facilitating glutamate release (Yang et al., 2019).

In inspiratory preBötC neurons, an MRS 2365-evoked increase in the frequency of spontaneous PSCs in ~44% of neurons (11/25), suggested that presynaptic $P2Y_1Rs$ may also facilitate transmitter release in a subpopulation of neurons. Of course, these data are no definitive since the increase in sPCS activity could simply reflect direct activation of action potentials in presynaptic neurons. However, we also observed that, following TTX to block action potential dependent transmission, two out of two inspiratory preBötC neurons responded to MRS 2365 with a 2.8 ± 1-fold reduction in IEI of mPSCs and an 0.1 ± 0.3-fold increase in mPSC amplitude. These data suggest that activation of presynaptic $P2Y_1Rs$ may facilitate transmitter release and contribute to

the excitatory actions of ATP on preBötC frequency. An important area of future investigation will be to increase sample size and also separately assess the effects of MRS 2365 on excitatory and inhibitory mPSCs by performing the mPSC analysis in the presence of glutamatergic or GABA/glycine receptor antagonists.

4.4 Role of excitatory vs inhibitory preBötC neurons in the effects of $P2Y_1R$ activation

Detailed mapping of the rhythmic slice from neonatal rats established that the preBötC is the site of maximum $P2Y_1R$ sensitivity and responsible for the $P2Y_1R$-mediated increase inspiratory-related frequency (Lorier et al., 2007). Similar preBötC sensitivity to $P2Y_1Rs$ was later established in neonatal mice *in vitro* (Zwicker et al., 2011). Whether this focal sensitivity reflects discrete distribution of $P2Y_1Rs$ in the preBötC, the unique function of the preBötC or both has never been clear until now. Detailed analysis of $P2Y_1R$ immunolabeling in the VRC revealed preferential distribution of $P2Y_1R$ immunolabeled neurons in the preBötC. This is very clear in Fig. 11 where the rostrocaudal and mediolateral distribution of $P2Y_1R$ immunolabeling in the VRC overlaps closely with SST immunolabeling. SST immunolabeling is arguably the most reliable marker of the preBötC in rodents (Stornetta et al., 2003; Tan et al., 2008; Gray et al., 2010). Mapping of $P2Y_1R$ immunolabeling to the preBötC is therefore an important contribution of this work. It is important to emphasize that the reliability of these data is greatly enhanced by the fact that we established the specificity of the $P2Y_1R$ antibody using a $P2Y_1R$ KO mouse obtained from Ute Krügel, from the Rudolf Boehm Institute of Pharmacology and Toxicology, Faculty of Medicine, Leipzig University. The strong staining in the preBötC of neonates and cerebellum of adult mice was not apparent in the KO animals. To our knowledge, the specificity of this antibody (or any $P2Y_1R$ antibody) has not previously been verified in KO animals. These data therefore indicate

that the sensitivity of the preBötC to ATP is due to the discrete distribution of $P2Y_1Rs$ in the network that generates inspiratory rhythm.

These data do not, however, provide insight into the subtype(s) of inspiratory preBötC neurons that underlie the $P2Y_1R$-mediated frequency increase. The preBötC comprises a heterogenous population of inspiratory neurons that include Dbx1-derived, NK1R+, glutamatergic neurons of multiple types (at least two types of pacemaker neurons, non-pacemaker neurons, rhythmogenic and pattern forming neurons), glycinergic neurons (pacemaker and non-pacemaker varieties) and GABAergic neurons (Gray et al., 2001; Kuwana et al., 2006; Tan et al., 2008; Winter et al., 2009; Bouvier et al., 2010; Gray et al., 2010; Koizumi et al., 2013; Baertsch and Ramirez, 2019). Our initial working model was that ATP mediates the increase in frequency through activation of $P2Y_1Rs$ on glutamatergic neurons. This hypothesis was based on several observations. To begin, the sensitivity of inspiratory rhythm to local application of non-NMDA glutamate receptor antagonists established almost three decades ago that inspiratory rhythm generation is dependent on AMPAR-mediated glutamatergic transmission within the preBötC (Smith et al., 1991; Funk et al., 1993). The primacy of glutamatergic signaling in inspiratory rhythm generation has been consistently reinforced by observations that: development of DBX1-derived glutamatergic neurons is essential for rhythm; targeted laser ablation of DBX1-derived, preBötC neurons eliminates rhythm (Wang et al., 2014); and that selective optogenetic stimulation of glutamatergic neurons increases preBötC rhythm (Cui et al., 2016; Baertsch et al., 2018; Vann et al., 2018). In addition, functionally unidentified NK1R-immunolabelled preBötC neurons co-label for $P2Y_1R$ immunolabeling (Lorier et al., 2007). Inspiratory preBötC, NK1R+ neurons are almost exclusively glutamatergic (Stornetta et al., 2003; Bouvier et al., 2010; Gray et al., 2010; Baertsch and Ramirez,

2019), suggesting that at least a subpopulation of $P2Y_1R$-expressing preBötC neurons are glutamatergic. However, there is evidence showing a small fraction of NK1+ neurons co-expressing GAD67 (~6%) or GLYT2 (~1%) mRNA in the preBötC (Wang et al., 2001). Considered together, these data have focused attention on the primary role of excitatory transmission in preBötC rhythm generation and led us to hypothesize that glutamatergic preBötC neurons underlie the $P2Y_1R$-mediated increase in frequency.

However, it is now apparent that ~50% of preBötC inspiratory neurons are inhibitory and that modulation of inhibitory activity can modulate rhythm (Baertsch et al., 2018; Ramirez and Baertsch, 2018; Baertsch and Ramirez, 2019). Most surprisingly, in 2018, it became clear that selective photostimulation of inhibitory preBötC neurons can increase preBötC frequency and in fact can be more effective than stimulation of glutamatergic neurons if timed appropriately (Baertsch et al., 2018).

Thus, a major goal of this study was to revisit our initial model and reassess whether $P2Y_1Rs$ act on excitatory (glutamatergic) or inhibitory (GABAergic or glycinergic) preBötC inspiratory neurons to increase inspiratory frequency. Several lines of evidence support our initial hypothesis that the $P2Y_1R$-mediated frequency increase is mediated primarily by excitatory neurons.

Most convincing is the observation in rat slices that the MRS 2365-evoked increase in inspiratory frequency of rhythmically active medullary slices is not affected by bath application of GABA and Glycine receptor antagonists, bicuculline and strychnine. Clearly, if the $P2Y_1R$-mediated frequency increase depends on GABA/Glycinergic neurons and synaptic inhibition, blocking

inhibition should abolish, or at least attenuate, the frequency increase. Neither happened. These pharmacological data indicate that $P2Y_1R$ activation of GABA/Glycinergic neurons is not necessary to cause the $P2Y_1R$-mediated excitation of the preBötC inspiratory network. Moreover, local application of MRS 2365 into the preBötC of rhythmic slices from mice evoked small inward currents in approximately one third of glutamatergic (vGLUT2+) inspiratory preBötC neurons. Most importantly, bath application of MRS 2365 in the presence of TTX increased intracellular Ca^{2+} fluorescence in a subpopulation of glutamatergic (vGLUT2+ neurons). This experiment is especially telling because the Ca^{2+} increase occurred in the presence of TTX, indicating that the MRS 2365 acted postsynaptically, directly on the vGLUT2+ neurons. Finally, virtually all the $P2Y_1R$ immunolabeled neurons in the preBötC were vGLUT2+; not a single $P2Y_1R$ immunolabeled neuron was glycinergic (GLYT2+).

Thus, we can conclude that synaptic inhibition is not essential for the MRS 2365-mediated increase in preBötC frequency and that glutamatergic neurons are sufficient for this response. An important point for consideration is that these experiments used rats and mice; the network responses and RNAScope data were obtained in rat while experiments involving positive identification of glutmatergic (vGLUT2+), nonglutamatergic (vGLUT2-) and glycinergic neurons (GLYT2+) could only be done in fluorescent reporter mice. Does this combination of species weaken or strengthen our conclusions? We argue that complimentary data from the two species strengthens our conclusions. First, the dependence of preBötC rhythm on glutamatergic signaling is common to rats and mice (Lorier et al., 2007; Huxtable et al., 2009; 2010; Zwicker et al., 2011). Second, while the enzyme systems in the preBötC that degrade ATP and the preBötC sensitivity to adenosine differ between mice and rats, preBötC sensitivity to $P2Y_1R$ activation is

indistinguishable between mice and rats (Zwicker et al., 2011). Thus, the fact that observations in rat and mice similarly support that $P2Y_1Rs$ act on glutamatergic neurons to increase preBötC frequency bolster our data.

Despite the strength of the data that the frequency increase evoked by $P2Y_1R$ activation in the preBötC, we cannot conclude that inhibitory neurons do not contribute. First, the dependence of the network rhythm on glutamatergic transmission means that the definitive experiment we performed to assess whether inhibitory transmission is essential; i.e., apply MRS 2365 after blocking glutamatergic synaptic transmission, could not be performed. Block of glutamatergic transmission stops preBötC rhythm, making it impossible to test whether MRS 2365 can increase frequency under these conditions. In addition, a subpopulation of inhibitory preBötC, inspiratory neurons appear sensitive to $P2Y_1R$ activation. A subpopulation of non-vGLUT2 inspiratory neurons in vGLUT2 mice respond to MRS 2365 with an increase in Ca^{2+} fluorescence. Also, in situ hybridization analysis using RNAScope technology revealed vGAT mRNA in at least one MRS 2365-sensitive inspiratory preBötC neuron. While these data suggest that inhibitory inspiratory preBötC neurons are $P2Y_1R$ sensitive, they provide no information as to whether the sensitive neurons are GABA or Glycinergic. Optogenetic activation of GABA or Glycinergic neurons can stimulate breathing *in vitro* (Baertsch et al., 2018). However, based on the fact that we did not find a single GLYT2+ neuron that showed $P2Y_1R$ immunolabeling, it appears most likely that GABAergic neurons are sensitive to $P2Y_1R$ activation. We used GAD67 reported mice to obtain direct evidence that GABAergic preBötC inspiratory are sensitive to MRS 2365. However, these efforts were not successful. We were unable to record from any GABAergic

(GAD67+) preBötC inspiratory neurons; zero of 28 GAD67+ preBötC neurons received inspiratory synaptic inputs.

5. Summary

Compelling evidence proposes that ATP released from astrocytes within the preBötC in response to hypoxia offsets the secondary hypoxic ventilatory depression (Gourine et al., 2005b; Angelova et al., 2015; Rajani et al., 2018). Work from our laboratory has shown that ATP excitation of the preBötC is mediated by activation of $P2Y_1Rs$ (Lorier et al., 2007) that involves the recruitment of a $G\alpha_{q/11}$-signalling pathway (Zhang et al., 2016a; 2016b). However, the cellular identity of inspiratory neurons that mediate the $P2Y_1R$-induced excitation of the inspiratory network remained unknown until the completion of this thesis. Here we present evidence suggesting the $G\alpha_{q/11}$-signalling pathway is recruited when $P2Y_1Rs$ are activated in the preBötC. This mechanism accounts for 50% of the $P2Y_1R$-mediated current. The remaining fraction of the $P2Y_1R$-evoked current can be attributed to parallel mechanisms, possibly Gs-coupled (Zhang et al., 2018). We also showed that BK_{Ca} channels is unlikley to mediate the $P2Y_1R$-induced excitation of preBötC inspiratory neurons. In addition, we presented evidence that suggest that $P2Y_1Rs$ could also be acting pre-synaptically to facilitate transmitter release.

We have also provided, for the first time, strong evidence that a cluster of $P2Y_1R$-expressing neurons is localized specifically in the preBötC region of the VLM. These data correlate with the focal ATP sensitivity of the preBötC (Lorier et al., 2008). Moreover, we presented evidence that while glutamatergic and nonglutamatergic, nonglycinergic neurons express $P2Y_1Rs$, the $P2Y_1R$-

mediated excitation of the preBötC network does not depend on inhibitory neurons; i.e., $P2Y_1Rs$ excite the preBötC primarily by exciting glutamatergic inspiratory neurons.

These findings help us deepen our knowledge of the mechanisms underlying ATP-mediated excitation of the preBötC that act to shape the secondary HVD and contribute to a more comprehensive understanding of purinergic modulation in the inspiratory network in particular, and the CNS in general. Additional experiments using single cell RNA sequencing on neurons sensitive to MRS 2365 versus non sensitive neurons could shed light on the possible ion channel(s) mediating the $P2Y_1R$-induced depolarization of preBötC inspiratory neurons. Experiments assessing the expression of $P2Y_1Rs$ and intracellular Ca^{2+} response on identifiable GABAergic neurons will provide additional information regarding the distribution of $P2Y_1Rs$ in the preBötC. Finally, *in vitro* and *in vivo* selective opto- or chemogenetic inhibition of glutamatergic and nonglutamatergic (i.e GABAergic) inspiratory preBötC neurons that express $P2Y_1Rs$ will be key in resolving the underlying mechanism and microcircuitry involved in the $P2Y_1R$-mediated excitation of the inspiratory network.

6. References

Abbott SBG, Stornetta RL, Coates MB, Guyenet PG (2011) Phox2b-expressing neurons of the parafacial region regulate breathing rate, inspiration, and expiration in conscious rats. Journal of Neuroscience 31:16410–16422.

Abbracchio MP, Burnstock G, Boeynaems J-M, Barnard EA, Boyer JL, Kennedy C, Knight GE, Fumagalli M, Gachet C, Jacobson KA, Weisman GA (2006) International Union of Pharmacology LVIII: Update on the P2Y G Protein-Coupled Nucleotide Receptors: From Molecular Mechanisms and Pathophysiology to Therapy. Pharmacol Rev 58:281–341.

Abbracchio MP, Burnstock G, Verkhratsky A, Zimmermann H (2009) Purinergic signalling in the nervous system: an overview. Trends in Neurosciences 32:19–29.

Abdel-Hady H (2015) Caffeine therapy in preterm infants. WJCP 4:81.

Amadio S, Vacca F, Martorana A, Sancesario G, Volonté C (2007) P2Y1 receptor switches to neurons from glia in juvenile versus neonatal rat cerebellar cortex. BMC Dev Biol 7:1–17.

Anderson TM, Garcia AJ, Baertsch NA, Pollak J, Bloom JC, Wei AD, Rai KG, Ramirez J-M (2016) A novel excitatory network for the control of breathing. Nature 536:76–80.

Anderson TM, Ramirez J-M (2017) Respiratory rhythm generation: triple oscillator hypothesis. F1000Res 6:139.

Angelova PR, Kasymov V, Christie I, SheikhBahaei S, Turovsky E, Marina N, Korsak A, Zwicker J, Teschemacher AG, Ackland GL, Funk GD, Kasparov S, Abramov AY, Gourine AV (2015) Functional Oxygen Sensitivity of Astrocytes. J Neurosci 35:10460–10473.

Aoki Y, Yamada E, Endoh T, Suzuki T (2004) Multiple actions of extracellular ATP and adenosine on calcium currents mediated by various purinoceptors in neurons of nucleus tractus solitarius. Neurosci Res 50:245–255.

Aranda JV, Turmen T, Davis J, Trippenbach T, Grondin D, Zinman R, Watters G (1983) Effect of caffeine on control of breathing in infantile apnea. The Journal of Pediatrics 103:975–978.

Baertsch NA, Baertsch HC, Ramirez J-M (2018) The interdependence of excitation and inhibition for the control of dynamic breathing rhythms. Nat Commun 9:843–17.

Baertsch NA, Ramirez J-M (2019) Insights into the dynamic control of breathing revealed through cell-type-specific responses to substance P. Elife 8:76.

Bansal V, Fisher TE (2017) Osmotic activation of a Ca2+-dependent phospholipase C pathway that regulates ΔN TRPV1-mediated currents in rat supraoptic neurons. Physiol Rep 5:8 e13259.

Bayliss DA, Barhanin J, Gestreau C, Guyenet PG (2015) The role of pH-sensitive TASK channels in central respiratory chemoreception. Pflugers Arch 467:917–929.

Benemei S, Patacchini R, Trevisani M, Geppetti P (2015) TRP channels. Curr Opin Pharmacol 22:18–23.

Berridge MJ, Bootman MD, Roderick HL (2003) Calcium: Calcium signalling: dynamics, homeostasis and remodelling. Nat Rev Mol Cell Biol 4:517–529.

Biancardi V, Saini J, Pageni A, Prashaad M H, Funk GD, Pagliardini S (2020) Mapping of the excitatory, inhibitory, and modulatory afferent projections to the anatomically defined active expiratory oscillator in adult male rats. Journal of Comparative Neurology 29:5806.

Bilmen JG, Wootton LL, Michelangeli F (2002) The mechanism of inhibition of the sarco/endoplasmic reticulum Ca2+ ATPase by paxilline. Arch Biochem Biophys 406:55–64.

Bissonnette JM, Hohimer RA, Chao CR, Knopp SJ, Notoroberto NF (1990) Theophylline Stimulates Fetal Breathing Movements during Hypoxia. Pediatr Res 28:83–86.

Bloodgood BL, Sabatini BL (2007) Nonlinear regulation of unitary synaptic signals by CaV(2.3) voltage-sensitive calcium channels located in dendritic spines. Neuron 53:249–260.

Bochorishvili G, Stornetta RL, Coates MB, Guyenet PG (2012) Pre-Bötzinger complex receives glutamatergic innervation from galaninergic and other retrotrapezoid nucleus neurons. Journal of Comparative Neurology 520:1047–1061.

Boison D, Alexander SPH (2013) Adenosine Kinase: Exploitation for Therapeutic Gain Alexander SPH, ed. Pharmacol Rev 65:906–943.

Bolser DC, Davenport PW (2002) Functional organization of the central cough generation mechanism. Pulm Pharmacol Ther 15:221–225.

Borvendeg SJ, Gerevich Z, Gillen C, Illes P (2003) P2Y receptor-mediated inhibition of voltage-dependent Ca2+ channels in rat dorsal root ganglion neurons. Synapse 47:159–161.

Bouvier J, Thoby-Brisson M, Renier N, Dubreuil V, Ericson J, Champagnat J, Pierani A, Chédotal A, Fortin G (2010) Hindbrain interneurons and axon guidance signaling critical for breathing. Nat Neurosci 13:1066–1074.

Brockhaus J, Ballanyi K (2001) Synaptic inhibition in the isolated respiratory network of neonatal rats. Eur J Neurosci 10:3823–3839.

Brown DA, Filippov AK, Barnard EA (2000) Inhibition of potassium and calcium currents in neurones by molecularly-defined P2Y receptors. J Auton Nerv Syst 81:31–36.

Brown TG (1914) On the nature of the fundamental activity of the nervous centres; together with an analysis of the conditioning of rhythmic activity in progression, and a theory of the evolution of function in the nervous system. The Journal of Physiology 48:18–46.

Burnstock G (2018) Purine and purinergic receptors. Brain Neurosci Adv 2:1–10

Burr D, Sinclair JD (1988) The effect of adenosine on respiratory chemosenstivity in the awake rat. Respiration Physiology 72:47–57.

Büsselberg D, Bischoff AM, Richter DW (2003) A combined blockade of glycine and calcium-dependent potassium channels abolishes the respiratory rhythm. NSC 122:831–841.

Chandaka GK, Salzer I, Drobny H, Boehm S, Schicker KW (2011) Facilitation of transmitter release from rat sympathetic neurons via presynaptic P2Y1 receptors. British Journal of Pharmacology 164:1522–1533.

Chen X, Kovalchuk Y, Adelsberger H, Henning HA, Sausbier M, Wietzorrek G, Ruth P, Yarom Y, Konnerth A (2010) Disruption of the olivo-cerebellar circuit by Purkinje neuron-specific ablation of BK channels. Proceedings of the National Academy of Sciences 107:12323–12328.

Contet C, Goulding SP, Kuljis DA, Barth AL (2016) BK Channels in the Central Nervous System. Int Rev Neurobiol 128:281–342.

Coppi E, Pedata F, Gibb AJ (2012) P2Y 1receptor modulation of Ca 2+-activated K +currents in medium-sized neurons from neonatal rat striatal slices. Journal of Neurophysiology 107:1009–1021.

Cui Y, Kam K, Sherman D, Janczewski WA, Zheng Y, Feldman JL (2016) Defining preBötzinger Complex Rhythm- and Pattern-Generating Neural Microcircuits In Vivo. Neuron 91:602–614.

Del Negro CA, Funk GD, Feldman JL (2018) Breathing matters. Nat Rev Neurosci 19:351–367.

Del Negro CA, Koshiya N, Robert J Butera J, Smith JC (2002) Persistent Sodium Current, Membrane Properties and Bursting Behavior of Pre-Bötzinger Complex Inspiratory Neurons In Vitro. Journal of Neurophysiology 88:2242–2250.

Del Negro CA, Morgado-Valle C, Hayes JA, Mackay DD, Pace RW, Crowder EA, Feldman JL (2005) Sodium and calcium current-mediated pacemaker neurons and respiratory rhythm generation. Journal of Neuroscience 25:446–453.

del Puerto A, Díaz-Hernández J-I, Tapia M, Gómez-Villafuertes R, Benitez MJ, Zhang J, Miras-Portugal MT, Wandosell F, Díaz-Hernández M, Garrido JJ (2012) Adenylate cyclase 5 coordinates the action of ADP, P2Y1, P2Y13 and ATP-gated P2X7 receptors on axonal elongation. J Cell Sci 125:176–188.

Deng P, Pang Z-P, Lei Z, Shikano S, Xiong Q, Harvey BK, London B, Wang Y, Li M, Xu ZC (2011) Up-Regulation of A-Type Potassium Currents Protects Neurons Against Cerebral Ischemia. J Cereb Blood Flow Metab 31:1823–1835.

DePuy SD, Kanbar R, Coates MB, Stornetta RL, Guyenet PG (2011) Control of Breathing by Raphe Obscurus Serotonergic Neurons in Mice. J Neurosci 31:1981–1990.

Doble A (1996) The pharmacology and mechanism of action of riluzole. Neurology 47:233S–241S.

Parkinson F, L Damaraju V, Graham K, Y M Yao S, A Baldwin S, E Cass C, D Young J (2011) Molecular Biology of Nucleoside Transporters and their Distributions and Functions in the Brain. CTMC 11:948–972.

Eldridge FL, Millhorn DE, Kiley JP (1984) Respiratory effects of a long-acting analog of adenosine. Brain Research 301:273–280.

Eldridge FL, Millhorn DE, Kiley JP (1985) Antagonism by theophylline of respiratory inhibition induced by adenosine. Journal of Applied Physiology 59:1428–1433.

Elnazir B, Marshall JM, Kumar P (1996) Postnatal development of the pattern of respiratory and cardiovascular response to systemic hypoxia in the piglet: the roles of adenosine. The Journal of Physiology 492:573–585.

Faber ESL, Delaney AJ, Sah P (2005) SK channels regulate excitatory synaptic transmission and plasticity in the lateral amygdala. Nat Neurosci 8:635–641.

Feldman JL, Del Negro CA (2006) Looking for inspiration: new perspectives on respiratory rhythm. Nat Rev Neurosci 7:232–241.

Feldman JL, Del Negro CA, Gray PA (2013) Understanding the Rhythm of Breathing: So Near, Yet So Far. Annu. Rev. Physiol 75:423–452.

Feldman JL, Smith JC (1989) Cellular mechanisms underlying modulation of breathing pattern in mammals. Annals of the New York Academy of Sciences 563:114–130.

Ferreira-Neto HC, Biancardi VC, Stern JE (2017) A reduction in SK channels contributes to increased activity of hypothalamic magnocellular neurons during heart failure. The Journal of Physiology 595:6429–6442.

Filippov AK, Brown DA, Barnard EA (2000) The P2Y1 receptor closes the N-type Ca2+ channel in neurones, with both adenosine triphosphates and diphosphates as potent agonists. British Journal of Pharmacology 129:1063–1066.

Filippov AK, Choi RCY, Simon J, Barnard EA, Brown DA (2006) Activation of P2Y1 nucleotide receptors induces inhibition of the M-type K+ current in rat hippocampal pyramidal neurons. Journal of Neuroscience 26:9340–9348.

Filippov AK, Fernández-Fernández JM, Marsh SJ, Simon J, Barnard EA, Brown DA (2004) Activation and inhibition of neuronal G protein-gated inwardly rectifying K(+) channels by P2Y nucleotide receptors. Molecular Pharmacology 66:468–477.

Fortuna MG, West GH, Stornetta RL, Guyenet PG (2008) Bötzinger Expiratory-Augmenting Neurons and the Parafacial Respiratory Group. J Neurosci 28:2506–2515.

Funk GD (2013) Neuromodulation: purinergic signaling in respiratory control. Compr Physiol 3:331–363.

Funk GD, Smith JC, Feldman JL (1993) Generation and transmission of respiratory oscillations in medullary slices: role of excitatory amino acids. Journal of Neurophysiology.

Gallego D, Hernández P, Clavé P, Jiménez M (2006) P2Y1 receptors mediate inhibitory purinergic neuromuscular transmission in the human colon. American Journal of Physiology-Gastrointestinal and Liver Physiology 291:G584–G594.

Gerevich Z, Borvendeg SJ, Schröder W, Franke H, Wirkner K, Nörenberg W, Fürst S, Gillen C, Illes P (2004) Inhibition of N-type voltage-activated calcium channels in rat dorsal root ganglion neurons by P2Y receptors is a possible mechanism of ADP-induced analgesia. Journal of Neuroscience 24:797–807.

Gestreau C, Heitzmann D, Thomas J, Dubreuil V, Bandulik S, Reichold M, Bendahhou S, Pierson P, Sterner C, Peyronnet-Roux J, Benfriha C, Tegtmeier I, Ehnes H, Georgieff M, Lesage F, Brunet J-F, Goridis C, Warth R, Barhanin J (2010) Task2 potassium channels set central respiratory CO2 and O2 sensitivity. Proc Natl Acad Sci USA 107:2325–2330.

Gonçalves J, Queiroz G (2008) Presynaptic adenosine and P2Y receptors. Handb Exp Pharmacol:339–372.

Gourine AV, Atkinson L, Deuchars J, Spyer KM (2003) Purinergic Signalling in the Medullary Mechanisms of Respiratory Control in the Rat: Respiratory Neurones Express the P2X2 Receptor Subunit. The Journal of Physiology 552:197–211.

Gourine AV, Kasymov V, Marina N, Tang F, Figueiredo MF, Lane S, Teschemacher AG, Spyer KM, Deisseroth K, Kasparov S (2010) Astrocytes Control Breathing Through pH-Dependent Release of ATP. Science 329:571–575.

Gourine AV, Llaudet E, Dale N, Spyer KM (2005a) ATP is a mediator of chemosensory transduction in the central nervous system. Nature 436:108–111.

Gourine AV, Llaudet E, Dale N, Spyer KM (2005b) Release of ATP in the Ventral Medulla during Hypoxia in Rats: Role in Hypoxic Ventilatory Response. J Neurosci 25:1211–1218.

Gray PA, Hayes JA, Ling GY, Llona I, Tupal S, Picardo MCD, Ross SE, Hirata T, Corbin JG, Eugenín J, Del Negro CA (2010) Developmental Origin of PreBötzinger Complex Respiratory Neurons. J Neurosci 30:14883–14895.

Gray PA, Janczewski WA, Mellen N, McCrimmon DR, Feldman JL (2001) Normal breathing requires preBötzinger complex neurokinin-1 receptor-expressing neurons. Nat Neurosci 4:927–930.

Gray PA, Rekling JC, Bocchiaro CM, Feldman JL (1999a) Modulation of Respiratory Frequency by Peptidergic Input to Rhythmogenic Neurons in the PreBötzinger Complex. Science 286:1566–1568.

Greer JJ, Smith JC, Feldman JL (1991) Role of excitatory amino acids in the generation and transmission of respiratory drive in neonatal rat. The Journal of Physiology 437:727–749.

Gu QD, Joe DS, Gilbert CA (2017) Activation of bitter taste receptors in pulmonary nociceptors sensitizes TRPV1 channels through the PLC and PKC signaling pathway. Am J Physiol Lung Cell Mol Physiol 312:L326–L333.

Guinamard R, Simard C, Del Negro C (2013) Flufenamic acid as an ion channel modulator. Pharmacology and Therapeutics 138:272–284.

Guyenet PG, Bayliss DA (2015) Neural Control of Breathing and CO2 Homeostasis. Neuron 87:946–961.

Guyenet PG, Bayliss DA, Stornetta RL, Kanbar R, Shi Y, Holloway BB, Souza GMPR, Basting TM, Abbott SBG, Wenker IC (2018) Interdependent feedback regulation of breathing by the carotid bodies and the retrotrapezoid nucleus. The Journal of Physiology 596:3029–3042.

Guyenet PG, Mulkey DK, Stornetta RL, Bayliss DA (2005) Regulation of ventral surface chemoreceptors by the central respiratory pattern generator. Journal of Neuroscience 25:8938–8947.

Guyenet PG, Stornetta RL, Bayliss DA (2010) Central respiratory chemoreception. Journal of Comparative Neurology 518:3883–3906.

Guyenet PG, Stornetta RL, Souza GMPR, Abbott SBG, Shi Y, Bayliss DA (2019) The Retrotrapezoid Nucleus: Central Chemoreceptor and Regulator of Breathing Automaticity. Trends in Neurosciences 42:807–824.

Guzman SJ, Gerevich Z, Hengstler JG, Illes P, Kleemann W (2005) P2Y1 receptors inhibit both strength and plasticity of glutamatergic synaptic neurotransmission in the rat prefrontal cortex. Synapse 57:235–238.

Hawryluk JM, Moreira TS, Takakura AC, Wenker IC, Tzingounis AV, Mulkey DK (2012) KCNQ Channels Determine Serotonergic Modulation of Ventral Surface Chemoreceptors and Respiratory Drive. J Neurosci 32:16943–16952.

Herlenius E, Lagercrantz H, Yamamoto Y (1997) Adenosine Modulates Inspiratory Neurons and the Respiratory Pattern in the Brainstem of Neonatal Rats. Pediatr Res 42:46–53.

Hu B, Boyle CA, Lei S (2020) Oxytocin receptors excite lateral nucleus of central amygdala by phospholipase Cβ- and protein kinase C-dependent depression of inwardly rectifying K+ channels. The Journal of Physiology 598:3501–3520.

Huckstepp RT, Henderson LE, Cardoza KP, Feldman JL (2016) Interactions between respiratory oscillators in adult rats. Elife 5:5613.

Huckstepp RTR, Bihi RI, Eason R, Spyer KM, Dicke N, Willecke K, Marina N, Gourine AV, Dale N (2010) Connexin hemichannel-mediated CO2-dependent release of ATP in the medulla oblongata contributes to central respiratory chemosensitivity. The Journal of Physiology 588:3901–3920.

Huckstepp RTR, Cardoza KP, Henderson LE, Feldman JL (2015) Role of Parafacial Nuclei in Control of Breathing in Adult Rats. J Neurosci 35:1052–1067.

Huxtable AG, Zwicker JD, Alvares TS, Ruangkittisakul A, Fang X, Hahn LB, de Chaves EP, Baker GB, Ballanyi K, Funk GD (2010) Glia Contribute to the Purinergic Modulation of Inspiratory Rhythm-Generating Networks. J Neurosci 30:3947–3958.

Huxtable AG, Zwicker JD, Poon BY, Pagliardini S, Vrouwe SQ, Greer JJ, Funk GD (2009) Tripartite purinergic modulation of central respiratory networks during perinatal development: the influence of ATP, ectonucleotidases, and ATP metabolites. Journal of Neuroscience 29:14713–14725.

Janczewski WA, Feldman JL (2006) Distinct rhythm generators for inspiration and expiration in the juvenile rat. The Journal of Physiology 570:407–420.

Janczewski WA, Tashima A, Hsu P, Cui Y, Feldman JL (2013) Role of inhibition in respiratory pattern generation. Journal of Neuroscience 33:5454–5465.

Johnson SM, Smith JC, Funk GD, Feldman JL (1994) Pacemaker behavior of respiratory neurons in medullary slices from neonatal rat. Journal of Neurophysiology 72:2598–2608.

Kawai A, Okada Y, Mückenhoff K, Scheid P (1995) Theophylline and hypoxic ventilatory response in the rat isolated brainstem-spinal cord. Respiration Physiology 100:25–32.

King AE, Ackley MA, Cass CE, Young JD, Baldwin SA (2006) Nucleoside transporters: from scavengers to novel therapeutic targets. Trends in Pharmacological Sciences 27:416–425.

Koch H, Zanella S, Elsen GE, Smith L, Doi A, Garcia AJ, Wei AD, Xun R, Kirsch S, Gomez CM, Hevner RF, Ramirez J-M (2013) Stable respiratory activity requires both P/Q-type and N-type voltage-gated calcium channels. Journal of Neuroscience 33:3633–3645.

Koizumi H, Koshiya N, Chia JX, Cao F, Nugent J, Zhang R, Smith JC (2013) Structural-functional properties of identified excitatory and inhibitory interneurons within pre-Botzinger complex respiratory microcircuits. Journal of Neuroscience 33:2994–3009.

Koizumi H, Mosher B, Tariq MF, Zhang R, Koshiya N, Smith JC (2016) Voltage-Dependent Rhythmogenic Property of Respiratory Pre-Bötzinger Complex Glutamatergic, Dbx1-Derived, and Somatostatin-Expressing Neuron Populations Revealed by Graded Optogenetic Inhibition. eNeuro 3(3)0081–16.2016.

Koos BJ, Kawasaki Y, Kim Y-H, Bohorquez F (2005) Adenosine A2A-receptor blockade abolishes the roll-off respiratory response to hypoxia in awake lambs. American Journal of Physiology - Regulatory, Integrative and Comparative Physiology 288:R1185–R1194.

Koos BJ, Mason BA, Punla O, Adinolfi AM (1994) Hypoxic inhibition of breathing in fetal sheep: relationship to brain adenosine concentrations. Journal of Applied Physiology. 77:2734–2739

Koos BJ, Matsuda K (1990) Fetal breathing, sleep state, and cardiovascular responses to adenosine in sheep. Journal of Applied Physiology 68:489–495.

Koshiya N, Smith JC (1999) Neuronal pacemaker for breathing visualized in vitro. Nature 400:360–363.

Kshatri AS, Gonzalez-Hernandez A, Giraldez T (2018) Physiological Roles and Therapeutic Potential of Ca2+ Activated Potassium Channels in the Nervous System. Front Mol Neurosci 11.

Kumar NN et al. (2015) Regulation of breathing by CO2 requires the proton-activated receptor GPR4 in retrotrapezoid nucleus neurons. Science 348:1255–1260.

Kuwana S-I, Tsunekawa N, Yanagawa Y, Okada Y, Kuribayashi J, Obata K (2006) Electrophysiological and morphological characteristics of GABAergic respiratory neurons in the mouse pre-Bötzinger complex. Eur J Neurosci 23:667–674.

Lagercrantz H, Yamamoto Y, Fredholm BB, Prabhakar NR, Euler von C (1984) Adenosine Analogues Depress Ventilation in Rabbit Neonates. Theophylline Stimulation of Respiration via Adenosine Receptors? Pediatr Res 18:387–390.

Leonard EM, Salman S, Nurse CA (2018) Sensory Processing and Integration at the Carotid Body Tripartite Synapse: Neurotransmitter Functions and Effects of Chronic Hypoxia. Front Physiol 9:225.

Li H-S, Xu X-ZS, Montell C (1999) Activation of a TRPC3-Dependent Cation Current through the Neurotrophin BDNF. Neuron 24:261–273.

Li P, Janczewski WA, Yackle K, Kam K, Pagliardini S, Krasnow MA, Feldman JL (2016) The peptidergic control circuit for sighing. Nature 530:293–297.

Lieske SP, Ramirez J-M (2006) Pattern-specific synaptic mechanisms in a multifunctional network. I. Effects of alterations in synapse strength. Journal of Neurophysiology 95:1323–1333.

Long WQ, Anthonisen NR (1994) Aminophylline partially blocks ventilatory depression with hypoxia in the awake cat. Can J Physiol Pharmacol 72:673–678.

Lopes JM, Davis GM, Mullahoo K, Aranda JV (1994) Role of adenosine in the hypoxic ventilatory response of the newborn piglet. Pediatr Pulmonol 17:50–55.

Lorier AR, Huxtable AG, Robinson DM, Lipski J, Housley GD, Funk GD (2007) P2Y1 Receptor Modulation of the Pre-Bötzinger Complex Inspiratory Rhythm Generating Network In Vitro. J Neurosci 27:993–1005.

Lorier AR, Lipski J, Housley GD, Greer JJ, Funk GD (2008) ATP sensitivity of preBötzinger complex neurones in neonatal rat in vitro: mechanism underlying a P2 receptor-mediated increase in inspiratory frequency. The Journal of Physiology 586:1429–1446.

Luthardt J, Borvendeg SJ, Sperlágh B, Poelchen W, Wirkner K, Illes P (2003) P2Y(1) receptor activation inhibits NMDA receptor-channels in layer V pyramidal neurons of the rat prefrontal and parietal cortex. Neurochem Int 42:161–172.

Mader F, Krause L, Tokay T, Hakenberg OW, Köhling R, Kirschstein T (2016) P2Y receptor-mediated transient relaxation of rat longitudinal ileum preparations involves phospholipase C activation, intracellular Ca 2+ release and SK channel activation. Acta Pharmacol Sin 37:617–628.

Marchenko V, Koizumi H, Mosher B, Koshiya N, Tariq MF, Bezdudnaya TG, Zhang R, Molkov YI, Rybak IA, Smith JC (2016) Perturbations of Respiratory Rhythm and Pattern by Disrupting Synaptic Inhibition within Pre-Bötzinger and Bötzinger Complexes. eNeuro 3:ENEURO.0011–16.

Martin RJ, Abu-Shaweesh JM, (2005) Control of breathing and neonatal apnea. Biol. Neonate 87:288–295.

Matschke LA, Rinné S, Snutch TP, Oertel WH, Dolga AM, Decher N (2018) Calcium-activated SK potassium channels are key modulators of the pacemaker frequency in locus coeruleus neurons. Molecular and Cellular Neuroscience 88:330–341.

Meredith AL, Wiler SW, Miller BH, Takahashi JS, Fodor AA, Ruby NF, Aldrich RW (2006) BK calcium-activated potassium channels regulate circadian behavioral rhythms and pacemaker output. Nat Neurosci 9:1041–1049.

Mironov SL, Richter DW (2000) Hypoxic modulation of L-type Ca2+ channels in inspiratory brainstem neurones: Intracellular signalling pathways and metabotropic glutamate receptors. Brain Research 869:166–177.

Montandon G, Liu H, Horner RL (2016a) Contribution of the respiratory network to rhythm and motor output revealed by modulation of GIRK channels, somatostatin and neurokinin-1 receptors. Sci Rep 6:1–15.

Montandon G, Qin W, Liu H, Ren J, Greer JJ, Horner RL (2011) PreBotzinger complex neurokinin-1 receptor-expressing neurons mediate opioid-induced respiratory depression. Journal of Neuroscience 31:1292–1301.

Montandon G, Ren J, Victoria NC, Liu H, Wickman K, Greer JJ, Horner RL (2016b) G-protein-gated Inwardly Rectifying Potassium Channels Modulate Respiratory Depression by Opioids. Anesthesiology 124:641–650.

Morgado-Valle C, Baca SM, Feldman JL (2010) Glycinergic Pacemaker Neurons in PreBötzinger Complex of Neonatal Mouse. J Neurosci 30:3634–3639.

Moss IR (2000) Respiratory responses to single and episodic hypoxia during development: mechanisms of adaptation. Respiration Physiology 121:185–197.

Mulkey DK, Stornetta RL, Weston MC, Simmons JR, Parker A, Bayliss DA, Guyenet PG (2004a) Respiratory control by ventral surface chemoreceptor neurons in rats. Nat Neurosci 7:1360–1369.

Mulkey DK, Stornetta RL, Weston MC, Simmons JR, Parker A, Bayliss DA, Guyenet PG (2004b) Respiratory control by ventral surface chemoreceptor neurons in rats. Nat Neurosci 7:1360–1369.

Mulkey DK, Talley EM, Stornetta RL, Siegel AR, West GH, Chen X, Sen N, Mistry AM, Guyenet PG, Bayliss DA (2007) TASK Channels Determine pH Sensitivity in Select Respiratory Neurons But Do Not Contribute to Central Respiratory Chemosensitivity. J Neurosci 27:14049–14058.

Nattie E, Li A (2009) Central chemoreception is a complex system function that involves multiple brain stem sites. Journal of Applied Physiology 106:1464–1466.

Neylon CB, Nurgali K, Hunne B, Robbins HL, Moore S, Chen MX, Furness JB (2004) Intermediate-conductance calcium-activated potassium channels in enteric neurones of the mouse: pharmacological, molecular and immunochemical evidence for their role in mediating the slow afterhyperpolarization. J Neurochem 90:1414–1422.

Ngo-Anh TJ, Bloodgood BL, Lin M, Sabatini BL, Maylie J, Adelman JP (2005) SK channels and NMDA receptors form a Ca 2+ -mediated feedback loop in dendritic spines. Nat Neurosci 8:642–649.

Onimaru H, Ballanyi K, Homma I (2003a) Contribution of Ca2+-dependent conductances to membrane potential fluctuations of medullary respiratory neurons of newborn rats in vitro. The Journal of Physiology 552:727–741.

Onimaru H, Homma I (2003b) A Novel Functional Neuron Group for Respiratory Rhythm Generation in the Ventral Medulla. J Neurosci 23:1478–1486.

Onimaru H, Ikeda K, Kawakami K (2008) CO2-Sensitive Preinspiratory Neurons of the Parafacial Respiratory Group Express Phox2b in the Neonatal Rat. J Neurosci 28:12845–12850.

Pagliardini S, Ren J, Greer JJ (2003) Ontogeny of the Pre-Bötzinger Complex in Perinatal Rats. J Neurosci 23:9575–9584.

Pagliardini S, Adachi T, Ren J, Funk GD, Greer JJ (2005) Fluorescent Tagging of Rhythmically Active Respiratory Neurons within the Pre-Bötzinger Complex of Rat Medullary Slice Preparations. J Neurosci 25:2591–2596.

Pagliardini S, Janczewski WA, Tan W, Dickson CT, Deisseroth K, Feldman JL (2011) Active expiration induced by excitation of ventral medulla in adult anesthetized rats. Journal of Neuroscience 31:2895–2905.

Pankratov Y, Lalo U, Krishtal OA, Verkhratsky A (2009) P2X receptors and synaptic plasticity. NSC 158:137–148.

Pascual O, Ben Achour S, Rostaing P, Triller A, Bessis A (2012) Microglia activation triggers astrocyte-mediated modulation of excitatory neurotransmission. Proc Natl Acad Sci USA 109:E197–E205.

Peng Y-J, Makarenko VV, Gridina A, Chupikova I, Zhang X, Kumar GK, Fox AP, Prabhakar NR (2019) H2S mediates carotid body response to hypoxia but not anoxia. Respiratory Physiology & Neurobiology 259:75–85.

Peng Y-J, Nanduri J, Raghuraman G, Souvannakitti D, Gadalla MM, Kumar GK, Snyder SH, Prabhakar NR (2010) H2S mediates O2 sensing in the carotid body. Proceedings of the National Academy of Sciences 107:10719–10724.

Picardo MCD, Weragalaarachchi KTH, Akins VT, Del Negro CA (2013) Physiological and morphological properties of Dbx1-derived respiratory neurons in the pre-Bötzinger complex of neonatal mice. The Journal of Physiology 591:2687–2703.

Pisanski A, Ding X, Koch NA, Pagliardini S (2020) Chemogenetic modulation of the parafacial respiratory group influences the recruitment of abdominal activity during REM sleep. Sleep 43:351.

Piskuric NA, Nurse CA (2012) Effects of chemostimuli on [Ca2+]i responses of rat aortic body type I cells and endogenous local neurons: comparison with carotid body cells. The Journal of Physiology 590:2121–2135.

Pitts T (2014) Airway protective mechanisms. Lung 192:27–31.

Pitts T, Morris K, Lindsey B, Davenport P, Poliacek I, Bolser D (2012) Co-ordination of cough and swallow in vivo and in silico. Exp Physiol 97:469–473.

Prabhakar NR (2013) Sensing hypoxia: physiology, genetics and epigenetics. The Journal of Physiology 591:2245–2257.

Prabhakar NR (2016) O2 and CO2 Detection by the Carotid and Aortic Bodies. In: Chemosensory Transduction, pp 321–338. Academic Press.

Pusch M, Neher E (1988) Rates of diffusional exchange between small cells and a measuring patch pipette. Pflugers Arch 411:204-211.

Rajani V, Zhang Y, Jalubula V, Rancic V, SheikhBahaei S, Zwicker JD, Pagliardini S, Dickson CT, Ballanyi K, Kasparov S, Gourine AV, Funk GD (2018) Release of ATP by pre-Bötzinger complex astrocytes contributes to the hypoxic ventilatory response via a Ca2+ -dependent P2Y1 receptor mechanism. The Journal of Physiology 596:3245–3269.

Rajani V, Zhang Y, Revill AL, Funk GD (2016) The role of P2Y1 receptor signaling in central respiratory control. Respiratory Physiology & Neurobiology 226:3–10.

Ramirez J-M, Baertsch NA (2018) The Dynamic Basis of Respiratory Rhythm Generation: One Breath at a Time. Annu Rev Neurosci 41:475–499.

Ramirez JM, Quellmalz UJA, Wilken B, Richter DW (1998) The hypoxic response of neurones within the in vitro mammalian respiratory network. The Journal of Physiology 507:571–582.

Reklow RJ, Alvares TS, Zhang Y, Miranda Tapia AP, Biancardi V, Katzell AK, Frangos SM, Hansen MA, Toohey AW, Cass CE, Young JD, Pagliardini S, Boison D, Funk GD (2019) The Purinome and the preBötzinger Complex - A Ménage of Unexplored Mechanisms That May Modulate/Shape the Hypoxic Ventilatory Response. Front Cell Neurosci 13:365.

Richter DW (1982) Generation and maintenance of the respiratory rhythm. Journal of Experimental Biology 100:93–107.

Richter DW, Ballantyne D, Remmers JE (1986) How Is the Respiratory Rhythm Generated? A Model. Physiology 1:109–112.

Richter DW, Heyde F, Gabriel M (1975) Intracellular recordings from different types of medullary respiratory neurons of the cat. Journal of Neurophysiology 38:1162–1171.

Richter DW, Schmidt-Garcon P, Pierrefiche O, Bischoff AM, Lalley PM (1999) Neurotransmitters and neuromodulators controlling the hypoxic respiratory response in anaesthetized cats. The Journal of Physiology 514:567–578.

Robert J Butera J, Rinzel J, Smith JC (1999) Models of Respiratory Rhythm Generation in the Pre-Bötzinger Complex. I. Bursting Pacemaker Neurons. Journal of Neurophysiology 82:382–397.

Rong W, Gourine AV, Cockayne DA, Xiang Z, Ford APDW, Spyer KM, Burnstock G (2003) Pivotal role of nucleotide P2X2 receptor subunit of the ATP-gated ion channel mediating ventilatory responses to hypoxia. Journal of Neuroscience 23:11315–11321.

Ruangkittisakul A, Schwarzacher SW, Secchia L, Poon BY, Ma Y, Funk GD, Ballanyi K (2006) High Sensitivity to Neuromodulator-Activated Signaling Pathways at Physiological [K+] of Confocally Imaged Respiratory Center Neurons in On-Line-Calibrated Newborn Rat Brainstem Slices. J Neurosci 26:11870–11880.

Ruffault P-L, D'Autréaux F, Hayes JA, Nomaksteinsky M, Autran S, Fujiyama T, Hoshino M, Hägglund M, Kiehn O, Brunet J-F, Fortin G, Goridis C (2015) The retrotrapezoid nucleus neurons expressing Atoh1 and Phox2b are essential for the respiratory response to CO_2. Elife 4:16410.

Runold M, Lagercrantz H, Prabhakar NR, Fredholm BB (1989) Role of adenosine in hypoxic ventilatory depression. Journal of Applied Physiology 67:541–546.

Saitow F, Murakoshi T, Suzuki H, Konishi S (2005) Metabotropic P2Y Purinoceptor-Mediated Presynaptic and Postsynaptic Enhancement of Cerebellar GABAergic Transmission. J Neurosci 25:2108–2116.

Sanchez M, McManus OB (1996) Paxilline inhibition of the alpha-subunit of the high-conductance calcium-activated potassium channel. Neuropharmacology 35:963–968.

Sausbier M, Hu H, Arntz C, Feil S, Kamm S, Adelsberger H, Sausbier U, Sailer CA, Feil R, Hofmann F, Korth M, Shipston MJ, Knaus HG, Wolfer DP, Pedroarena CM, Storm JF, Ruth P (2004) Cerebellar ataxia and Purkinje cell dysfunction caused by Ca2+-activated K+ channel deficiency. Proceedings of the National Academy of Sciences 101:9474–9478.

Schicker KW, Chandaka GK, Geier P, Kubista H, Boehm S (2010) P2Y1 receptors mediate an activation of neuronal calcium-dependent K+ channels. The Journal of Physiology 588:3713–3725.

Schmid K, Foutz AS, Denavit-Saubié M (1996) Inhibitions mediated by glycine and GABAA receptors shape the discharge pattern of bulbar respiratory neurons. Brain Research 710:150–160.

Schmidt B, Anderson PJ, Doyle LW, Dewey D, Grunau RE, Asztalos EV, Davis PG, Tin W, Moddemann D, Solimano A, Ohlsson A, Barrington KJ, Roberts RS, Caffeine for Apnea of Prematurity (CAP) Trial Investigators (2012) Survival without disability to age 5 years after neonatal caffeine therapy for apnea of prematurity. JAMA 307:275–282.

Schmidt B, Roberts RS, Davis P, Doyle LW, Barrington KJ, Ohlsson A, Solimano A, Tin W (2009) Long-Term Effects of Caffeine Therapy for Apnea of Prematurity. 357:1893–1902.

Schmidt B, Roberts RS, of PDEJ (2006) Caffeine therapy for apnea of prematurity. Mass Medical Soc. 3454:2112–2121.

Schmidt C, Bellingham MC, Richter DW (1995) Adenosinergic modulation of respiratory neurones and hypoxic responses in the anaesthetized cat. The Journal of Physiology 483:769–781.

Schulz R, Kirschstein T, Brehme H, Porath K, Mikkat U, Köhling R (2012) Network excitability in a model of chronic temporal lobe epilepsy critically depends on SK channel-mediated AHP currents. Neurobiology of Disease 45:337–347.

Shao XM, Feldman JL (1997) Respiratory Rhythm Generation and Synaptic Inhibition of Expiratory Neurons in Pre-Bötzinger Complex: Differential Roles of Glycinergic and GABAergic Neural Transmission. Journal of Neurophysiology 77:1853–1860.

SheikhBahaei S, Turovsky EA, Hosford PS, Hadjihambi A, Theparambil SM, Liu B, Marina N, Teschemacher AG, Kasparov S, Smith JC, Gourine AV (2018) Astrocytes modulate brainstem respiratory rhythm-generating circuits and determine exercise capacity. Nat Commun 9:1–10.

Sherman D, Worrell JW, Cui Y, Feldman JL (2015) Optogenetic perturbation of preBötzinger complex inhibitory neurons modulates respiratory pattern. Nat Neurosci 18:408–414.

Shipston MJ (2018) Control of anterior pituitary cell excitability by calcium-activated potassium channels. Molecular and Cellular Endocrinology 463:37–48.

Sickmann T, Klose A, Huth T, Alzheimer C (2008) Unexpected suppression of neuronal G protein-activated, inwardly rectifying K+ current by common phospholipase C inhibitor. Neuroscience Letters 436:102–106.

Smith JC, Abdala APL, Borgmann A, Rybak IA, Paton JFR (2013) Brainstem respiratory networks: building blocks and microcircuits. Trends in Neurosciences 36:152–162.

Smith JC, Ellenberger HH, Ballanyi K, Richter DW, Feldman JL (1991) Pre-Botzinger complex: a brainstem region that may generate respiratory rhythm in mammals. Science 254:726–729.

Smith JC, Feldman JL (1987) In vitro brainstem-spinal cord preparations for study of motor systems for mammalian respiration and locomotion. Journal of Neuroscience Methods 21:321–333.

Sobrinho CR, Wenker IC, Poss EM, Takakura AC, Moreira TS, Mulkey DK (2014) Purinergic signalling contributes to chemoreception in the retrotrapezoid nucleus but not the nucleus of the solitary tract or medullary raphe. The Journal of Physiology 592:1309–1323.

Solomon IC (2005) Glutamate Neurotransmission Is Not Required for, But May Modulate, Hypoxic Sensitivity of Pre-Bötzinger Complex In Vivo. Journal of Neurophysiology 93:1278–1284.

Solomon IC, Edelman NH, Neubauer JA (2000) Pre-Bötzinger Complex Functions as a Central Hypoxia Chemosensor for Respiration In Vivo. Journal of Neurophysiology 83:2854–2868.

Stemkowski PL, Tse FW, Peuckmann V, Ford CP, Colmers WF, Smith PA (2002) ATP-Inhibition of M Current in Frog Sympathetic Neurons Involves Phospholipase C But Not Ins P(3), Ca(2+), PKC, or Ras. J Neurophysiol 88:277-288.

Stocker M, Pedarzani P (2000) Differential Distribution of Three Ca2+-Activated K+ Channel Subunits, SK1, SK2, and SK3, in the Adult Rat Central Nervous System. Molecular and Cellular Neuroscience 15:476–493.

Stornetta RL, Moreira TS, Takakura AC, Kang BJ, Chang DA, West GH, Brunet J-F, Mulkey DK, Bayliss DA, Guyenet PG (2006) Expression of Phox2b by Brainstem Neurons Involved in Chemosensory Integration in the Adult Rat. J Neurosci 26:10305–10314.

Stornetta RL, Rosin DL, Wang H, Sevigny CP, Weston MC, Guyenet PG (2003) A group of glutamatergic interneurons expressing high levels of both neurokinin-1 receptors and somatostatin identifies the region of the pre-Bötzinger complex. J Comp Neurol 455:499–512.

Suzue T (1984) Respiratory rhythm generation in the in vitro brain stem-spinal cord preparation of the neonatal rat. The Journal of Physiology 354:173–183.

Tan W, Janczewski WA, Yang P, Shao XM, Callaway EM, Feldman JL (2008) Silencing preBötzinger Complex somatostatin-expressing neurons induces persistent apnea in awake rat. Nat Neurosci 11:538–540.

Tan Z, Liu Y, Xi W, Lou H-F, Zhu L, Guo Z, Mei L, Duan S (2017) Glia-derived ATP inversely regulates excitability of pyramidal and CCK-positive neurons. Nat Commun 8:1–14.

Thoby-Brisson M, Karlén M, Wu N, Charnay P, Champagnat J, Fortin G (2009) Genetic identification of an embryonic parafacial oscillator coupling to the preBötzinger complex. 12:1028–1035

Thoby-Brisson M, Ramirez J-M (2000) Role of Inspiratory Pacemaker Neurons in Mediating the Hypoxic Response of the Respiratory Network In Vitro. J Neurosci 20:5858–5866.

Tse A, Yan L, Lee AK, Tse FW (2012) Autocrine and paracrine actions of ATP in rat carotid body. Can J Physiol Pharmacol 90:705–711.

Vann NC, Pham FD, Dorst KE, Del Negro CA (2018) Dbx1 Pre-Bötzinger Complex Interneurons Comprise the Core Inspiratory Oscillator for Breathing in Unanesthetized Adult Mice. eNeuro 5(3) e0130-18.2018.

Vigil FA, Carver CM, Shapiro MS (2020) Pharmacological Manipulation of Kv7 Channels as a New Therapeutic Tool for Multiple Brain Disorders. Front Physiol 11:688.

Wallén-Mackenzie Å, Gezelius H, Thoby-Brisson M, Nygård A, Enjin A, Fujiyama F, Fortin G, Kullander K (2006) Vesicular Glutamate Transporter 2 Is Required for Central Respiratory Rhythm Generation But Not for Locomotor Central Pattern Generation. J Neurosci 26:12294–12307.

Wang H, Stornetta RL, Rosin DL, Guyenet PG (2001) Neurokinin-1 receptor-immunoreactive neurons of the ventral respiratory group in the rat. J Comp Neurol 434:128–146.

Wang S, Benamer N, Zanella S, Kumar NN, Shi Y, Bévengut M, Penton D, Guyenet PG, Lesage F, Gestreau C, Barhanin J, Bayliss DA (2013) TASK-2 Channels Contribute to pH Sensitivity of Retrotrapezoid Nucleus Chemoreceptor Neurons. J Neurosci 33:16033–16044.

Wang X, Hayes JA, Revill AL, Song H, Kottick A, Vann NC, LaMar MD, Picardo MCD, Akins VT, Funk GD, Del Negro CA (2014) Laser ablation of Dbx1 neurons in the pre-Bötzinger complex stops inspiratory rhythm and impairs output in neonatal mice. Elife 3:e03427.

Weese-Mayer DE, Berry-Kravis EM, Ceccherini I, Keens TG, Loghmanee DA, Trang H (2010) An Official ATS Clinical Policy Statement: Congenital Central Hypoventilation Syndrome. Am J Respir Crit Care Med 181:626–644.

Wei AD, Ramirez J-M (2019) Presynaptic Mechanisms and KCNQ Potassium Channels Modulate Opioid Depression of Respiratory Drive. Front Physiol 10:1407.

Wilson CG, Martin RJ, Jaber M, Abu-Shaweesh J, Jafri A, Haxhiu MA, Zaidi S (2004) Adenosine A2A receptors interact with GABAergic pathways to modulate respiration in neonatal piglets. Respiratory Physiology & Neurobiology 141:201–211.

Winter SM, Fresemann J, Schnell C, Oku Y, Hirrlinger J, Hülsmann S (2009) Glycinergic interneurons are functionally integrated into the inspiratory network of mouse medullary slices. Pflugers Arch 458:459–469.

Wu J, Capelli P, Bouvier J, Goulding M, Arber S, Fortin G (2017) A V0 core neuronal circuit for inspiration. Nat Commun 8:544–12.

Wu J, Ding W-G, Matsuura H, Horie M (2012) Regulatory mechanisms underlying the modulation of GIRK1/GIRK4 heteromeric channels by P2Y receptors. Pflugers Arch 463:625–633.

Xu J, Tse FW, Tse A (2003) ATP triggers intracellular Ca2+ release in type II cells of the rat carotid body. The Journal of Physiology 549:739–747.

Xu J, Xu F, Tse FW, Tse A (2005) ATP inhibits the hypoxia response in type I cells of rat carotid bodies. J Neurochem 92:1419–1430.

Yamamoto M, Nishimura M, Kobayashi S, Akiyama Y, Miyamoto K, Kawakami Y (1994) Role of endogenous adenosine in hypoxic ventilatory response in humans: a study with dipyridamole. Journal of Applied Physiology 76:196–203.

Yan S, Laferriere A, Zhang C, Moss IR (1995) Microdialyzed adenosine in nucleus tractus solitarii and ventilatory response to hypoxia in piglets. Journal of Applied Physiology 79:405–410.

Yang CF, Feldman JL (2018) Efferent projections of excitatory and inhibitory preBötzinger Complex neurons. Journal of Comparative Neurology 526:1389–1402.

Yang C-T, Hung S-Y, Hsu S-F, MacDonald I, Lin J-G, Luo S-T, Lin P-L, Chen Y-H (2019) Inhibiting the LPS-induced enhancement of mEPSC frequency in superficial dorsal horn neurons may serve as an electrophysiological model for alleviating pain. Sci Rep 9:16032–14.

Yang H, Zhang G, Cui J (2015) BK channels: multiple sensors, one activation gate. Front Physiol 6:29.

Yoshioka K, Hosoda R, Kuroda Y, Nakata H (2002) Hetero-oligomerization of adenosine A1 receptors with P2Y1 receptors in rat brains. FEBS Lett 531:299–303.

Zaika O, Tolstykh GP, JAFFE DB, Shapiro MS (2007) Inositol triphosphate-mediated Ca2+ signals direct purinergic P2Y receptor regulation of neuronal ion channels. Journal of Neuroscience 27:8914–8926.

Zavala-Tecuapetla C, Aguileta MA, Lopez-Guerrero JJ, González-Marín MC, Peña F (2008) Calcium-activated potassium currents differentially modulate respiratory rhythm generation. Eur J Neurosci 27:2871–2884.

Zhang J, Chen L, He Y, Ding Y, Zhou H, Hu H, Tang Y, Zheng Y (2010) Large-conductance calcium-activated potassium channels in the neurons of pre-Bötzinger complex and their participation in the regulation of central respiratory activity in neonatal rats. Neuroscience Letters 481:159–163.

Zhang Y, Gourine A, Kasparov S, Alvares T, Funk GD (2016a) ATP Excitation of the PreBötzinger Complex and Inspiratory Neurons in vitro is Mediated in Part via a PLC/IP3-mediated increase In [Ca2+]i. FASEB. Online.

Zhang Y, Gourine AV, Kasparov S, Alvares T, Funk GD (2016b) ATP excites the preBötzinger Complex network in vitro via activation of a Gαq-signaling pathway. SFN. San Diego. Online.

Zhang Y, Jaib AT, Gourine A, Kasparov S, Alvares T, Funk GD (2018) cAMP-dependent modulation of Ih underlies the P2Y1 receptor-mediated excitation of the preBötzinger Complex inspiratory network in vitro. SFN. San Diego. Online.

Zhao MG, Hülsmann S, Winter SM, Dutschmann M, Richter DW (2006) Calcium-regulated potassium currents secure respiratory rhythm generation after loss of glycinergic inhibition. Eur J Neurosci 24:145–154.

Zhou Y, Lingle CJ (2014) Paxilline inhibits BK channels by an almost exclusively closed-channel block mechanism. J Gen Physiol 144:415–440.

Zoccal DB, Silva JN, Barnett WH, Lemes EV, Falquetto B, Colombari E, Molkov YI, Moreira TS, Takakura AC (2018) Interaction between the retrotrapezoid nucleus and the parafacial respiratory group to regulate active expiration and sympathetic activity in rats. Am J Physiol Lung Cell Mol Physiol 315:L891–L909.

Zwicker JD, Rajani V, Hahn LB, Funk GD (2011) Purinergic modulation of preBötzinger complex inspiratory rhythm in rodents: the interaction between ATP and adenosine. The Journal of Physiology 589:4583–4600.

II. Chapter 2: Circuitry underlying NPY-induced stress resilience.

Publication disclosure

II Chapter 2. Circuitry underlying NPY-induced stress resilience.
All data included in this thesis Chapter represent my original work. Some of the data included in this Chapter have already been published in Michaelson et al., 2020, a paper on which I am second author. For clarity, I include below a complete list of the data that have been published by referring to specific figures and panels of the thesis and the published paper.

Data in "Figure 5: Effect of repeated BLA injections of a Y_1R agonist [F7, P34]NPY on anxiety-like behavior in the social interaction test" are published in Michaelson et al., 2020 (Fig. 10).

Capacitance measurements of the group treated with 100 nM cPP in "Figure 7J: Effect of repeated treatment with three concentrations of the Y_5R agonist [cPP(1-7),NPY(19-23),Ala31,Aib32, Gln34]hPP (cPP) on the passive resting properties of BLA OTC" are published in Michaelson et al., 2020 (Fig. 9).

Data in "Figure 8: Effect of the Y_5R agonist, cPP, on synaptic activity of BLA OTCs neurons" are published in Michaelson et al., 2020 (Fig. 7).

Measurements of Total dendritic length (A), number of branch points (B), sholl analysis (C) and number of 1^{st}, 2^{nd}, 3^{rd}, 4^{th} and 5^{th} order dendrites of the group treated with 100 nM cPP in "Figure 9: Morphometric analysis of BLA OTCs treated with the Y_5R agonist, cPP" are published in Michaelson et al., 2020 (Fig. 9).

Capacitance measurements of the group treated with NPY+Y_5R antagonist in "Figure 10J: Effect of the co-treatment of NPY and the Y_5R antagonist CGP71683A (CGP) on BLA OTC neurons" are published in Michaelson et al., 2020 (Fig. 9).

Measurements of Total dendritic length (A), sholl analysis (B), number of branch points (C) and number of 1^{st}, 2^{nd}, 3^{rd}, 4^{th} and 5^{th} order dendrites (D) of the group treated with NPY+Y_5R antagonist in "Figure 11: Morphometric analysis of BLA OTCs treated with NPY + Y_5R antagonist" are published in Michaelson et al., 2020 (Fig. 9).

Data in “Figure 12: Effect of repeated BLA injections of a Y_5R agonist on anxiety-like behavior” are published in Michaelson et al., 2020 (Fig 10).

Capacitance measurements in “Figure 13F: Effect of the Y_5R agonist cPP and NPY + Y_5R antagonist on passive properties of BLA pyramidal neurons” are published in Michaelson et al., 2020 (Fig. 9).

Measurements of Total dendritic length (A), sholl analysis (B), number of branch points (C) and number of 1^{st}, 2^{nd}, 3^{rd}, 4^{th} and 5^{th} order dendrites (D) Total dendritic length (A), sholl analysis (B), number of branch points (C), number of 1^{st}, 2^{nd}, 3^{rd}, 4^{th} and 5^{th} order dendrites in “Figure 14: Morphometric analysis of BLA neurons from animals treated with the Y_5R agonist cPP, NPY + the Y_5R antagonist CGP” are published in Michaelson et al., 2020 (Fig. 9).

List of Figures

List of Abbreviations

Abbreviation	Definition
AHA	Anterior hypothalamic area
AMPA	α-amino-3-hydroxy-5-methyl-4-isoxazolepropionic acid
AST	Amygdala striataltransition area
BA	Basal amygdala nucleus
BDNF	Brain derived neurotrophic factor
BLA	Basolateral amygdala
BLA OTC	Organotypic slice culture of the basolateral amygdala
BM	Basomedial amygdala nucleus
BNST	Bed nucleus of the stria terminalis
CaMKII	Calcium/calmodulin-dependent protein kinase II
CCK	Cholecystokinin
CeA	Central amygdala
CeL	Lateral central amygdala
CeM	Medial central amygdala
CGP71683	NPY Y_5 receptor antagonist
ChR2	Channelrhodopsin type 2
CNQX	6-cyano-7-nitroquinoxaline-2,3-dione
CNS	Central nervous system
cPP	cPP^{1-7},$NPY^{19–32}$, Ala^{31},Aib^{32},Gln^{34}]human pancreatic Polipeptide
CRF	Corticotrophin releasing factor
CRFR2	Type 2 corticotropin releasing factor receptor

CSF	Cerebrospinal fluid
DV	Dorsoventral
EGTA	Ethylene glycol-bis(β-aminoethyl ether)-N,N,N′,N′-tetraacetic acid
EPM	Elevated plus maze
EPSC	Excitatory postsynaptic currents
F^7,P^{34}[NPY]	NPY Y_1 receptor agonist
GABA	Gamma aminobutyric acid
GABAAR	$GABA_A$ receptor
GABABR	$GABA_B$ receptor
HCN1	Hyperpolarization activated cyclic nucleotide gated potassium channel 1
HEPES	4-(2-hydroxyethyl)-1-piperazineethanesulfonic acid
HPC	Hippocampus
IEI	Inter event interval
IIR	Inward rectifying current
IL	Infralimbic
IPSC	Inhibitory postsynaptic currents
IR	Input resistance
LA	Lateral amygdala
LTD	Long-terms depression
LTP	Long-terms potentiation
MEM	Minimum essential medium
mPFC	Medial prefrontal cortex

NMDA	N-Methyl-D-aspartic acid or N-Methyl-D-aspartate
NPY	Neuropeptide Y
NPYR	NPY receptor
OTC	Organotypic slice culture
PBS	Phosphate buffered saline
PFC	Prefrontal cortex
PL	Prelimbic cortex
PKC	Protein kinase C
PNs	Principal neurons
PTSD	Post-traumatic stress disorder
PV	Parvalbumin
RMP	Resting membrane potential
SK2	Small conductance potassium channels subtype 2.
SST	Somatostatin
SSRI	Serotonin reuptake inhibitor
VGCC	Voltage gates calcium channels
Y_1R	NPY Y_1 receptor
Y_2R	NPY Y_2 receptor
Y_5R	NPY Y_5 receptor

1. Literature Review

1.1 Emotions

Emotions are complex behavioral patterns that have been shaped in the course of evolution by repetitive encounters with adaptive challenges to favour the survival and reproductive success of the species (Nesse, 1994). Challenges to an organism that represent an opportunity (like food, water or social encounters) will elicit motivation and ultimately, pleasure, positively reinforcing the behavior. Once consummated, the motivated behaviors help guarantee survival and reproductive success. Threatening challenges, on the other hand, evoke emotions like fear and anxiety, resulting in defensive behaviors. If those responses are effective, the organism is temporarily relieved, and its survival is also guaranteed. However, if the threat is severe or prolonged, those responses become maladaptive (ie. a rodent that does not forage due to predators could potentially starve and die, or a person that undergoes a severe trauma could develop psychiatric conditions such as post-traumatic stress disorder (PTSD)) (Nesse, 1990).

The resistance to stressful stimuli; or resilience; seems to be a key feature in preventing the development of maladaptive states. It is known that NPY is associated with less anxious states in human. NPY is also a potent anxiolytic and also induces stress resilience in rodents. It is also known that Y_1Rs are the primary receptor subtype mediating the acute anxiolytic actions of NPY. However, cellular mechanism by which NPY induces stress resilience remains unknown. In this thesis I will study the role of different NPY receptors subtype, in particular Y_1Rs and Y_5Rs in NPY-induced stress resilience. In addition, I will study the effect of NPY on BLA neurons that project to two regions associated to fear and anxiety, the mPFC and the BNST respectively.

1.2 Fear and anxiety

The definition of fear and anxiety has been a matter of controversy for years. On many occasions fear and anxiety are terms thar are used interchangeably and despite that both, fear and anxiety, have overlapped neural pathways, they are distinct emotional states. While fear is triggered by a discrete, acutely threatening stimulus, anxiety can be understood as the emotion evoked in response to an uncertainty about a future potential threat (Davis et al., 2010; Grupe and Nitschke, 2013). Fear begins and dissipates rapidly once a threat is encountered and removed and it coordinates active defensive responses (ie. fight of flight). Anxiety, on the other hand, is a long-lasting state of apprehension (Davis et al., 2010). These characteristics, in particular the anticipatory nature and the uncertainty of a threat differentiate what we experience as anxiety from fear.

Assessing fear and anxiety in humans involves self-assessment of symptoms from questionnaires and despite the subjective nature of the assessment, they are crucial to identify fear and anxiety disorders (Rose and Devine, 2014). This distinction between fear and anxiety has ethological support and validity based on rodents' defensive behaviors and responses. In rodents, the most common animal model to study fear and anxiety in the laboratory, their defensive responses have three main stages and they emerge as a continuum. (i) Pre-encounter defense emerges in an area where a predator has been encountered in the past. (ii) Post-encounter is activated when a predator is physically identified at distance. Here, there is a sustained assessment of the risk. And finally, when physical contact with the predator is achieved (iii) Circa-strike defense (fight or flight) is activated. In this way, anxiety is evoked by a potential presence of a predator (future-based

emotion) and relates to stages I (and II), while fear is elicited by close contact with a predator (Stage III) (Davis et al., 2010).

1.3 Measuring fear and anxiety

Most animal models of fear and anxiety are based on classic Pavlovian conditioning (Fig. 1A). First described by the Russian physiologist Ian Pavlov in the early 1900s, conditioning involves the pairing of two components. A neutral innocuous sensory cue, soon-to be a conditioned stimulus (CS, ie. the sound of a bell) is time locked to an unconditioned stimulus (US, ie. food). In fear conditioning, the CS usually involves a light or a tone while the US is typically presented as a mild, yet aversive, footshock. This pairing (CS followed by US) is repeated over time until the CS is now recognized as aversive and evokes fear behaviors (ie. freezing) without the need of the US (LeDoux, 2000; Nieh et al., 2013; Tovote et al., 2015). Following fear conditioning, the repeated presentation of the CS in absence of the US results in a dissociation of CS-US and a reduction in the CS-elicited fear. This processed, called “fear extinction”, is not forgetting that the CS was a fear stimulus but rather involves re-learning that the CS no longer represents a threat (Myers and Davis, 2002).

This type of conditioning has been shown across a wide range of species including fly, worm, snail, fish, pigeon, rabbit, rat, mouse, cat, monkey and humans (LeDoux, 2000) which suggest that the neural pathways of fear are highly conserved. In fact, the amygdala (the neural substrate of fear learning), or amygdala-like structures, have been identify in other vertebrates beside mammals, such as fish, lizard and birds (Johnston, 1923; Lanuza et al., 1998; Jarvis et al., 2005).

Originally developed by Brown et al. (Brown, 1951), Fear-potentiated startle consist of the pairing of a neutral cue (ie. a tone, light or odor) with an aversive unconditioned stimulus (US – a footshock). Once this pairing between the neutral cue (now a conditioned stimulus, CS – a tone) and the US is acquired, rodents are tested for fear evoked by the presentation of the CS in the presence of bursts of noise. This way, a startle response (evoked by the burst of noise) is potentiated in the presence of the CS (the tone previously associated with the aversive footshock). In humans, images are presented paired with a shock. The potentiation of startle (which is evoked by a loud noise) is evaluated measuring eyeblink (Davis et al., 2010).

Most anxiety assays are based in an approach-avoidance conflict model. Rodents are driven to explore novel areas (to forage and find mates) and to avoid unprotected open, bright spaces that represent vulnerability to threats. In all these tasks, rodents tend to spend more time in enclosed, dark safe zones of the arena when more anxious. Several tests had been used to measure anxiety-like behaviors in rodent and I will provide a brief description in the following section.

The most widely used anxiety test is the elevated plus maze (EPM) (Fig. 1C). In this test, rodents are placed on an elevated X maze that consists of two open (unprotected) and to enclosed (protected) arms. Anxious rodents avoid the open arms in favor of the enclosed arms. Rodents are placed in the center and are allowed to explore freely all arms of the maze. The time and number of entries into both open and both closed arms are scored as a measure of anxiety (Calhoon and Tye, 2015).

Other paradigm to evaluate anxiety in rodents is the open field test (OFT) (Fig. 1D). In this paradigm, rodents are placed in an open squared arena surrounded by walls and left to explore freely. The center of the arena represents a more vulnerable area. Less anxious mice and rats will explore the center of the arena while more anxious rodents will remain close to the edges of the arena (Calhoon and Tye, 2015).

In the light-dark test (Fig. 1E) rodents are allowed to explore an enclosure with two compartments, a light and a dark area. Anxious animals will prefer spent time in the dark vs the light compartment (Calhoon and Tye, 2015).

One problem that arises with the tests describe above is that animals quickly habituate to the test conditions if the test is repeated. This makes difficult the study of long-lasting behaviors that required multiple behavioral evaluations on the same individuals. The social interaction (SI) (Fig. 1F) test was developed in 1978 by File and Hyde as an alternative to measure anxiety in rodents. Unlike the tests described above, the SI test can be repeated over time. This model is based in the need of two animals of the same species (ie. rats) to engage in social interaction to stablish territory when placed together. They can exhibit a variety of behaviors including sniffing, chasing, walking over, crawling under and grooming. In this way, rats that have a less anxious phenotype will spend more time in interaction with their counterparts (File and Seth, 2003).

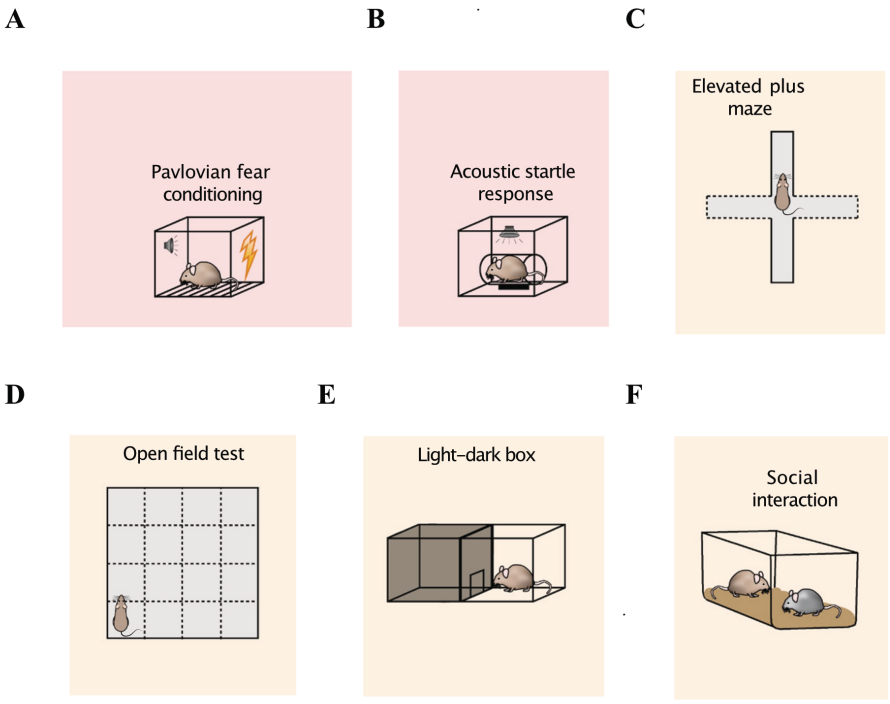

Figure 1: Some of the validated tests to assay fear and anxiety in rodents. A. Fear conditioning. B. Acoustic startle response. C. Elevated plus maze. D. Open field test. E. Ligh-dark box. F. Social Interaction. Adapted with permission from (Calhoon and Tye, 2015).

1.4 The amygdala complex

The amygdala complex (Fig 2), first identified by Burdach in the 19th century, is an almond-shaped structure located bilaterally in the anterior medial temporal lobes (Sah et al., 2003) (Fig. 2A). The amygdala encompasses 13 highly heterogeneous regions that are grouped based on connectivity and behavioral function (Sah et al., 2003). Three mayor subdivisions of the amygdala complex had been classified (Fig. 2B). The basolateral nuclei (BLA), the cortical-like nuclei and the centromedial nuclei of the amygdala (CeA). Additional groups are the intercalated cell masses and the amygdalohippocampal region (AHA) and the extended amygdala (Sah et al., 2003). In this section I will describe in detail the BLA and the CeA.

A

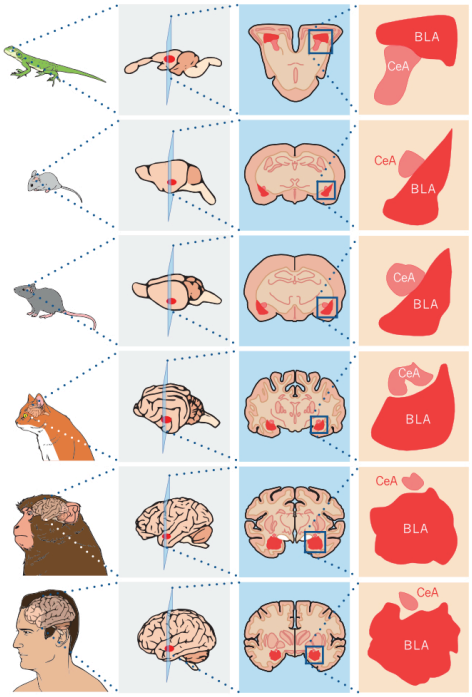
BLA
CeA
CeA
BLA
CeA
BLA
CeA
BLA
CeA
BLA
CeA
BLA

B

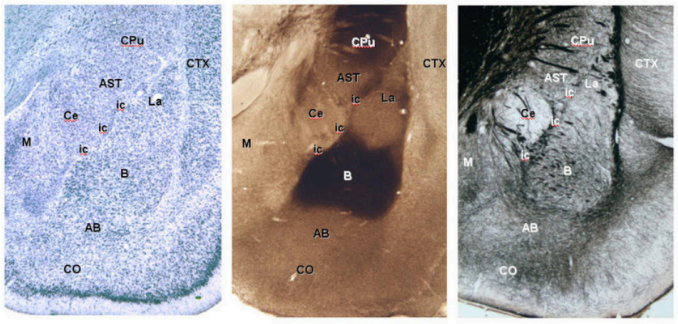
CPu
CTX
AST
ic
La
Ce
ic
M
ic
B
AB
CO
CPu
CTX
AST
ic
La
Ce
ic
M
ic
B
AB
CO
CPu
CTX
AST
ic
La
Ce
ic
M
ic
B
AB
CO

Figure 2. The amygdala complex. A. Diagram showing the location of principal amygdala nuclei across different species including lizards, mice, rats, cats, primates and humans. From (Janak and Tye, 2015). B. Rat brain slices containing the amygdala showing the principal subdivision of the basolateral and central amygdala. Left: Nissil staining. Middle: acetylcholinesterase staining. Right: silver staining. Abbreviations: La, lateral amygdala nucleus; B, basal amygdala nucleus; AB, basal medial nucleus; Ce, central amygdala nucleus; ic, intercalated cell mass; M, medial amygdala; CO, cortical-like nucleus. AST, amygdala striataltransition area; CTX, cortex; CPu, caudate putamen. From Ledoux et al. (2008) Scholapedia.

1.4.1 The basolateral amygdala

The basolateral amygdala (BLA) is located lateral to the central amygdala and striatum and medial to the cortex (Fig. 2B). The BLA is delimited medial and lateral by two sets of fibre bundles. The longitudinal association bundles which border medially separates the BLA from the central amygdala. The external capsule which borders laterally separates the BLA from the cortex (Fig. 2B). The BLA comprises two distinct subnuclei. The lateral nucleus (LA) is located dorsally and abuts ventrally with the basal (Ba) nucleus. The third region is the accessory basal or basomedial (BM) group, which is located ventral to the BA nucleus, adjacent to the AHA, but due to lack of clear anatomical boundaries it is considered together with the Ba. The principal focus of this thesis is the BA nucleus of the BLA since anxiety expression and the effect of stress and NPY reside in the BA.

In a series of elegant anatomical studies, Alexander J McDonald (1984, 1996) showed that the BLA is composed primarily by pyramidal cortical-like spiny projection neurons, comprising about 80% of the BLA neuronal population. These neurons are commonly called principal neurons (PNs) and use glutamate as neurotransmitter (McDonald, 1984; 1996). PNs (originally classified as Class I) can be further divided into pyramidal-like neurons and stellate-like neurons. Pyramidal neurons in the BLA have large, ~20 μm, somas and are characterized by spine-laden dendrites and elaborated dendritic arborizations. They typically have 4-7 primary dendrites, with one prominent apical dendrite from where they give rise to their complex dendritic arborization. Pyramidal neurons have the highest (~65 MΩ) input resistance, long duration action potentials (AP) (> 1 ms), long time constant of membrane charging, regular firing patter with characteristic spike frequency adaptation (McDonald, 1982; Rainnie et al., 1993; Ryan et al., 2016). Stellate-like neurons

dendrites are also densely covered in spines but are smaller in size than pyramidal neurons. They present lower input resistance (~40 MΩ), shorter time constant of membrane charging, shorter duration AP and burst firing pattern. PNs express $Ca2^{+}$/calmodulin-dependent protein kinase II (McDonald et al., 2002; Rostkowski et al., 2009) which has been used as their neuronal marker.

The remaining 20% of the BLA neurons correspond to inhibitory GABAergic interneurons (or Class II neurons) and form part of the BLA local microcircuit (McDonald, 1984; 1985; Polepalli et al., 2020). They are characterized by their small soma size; they are multipolar, and their dendrites are completely devoid of spines. They have intermediate (~55 MΩ) input resistance, intermediate time constant of membrane charging and shorter (<1 ms) AP duration. They have regular firing with no accommodation (McDonald, 1984; Rainnie et al., 1993). GABAergic interneurons also co-express a variety of neuropeptides, including neuropeptide Y, somatostatin (SST), parvalbumin, cholecystokinin (CCK), parvalbumin (PV) and calbindin (McDonald, 1989; McDonald and Pearson, 1989; McDonald and Mascagni, 2001; Mascagni and McDonald, 2003; Polepalli et al., 2020; Krabbe et al., 2017).

In simplified terms, the amygdala basic circuitry goes as follow. The BLA receives excitatory sensory information from the environment form the sensory thalamus and sensory cortices which project to the LA. This information is further processed in the Ba/BM to finally leave the amygdala through the central amygdala (CeA) (Fig. 3).

1.4.2 The lateral amygdala

The LA is located dorsal to the Ba (Fig. 2B) and receives most of the sensory information that enters the amygdala complex (Fig. 3), which is why the LA is considered the gatekeeper of the amygdala complex. Most auditory, visual, somatosensory, olfactory and gustatory centers provide inputs to the BLA via the LA (LeDoux et al., 1990; Sah et al., 2003; Polepalli et al., 2020). As described above, the LA sends information to Ba and BM which in turns project to the (CeA), the major output of the amygdala complex (LeDoux, 2000; Calhoon and Tye, 2015, Tovote et al., 2015). However, direct projections from the LA to the CeA have also been described (Li et al., 2013) (Fig. 3). The LA has been the focus of extensive research since is the neural subtract of Pavlovian conditioning. (LeDoux, 2000). Is in the LA where associations between sensory information (ie. a tone) and noxious stimulus (i.e a footstock) are made. This associative process, known as fear conditioning, is lost when the LA is lesioned (Nader et al., 2001; Tazumi and Okaichi, 2002). On the other hand, optogenetic activation of presynaptic auditory terminals on the LA induces fear, similar to a noxious stimulus (Kwon et al., 2014; Li et al., 2020). Similarly, optogenetic activation of LA PNs induces fear responses in the absence of an aversive stimulus (Johansen et al., 2010; Tipps et al., 2018). In addition, optogenetic inhibition of LA synapses from the thalamus blocks fear-related memories (Nabavi et al., 2014).

1.4.3 The basal amygdala

The BA resides ventral to the LA and it comprises two nuclei, the Ba and the Bm which is located ventral to the Ba (Fig. 2B). It receives dense innervation from the LA but also from the thalamus and association cortices (Sah et al., 2003; Polepalli et al., 2020). The BA receive information form the LA (the main entry from all sensory information) and in turn projects to the CeA_M (Fig. 3).

Early inactivation studies showed that infusions of NMDA antagonists into the BLA blocked the acquisition and expression of fear (Miserendino et al., 1990; Kim et al., 1993). In similar way, infusion of NMDA receptor (NMDAR) antagonists into the BLA block the extinction of a previously acquired fear memory (Davis et al., 2003). However, this approach included inactivation of the whole BLA, making difficult to differentiate between the role of the LA, Ba and Bm. Later, Amaro et al (2011) showed that neurons from the Ba increased their firing during fear and that inactivating the Ba impaired both fear expression and extinction (Amano et al., 2011). More relevant to this thesis is that NPY in the Ba, has been reported to facilitate the extinction of fear (Gutman et al., 2008), reduce anxiety behaviors (Sajdyk et al., 1999) and induce stress resilience (Sajdyk et al., 2008b; Silveira Villarroel et al., 2018).

1.4.4 The central amygdala

The CeA is located medial to the BLA (Fig. 2B, Fig. 3). It is a striatum-like structure composed of GABAergic medium spiny projection neurons (Sun and Cassell, 1993; Swanson and Petrovich, 1998; Sah et al., 2003). The CeA is subdivided into the lateral central amygdala (CeL) and medial central amygdala (CeM) and have distinctive functions in the expression of fear. While the CeL is associated with the acquisition of fear, the CeM is considered the main autonomic output. Optogenetic stimulation of the CeM evokes fear (ie. freezing response) and pharmacological inactivation of CeM abolishes fear responses. On the other hand, inactivation of the CeL, not the CeM, prevented the acquisition of fear (Ciocchi et al., 2010). Using *in vivo* single unit recordings, Ciocchi et al. (2010) found two functionally distinct CeL neuronal populations. Fear-ON neurons increase their firing during fear and Fear-OFF neurons decrease their firing in presence of the fear stimulus (Ciocchi et al., 2010). In a later study, Fear-OFF neurons were found to express the

protein kinase C δ isoform (PKC δ) and optogenetic activation of this neuronal population inhibits CeM output neurons and blocks the expression of fear (Haubensak et al., 2010). Overall, authors proposed a model in which in the presence of a fear stimulus, CeL Fear-ON neurons are activated and inhibit CeL Fear-OFF neurons, disinhibiting CeM output neurons allowing the expression of fear responses (Fig. 3) (Haubensak et al., 2010).

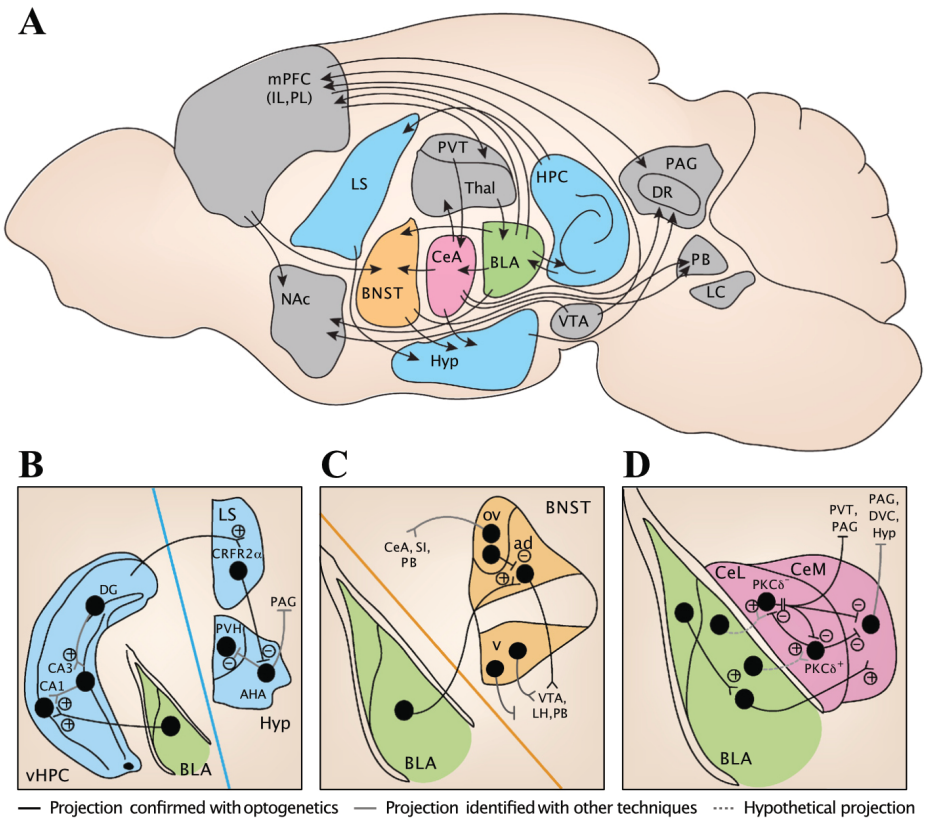

Figure 3. Amygdala circuit mediating fear and anxiety. A. Sagittal view of the rodent brain showing anxiety-related neural pathways. B. BLA projections to the ventral hippocampus related to anxiety. C. BLA-BNST circuit related to anxiety. D. BLA and CeA microcircuit modulating anxiety. Sensory information converges into LA. The BLA project to the CeL to modulate anxiety behaviors. Here, PKC δ- (CeL_{ON})and PKC δ+ (CeL_{OFF}) neurons form a reciprocal inhibitory circuit. PKC δ+ neurons inhibit CeM output neurons. This CeM neurons project to effector structures such as the the PAG. CeL projections also inhibit the BNST. Solid lines represent optogenetic findings. Abbreviations: d, anterodorsal nucleus of the BNST; AHA, anterior hypothalamic area; BLA, basolateral amygdala; BNST, bed nucleus of the stria terminalis; CeA,

central amygdala; CeL, lateral subdivision of the central amygdala; CeM, centromedial subdivision of the amygdala; CRFR2α, type 2 corticotropin releasing factor receptor; DR, dorsal raphe nucleus; DVC, dorsal vagal complex; HPC, hippocampus; Hyp, hypothalamus; IL, infralimbic division of the mPFC; LC, locus coeruleus; LH, lateral hypothalamus; LS, lateral septum; mPFC, medial prefrontal cortex; NAc, nucleus accumbens; ov, oval nucleus of the BNST; PAG, periaqueductal gray; PB, parabrachial nucleus; PL, prelimbic division of the mPFC; PVH, paraventricular nucleus of the hypothalamus; PVT, paraventricular thalamus; SI, substantia innominata; Thal, thalamus; v, ventral nucleus of the BNST; vHPC, ventral hippocampus; VTA, ventral tegmental area. Adapted with permission from (Calhoon and Tye, 2015).

1.5 Role of the BLA in fear and anxiety

1.5.1 Role of the amygdala in fear

The first clues indicating the role of the amygdala in fear learning came from Brown and Schäffer in 1888. They noticed that a rhesus monkey showed reduced aggression, fear and defensive behaviors after they performed a bilateral ablation of the temporal lobe. Later, in 1956, Lawrence Weiskrantz found that after lesioning the amygdala, monkeys were less afraid of humans and had impaired fear responses acquired before the lesion but the extinction of fear was enhanced (Weiskrantz, 1956). These early studies precipitate a cascade research in both, rodents and humans aimed to understand the role of the amygdala in fear. Amygdala lesions in rodents were later reported to have a similar outcome. Blanchard and Blanchard (1972) lesioned the amygdala of rats and exposed them to a cat, or to a fear conditioned training. As a result, rats showed reduced response both, innate (the cat) and learned fear (fear conditioning) (Blanchard and Blanchard, 1972). A key study in rodents was done by Ledoux et al. (1990). They found that electrical bilateral lesions restricted to the lateral region of the amygdala (the amygdala region that receive dense auditory information) interfered with fear conditioning. This is, lesioned rats do not show fear responses to a CS (LeDoux et al., 1990). In humans, the first direct evidence linking the amygdala with emotional regulation was the study of patient S.M, by Adolphs et al. (1994). S.M, known as the woman without fear, suffered from a rare autosomal recessive condition called Urban-Weithe that causes bilateral calcification (destruction) of the amygdala. The authors presented S.M with different facial expressions and ask her to assign an emotional adjective. The most predominant characteristic of S.M is that she specifically failed to recognize fear (Adolphs et al., 1994). Additionally, fMRI studies in humans showed that the amygdala is activated during fear

conditioning and the degree of activation correlates with fear intensity and this activation decreases with extinction (LaBar et al., 1998).

Quirk et al. (1997) reported that, in rats, BLA neurons increased their firing rate during fear conditioning (Quirk et al., 1997). Interestingly, during extinction the activity of another population of BLA neurons also increases. Amaro et al. (2011) showed that neurons from the BA increased their firing in anticipation during fear-associated cues (Amano et al., 2011). Next, they evaluated the effect of Ba and Bm inactivation. Using muscimol injections they determined that the expression of fear is blocked when both Ba and Bm are inactivated (Amano et al., 2011). In addition, inactivation of Ba and Bm also produces deficits on fear extinction (Herry et al., 2008; Amano et al., 2010). This suggest that within the BA there are populations of neurons that exert a bidirectional control of fear. In a beautiful work done by Herry et al. in 2008 it was demonstrated that the selective inactivation of BA impaired extinction and also impaired the reestablishment of a previously extinct fear memory (Herry et al., 2008). Using behavioral conditioning and extracellular recording on behaving mice they found that the BA has two distinct neuronal groups. "Fear Neurons" were found to be active during fear learning and were silent during fear extinction. "Extinction Neurons" were found to be silent during fear learning and their activity increased during fear extinction. Herry et al. (2008) also showed that fear neurons receive inputs form the hippocampus while extinction neurons are reciprocally connected to the mPFC (Herry et al., 2008). Recently, Johansen et al. (2010) reported that the activation of LA PNs is necessary for fear learning. Using optogenetic and fear conditioning, the authors replaced the US for optogenetic depolarization of LA neurons. First, they and found that LA photostimulation was sufficient to elicit fear. Then, they repeatedly paired a CS with LA depolarizations and found that, after a

training period, the CS alone was capable of elicit fear (Johansen et al., 2010). In the following study they demonstrated that inhibition of LA PNs disrupted fear conditioning (Johansen et al., 2014). Similar observations were made by Tipps et al. (2018). The authors found that the chemogenetic inhibition of LA PNs, and not BA PNs, impaired auditory fear conditioning (Tipps et al., 2018). However, they also found that the inhibition of BA PNs also impaired fear conditioning.

As described above, GABAergic interneurons give account for only a small fraction (~20%) of the entire BLA neuronal population. They are classified into several subgroups based on the expression of cytosolic markers and connection patterns (Spampanato et al., 2011). The two more prominent groups are the GABAergic interneurons that express the calcium-binding albumin protein parvalbumin (PV) which provide perisomatic inhibition to PNs; and GABAergic interneurons that express somatostatin (SST) which provide dendritic inhibition of PNs (Spampanato et al., 2011). Despite their numerical disadvantage, BLA GABAergic interneurons exert powerful inhibitory control over PNs. As a result, BLA PNs have low basal activity both, *in vivo* and *in vitro* (Li et al., 1996; Rosenkranz and Grace, 1999; Bissière et al., 2003). This is supported by a series of studies. First, loss of BLA GABAergic inhibition is associated with potentiation of fear (Shaban et al., 2006). Chemogenic inhibition of BA GABAergic interneurons, and not PNs, impairs fear learning while GABAergic interneurons activation during the presentation of a neutral auditory is sufficient to elicit freezing behaviors. (ie. Inhibition of BA GABAergic interneurons promotes the association between a neutral cue and fear in the absence of a noxious stimulus) (Tipps et al., 2018). Later, Wolff et al. (2014) using an optogenetic approach demonstrated that the activation of BLA GABAergic interneurons expressing PV result in

dendritic disinhibition of PNs by silencing SST-expressing interneurons, promoting fear. On the other hand, photoactivation of SST interneurons reduced fear by direct inhibition of BA PNs (Wolff et al., 2014). A Rovira-Esteban et al. (2019) recently reported that the optogenetic photoactivation of BA GABAergic interneurons expressing CCK (that also co-express either NPY or PV) promotes the extinction of fear (Rovira-Esteban et al., 2019).

1.5.2 Neural mechanisms of fear

The association of the cue-stimulus paring that occurs during fear conditioning appears to be mediated by Hebbian mechanisms of LTP in the amygdala (Johansen et al., 2014). Rogan et al. (1997) were the first to demonstrate that the LA undergoes associative LTP following fear conditioning (Rogan et al., 1997). In the LA, synapses coding for weak sensory synaptic inputs (CS) coincide with a strong aversive (US) LA neurons depolarization, allowing the strengthening of the circuit. When the CS is presented, glutamate is released from sensory inputs and binds to glutamate AMPA and NMDA receptors at the post-synaptic LA neuron. This evokes small excitatory post synaptic currents (EPSC). Then, when the US is presented, it induces LA neurons depolarization, backpropagation of AP and activation of VGCC. This results in Ca^{2+} entry and remotion of Mg^{2+} block from NMDA receptors allowing weak CS inputs to strengthen (Blair et al., 2001; Maren and Quirk, 2004). This was later demonstrated by Johansen et al. (2010). Using optogenetic and fear conditioning, they and found that LA photostimulation was sufficient to elicit fear and that when paired a CS with LA depolarizations, the CS alone was capable of evoke fear (Johansen et al., 2010; Tovote et al., 2015).

1.5.3 Role of the amygdala in anxiety

In humans, increased amygdala activity amygdala has also been associated to anxiety (Etkin et al., 2009; Grupe and Nitschke, 2013; Boehme et al., 2014). Etking et al. (2019) using fMRI showed patients diagnosed with generalized anxiety disorder have deficiencies in amygdala functional connectivity (Etkin et al., 2009). Additionally, both increased and decreased amygdala size was correlated to anxiety disorders in humans (Irle et al., 2010; Machado-de-Sousa et al., 2014). Later, Boehme et al. (2014), using fMRI found that the amygdala was activated during anticipatory anxiety to public speaking (Boehme et al., 2014).

Early studies done by Davis et al. (2010) demonstrated that pharmacological inactivation of the BLA using AMPA receptors antagonists blocks anxiety (Davis et al., 2010). The exposure to a anxiogenic stimulus increases c-fos (the protein product of the immediate early gene *c-fos* that is a marker of neuronal activity) activity in the BLA, indicating neuronal activation (Butler et al., 2012). Additionally, bilateral pharmacological inactivation of the BLA using $GABA_A$ receptor ($GABA_AR$) antagonists results in an anxiogenic outcome while the pharmacological activation of the amygdala with $GABA_AR$ is anxiolytic in the social interaction test (Sanders and Shekhar, 1995).

Groundbreakingly work dissecting the role of the BLA in anxiety was done by Kay Tye in 2011. Using expression of ChR2 on PNs, it was demonstrated that the specific photostimulation of BLA PNs somatas promotes anxiety-like behavior in mice. Photoactivation of BLA PNs neurons terminals in the CeL decreased anxiety-like behavior (Fig. 3C). On the other hand, inhibition of BLA terminals in the CeL with NpHR, increased anxiety (Tye et al., 2011). One of the main targets

of the BLA that is recruited during anxiety, is the bed nucleus of the stria terminalis (BNST) (Fig. 3A, C) and it has been long considered that the activation of the BLA leads to increased activity on the BNST, resulting in high anxiety (Walker and Davis, 2008; Davis et al., 2010). Kim et al. (2013a) showed that the photostimuation of BLA excitatory inputs to the BNST reduces anxiety; and their inhibition is anxiogenic (Kim et al., 2013a). These paradoxical results suggest that the BLA exert a bidirectional modulation over BNST activity that result on reversible control of anxiety. Perhaps in the BLA exist PNs that modulate anxiety in a similar what that fear and extinction neurons are recruited to modulate fear and extinction. Additionally, BLA PNs inputs to the hippocampus also have a role in modulating anxiety. Optogenetic stimulation of BLA terminals into the ventral hippocampus (vHIPP) increases anxiety behavior in mice (Fig. 3A) (Felix-Ortiz and Tye, 2014).

1.6 Stress, fear, anxiety; and the Amygdala.

Stress was first defined by the endocrinologist Hans Selye in 1936 as "…the expression of a general alarm of the organism…", produced by "…acute non-specific nocuous agents…" in "…a generalized effort of the organism to adapt itself to new conditions…" (Selye, 1936). The stress response is now defined as the emergency state of an organism elicited by any real or potential threats (stressors) that challenge its homeostasis (Chrousos, 2009; McEwen and Gianaros, 2011).

The biological role of stress is to ensure adaptation and the survival of the organism. During a stressful situation the organism orchestrates an integrated reaction including behavioral and physiological (autonomic and hormonal) responses. However, when stressor has a high psychological impact or is sustained over time it can become maladaptive contributing to the

development of anxiety-related disorders such as PTSD, social and generalized anxiety. A stressor can be systemic (ie. hypoglycemia, hypoxia, hypovolemia) or psychological. The key characteristic of psychological stressors is that they are anticipatory in nature and include any circumstance that can potentially lead to danger and homeostatic imbalance in the future. (McEwen et al., 2012; Daviu et al., 2019), and is represented as heightened anxiety.

It is well stablished that stress can impact the brain in a way that cause imbalance of neural pathways of cognition, decision making, fear and anxiety (LeDoux, 2000; Roozendaal et al., 2009; Leuner and Shors, 2013; Daviu et al., 2019), including the medial prefrontal cortex (mPFC), hippocampus and amygdala. Neurons on these regions are extremely sensitive to the effect of stress and anxiety.

Spontaneously more anxious rats have larger BLA PNs and smaller hippocampal neurons that less anxious rats (Adamec et al., 2012). Compared to less anxious rats, more anxious have increased dendritic spines in BLA PNs and decreased dendritic spines hippocampal pyramidal neurons (Adamec et al., 2012).

Mitra et al. (2005) reported that the exposure to an acute stress consisting of complete physical immobilization induced synaptogenesis in the BLA, but this effect dissipates quickly (Mitra et al., 2005). Work done by Vyas et al. (2002) addressed the effects chronic stress in neurons of the amygdala and hippocampus. First, the authors subjected rats to a chronic stress protocol consisting in complete physical immobilization, 2 h a day for 21 days. They found that stressed animals were more anxious. Then, they examined how stress have impacted neurons of the BLA and

hippocampus. They found that the increase in anxiety was correlated with hypertrophy and increased dendritic spines on PNs of the BLA. Strikingly, in the hippocampus the effect of stress was exactly the opposite. Stress induced hypotrophy of pyramidal neurons and a decrease on spines on hippocampal pyramidal neurons. (Vyas et al., 2002). Using a different stress model, Patel et al. (2018) made the same observations. Social defeat stress (a model in which rats are subjected to an territorial aggressive rat) induces dendritic hypertrophy of BLA neurons and atrophy of hippocampus neurons (Patel et al., 2018). In a following study, Vyas et al. (2006) demonstrated that the effect of stress on BLA PNs dendritic remodeling and anxiety behavior was persistent and lasted up to 3 weeks after the stress protocol was ended (stress-free period) while the effect of stress in the hippocampus reversed after a stress-free period (Vyas et al., 2006). Similar, stress-induced dendritic retraction was reported in the mPFC of male rats. Interestingly, in females, stress induced hypertrophy of mPFC pyramidal neurons (Garrett and Wellman, 2009; Urban and Valentino, 2016). However, caution needs to be made regarding the effect of stress on BLA PNs since all the studies described above were conducted on male rats. A recent study evaluated the effect of stress on dendritic remodeling of BLA PNs of female rats. Blume et al. (2019) reported that in female rats restrain stress causes hypertrophy of LA PNs but does not affect BA PNs morphology while in males, restrain stress produces hypertrophy of BA PNs without having any effect on LA PNs morphology (Blume et al., 2019).

It was later observed that reducing BLA overall activity with the overexpression of SK2 channels decreases both, anxiety and stress-induced hypertrophy of BLA neurons (Mitra et al., 2009). Additionally, SK channel activators reduce chronic stress-induced BLA excitability (Rosenkranz et al., 2010). The structural changes on BLA neurons induced by stress were found to be dependent

on brain derived neurotrophic factor (BDNF). Chronic stress produces a long-lasting increase in BDNF expression on the BLA (Lakshminarasimhan and Chattarji, 2012). However, BDNF overexpression in the BLA results in increased anxiety and spine density but paradoxically blunted stress-induced dendritic hypertrophy (Govindarajan et al., 2006).

1.7 Neuromodulation in the BLA

Neuropeptides are expressed throughout the CNS and play important roles in modulating neuronal activity. Unlike classical neurotransmitters, neuropeptides are stored in dense core vesicles, have slow vesicle recycling cycles, they can diffuse longer distances (volume transmission) and modulate G-protein coupled receptors. Classically released in terminals, there is evidence that neuropeptides can also be resealed by dendrites (van den Pol, 2012). The BLA activity is under modulation of a wide range of neuropeptides including NPY, corticotrophin releasing factor (CRF), CCK and SST (Sajdyk et al., 2008b; Giesbrecht et al., 2010a; Rostkowski et al., 2013; Wolff et al., 2014; Leitermann et al., 2016; Rovira-Esteban et al., 2019). Relevant for this thesis are the actions of NPY in the BLA and anxiety. I will review in detail the role of NPY in the following section.

1.7.1 Neuropeptide Y

The BLA contains high levels of Neuropeptide Y (NPY) (Adrian et al, 1983; De Quidt and Emson, 1986a; 1986b), a strongly evolutionary-conserved, 36-amino acid peptide, widely distributed in the central and peripheral nervous systems (Tatemoto et al., 1982; Blomqvist et al., 1992). Biological responses to NPY are mediated by the activation of five G-protein coupled receptors, Y_1, Y_2, Y_4, Y_5 and Y_6 (Michael et al., 1998). NPY Y_1, Y_2 and Y_5 receptors have been identify in

neurons and fibers of the BLA. NPY has long been associated with anxiety- and depression-related disorders and is considered an important stress resilience factor.

The first clue linking NPY with psychiatric disorders came from observations made by Widerlov in the late 90s. Using a radioimmuno assay of NPY on cerebrospinal fluid (CSF) of subjects diagnosed with major depressive disorder and schizophrenia. Widerlöv et al. (1988) found that NPY- like immunoreactivity (NPY-ir) on CSF from patients with depression was lower than from patients diagnosed with schizophrenia and healthy controls (Widerlöv et al., 1988). This was followed by several studies, in both humans and rodents, aimed to dilucidate the role of NPY on psychiatric conditions. Heiling et al. (2004) studied the NPY-ir on CSF from patients diagnosed with unipolar depression. Similar to the study described earlier, they found a pronounced reduction of NPY levels in CSF from patients diagnosed with depression compared to healthy volunteers (Heilig et al., 2004). On patients treated with electroconvulsive therapy CSF NPY levels were elevated compared to pre-treatment levels (Mathé et al., 1995). NPY levels on patients with major depression treated with citalopram (a Selective Serotonin Reuptake Inhibitor, SSRI) were also increased compared to pre-treatment levels (Nikisch et al., 2005). In the early 2000s, Rasmusson et al. (2000) reported that combat-exposed subject diagnosed with PTSD have lower circulating plasma NPY levels compared with healthy control subjects (Rasmusson et al, 2000). Similar observations were made later by Sah et al. (2009). NPY CSF levels of combat veterans diagnosed with PTSD was reduced compared to healthy volunteers (Sah et al., 2009). Interestingly, combat-exposed veterans previously diagnosed with PTSD but that later recovered showed increased NPY plasma levels compared to veterans diagnosed with PTSD who did not recovered (Yehuda et al., 2006).

Further evidence suggesting the role of NPY in resistance to stress came from Morgan III et al. (2000, 2001, 2002). In a series of studies, they showed first that, in humas, NPY is released after acute uncontrollable stress and after military interrogation. Second, NPY plasma levels correlate positively with plasma levels of cortisol and noradrenaline (two markers of stress). And third, subjects with greater plasma levels of stress-induced NPY exhibit less psychological distress (Morgan et al., 2000; 2001; 2002). These series of studies not only link NPY to psychiatric disorders but they also suggest an association between NPY levels and resistance to stress, or resilience. More recently, a single nucleotide polymorphism (SNPrs16147) located in the NPY promoter region decreases NPY expression and was correlated with high amygdala activation and less resilience (Zhou et al., 2008)

In line with human studies, NPY has been shown to have anxiolytic properties in rodents. Intracerebroventricular (i.c.v) delivery of NPY increased the time that rats spend in the open arms of the EPM (Heilig et al., 1989). Later, Sergeyev et al. (2005) found that on rats exposed to chronic mild stress NPY mRNA levels in the hippocampus were decreased (Sergeyev et al., 2005). In line with this observation, it was reported that early maternal separation stress decreased NPY-ir in the hippocampus when evaluated 12 weeks after the stress (Jimenez-Vasquez et al., 2001).

1.7.2 NPY effects on the basolateral amygdala

As described above, the BLA is particularly rich in NPY expression and BLA PNs express the three subtypes of NPY receptors found in the CNS, Y_1R, Y_2R and Y_5R. The BLA is also involve

in emotional regulation. Thus, it seems reasonable that NPY could act on the BLA to modulate anxiety.

The participation of NPY on the BLA and anxiety was first studied in rodents by Heilig et al. (1993). The authors first showed that NPY and a selective Y_1R agonist, when infused into the BLA of rats, decreases anxiety (Heilig et al., 1993). On a later study, Heilig et al. (1995), first showed that bilateral injections of NPY into the BLA of rats decreases anxiety in the EPM. Then, they injected (i.c.v) an Y_1R antisense oligonucleoutide to reduce the global Y_1Rs expression and found that rats were more anxious. Finally, they injected NPY into the BLA of rats previously treated i.c.v with the Y_1R antisense oligonucleoutide and found that NPY failed to reduce anxiety (Heilig, 1995). This was later confirmed by Sajdyk et al. (1999). They first showed that the acute administration of NPY into the BLA decrease anxiety in the SI test. Then they were able to block the NPY-induced anxiolysis by co-administrating a Y_1R antagonist (Sajdyk et al., 1999). These studies described above suggest that NPY, acting through Y_1Rs decreases anxiety.

The effects of stress on NPY-induced anxiolysis have also being studied. In homogenates tissue from the amygdala of rats, NPY mRNA levels were decreased following exposure of an acute stress (Thorsell et al., 1998). In a subsequent study, Thorsell et al. (2000) used NPY transgenic rats, which overexpress NPY in all NPY neurons, and evaluated the effect of stress on anxiety behavior on the EPM. In agreement with previous studies, they found that stress increased anxiety on wild type rats. Then, they subjected the NPY overexpressing rats to stress and they found stress did not increase anxiety on NPY transgenic rats, suggesting that NPY attenuates sensitivity to stress. (Thorsell et al., 2000).

The anxiolytic actions of NPY into the BLA were further demonstrated on a series of studies by Sajdyk et al. (2006, 2008b). First, the authors injected urocortin (a corticotrophin releasing factor receptor agonist which is highly anxiogenic) into the BLA of rats and evaluated anxiety. They found that urocortin injected into the BA increase anxiety. Then, they injected NPY into the BA prior to injecting urocortin and measured anxiety. They observed that NPY prevented the urocortin-induced increase in anxiety. Then, a group of rats were subjected to restrain stress for five days and following the stress procedure a single dose of NPY was injected into the BA. They found that NPY blocked the increase in anxiety induced by stress (Sajdyk et al., 2006). On a following study, Sajdyk et al. (2008b) demonstrated that NPY can induce the development of stress resilience. They repeatedly injected NPY into the BLA of rats once a day for five days and evaluated anxiety-behavior 8 weeks after the treatment with NPY in the SI test. They observed that rats treated with NPY had less anxiety basal levels compared with vehicle-treated rats. In the same study, authors also evaluated the effect of NPY treatment on restrain stress sensitivity. They found that rats treated with NPY were less anxious following restrain stress than controls that underwent the same stress (Sajdyk et al., 2008b). Whether Y_1Rs are responsible for the long-lasting actions of NPY on anxiety remains unclear. However, it is tempting to suggest, based on the experiments described above, that NPY, via Y_1Rs, induce stress resilience.

NPY Y_1, Y_2 and Y_5 receptors are expressed in the BLA. While Y_1Rs are reported to mediate the acute actions of NPY, little is known about Y_2Rs and Y_5Rs and their role in anxiety. Sajdyk et al. (2002a) tested the effects of a Y_2R/Y_5R preferring agonist, injected into the BLA, on anxiety behavior of rats. They found that anxiety was increased when low doses (which activate Y_2

receptors) were used. On the other hand, high doses of the same agonist (which they argue activates Y_5Rs) were anxiolytic (Sajdyk et al., 2002a). This is the first evidence involving Y_5Rs on NPY-mediated anxiolysis. More recently, it was reported that Y_2Rs increase BLA pyramidal neurons excitability acutely (Mackay et al., 2019).

Work done previously at the Colmers laboratory showed that when applied to acute brain slices containing BLA, NPY hyperpolarizes and reduces the excitability of a population of BLA pyramidal output neurons in part by suppressing the voltage-dependent activation of the h-current (I_h) (Giesbrecht et al., 2010), a hyperpolarization-activated depolarizing current (Robinson and Siegelbaum, 2003). This effect is blocked by a Y_1R antagonist (Giesbrecht et al., 2010). Furthermore, the laboratory demonstrated that compared to saline-injected animals, repeated administration of NPY into the BLA produces a long-lasting hyperpolarization and reduction in the maximum I_h amplitude that lasts at least 4 weeks after treatment (Silveira Villarroel et al., 2018). Acute application of NPY to BLA slices from NPY-treated animals neither hyperpolarizes nor reduces the excitability of BLA output neurons, suggesting that the NPY treatment in some way desensitizes NPY-sensitive neurons of the BLA, or these neurons are to depressed to respond to the inhibitory actions of NPY (Silveira Villarroel et al., 2018). Using an organotypic slice culture model of the BLA (BLA OTC), work done by the Colmers group showed that incubations of NPY on BLA OTC for five days produces a long-lasting decrease in cell membrane capacitance and dendritic hypotrophy of BLA OTC PNs (Michaelson et al., 2020). Dendritic remodeling was also observed *in vivo* after repeated NPY administration into the BLA. Michaelson et al. (2020) found that NPY decreases whole-cell capacitance and morphological complexity of the dendritic arbors of BLA PNs (Michaelson et al., 2020). These data strongly suggest that NPY-induced structural

plasticity in BLA pyramidal neurons, which appears to account for the long-lasting anxiolytic effects. The NPY receptor subtype responsible for the long-term effects of NPY on both, anxiety and structural remodeling of BLA PNs remains to be resolved. The focus of this thesis is to investigate the cellular mechanism by which NPY induced stress resilience, in particular the role of Y_1Rs and Y_5Rs.

1.8 Neural pathways of fear and anxiety

As discussed earlier, the BLA receives sensory information from every modality. In the BLA, information if further processed and transmitted to downstream structure to orchestrate an appropriated response. We have also discussed that NPY reduced BLA excitability and promote stress resilience, however, the neural pathways underlying NPY-induced resilience (i.e the downstream targets of NPY-sensitive neurons) remains unresolved. In this section I will discuss the neural pathways of fear and anxiety that may underlie NPY-induced stress resilience.

1.8.1 Basolateral amygdala – medial prefrontal cortex.

The posterior BLA projects heavily to the medial prefrontal cortex (mPFC) (Fig. 3, Fig 4) (Hoover and Vertes, 2007), principally to layers V and II of the infralimbic mPFC (IL), a region of the cortex involved in the acquisition and expression of fear extinction, and prelimbic mPFC (PL), a region of the cortex highly involved in fear expression (Maren and Holmes, 2015). Moreover, cortical pyramidal neurons from layers V and II that receive inputs from the BLA project back to the amygdala, forming a strong reciprocal circuit regulating emotion (Little and Carter, 2013). Activity in the BLA inhibits activity in the mPFC evoked by aversive stimuli (Garcia et al., 1999). In contrast, pharmacological inactivation of the BLA using the $GABA_AR$ antagonist, muscimol,

decreases the firing rate of PL mPFC pyramidal neurons of fear-conditioned rats and abolishes conditional tone responses (Sotres-Bayon et al., 2012a). Fear extinction induces Fos expression in BLA neurons that project to the mPFC. More specifically, fear conditioning produced an increase in Fos expression predominantly in BLA neurons projecting to the PL mPFC. In contrast, fear extinction induces Fos expression in the BLA neurons projecting to IL mPFC. Additionally, photoinhibition of BLA-IL projecting neurons reduces extinction learning, while inactivation of BLA-PL projecting neurons results in increased extinction learning (Senn et al., 2014). This is of particular interest for this thesis because evidence suggests that intra-BLA injections of NPY inhibit fear expression, and a Y_1R antagonist injection into the BLA blocks fear extinction (Gutman et al., 2008). As discussed earlier, Herry et al. (2008) reported that the BLA contains two population of neurons with distinct function on fear. Fear neurons are active during fear and silent during extinction while extinction neurons are silent during fear and active during extinction (Herry et al., 2008). More recently, Uliana et al. (2020) studied the effect of stress in the BA-mPFC pathway. First, they found that stress increases the number of spontaneously active of BLA pyramidal neurons. Then, they stimulated BA neurons and simultaneously recorded the activity on the mPFC. In naïve rats (no stress) BA stimulation (which resembles increased BA activity induced by stress) induces LTD on mPFC. On rats subjected to stress, BA stimulation leads to a greater LTD on the mPFC (Uliana et al., 2020) that lasted 2 weeks, however no distinction was made between PL and IL mPFC. I believe that it is possible that NPY acts on BLA neurons (perhaps on fear neurons) that project to the PL mPFC to reduce their excitability, resulting in less fear.

1.8.2 Basolateral amygdala – bed nucleus of the stria terminalis - central amygdala

The BLA relays information both to the CeA and BNST (Fig 3B, Fig. 4). Outputs from both these structures project to numerous target areas and modulate the behavioral, autonomic and endocrine response to stress, which ultimately results in the elaboration of an integrated stress response. Davis and et al. (2009) have hypothesized that a long-lasting stimulus activates the BLA, whose projections then mediate the activation of CeM, to produce a phasic fear response. At the same time, the lateral division of the CeL facilitates the BLA direct excitatory drive to the BNST, via CRF release, to produce a sustained fear response (Walker et al., 2009), making a permanent record of the response, and representing a potential substrate for maladaptive responses such as PTSD. Work done by Tye et al. (2011) showed that the photostimulation and inhibition of BLA PNs terminals into the CeL of mice produce an acute decrease and increase in anxiety-like behaviors respectively, mostly by a feedforward inhibition of the CeM (Tye et al., 2011). Furthermore, in a two-chamber test, photostimulation specifically of BLA-CeM projecting neurons increases avoidance of the stimulus-paired chamber, promoting negative reinforcement (Namburi et al., 2015). Pharmacological inactivation of the BNST dampens anxiety-like behaviors (Walker and Davis, 1997), while its activation produces potentiates anxiety (Sajdyk et al., 2008a). Stress induces structural plasticity in BNST neurons. Specifically, repeated immobilization stress causes an increase in dendritic size and branching (Vyas et al., 2003), an effect that has been correlated with increased anxiety levels. Stress also increases CRF expression in the BNST and CeA (Walker et al., 2009) and repeated activation of CRF receptors in the BNST increases social anxiety (Lee et al., 2008). Recent studies have shown that photoinhibition and photostimulation of the BNST in mice decreases and increases anxiety-like behaviors, respectively (Kim et al., 2013b). Based on

the evidence describe above, I believe that it is possible that NPY acts on BLA neurons that project to the BNST to reduce their excitability, resulting in less anxiety.

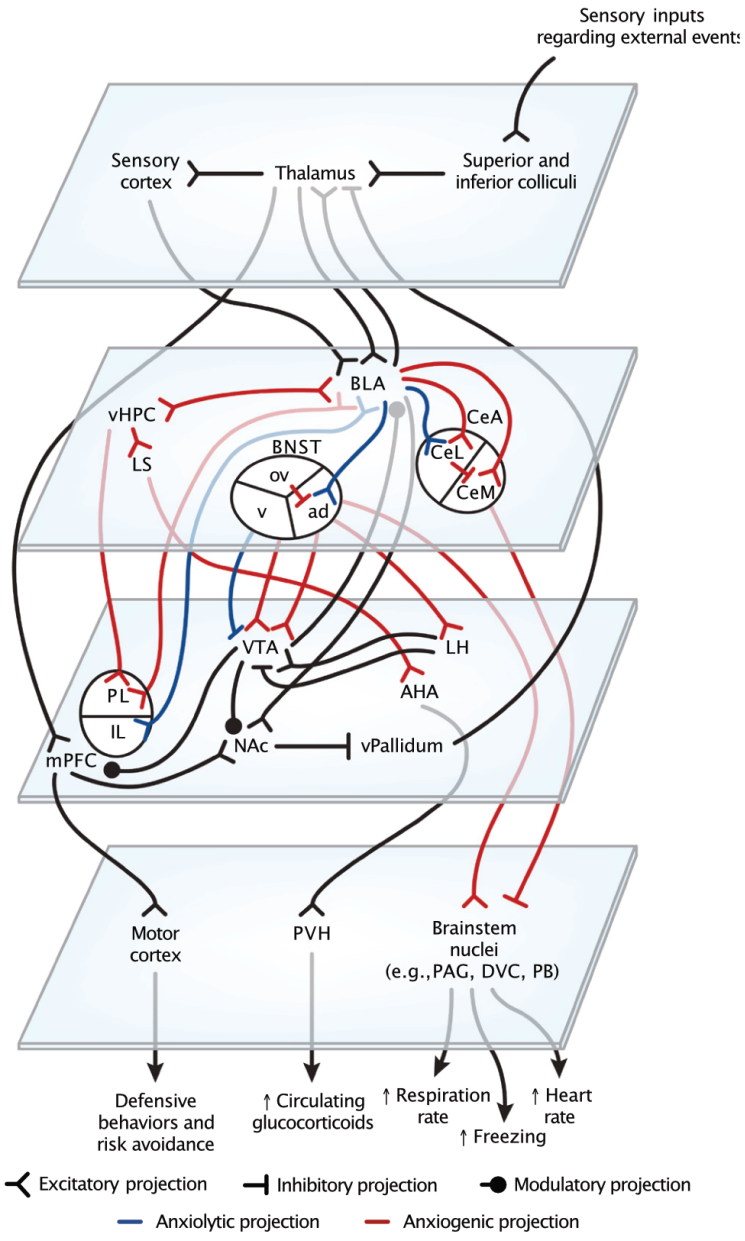

Figure 4: Neural pathways of anxiety proposed by Calhoon and Tye (2015). The BLA receives sensory thalamic and also cortical inputs. The BLA projects to a wide range of downstream regions to coordinate an appropriate emotional response. Abbreviations: ad, anterodorsal nucleus of the BNST; AHA, anterior hypothalamic area; BLA, basolateral amygdala; BNST, bed nucleus of the stria terminalis; CeA, central amygdala; CeL, lateral central amygdala; CeM, centromedial

amygdala; DVC, dorsal vagal complex; IL, infralimbic division of the mPFC; LH, lateral hypothalamus; LS, lateral septum; mPFC, medial prefrontal cortex; NAc, nucleus accumbens; ov, oval nucleus of the BNST; PAG, periaqueductal gray; PB, parabrachial nucleus; PL, prelimbic division of the mPFC; PVH, paraventricular nucleus of the hypothalamus; v, ventral BNST; vHPC, ventral hippocampus; vPallidum, ventral pallidum; VTA, ventral tegmental area.

1.9 Thesis Objectives

NPY produces anxiolysis by supressing I_h and reducing excitability of a subpopulation of BLA pyramidal neurons (Giesbrecht et al., 2010b). NPY also produces a sustained state of anxiolysis, or stress resilience, via downregulation of I_h (Silveira Villarroel et al., 2018) and dendritic hypotrophy of pyramidal BLA pyramidal neurons (Michaelson et al., 2020). The acute effects of NPY are mediated by Y_1Rs, however there is evidence suggesting that Y_5Rs also play a role in NPY-induced anxiolysis (Sajdyk et al., 2002a). The cellular mechanisms responsible for the long-term effects of NPY are unknown.

The specific objectives of this component of the thesis are to test:

a) the hypothesis that Y_1Rs and not Y_5Rs of the BLA mediate the long-lasting anxiolytic actions of NPY, reduce BLA PNs excitability and promote dendritic hypotrophy. To test the participation of Y_1Rs, I will inject a selective Y_1R agonist or vehicle into the BLA of rats for five days. Then I will study anxiety behavior on the SI test followed by the basic electrical properties and morphology of BLA PNs. To test the participation of Y_5Rs I will use BLA OTCs treated with a selective Y_5R agonist and NPY + a Y_5R antagonist. Then, I will study the basic electrical properties and morphology of BLA OTC. Finally, I will inject a selective Y_5R agonist, NPY + a Y_5R antagonist or vehicle into the BLA of rats for five days and then study anxiety behavior on the SI test followed by *in vitro* analysis of the basic electrical properties and morphology of BLA PNs from all groups.

b) that NPY acts on BLA neurons that project to the PL mPFC and BNST to reduce overall fear and anxiety. To test his hypothesis first I will inject a retrograde tracer into the PL mPFC or the BNST. Then, I will study the effect of NPY on the excitability of BLA PNs that specifically project to the PL mPFC or BNST using acute BLA slices. After, I will inject NPY into the BLA for five days and study the effect of an NPY treatment on BLA neurons that project to the PL mPFC and BNST.

2. Methods

2.1 Animals

Male Sprague – Dawley rats aged 5 weeks were pair housed throughout the experiment and given water and food *ad libitum*. The housing room was maintained on a 12 h light/dark cycle (7:00 A.M./7:00 P.M.) at 22°C. One week of acclimatization was allowed before the animals were included in any experimental procedures. During this one-week period all animals were handled daily, twice a day for 10 minutes per animal, to ensure that all animals were habituated to our experimental procedures, manipulations and to reduce the stress related to transport and novel environment. All procedures were in approved by the University of Alberta Animal Ethics Committees and performed in accordance with their guidelines for the care, handling, and treatment of experimental animals.

2.2 Stereotaxic Surgery

Stereotaxic surgery was performed as described previously (Silveira Villarroel et al., 2018) with minor modifications. Rats were deeply anesthetized with ketamine (90 mg/kg, i.p.) and xylazyine (10 mg/kg, i.p.) or isofluorane 2.5% using a SomnoSuite low flow vaporizer (Kent Scientific) and placed in a stereotaxic apparatus with a digital readout (David Kopf, Tujunga, California include the model). Anesthesia was carefully monitored, by pinching the four paws, to maintain surgical plane throughout and animals were kept at 36.5˚C with a temperature-controlled heating pad (Harvard Apparatus). Bilateral guide cannulas (26 gauge; length, Plastics One, Roanoke, VA) were implanted into the BLA [anteroposterior (AP): -2.3; mediolateral (ML): ±5.0; dorsoventral (DV): -6.4; incisor bar: -3.2 mm] according to the stereotaxic atlas of the rat brain (Paxinos and Watson,

1986). The guide cannulas were secured to the skull with four stainless steel screws (0-80 x 1/8; Plastics One) and self-curing acrylic resin (Lang Dental Manufacturing Company, Inc., IN).

For retrograde tracing experiments, 46 nl of red or green fluorescent latex microspheres (Lumafluor Inc., NC) were unilaterally injected via borosilicate glass capillarie using a Nanojector II (Drummond Sci., PA) on the following coordinates: PL mPFC [anteroposterior (AP): +1.75 mm; mediolateral (ML): ± 0.3mm; dorsoventral (DV): -2.3 mm; incisor bar: -3.2 mm] (Senn et al., 2014), IL mPFC [anteroposterior (AP): +1.75 mm; mediolateral (ML): ± 0.3 mm; dorsoventral (DV): -2.5 mm; incisor bar: -3.2 mm] (Senn et al., 2014) or BNST [anteroposterior (AP): -0.26 mm; mediolateral (ML): ± -1.6 mm; dorsoventral (DV): -0.64 mm; incisor bar: -3.2 mm] (Kim et al., 2013a). The injector remained in place for 1 extra minute after the injection to backflow and to avoid spreading of the retrobeads to surrounding areas during capillary removal. 1 week was allowed from the procedure to ensure retrograde labelling.

After completion of surgeries, all animals received meloxicam (Boerhringer Ingelheim, Burlington, Ontario; 1 mg/kg, s.c.), 10 ml of saline 0.9% s.c., and were placed on a warm heating pad until they had fully recovered from the anesthetic. A general score was assigned following our animal post-operative monitoring SOP which includes body condition, responsiveness score, respiration score, posture, gait, hair coat and vocalization. Full recovery (60-90 min) from the anesthesia was determined by evaluating attentiveness, responsiveness to touch and food and water consumptions. Rats remained single housed for three days to recover from the procedure and then housed in pairs and kept together throughout the remainder of the experiment.

2.3 Intracranial microinjections procedures.

All compounds were administrated as described previously (Silveira Villarroel et al., 2018). Drugs were delivered bilaterally into the BLA for five consecutive days via two injection cannulas (33 Ga; Plastics One, Roanoke, VA) that extended 2 mm past the distal end of the guide cannulae. Injection cannulae were each connected via polyethylene tubing (PE50; Plastics One, Roanoke, VA) to a 1 μL Hamilton syringe placed on an infusion pump (Harvard Apparatus, Holliston, MA; model PHD ULTRA). Animals were conscious and gently hand-restrained during the procedure. Vehicle (sterile saline) alone or containing drugs was delivered at 100 nl/30 s per side. The injection cannulae were left in place for 1 min afterward to prevent backflow. The injection cannulae remained in place for an additional 2 minutes post injection to ensure complete delivery of the solution and to minimize backflow once the cannulae were removed. The injectors were then removed and tested for proper flow to ensure that that had not become obstructed during the drug administration. Injector caps were placed into the guide cannulas immediately after the cannulae were removed and animals returned to their homecages.

2.4 Behavioral Test.

The social interaction (SI) test was performed according to (Sajdyk et al., 2008b) with minor modifications. Briefly, experimental animals were simultaneously placed into the SI box (96 cm long x 96 cm wide x 30 cm high with an open top) with a partner rat. All partner rats were of same sex, similar age and weight, housed under identical conditions and had no previous contact with the experimental animal. A 10 min test was performed under high-light familiar conditions. All testing was video-taped for subsequent analysis. The total amount of time the experimental animal spent initiating interaction (i.e., grooming, sniffing, crawling, playing) with the partner rat was

registered. Time spent displaying aggressive behavior, defined as fighting and biting was not included as part of the interaction time. Before any behavioral test, a sham injection was performed to ensure animals were habituated to the injection procedure. The following day, rats were injected vehicle and thirty minutes later baseline anxiety-like levels were established by exposing rats to the SI test. Two days after, rat anxiety behavior was re-evaluated on the SI test 30 min after the first injection (D1). This was repeated on day 5, again 30 min after the fifth drug injection (D5), and again at two and four weeks (W2 and W4 respectively) after the first injection on D1. All drug administration and SI testing was conducted between 8:00 A.M. and 1:00 P.M.

2.5 Acute slice preparation

Rates, aged P70, were decapitated, and their brains were rapidly submerged in ice-cold (4˚C) aCSF slicing solution, containing the following (in mM): 118 NaCl, 3 KCl, 1.3 $MgSO_4$, 1.4 NaH_2PO_4, 5.0 $MgCl_2$, 10 D-glucose, 26 $NaHCO_3$, 2.5 $CaCl_2$, and 1.0 kynurenic acid and bubbled with carbogen (95% O_2, 5% CO_2) (Giesbrecht et al., 2010b; Silveira Villarroel et al., 2018). Brains were trimmed and the tissue containing the BLA was secured to the vibrating slicer chamber with cyanoacrylate glue and hemisected. Meninges and blood vessels were carefully removed, and tissue was immersed on ice-cold (4˚C) aCSF slicing solution. Coronal sections 300 µm thick were cut serially from rostral to caudal using a vibratome slicer (HR2; Sigmann Elektronik). Four slices per hemisphere containing the BLA (as determined visually by the almond-shaped structure surrounded medially and laterally by the internal and external capsule, respectively) were prepared. Slices were then transferred to a room temperature (23˚C), carbogenated aCSF containing the following (in mM): 124 NaCl, 3 KCl, 1.3 $MgSO_4$, 1.4 NaH_2PO_4, 10 D-glucose, 26

$NaHCO_3$, and 2.5 $CaCl_2$. Osmolality for both aCSF was adjusted to 300 mOsm/kg. Slices were kept at room temperature for at least of 60 min before being placed into the recording chamber.

2.6 Organotypic slice preparation.

Organotypic cultures were prepared using the interface method described previously (Stoppini et al., 1991) with minor modifications. Briefly, P14 rats were decapitated, their brains rapidly removed under sterile conditions and submerged in ice-cold (4˚C) Hanks balanced salt solution containing 0.6% D-glucose and 30 mM kynurenic acid. The brain was imbedded in agarose. Trimmed agarose-brain blocks were secured with cyanoacrylate glue to a custom slicing chamber, immersed in cold (4˚C) slicing solution. Coronal slices 350 μm thick were cut serially from rostral to caudal using a vibratome and trimmed to size. Four slices per hemisphere containing the BLA (as determined visually under a dissecting microscope) were allowed to stabilize in slicing solution at 4˚C for 30-45 min. Slices where mounted on individual semiporous membrane inserts (Millicell Culture plate inserts, Fisher) and placed in 24-well plates with 300 ml of culture media (50% minimum essential medium (MEM), 25% heat-inactivated horse serum, 25% Hanks balanced salt solution, supplemented with: 1 mM Glutamax, 1% D-glucose, 0.5 mM L-ascorbic acid, and 25 U/ml penicillin/streptomycin). After 48 h, slices were treated with an antimitotic solution of 1:1:1 cytosine-b -D-arabinofuranoside, uridine, and 5-fluro-29-deoxyuridine added on the culture media at a 0.5 mM final concentration for 24 h to prevent glial proliferation. Slices were maintained at 37°C in 5%/95% CO2/air. Slices remained in culture for 4 weeks prior to any manipulation. Media was changed three times per week for the duration of the experiment, except during drug incubations.

2.7 Whole-cell electrophysiology

Intracellular whole-cell recordings of BLA neurons were made under voltage- or current-clamp configuration on brain slices prepared acutely from P70 rats or Equivalent Postnatal (EP) 9-10 weeks OTC slices that were still attached to the culture insert membrane. Recordings were obtained under infrared-differential interference contrast (60x) optics microscope (Axioskop FS2; Carl Zeiss). Patch pipettes were pulled from borosilicate glass (6 mm, 1.2 mm OD, 1.12 mm ID. TW150F; World Precision Instruments) with a two-stage puller (PP-83; Narishige) and had resistances of 4-6 MΩ when filled an internal solution containing the following (in mM): 126 K-gluconate, 4 KCl, 10 HEPES, 5 MgATP, 0.3 NaGTP, 1 EGTA, 0.3 CaCl2, and 0.2% neurobiotin (pH 7.27, 275 mOsm/L for acute slices and 300 mOsm/L for OTCs). Recordings were made using either a Multiclamp 700B or AxoClamp2A amplifiers and data was acquired using pClamp (version 10.4) via a DigiData 1322 or Digidata 1440 interface (all Molecular Devices, need city). Acute and organotypic slices were held submerged by a platinum and polyester fiber "harp" in a fixed-stage 5 mL recording chamber (Giesbrecht et al., 2010) and viewed with a movable upright microscope (Axioskop FS2; Carl Zeiss). Slices were perfused continuously with warm (34˚C ± 0.5˚C), carbogenated aCSF between 2 and 2.5 ml/min for 20 min before any recordings were made. Osmolarity was adjusted to 300 mOsm/L for acute slices and 320 mOsm/L for organotypic slices. The BLA from acute and OTCs slices was identified under a 5X objective as the basal and lateral region between the internal and external capsule using criteria based on the Paxinos and Watson (1986) rat brain atlas. BLA PNs were visually identified under a 60X objective using infrared-differential contrast optics (ir-DIC) and appropriate epifluorescence illumination. BLA PNs were selected from random locations throughout the BLA based on their large pyramidal-shaped soma with a prominent apical dendrite. BLA neurons were also characterized by their very negative

resting membrane potential (-75 – 85 mV), low input resistance (40 – 100 ΩOhm), >1ms half-width APs (double of most interneurons), and spike frequency adaptation (Washburn and Moises, 1992; Giesbrecht et al., 2010a; Silveira Villarroel et al., 2018; Mackay et al., 2019; Michaelson et al., 2020). GigOhm seals were established on either voltage or current clamp mode. Once a seal was formed, the command potential was set near the estimated resting membrane potential (-75 mV, corrected for +15 mV of liquid junction potential) and the patch was ruptured by gentle suction. Voltage-clamp data were low-pass filtered at 3 kHz and digitized at 10kHz. Access resistance was measured throughout the experiment, and only those cells with changes lower than 20% were included in the analyses. Capacitance was calculated offline with pClamp from the area under the curve of the current response evoked by a 200 ms, 10 mV hyperpolarizing voltage step. No capacitance compensation was applied. Spontaneous synaptic activity was recorded (20 kHz sampling rate) in voltage clamp at a (liquid junction potential-corrected) at holding potential of -55 mV (corrected for +15 mV of liquid junction potential) and spontaneous event detection was performed offline using MiniAnalysis software (Synaptosoft). For ach neuron the first 400 synaptic events of each polarity were analyzed using the predetermined suggested thresholding parameters for IPSCs and EPSCs.

Reagents and drugs. NPY (human, rat) was purchased from the Polypeptide Group (CA, USA). The NPY Y_1R-agonist (F^7,P^{34}-NPY) and the NPY Y_5R-agonist ([cPP$^{1-7}$,NPY$^{19–32}$, Ala^{31},Aib^{32},Gln^{34}]hPP) were generous gifts from Dr A.G. Beck-Sickinger. The Y_5R antagonist, CGP71683, was purchased from Tocris Bioscience. Culture reagents were all obtained from Invitrogen, except for cytosine-b-D-arabinofuranoside, uridine, and 5'fluro-2'deoxyuridine, which

were from Sigma- Aldrich. Pipette solution reagents were all from Sigma-Aldrich, except for Na-GTP (Roche Diagnostics).

2.8 Cell processing and labeling.

Neurons from BLA and OTC slices were all processed, stained, imaged, reconstructed, and subjected to morphologic analyses. Following whole-cell recordings, OTCs and acute slices were fixed with 10% formalin (Thermo Fisher Scientific) for 24-72 h at 4° C. Slices were then transferred to 0.2% sodium azide in phosphate buffered saline (PBS, 1X) for storage and kept at 4°C for posterior processing. Free-floating slices were washed 3 x 10 min each in PBS before blocking and permeabilization for 2 h with 0.3% Triton X-100 in PBS and 4% normal goat serum (Sigma-Aldrich). Slices were incubated with streptavidin conjugated with AlexaFluor-555 or -546 (1:1000; Invitrogen) in 0.3% Triton X-100 in PBS with 4% normal goat serum for 3 h at room temperature. Slices were washed 4 x 10 min each in PBS, mounted on Superfrost Plus slides, and coverslips were applied with Prolong Gold mounting media (Thermo Fisher Scientific). Slides were allowed to air dry in the dark at room temperature before imaged via confocal microscopy.

2.9 Imaging and neuronal reconstruction.

For morphologic analysis of filled neurons, z-stack images were obtained with a 20x objective, 1024 x 1024 resolution and 100 Hz for a series of 0.8 mm steps. An excitation wavelength of 543 nm with a laser scanning confocal microscope (TCS SP5; Leica Microsystems. Imaging Core University of Alberta). Multiple single-plane images at 10x magnification, 512x512 resolution and 100 Hz were taken to determine the position of each neuron within the slice and stitched together using Leica LAS AF software. Only those neurons whose dendritic arbor was healthy looking,

distal dendrites were not trunked or retracted, cell body was clearly within the boundaries of the BLA and had stable electrophysiological recordings were included in the analyses. The neurite tracer function in FIJI (National Institutes of Health) was used for neuronal reconstruction. Sholl analysis (SHOLL, 1953) of the entire dendritic reconstruction was performed using a 10 µm increasing concentric radii with FIJI software. Total dendritic length and dendritic branching were calculated using FIJI and Excel software.

2.9 Statistical analysis

Electrophysiological data were viewed and analyzed offline using pCLAMP 10.3. All membrane potential data were corrected offline for the calculated 15mV, liquid junction potential associated with K-gluconate solution (Chee et al., 2010; Giesbrecht et al., 2010a; Silveira Villarroel et al., 2018; Mackay et al., 2019; Michaelson et al., 2020). Traces from electrophysiological recordings, statistical analysis, and graphs were prepared using versions 7-8 of Prism software (GraphPad). Neuronal reconstruction and Sholl analysis were performed using the FIJI software (National Institutes of Health). All data are presented as mean ± SEM. One-way ANOVA with Tukey's post hoc multiple comparisons test or two-way RM ANOVA with Tukey's post hoc test for multiple comparisons, two-tailed Student's t test or Mann-Whitney U tests were performed when appropriated.

3. Results

3.1 Y_1R agonist fails to produce a durable anxiolytic phenotype.

Repeated injections of NPY into the BLA for five days produces a long-term increase in social interaction compared to vehicle (Sajdyk et al., 2008b; Silveira Villarroel et al., 2018), which corresponds to a less anxious behavioral phenotype or stress resilience. This is accompanied by hyperpolarization, suppression of I_h, decrease in excitability, reduction of inward rectifying current (I_{IR}) (Silveira Villarroel et al., 2018) and cell capacitance, and hypotrophy of BLA pyramidal neurons (Michaelson et al., 2020). Additionally, the acute anxiolytic actions of NPY in the BLA are mediated principally by the activation of Y_1Rs (Sajdyk et al., 1999; Giesbrecht et al., 2010a), however the mechanisms underlying stress resilience are unknown. Thus, the first question we asked is whether repeated activation of Y_1Rs in the BLA is responsible for the long-term anxiolytic actions of NPY. We hypothesized that the repeated activation of BLA Y_1Rs will result stress resilience, decreased excitability and hypotrophy of BLA pyramidal neurons that outlasts the period of agonist administration. We evaluated the effect of bilateral injections of 10 pmol of the Y_1R-selective agonist [F^7, P^{34}]NPY, or vehicle, for five days (D1 – D5) into the BLA on anxiety behavior using the social interaction (SI) test. We evaluated SI time before the beginning of the treatment (pre-treatment baseline), at D1, D5, 2 (W2) and 4 weeks (W4) after the beginning of the treatment. After W4, we performed electrophysiological experiments on BLA neurons from the Y_1R agonist- and vehicle-treated groups to assess lasting changes in passive membrane properties, excitability and morphology.

Administration of the Y_1R agonist increased SI time by 40 ± 14% ($p < 0.05$, RM two-way ANOVA, Tukey's multiple comparisons test) at D1 and by 82 ± 23 % ($p < 0.001$, RM two-way

ANOVA, Tukey's multiple comparisons test) at day 5 compared to pre-treatment baseline (n = 9) and compared to the control-treated group (n = 7). However, this increase in SI time evoked by the Y_1R agonist did not persist. At Week 2 and week 4 SI was not different than baseline levels (Fig. 5. W2: 128 ± 11 %, p=0.96. W4: 131 ± 12%, p=0.99. RM two-way ANOVA, Tukey's multiple comparisons test). This result suggests that Y_1Rs activation produces an acute decrease in anxiety (D1-D5) but, more importantly, the activation of Y_1Rs does not lead to a long-term reduction in anxiety (W2-W4). Thus, the mechanisms underlying the NPY-induced stress resilience are not due to the repeated activation of Y_1Rs.

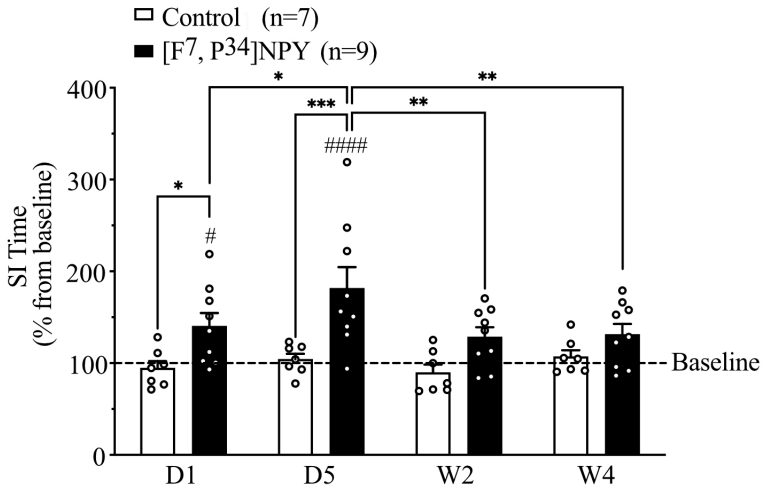

Figure 5: Effect of repeated BLA injections of a Y_1R agonist [F^7, P^{34}]NPY on anxiety-like behavior in the social interaction test. Time course of social interaction time as a percentage of baseline of rats that received an injection of either vehicle (control) or a the Y_1R-selective agonist directly into the BLA, daily for five consecutive days. SI time was measured before any treatment to account for baseline anxiety levels, at Day 1 (D1) and Day 5 (D5) of treatment, and 2 (W2) and 4 weeks (W4) from the first injection. Data represent the Mean ± SEM. *p = significantly different from vehicle. #p = Significantly different from baseline.

We know that NPY, when given repeatedly for five days, triggers plastic changes on BLA pyramidal neurons that can give account for the decrease in anxiety levels (Silveira Villarroel et al., 2018; Michaelson et al., 2020). When a treatment, in this case the Y_1R agonist, brings about a change in behaviour that reverses upon removal of the drug, one possible explanation is that the actions of the drug were acute and had no long-lasting effect on neuronal or network function. Another possibility is that compensatory mechanisms developed that returned anxiety levels to normal despite permanent changes on BLA neurons. Therefore, we next studied whether BLA pyramidal neurons form animals treated with the Y_1R agonist were different from controls. Specifically, we evaluated if the treatment with [F^7, P^{34}]NPY changes in the amplitude of I_h and inward rectifying (I_{IR}) current, as well as resting membrane potential and rheobase.

The max I_h amplitude of BLA pyramidal neurons from animals treated with the Y_1R agonist was not different from controls (Fig. 6A. Control: -351 ± 26 pA n = 40; [F^7, P^{34}]NPY: -333 ± 19 pA n = 54, p>0.99, Two-way ANOVA, Bonferroni's multiple comparisons test). The I_{IR} current of BLA pyramidal neurons from the Y_1R agonist-treated group was not different form controls (Fig. 6B. Control: -1006 ± 42 pA n = 31; [F^7, P^{34}]NPY: -1000 ± 41 pA, n = 50, p=0.99, Two-way ANOVA, Bonferroni's multiple comparisons test). Surprisingly, we found that the resting membrane potential of pyramidal neurons from the Y_1R agonist-treated group was 3.1 ± 1.2 mV more hyperpolarized than controls (Fig. 6C. Control: -78.9 ± 0.8 mV, n = 38; [F^7, P^{34}]NPY: -82.0 ± 0.9 mV, n = 39, p=0.013, unpaired student's test). This more hyperpolarized state on BLA pyramidal neurons from the Y_1R agonist-treated group was accompanied by an increased rheobase compared to controls (Fig, 6D. Control: 317 ± 13 pA, n = 39; [F^7, P^{34}]NPY: 374 ± 19 pA, n = 38, p=0.017, unpaired student's test), suggesting that the repeated activation of Y_1Rs hyperpolarizes and

decreases excitability of BLA pyramidal neurons without suppressing I_h or reducing I_{IR}. Finally, we found no difference in capacitance (Fig. 6E. Control: 231 ± 6 pF, n = 64, Y_1R agonist: 239 ± 6 pF, n = 57, p=0.34, unpaired student's test). Taken together, these results suggest that the repeated activation of Y_1R in the BLA produces a long-term hyperpolarization and a decrease in excitability of BLA pyramidal neurons *in vivo*, however, this is not sufficient to maintain a persistent less anxious phenotype.

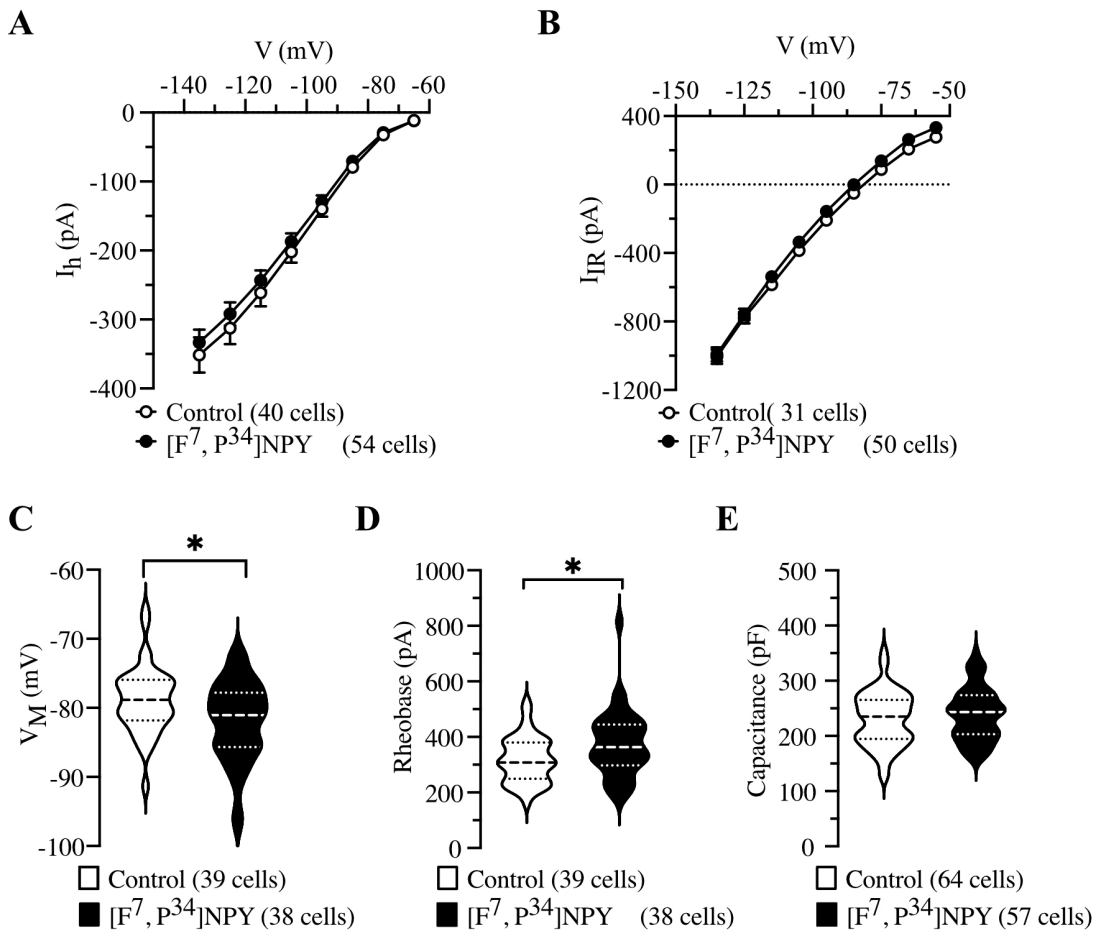

Figure 6: Passive resting properties of BLA pyramidal neurons from animals treated with the Y_1R agonist [F^7, P^{34}]NPY. A-E. Effect of [F^7, P^{34}]NPY on I_h amplitude (A), I_{IR} (B), RMP (C), rheobase (D) and cell capacitance (E) of BLA pyramidal neurons. Data represent the Mean ± SEM. *p = significantly different relative to control-treated animals. Violin plots on C, D and E show the 1st and 3rd quartile in lower and upper dotted lines, respectively, and the median in a dashed line. Violin plot shapes indicate the density of the data at different values smoothed by a Kerner density estimator.

3.2 Effect of Y_5R activation on resting properties of BLA OTCs neurons.

The observation that Y_1R-agonism produces an acute, but not long-lasting anxiolytic *in vivo* (Fig. 1), suggests that other NPY receptors are involved in the development of stress resilience. Y_2 receptors promote anxiety (Nakajima et al., 1998; Sajdyk et al., 2002b) and increase BLA pyramidal neurons excitability acutely (Mackay et al., 2019), making the activation of Y_2R unlikely to mediate the anxiolytic actions of NPY. There is also evidence suggesting that Y_5 receptors regulate anxiety. Intra-BLA microinjections of a Y_2R/Y_5R preferring agonist at doses that activate Y_5R decreases anxiety levels (Sajdyk et al., 2002a). Thus, we explored the role of Y_5R in mediating long term changes in BLA pyramidal neuron properties. We used a novel organotypic slice culture model of the BLA as an intermediate interface to test the role of Y_5R because (i) it allows for easier acute and long-term pharmacological manipulations than *in vivo* models, (ii) we have reported that BLA OTC neurons develop and resemble BLA neurons from adult rats (Michaelson et al., 2020) and (iii) work done previously by Dr. Michaelson shows that NPY decreases I_h amplitude, reduces the excitability (Michaelson & Colmers, unpublished), whole-cell capacitance and causes hypotrophy of BLA OTC neurons, resembling the effects of NPY *in vivo* (Michaelson et al., 2020). We hypothesized that the persistent activation of BLA OTC Y_5R using a selective Y_5R agonist will result in decreased I_h, reduced neuronal excitability and membrane capacitance, and hypotrophy of BLA pyramidal neurons. To test this, we administered vehicle (control group) or the Y_5R-selective agonist, [cPP($^{1-7}$),NPY($^{19-23}$),Ala^{31},Aib^{32}, Gln^{34}]hPP (cPP, 0, 1, 10, 100 nM) to BLA OTCs for five days and evaluated passive membrane properties and morphology of BLA OTC neurons 1-2 weeks after the treatment (controls vs Y_5R agonist).

Incubation of BLA OTC neurons with the Y_5R agonist, cPP, did not change the max I_h amplitude (Fig. 7A. Control: -364 ± 38 pA, n = 30, p>0.9; 1 nM: -409 ± 54 pA, n = 29, p>0.9; 10 nM: -335 ± 37 pA, n = 42, p>0.9; 100 nM: -308 ± 53, n = 32, p>0.9. Two-way ANOVA, Tukey's multiple comparisons test), nor the max I_h density (Fig. 7B. Control: -2.3 ± 0.2 pA/pF, n = 30; 1nM: -2.6 ± 0.3 pA/pF, n = 29, p=0.6; 10 nM: -2.8 ± 0.4 pA/pF, n = 42, p=0.2; 100 nM: -2.3 ± 0.3 pA/pF, n = 32, p>0.9. Two-way ANOVA, Tukey's multiple comparisons test). Kinetic analysis of I_h revealed a faster activation of I_h (Fig. 7C). Specifically, 100 nM cPP decreased the fast component of the time constant (τ fast) of the I_h activation curve (Fig. 7C. Control: 10.6 ± 1.4 ms, n = 31; 1 nM: 9.1 ± 1.3 ms, n = 29, p=0.7; 10 nM: 7.5 ± 0.9 ms, n = 40, p=0.1; 100 nM: 5.3 ± 0.5 ms, n = 29, p = 0.047, One-way ANOVA, Tukey's multiple comparisons test). There was no difference in the slow component (τ slow) of I_h activation curve (Fig. 7D. Control: 66.8 ± 5.1 ms, n = 31; 1 nM: 74.4 ± 7.3 ms, n = 29, p=0.7; 10 nM: 55.8 ± 4.2 ms, n = 40, p=0.4; 100 nM: 50.9 ± 2.7 ms, n = 30, p=0.1. One-way ANOVA, Tukey's multiple comparisons test). There was also no difference in half activation voltage (V50) if I_h (Fig. 7E. Control: -98.45 ± 2.1 mV, n = 32; 1 nM: -101.6 ± 2.4 mV, n = 32, p=0.8; 10 nM: -99.6 ± 2.0 mV, n = 44, p=0.9; 100 nM: -100.9 ± 2.5 mV, n = 32, p=0.9. One-way ANOVA, Tukey's multiple comparisons test).

Treatment with the Y_5R agonist was also without effect on max I_{IR} (Fig. 7F. Control: -1095± 95 pA, 100 nM: -1032 ± 98, n = 32, p>0.9, Two-way ANOVA, Bonferroni's multiple comparisons test), resting membrane potential (Fig. 7G. Control: -78.7 ± 0.9 mV, n = 30, 1 nM: -82.8 ± 1.4 mV, n = 32, p=0.1, 10 nM: -81.6 ± 1.0 1 mV, n = 46, p=0.3; 100 nM: -81.8 ± 1.2 mV, n = 34, p=0.3. One-way ANOVA, Tukey's multiple comparisons test) or rheobase (Fig. 7H. Control: 300 ± 27 pA, n = 30; 1 nM: 338 ± 40 pA, n = 32, p=0.9; 10 nM: 321 ± 27 pA, n = 46, p=0.9; 100 nM: 300

± 39 pA, n = 34, p>0.9. One-way ANOVA, Tukey's multiple comparisons test). There was no change in input resistance (Fig. 7I. Controls: 104.3 ± 8.6 MΩ, n = 30; 1nM: 108.3 ± 12.8 MΩ, p=0.9, n = 32, 10 nM: 1007.0 ± 6.0 MΩ, n = 50, p=0.9; 100 nM: 113.6 ± 8.2 MΩ, n = 34, p=0.9. One-way ANOVA, Tukey's multiple comparisons test). Compared to control BLA OTC neurons, those treated with the the Y_5R agonist at 10 nM and 100 nM had smaller membrane capacitance. (Fig. 7J. Control: 160 ± 12 pF, n = 30; 1 nM: 154 ± 12 pF, n = 32; 10 nM: 121 ± 5 pF, n = 47, p=0.009; 100 nM: 119 ± 6 pF, n = 34, p=0.01. One-way ANOVA, Tukey's multiple comparisons test).

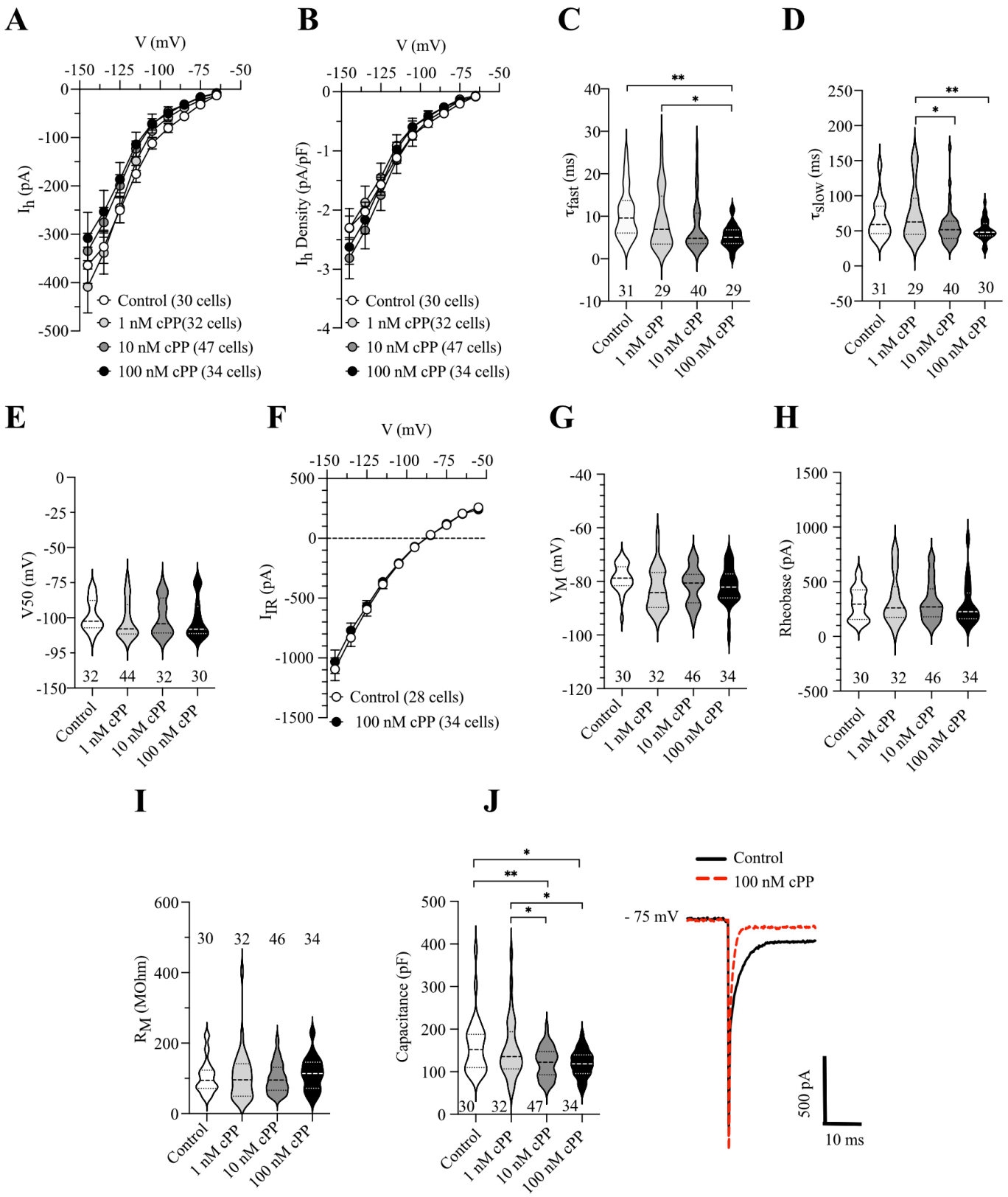
A
V (mV)
-150 -125 -100 -75 -50
0
-100
-200
-300
-400
-500
I_h (pA)
Control (30 cells)
1 nM cPP(32 cells)
10 nM cPP (47 cells)
100 nM cPP (34 cells)
B
V (mV)
-150 -125 -100 -75 -50
0
-1
-2
-3
-4
I_h Density (pA/pF)
Control (30 cells)
1 nM cPP(32 cells)
10 nM cPP (47 cells)
100 nM cPP (34 cells)
C
τ_{fast} (ms)
40
30
20
10
0
-10
**
*
31 29 40 29
Control
1 nM cPP
10 nM cPP
100 nM cPP
D
τ_{slow} (ms)
250
200
150
100
50
0
-50
**
*
31 29 40 30
Control
1 nM cPP
10 nM cPP
100 nM cPP
E
V50 (mV)
0
-25
-50
-75
-100
-95
-150
32 44 32 30
Control
1 nM cPP
10 nM cPP
100 nM cPP
F
V (mV)
-150 -125 -100 -75 -50
500
0
-500
-1000
-1500
I_{IR} (pA)
Control (28 cells)
100 nM cPP (34 cells)
G
V_M (mV)
-40
-60
-80
-100
-120
30 32 46 34
Control
1 nM cPP
10 nM cPP
100 nM cPP
H
Rheobase (pA)
1500
1000
500
0
-500
30 32 46 34
Control
1 nM cPP
10 nM cPP
100 nM cPP
I
R_M (MOhm)
600
400
200
0
30 32 46 34
Control
1 nM cPP
10 nM cPP
100 nM cPP
J
Capacitance (pF)
500
400
300
200
100
0
*
**
*
*
30 32 47 34
Control
1 nM cPP
10 nM cPP
100 nM cPP
Control
100 nM cPP
- 75 mV
500 pA
10 ms

Figure 7: Effect of repeated treatment with three concentrations of the Y_5R agonist [cPP(1-7),NPY(19-23),Ala31,Aib32, Gln34]hPP (cPP) on the passive resting properties of BLA OTC neurons. A-J. Effect of cPP on I_h amplitude (A), time constant of I_h activation (B, C), V1/2 of I_h (D), I_h density (E), inward rectifying current (F), RMP (G), rheobase (H), input resistance (I) and whole-cell capacitance (J). Data on A, B, F represent the Mean ± SEM. Violin plots on C, D and E show the 1st and 3rd quartile in lower and upper dotted lines, respectively, and the median in a dashed line. Violin plot shapes indicate the density of the data at different values smoothed by a Kerner density estimator.*$p < 0.05$, **$p<0.01$. *p = significantly different relative to control-treated animals.

The Y_5R agonist also increased inter event interval (IEI) of spontaneous excitatory post-synaptic currents (sEPSCs, Fig. 8A, B, C. Mann-Whitney U test; U = 299.0, p = 0.80) and decreased of spontaneous inhibitory post-synaptic currents IEI (sIPSCs, Fig. 8A, B, C. Mann-Whitney U test; U = 269.0, p =0.40). sPSC amplitude was unaffected (Figure 8A, B, D. sEPSCs amplitude ann-Whitney U test; U = 259.0, p = 0.30. sIPSCs amplitude Mann-Whitney U test; U = 111.0, p <0.0001). This reduction in capacitance and decrease in excitatory observed with the Y_5R agonist was similar to the effect of NPY reported on this model (Michaelson et al., 2020).

In summary, we show that the persistent activation of Y_5Rs for five days in culture decreases the size of BLA OTC neurons and reduces excitatory drive while increasing inhibitory drive onto BLA OTC neurons *in vitro*. Thus, our results support the possibility that Y_5Rs might contribute to the hypotrophy and reduction in overall excitability of BLA neurons that is induced by NPY.

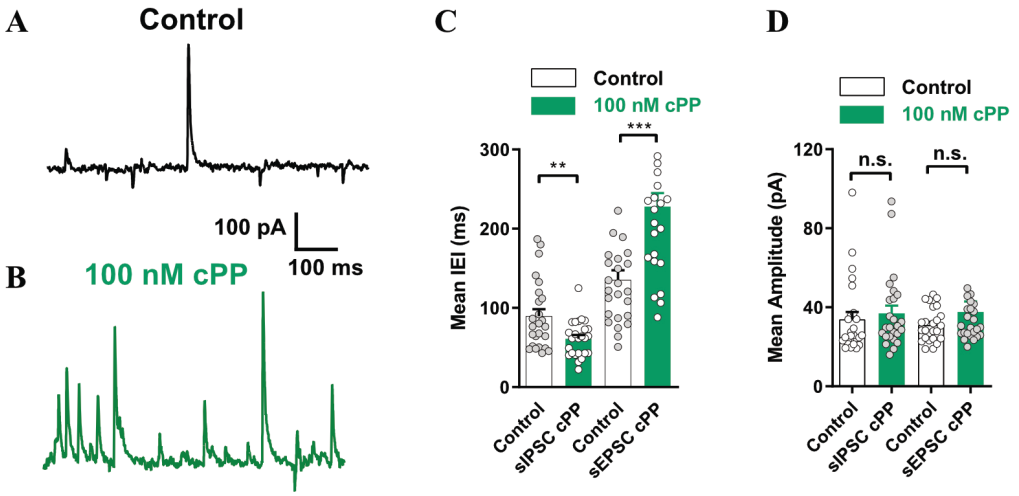

Figure 8: Effect of the Y_5R agonist, cPP, on synaptic activity of BLAOTCs neurons. A, B. Representative traces of a BLAOTC control neuron (A) and a neuron treated with 100 nM cPP (B). C. Mean sIPSC and sEPSC inter-event interval from controls neurons and neurons treated with 100 nM cPP. D. Mean sIPSC and sEPSC amplitude from controls neurons and neurons treated with 100 nM cPP. Data represent the Mean ± SEM. **p<0.01, ***p<0.001. Modified with permission from (Michaelson et al., 2020).

3.3 Repeated activation of Y_5Rs induces hypotrophy on BLA OTC neurons.

NPY causes hypotrophy of BLA OTC neurons (Michaelson et al., 2020). That, together with our observations that Y_5R activation decreased cell capacitance suggests that Y_5R are responsible for the NPY-induced hypotrophy. Thus, we studied the morphology of BLA OTC neurons 1-2 weeks after 5-days administration of the Y_5R agonist, cPP. We hypothesize that the activation of Y_5R will induce hypotrophy of BLA OTC neurons.

BLA OTC neurons treated with the Y_5R agonist, cPP at 10 and 100 nM, had reduced total dendritic length compared to controls (Fig. 9A. Control: 3734 ± 265 µm, n = 26; 1 nM: 3232 ± 399 µm, p=0.4, n = 24; 10 nM: 2558 ± 201 µm, n = 31, p=0.006; 100 nM: 2513 ± 125 µm, n = 32, p=0.004. One-way ANOVA, Tukey's multiple comparisons test). This reduction on total dendritic length was accompanied by a decrease on number of branch points in BLA OTC neurons treated with 100 nM of the Y_5R agonist compared to controls (Fig. 9B. Control: 21.8 ± 1.1, n = 26; 1 nM: 22.3 ± 2.8, n = 24, p>0.9; 10 nM: 17.8 ± 1.7, n = 31, p=0.4; 100 nM: 15.5 ± 1.1, n = 32, p=0.04, One-way ANOVA, Tukey's multiple comparisons test). Sholl analysis (Fig. 9C) revealed a decrease in dendritic arborisation between 150 – 210 µm with 1 nM ($p<0.05$), 100 – 220 µm with 10 nM ($p<0.01$) and 60 – 210 µm with 100 nM ($p<0.01$, Two-way ANOVA, Tukey's multiple comparisons test). Incubation with 1nM cPP has no effect on the number of 1^{st}, 2^{nd}, 3^{rd}, 4^{th} or 5^{th} order dendrites (Fig 9D. 1^{st}: 3.1 ± 0.1, p=0.9; 2^{nd}: 12.4 ± 1.1, p=0.9; 3^{rd}: 7.9 ± 1.3; p>0.9; 4^{th}: 1.7 ± 0.6, p=0.9; 5^{th}: 0.2 ± 0.1, p=0.9, n=24. Two-way ANOVA, Tukey's multiple comparisons test). Incubation with 10 nM cPP reduced the number of 3^{rd} order dendrites (Fig 9D. 1^{st}: 3.1 ± 0.09, p=0.9; 2^{nd}: 10.9 ± 0.9, p=0.48; 3^{rd}: 5.6 ± 0.7; p=0.02; 4^{th}: 1.1 ± 0.3, p=0.9; 5^{th}: 0.07 ± 0.05, p=0.9, n=31. Two-way ANOVA, Tukey's multiple comparisons test) compared to controls.

Administration of 100 nM Y_5R agonist (n = 32) reduced the number of $2^{nd}$and 3^{rd} order dendrites (1^{st}: 3.1 ± 0.06, p=0.9; 2^{nd}: 9.9 ± 0.6, p=0.03; 3^{rd}: 4.7 ± 0.5, p=0.0001; 4^{th}: 0.9 ± 0.2, p=0.6; 5^{th}: 0.03 ± 0.03, p=0.9, n=32) compared to controls (1^{st}: 2.9 ± 0.04; 2^{nd}: 12 ± 0.6; 3^{rd}: 7.9 ± 0.6; 4^{th}: 1.7 ± 0.3; 5^{th}: 0.2 ± 0.07, Two-way ANOVA, Tukey's multiple comparisons test). Analysis of dendritic branching as a function of distance from the soma showed a decrease in dendritic branching on more distal dendrites (Fig. 9E) with 10nM and 100 nM compared to controls (Control: 1.2 ± 0.3, n = 26; 10nM: 0.3 ± 0.2, n = 31, p=0.01; 100 nM: 0.3 ± 0.1, n = 32, p=0.006, Two-way ANOVA, Tukey's multiple comparisons test) was 180 μm from the soma compared to controls (1.2 ± 0.3, n = 26). Taken together, these data suggest that Y_5R activation causes lasting hypotrophy of BLA OTC neurons.

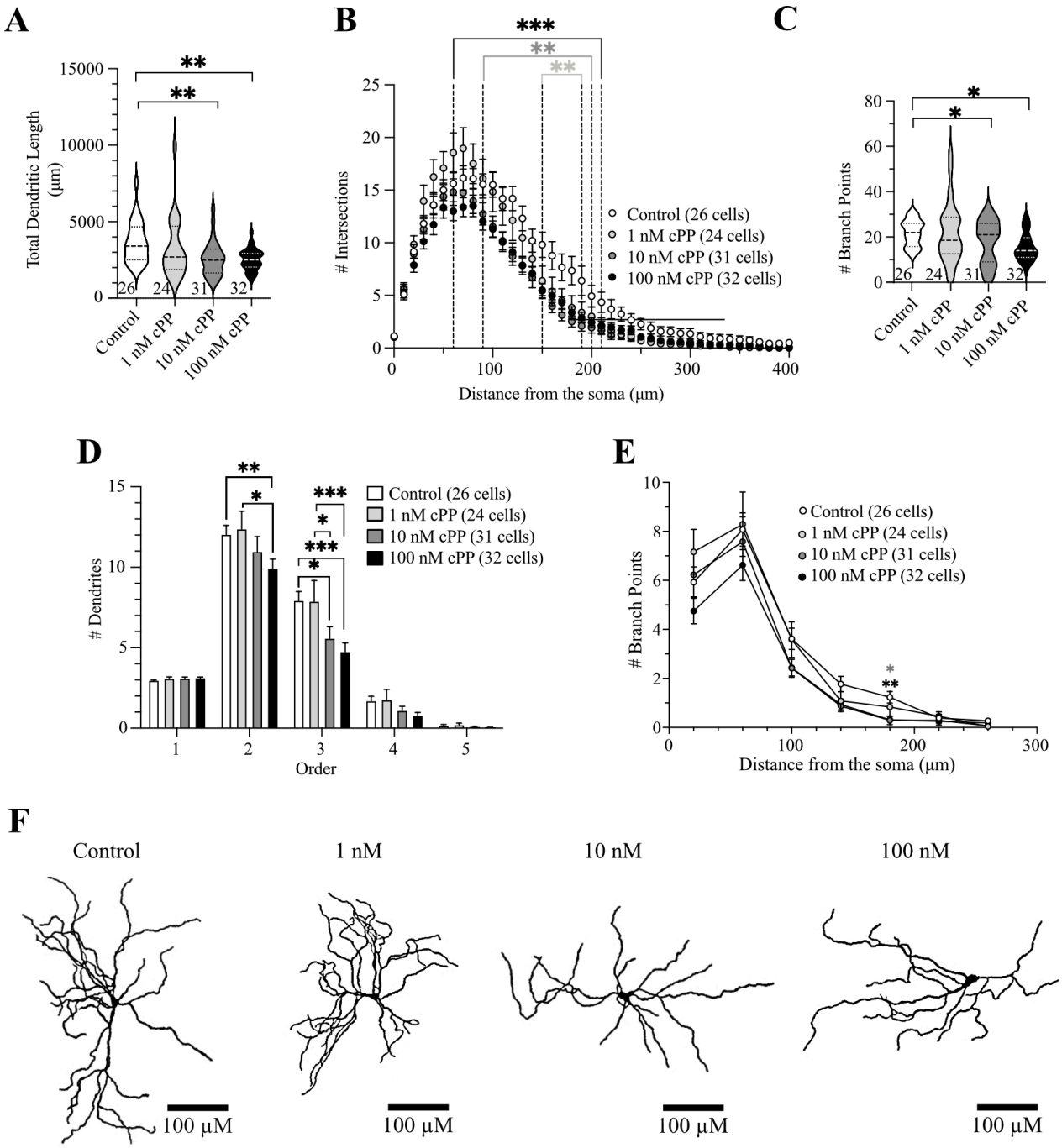

Figure 9: Morphometric analysis of BLA OTCs treated with the Y_5R agonist, cPP. A-E. Total dendritic length (A), number of branch points (B), sholl analysis (C), number of 1st and 2nd, 3rd, 4th and 5th order dendrites (D) and number of branch points as a function of distance from the

soma (E). Bottom: representative traces of a BLAOTC neuron from control, 1 nM, 10 nM and 100 nM cPP incubations. Data on B, D and E represent the Mean ± SEM. Violin plots on A and C show the 1st and 3rd quartile in lower and upper dotted lines, respectively, and the median in a dashed line. Violin plot shapes indicate the density of the data at different values smoothed by a Kerner density. *$p<0.05$, **$p<0.01$, ***$p<0.001$.

3.4 Antagonizing Y_5R prevented the effects of NPY on BLA OTC neurons.

NPY supresses reduces excitability and induces hypotrophy of BLA pyramidal neurons *in vitro* and *in vivo* (Giesbrecht et al., 2010a; Silveira Villarroel et al., 2018; Michaelson et al., 2020). Data obtained from Dr. Michaelson have shown that NPY also hyperpolarizes and decreases excitability and the time constant of I_h activation without suppressing I_h of BLA OTC PNs (Michaelson & Colmers, unpublished data), reduces whole-cell capacitance and induces hypotrophy of BLA OTC neurons (Michaelson et al., 2020). We hypothesize that, if Y_5Rs mediate the effects of NPY on passive properties and morphology of BLA OTC neurons, antagonizing Y_5R will block the NPY-induced changes in passive properties and morphology of BLA OTC. To confirm that NPY acts via Y_5R to produce long-term changes on the morphology of BLA OTC neurons, we coapplied 10 nM NPY with the Y_5R antagonist, 30 nM CGP 71683A (CGP), on BLA OTC neurons for 5 days, and examined neuronal properties 1-2 weeks after the drug treatment.

Unlike NPY alone, which did not affect I_h or on BLA OTC neurons (Michaelson & Colmers, unpublished), co-administration of NPY and a Y_5R antagonist potentiated I_h on BLA OTC neurons (fig 10) compared to controls (Control: -125mV: -204.9 ± 27.4; -135 mV: -236.1 ± 33.1 pA. -145 mV: -255.7 ± 36.7 pA, n=31. NPY+CGP: -125 mV: -288.0 ± 26.7, p=0.04; -135 mV: -362.0 ± 32.3 pA, p=0.006; -145 mV: -429.4 ± 38.6 pA, n = 44, p<0.0001. Two-way ANOVA, Tukey's multiple comparisons test). Neurons from BLA OTC treated with the Y_5R antagonist alone also showed increased I_h amplitude compared to controls (CGP: -125mV: -300.7 ± 35.3, p=0.03; -135 mV: -359.7 ± 38.8 pA, p=0.003; -145 mV: -392.1 ± 41.4 pA, p=0.0007, n=29. Two-way ANOVA, Tukey's multiple comparisons test). Administration of NPY plus Y_5R antagonist had no effect on

I_h density (Fig. 10B. Control: -1.7 ± 0.2 pA/pF, n = 31; NPY + CGP: -2.3 ± 0.2 pA/pF, n = 44, CGP: -2.2 ± 0.3 pA/pF, n = 29. Two-way ANOVA, Tukey's multiple comparisons test).

NPY alone decreases time constant of I_h activation (Michaelson & Colmers, unpublished). In contrast, our co-administration of NPY and Y_5R antagonist, or Y_5R antagonist alone had no effect on the τ fast component of I_h activation of BLA OTC neurons compared to controls (Fig. 10C. Control: 13.3 ± 1.4 ms, n = 27; NPY+CGP: 15.4 ± 1.4 ms, n = 38, p=0.6; CGP: 15.9 ± 2.1 ms, n = 24, p=0.5. One-way ANOVA, Tukey's multiple comparisons test). The τ slow component of I_h activation was also not different from controls (Fig. 10D. Control: 89.5 ± 7.9 ms, n = 27; NPY + CGP: 100.8 ± 9.6 ms, n = 38, p=0.7; CGP: 101.8 ± 11.6 ms, n = 24, p=0.7. One-way ANOVA, Tukey's multiple comparisons test). NPY plus Y_5R antagonist had no effect on I_h V50 (Fig. 10E. Control: -86.6 ± 2.7 mV, n = 30; NPY + CGP: -94.4 ± 2.2 mV, n = 44, p=0.06; CGP: -91.7 ± 2.4 mV, n = 28, p=0.4. One-way ANOVA, Tukey's multiple comparisons test).

Additionally, unlike NPY which has no effect on I_{IR} or on BLA OTC neurons (Michaelson & Colmers, unpublished), co-administration of the Y_5R antagonist and NPY increases I_{IR} (Fig. 10F) compared to controls (Control -115mV: -396.2 ± 38.5 pA; -125 mV: -611.9 ± 57.8 pA; -135 mV: -848.6 ± 77.4 pA; -145 mV: -1118.3 ± 99.7 pA, n=26. NPY+CGP -115 mV: -624.3 ± 62.9 pA, p=0.03; -125 mV: -986.7 ± 62.9 pA, p<0.0001; -135 mV: -1382.9 ± 137.5 pA, p<0.0001; -145 mV: -1791 ± 175.3 pA, p< 0.0001, n=19. Two-way ANOVA, Tukey's multiple comparisons test). This increase on I_h and I_{IR} observed with the administration of NPY plus the Y_5R antagonist resemble the effects observed with the activation of Y_2 receptors (Michaelson & Colmers, unpublished) where the administration of a Y_2 agonist induces and increase on max I_h and

potentiates I_{IR} on BLA OTC neurons. The increase on I_h observed with the administration of the Y_5R antagonist alone (CGP) also suggest that NPY may be tonically released and acting on Y_2.

Unlike NPY, which result on more hyperpolarized BLA OTC neurons (Michaelson & Colmers, unpublished), co-administration of Y_5R antagonist plus NPY did not have any effect on RMP (Fig. 10G. Control: -76.3 ± 1.3 mV, n = 32; NPY + CGP: -79.8 ± 1.3 mV, n = 45, p=0.16; CGP: -77.0 ± 1.5 mV, n = 30, p=0.9. One-way ANOVA, Tukey's multiple comparisons test). However, similar to NPY (Michaelson & Colmers, unpublished), co-administration of Y_5R antagonist plus NPY resulted on increased rheobase (Fig. 10H. Control: 195.8 ± 29.2 pA, n = 32; NPY + CGP: 365.2 ± 39.5 pA, p=0.003, n = 45; CGP: 250.4 ± 31.4 pA, n = 30, p=0.6. One-way ANOVA, Tukey's multiple comparisons test). CGP alone had no effect on wither RMP or rheobase. Input resistance from neurons incubated with NPY plus Y_5R antagonist was reduced compared controls (Fig. 10I. Control: 119.5 ± 11.8 MΩ, n = 15, NPY + CGP: 70.7 ± 10.6 MΩ, p=0.007, n = 19; CGP: 87.2 ± 10.72 MΩ, p=0.6, n = 10. One-way ANOVA, Tukey's multiple comparisons test). This increase in rheobase was not observed with NPY alone (Michaelson & Colmers, unpublished). Administrations of NPY alone is result in BLA OTC neurons with reduced capacitance (Michaelson et al., 2020). contrary to NPY alone which reduced whole-cell capacitance (Michaelson et al., 2020), antagonizing Y_5R in the presence of NPY resulted in increased on whole-cell capacitance compared to controls (Fig. 10J. Control: 142.6 ± 7.7 pF, n = 32; NPY + CGP: 183.7 ± 9.3 pF, n = 45, p=0.05; CGP: 162.7 ± 8.8 pF, n = 32, p=0.2. One-way ANOVA, Tukey's multiple comparisons test).

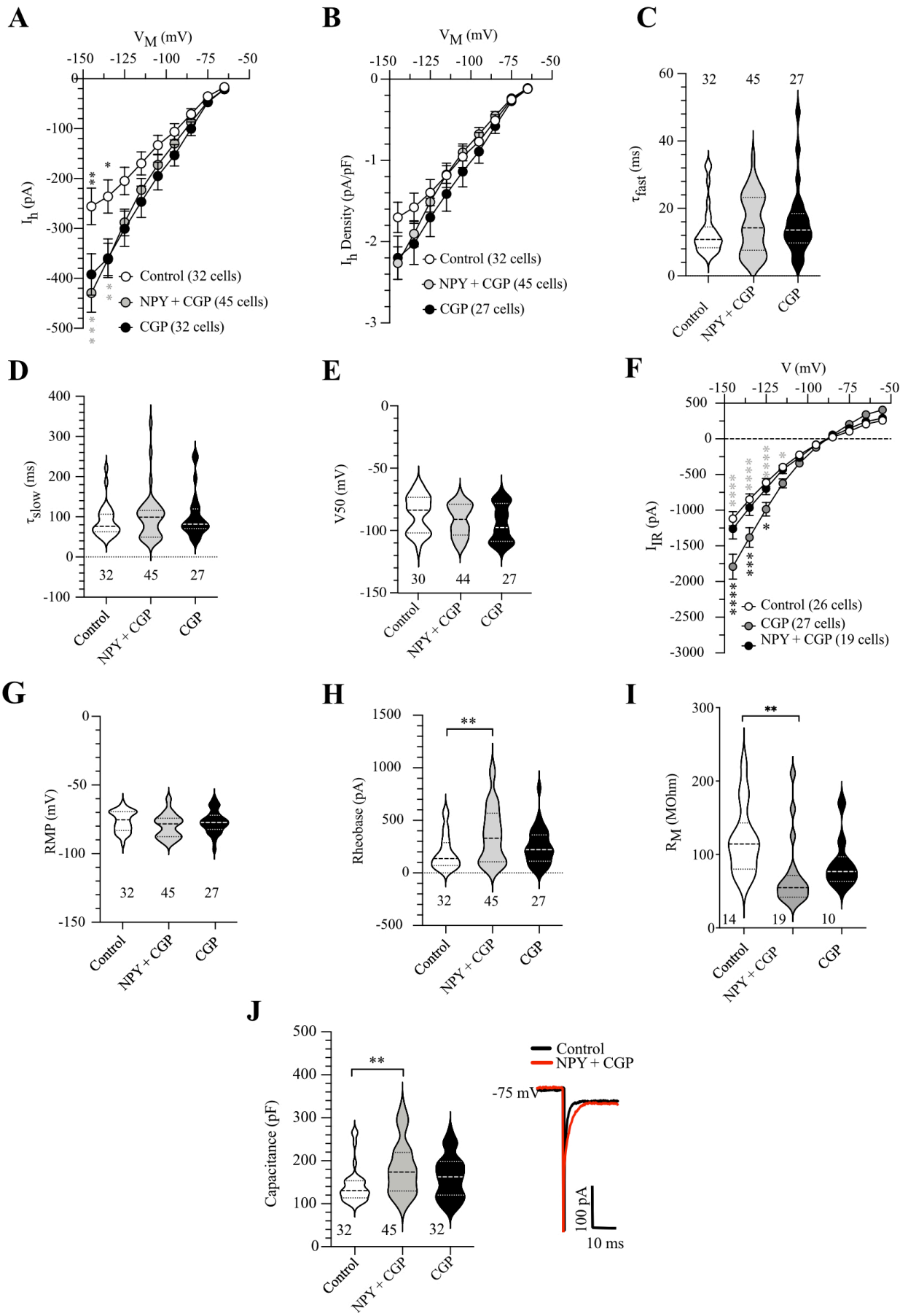
A
V_M (mV)
-150 -125 -100 -75 -50
0
-100
-200
-300
-400
-500
I_h (pA)
Control (32 cells)
NPY + CGP (45 cells)
CGP (32 cells)
B
V_M (mV)
-150 -125 -100 -75 -50
0
-1
-2
-3
I_h Density (pA/pF)
Control (32 cells)
NPY + CGP (45 cells)
CGP (27 cells)
C
60
40
20
0
τ_fast (ms)
32 45 27
Control
NPY + CGP
CGP
D
400
300
200
100
0
-100
τ_slow (ms)
32 45 27
Control
NPY + CGP
CGP
E
0
-50
-100
-150
V50 (mV)
30 44 27
Control
NPY + CGP
CGP
F
V (mV)
-150 -125 -100 -75 -50
500
0
-500
-1000
-1500
-2000
-2500
-3000
I_IR (pA)
Control (26 cells)
CGP (27 cells)
NPY + CGP (19 cells)
G
0
-50
-100
-150
RMP (mV)
32 45 27
Control
NPY + CGP
CGP
H
1500
1000
500
0
-500
Rheobase (pA)
**
32 45 27
Control
NPY + CGP
CGP
I
300
200
100
0
R_M (MOhm)
**
14 19 10
Control
NPY + CGP
CGP
J
500
400
300
200
100
0
Capacitance (pF)
**
32 45 32
Control
NPY + CGP
CGP
Control
NPY + CGP
-75 mV
100 pA
10 ms

Figure 10: Effect of the co-treatment of NPY and the Y_5R antagonist CGP71683A (CGP) on BLA OTC neurons. A-K. Effect of NPY + CGP or CGP alone on I_h amplitude (A), I_h density (B), time constant of I_h activation (C, D), V50 of I_h (E), inward rectifying current (F), RMP (G), rheobase (H), input resistance (I) and capacitance (J). Data on A, B and F represent the Mean ± SEM. Violin plots on C, D, E, G, H, I, J and F show the 1st and 3rd quartile in lower and upper dotted lines, respectively, and the median in a dashed line. Violin plot shapes indicate the density of the data at different values smoothed by a Kerner density. *$p < 0.05$, **$p < 0.01$, ***$p < 0.001$, ****$p<0.0001$.

3.5 Antagonizing Y_5Rs prevented the NPY-induced hypotrophy of BLA OTC neurons.

NPY (Michaelson et al., 2020) and a Y_5R agonist (Fig. 9) produced hypotrophy of BLA OTC neurons and antagonizing Y_5Rs prevented the NPY-induced decrease in whole-cell capacitance (Fig. 10). Thus, we hypothesize that blocking Y_5Rs will prevent the NPY-induced dendritic hypotrophy of BLA OTC neurons.

Unlike NPY alone (Michaelson et al., 2020) and the Y_5R agonist (Fig. 9) which produced hypotrophy of BLA OTC neurons, the co-administration of NPY plus Y_5R antagonist induced dendritic hypertrophy. Co-administration of NPY and the Y_5R antagonist increased total dendritic length ($p < 0.01$) on BLA OTC neurons compared to controls (Fig. 11A. Control: 3598.2 ± 160.9 μm, n = 53; NPY + CGP: 4739.2 ± 292.4 μm, n = 34, p=0.01; CGP: 4071.3 ± 304.6 μm, n = 24. One-way ANOVA, Tukey's multiple comparisons test). This increase was accompanied by an increase in the number of branch points compared to controls (Fig. 11B. Control: 20.8 ± 1.1, n = 53; NPY + CGP: 32.2 ± 2.3, n = 34, p<0.0001; CGP: 26.4 ± 2.9, n = 24). Sholl analysis revealed that compared to controls, the increase in dendritic complexity induced by NPY plus Y_5R antagonist occurred at distances from the soma between 40 – 200 μm ($p < 0.001$), while compared to the Y_5R antagonist alone the increase in complexity occurred between 50 – 100 μm ($p < 0.01$) from the soma (Fig. 11C). Co-administration of NPY plus Y_5R antagonist also increased the number of 2^{nd}, 3^{rd} and 4^{th} dendrites compared to controls (Fig. 7D. Control 1^{st}: 4.1 ± 0.2; 2^{nd}: 12.5 ± 0.6; 3^{rd}: 6.94 ± 0.53; 4^{th}: 1.3 ± 0.2; 5^{th}: 0.09 ± 0.3, n = 53. NPY + CGP 1^{st}: 3.6 ± 0.1; 2^{nd}: 15.35 ± 1.0, p=0.0007; 3^{rd}:11.9 ± 1.01, p<0.0001; 4^{th}" 4.2 ± 0.6, p=0.0005, 5^{th}: 0.7 ± 0.3, n = 34, p=0.7. Two-way ANOVA, Tukey's multiple comparisons test). Administration of Y_5R antagonist alone increased 3^{rd} order dendrites compared to controls (CGP 1^{st}: 3.1 ± 0.08; 2^{nd}: 13.8 ± 1.1; 3^{rd}: 10.0

± 1.3; 4th: 2.3 ± 0.5; 5th: 0.3 ± 0.1, n = 24). Analysis of dendritic branching as a function of distance from the soma revealed that the increase in dendritic branching seen with NPY plus Y_5R antagonist occurred between 20 – 140 µm from the soma (Fig. 11E. Control 20 µm: 4.7 ± 0.4; 60 µm: 7.2 ± 0.6; 100 µm: 3.7 ± 0.4. 140 µm: 2.0 ± 0.3, 180 µm: 0.9 ± 0.1; 220 µm: 0.7 ± 0.2; 260 µm: 0.4 ± 0.1, n = 53. NPY + CGP 20: 8.1 ± 1.1, $p<0.0001$; 60 µm: 9.1 ± 1.2, $p=0.03$; 100 µm: 5.4 ± 0.6, $p=0.07$. 140 µm: 4.1 ± 0.5, $p=0.02$, 180 µm: 2.2 ± 0.5, $p=0.3$; 220 µm: 1.4 ± 0.5, $p=0.6$; 260 µm: 0.9 ± 0.3, $p=0.8$, n = 34. Two-way ANOVA. Tukey's multiple comparisons test). No effect was found with the Y_5R antagonist alone (CGP: 5.2 ± 0.0, $p=8$; 60 µm: 7.8 ± 1.6, $p=0.7$; 100 µm: 4.5 ± 0.6, $p=0.07$. 140 µm: 2.3 ± 0.4, $p=0.9$, 180 µm: 1.7 ± 0.3, $p=0.7$; 220 µm: 1.5 ± 0.4, $p=0.6$; 260 µm: 0.5 ± 0.2, $p=0.9$, n = 24. Two-way ANOVA. Tukey's multiple comparisons test). Taken together, these results support our previous findings showing that NPY, through activation of Y_5R causes dendritic hypotrophy on BLA OTC. Our results also suggest that the hypertrophy observed with the co-administration of NPY and the Y_5R antagonist can be due to the activation of another NPY receptors, most likely the Y_2R as incubations with a Y_2R agonist result in dendritic hypertrophy of BLA OTC neurons (Michaelson et al., 2020).

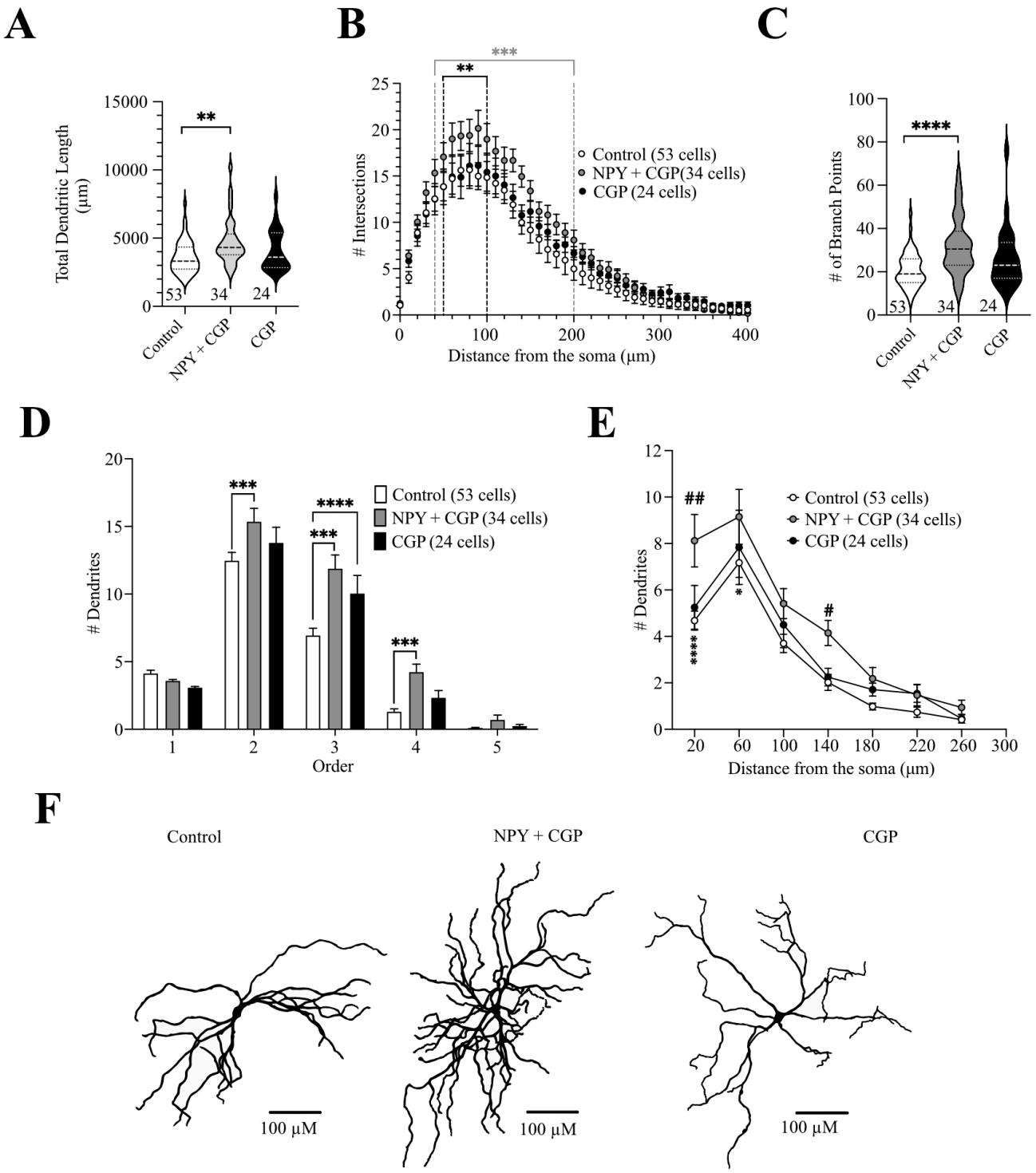
A
Total Dendritic Length (µm)
15000
10000
5000
0
**
53
34
24
Control
NPY + CGP
CGP
B
***
**
25
20
15
10
5
0
Intersections
0
100
200
300
400
Distance from the soma (µm)
Control (53 cells)
NPY + CGP(34 cells)
CGP (24 cells)
C
# of Branch Points
100
80
60
40
20
0
****
53
34
24
Control
NPY + CGP
CGP
D
Dendrites
20
15
10
5
0
***
****
***
***
1
2
3
4
5
Order
Control (53 cells)
NPY + CGP (34 cells)
CGP (24 cells)
E
Dendrites
12
10
8
6
4
2
0
##
****
*
#
20
60
100
140
180
220
260
300
Distance from the soma (µm)
Control (53 cells)
NPY + CGP (34 cells)
CGP (24 cells)
F
Control
NPY + CGP
CGP
100 µM
100 µM
100 µM

Figure 11: Morphometric analysis of BLA OTCs treated with NPY + Y_5R antagonist. A-E. Total dendritic length (A), sholl analysis (B), number of branch points (C), number of 1st, 2nd, 3rd, 4th and 5th order dendrites (D) and number of branch points as a function of distance from the soma (E). F. Representative traces of BLA OTC neurons from control and treated with NPY + CGP and CGP. Data on B, D, E represent the Mean ± SEM. Violin plots on A and C show the 1st and 3rd quartile in lower and upper dotted lines, respectively, and the median in a dashed line. Violin plot shapes indicate the density of the data at different values smoothed by a Kerner density. **p< 0.01, ***p< 0.001, ****p<0.0001 NPY + CGP compared to control. ##p<0.01 NPY + CGP compared to CGP alone.

3.6 Repeated activation of Y_5Rs *in vivo* produces stress resilience and hypotrophy of BLA pyramidal neurons

The *in vitro* results described above suggest that NPY may act through Y_5Rs to produce stress resilience possibly by inducing hypotrophy of BLA pyramidal neurons. Thus, we hypothesize that activation of BLA Y_5Rs *in vivo* will decrease anxiety and cause hypotrophy of BLA pyramidal neurons. We also predict that administration of the Y_5R antagonist, CGP, will block the NPY-induced stress resilience and the hypotrophy of BLA pyramidal neurons.

Injections of 10 pmol/100 nl of the Y_5R agonist, cPP (n = 7) directly into the BLA for five consecutive days (D1 – D5), increased SI time during the treatment period. Specifically, treatment with the Y_5R agonist increased SI time by 58.5 ± 13.8 % at D1 and by 62.8 ± 10.4 % at D5 compared to pre-treatment baseline (Fig: 12. D1 $p=0.0004$; D5 $p=0.0001$, RM two-way ANOVA, Tukey's multiple comparisons test) and compared to vehicle-treated controls (D1 $p=0.02$; D5 $p<0.003$). Most importantly, the Y_5R-induced increase in SI time persisted at W2 and W4 (W2: 75.9 ± 14.9 %, $p<0.0001$. W4: 68.9 ± 16.7 %, $p<0.0001$) compared to the pre-treatment baseline and to the control-treated group (W2 $p=0.003$; W4 $p=0.04$, n = 8).

Consistent with this data, injections of the Y_5R antagonist, 10 pmoles/100 nl CGP, for 5 consecutive days into the BLA 20 minutes before the injection of NPY 10 pmoles/100 nl blocked the development of the NPY-mediated reduction in anxiety. Specifically, co-administration of NPY + Y_5R antagonist resulted in an increased SI time during the treatment period by 55.2 ± 6.7 % at D1 compared to the pre-treatment baseline (Fig. 12. $p=0.05$, RM two-way ANOVA, Tukey's multiple comparisons test) and controls ($p=0.02$, RM two-way ANOVA, Tukey's multiple

comparisons test) and by 51.1 ± 13.9 % at D5 compared to pre-treated baseline (p=0.02, RM two-way ANOVA, Tukey's multiple comparisons test). However, injections of NPY + Y_5R antagonist prevented the increase in SI time at W2 and W4 (Fig. 12. W2: 116 ± 13.8 %, p=0.5. W4: 102.7 ± 17.1 %, p=0.9, RM two-way ANOVA, Tukey's multiple comparisons test) compared to pre-treatment baseline, Y_5R agonist and controls. This results strongly support the role of Y_5R in NPY-induced stress resilience. NPY-induced stress resilience is due in part by suppression of I_h, hyperpolarization and reduced excitability and hypotrophy of BLA pyramidal neurons. We next asked whether BLA neurons from animals treated with either the Y_5R agonist or NPY + Y_5R antagonist were less excitable. Thus, we studied the basic properties of BLA pyramidal neurons from these groups.

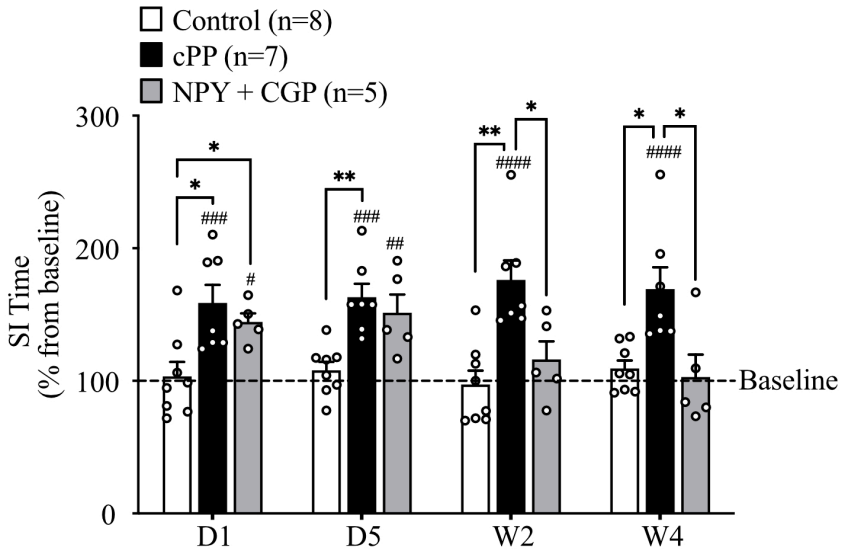

Figure 12: Effect of repeated BLA injections of a Y_5R agonist on anxiety-like behavior. Time course of social interaction time as a percentage of each individual animal's baseline of rats that received an injection of either vehicle (control), the Y_5R-selective agonist or NPY + Y_5R-selective antagonist directly into the BLA, daily for five consecutive days. SI time was measured before any treatment to account for baseline anxiety levels, at Day 1 (D1) and Day 5 (D5) of treatment, and 2 (W2) and 4 weeks (W4) from the first injection. Data represent the Mean ± SEM. *p< 0,05, **p< 0.01, ***p< 0.001, ****p<0.0001 compared to control. ##p< 0.01, ###p< 0.001, ####p<0.0001 compared to pre-treatment baseline.

BLA pyramidal neurons from animals that received Intra-BLA injections of the Y_5R agonist have reduced I_h amplitude compared to BLA neurons from animals that received injections of NPY + Y_5R antagonist and controls (Fig. 13A. Control -105 mV: -202.2 ± 15.5 pA, -115 mV: -261.4 ± 19.5 pA, -125 mV: -312.6 ± 23.1 pA, -135 mV: -351.4 ± 25.5 pA, n = 40; cPP -105 mV: -151.4 ± 7.9 pA p=0.002 vs controls p=0.02 vs NPY+CGP, -115 mV: -195.1 ± 9.3 pA p<0.0001 vs controls p=0.01 vs NPY + CGP, -125 mV: -235.6 ± 10.4 pA p<0.0001 vs controls p=0.01 vs NPY + CGP, -135 mV: 270.8 ± 12.1 pA p<0.0001 vs controls p=0.02 vs NPY+CGP, n = 86; NPY+CGP -95 mV: -141.5 ± 8.1 pA p=0.02, -105 mV: -187.9 ± 9.7 pA, -115 mV: -233.0 ± 10.8 pA, -125 mV: -273.4 ± 11.6 pA, -135 mV: -307.8 ± 12.5 pA, n = 51. Two-way ANOVA, Tukey's multiple comparisons test). I_h from neurons treated with NPY + Y_5R antagonist was also different from controls at -125 mV (p=0.04) and -135 mV (p=0.02). I_{IR} current from BLA pyramidal neurons from animals treated with Y_5R agonist was not different from control. However, administration of NPY + Y_5R antagonist resulted on increased I_{IR} current compared to controls and Y_5R agonist (Fig. 13B. Control -105 mV: -390.4 ± 22.5 pA, -115 mV: -596.5 ± 30.6 pA, -125 mV: -805.8 ± 41.0 pA, -135 mV: -1043.1 ± 51.0 pA, n = 22; cPP -105 mV: -402.1 ± 16.8 pA, -115 mV: -608.0 ± 22.1 pA, -125 mV: -829.4 ± 28.1 pA, -135 mV: -1063.2 ± 34.7 pA, n = 86; NPY + CGP -105 mV: -480.9 ± 23.4 pA p=0.03 vs cPP, -115 mV: -721.8 ± 28.6 p=0.01 vs controls p=0.0009 vs cPP, -125 mV: -984.6 ± 34.9 pA p=0.0002 vs controls p<0.0001 vs cPP, -135 mV: -1261.2 ± 41.5 p<0.0001 vs controls and cPP, n = 45. Two-way ANOVA, Tukey's multiple comparisons test). The Y_5R agonist or NPY + Y_5R antagonist had no effect on resting membrane potential compared to controls (Fig. 13C. Control: -79.5 ± 0.6 mV, n = 37; cPP: -80.7 ± 0.5 mV p=0.4, n = 83; NPY + CGP: -79.4 ± 0.7 mV p=0.9, n = 51. One-way ANOVA, Tukey's multiple comparisons test). We found no difference on rheobase of BLA neurons trearted with the Y_5R agonist. However,

BLA neurons treated with NPY + Y_5R antagonist were less excitable than controls (Fig. 13D. Control: 319.7± 10.4 pA, n = 53; cPP: 353.9 ± 14.5 pA, n = 92 p=0.3; NPY + CGP: -385.9 ± 20.3 pA, n = 45 p=0.02. One-way ANOVA, Tukey's multiple comparisons test) or input resistance (Fig. 9E. Control: 65.6 ± 3.3 MΩ, n = 40; cPP: 71.3 ± 2.8 MΩ, n = 87 p=0.1; NPY + CGP: 56.4 ± 2.4 MΩ, n = 51 p=0.4. One-way ANOVA, Tukey's multiple comparisons test). Finally, the capacitance of neurons from the Y_5R agonist-treated group was reduced compared to controls and to NPY + Y_5R antagonist (Fig. 9F. Control: 230.7 ± 6.09 pF, n = 64; cPP: 201.7 ± 4.99 pF, n = 95 p=0.0004 vs controls, p=0.008 vs NPY+CGP; NPY + CGP: 225.7 ± 4.88 pF, n = 51. One-way ANOVA, Tukey's multiple comparisons test).

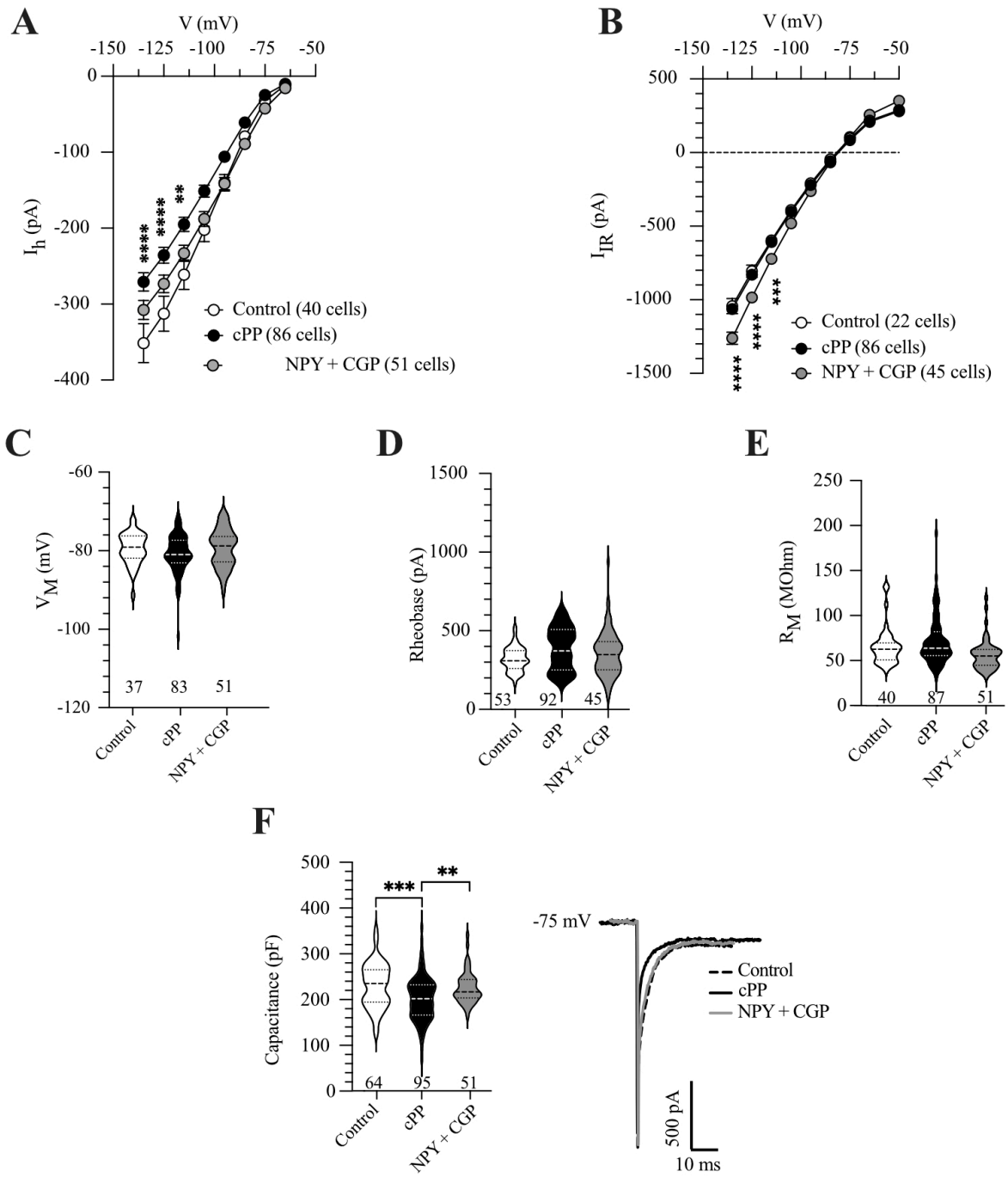
A
V (mV)
-150 -125 -100 -75 -50
0
-100
-200
-300
-400
I_h (pA)
****
****
**
Control (40 cells)
cPP (86 cells)
NPY + CGP (51 cells)
B
V (mV)
-150 -125 -100 -75 -50
500
0
-500
-1000
-1500
I_{IR} (pA)
***
****
****
Control (22 cells)
cPP (86 cells)
NPY + CGP (45 cells)
C
-60
-80
-100
-120
V_M (mV)
37 83 51
Control
cPP
NPY + CGP
D
1500
1000
500
0
Rheobase (pA)
53 92 45
Control
cPP
NPY + CGP
E
250
200
150
100
50
0
R_M (MOhm)
40 87 51
Control
cPP
NPY + CGP
F
500
400
300
200
100
0
Capacitance (pF)
***
**
64 95 51
Control
cPP
NPY + CGP
-75 mV
Control
cPP
NPY + CGP
500 pA
10 ms

Figure 13: Effect of the Y_5R agonist cPP and NPY + Y_5R antagonist on passive properties of BLA pyramidal neurons. A-E. Effect of cPP, NPY + CGP and CGP on I_h amplitude (A), I_{IR} (B), resting membrane potential (C), rheobase (D) input resistance (E) and cell capacitance (F) of BLA pyramidal neurons. Data on A and B represent the Mean ± SEM. *p = significantly different relative to control. Violin plots on B-E show the 1st and 3rd quartile in lower and upper dotted lines, respectively, and the median in a dashed line. Violin plot shapes indicate the density of the data at different values smoothed by a Kerner density

This Y_5R agonist-mediated decrease in capacitance was associated with hypotrophy of BLA pyramidal neurons (Fig. 14). Total dendritic length of BLA neurons from the Y_5R agonist-treated group was decreased compared to controls and to the NPY + Y_5R antagonist group. (Fig. 14A. Control: 8741.7 ± 232.69 µm, n = 52; cPP: 7026.3 ± 223.53 µm, n = 50, $p<0.0001$ vs control and NPY + CGP; NPY + CGP: 9545.8 ± 356.6 µm, n = 35 $p=0.01$ vs control. One-way ANOVA, Tukey's multiple comparisons test). Y_5R agonist also decreased dendritic branching compared to controls and the NPY + Y_5R antagonist group (Fig. 14B. Control: 45.56 ± 1.42, n = 52; cPP: 36.22 ± 1.52, n = 50 $p<0.0001$ vs control and NPY + CGP; NPY + CGP: 47.80 ± 1.69, n = 35 $p=0.6$ vs control. One-way ANOVA, Tukey's multiple comparisons test). Sholl analysis revealed that the decrease in dendritic arborisation induced by Y_5R agonist occurred between 110 – 260 and 90 – 280 µm from the soma ($p < 0.001$) compared to controls and to NPY + Y_5R antagonist, respectively (Fig. 14C). The Y_5R agonist also decreased 2^{nd}, 3^{rd} and 4^{th} order dendrites compared to control and NPY + Y_5R antagonist (Fig. 14D. Control 1^{st}: 3.8 ± 0.1; 2^{nd}: 20.1 ± 0.6; 3^{rd}: 18.3 ± 0.8; 4^{th}: 5.9 ± 0.4; 5^{th}: 1.3 ± 0.3, n = 52. cPP 1^{st}: 3.8 ± 0.1, 2^{nd}: 18.1 ± 0.7 $p=0.02$ vs controls $p=0.0004$ vs NPY + CGP; 3^{rd}: 14.2 ± 0.8 $p<0.0001$ vs control and NPY + CGP; 4^{th}: 3.7 ± 0.4 $p=0.01$ vs control $p=0.04$ vs NPY + CGP; 5^{th}: 0.5 ± 0.1 p, n=50. NPY + CGP 1^{st}: 3.9 ± 0.2; 2^{nd}: 21.2 ± 0.8; 3^{rd}: 19.9 ± 1.0; 4^{th}: 5.7 ± 0.6; 5^{th}: 0.8 ± 0.2, n = 35. Two-way ANOVA, Tukey's Multiple comparisons). Analysis of dendritic branching as a function of distance from the soma revealed that the decrease in branching seen with the Y_5R agonist treatment was between 60 – 120 µm from the soma. No changes were observed with the NPY + Y_5R antagonist treatment compared to controls (Fig. 14F. Control 20 µm: 7.9 ± 0.4; 60 µm: 15.6 ± 0.7; 100 µm: 9.1 ± 0.6. 140 µm: 4.4 ± 0.4, 180 µm: 2.4 ± 0.2; 220 µm: 1.2 ± 0.2; 260 µm: 0.6 ± 0.1, n = 52. cPP: 20 µm: 6.8 ± 0.4; 60 µm: 13.7 ± 0.7 $p=0.003$ vs control $p<0.0001$ vs NPY + CGP; 100 µm: 7.1 ± 0.4 $p=0.001$ vs control $p=0.0001$ vs

NPY + CGP; 140 µm: 3.3 ± 0.4 p=0.2, 180 µm: 1.5 ± 0.2 p=0.2; 220 µm: 1.0 ± 0.2 p=0.9; 260 µm: 0.6 ± 0.1 p=0.9, n = 50. NPY + CGP 20 µm: 7.2 ± 0.5 p=0.5; 60 µm: 16.7 ± 0.9 p=0.1; 100 µm: 9.7 ± 0.7 p=0.6; 140 µm: 5.5 ± 0.5 p=0.2; 180 µm: 2.3 ± 0.3 p=0.9; 220 µm: 1.7 ± 0.2 p=0.8; 260 µm: 1.0 ± 0.2 p=0.8, n = 35. Two-way ANOVA. Tukey's multiple comparisons test). Taken together, our data suggest that NPY, acting via Y_5Rs, produces a persistent reduction in anxiety that outlasts the duration of agonist administration for at least two weeks that is associated with hypotrophy of BLA pyramidal neurons *in vivo*. Figure 12: Effect of repeated BLA injections of a Y_5R agonist on anxiety-like behavior.

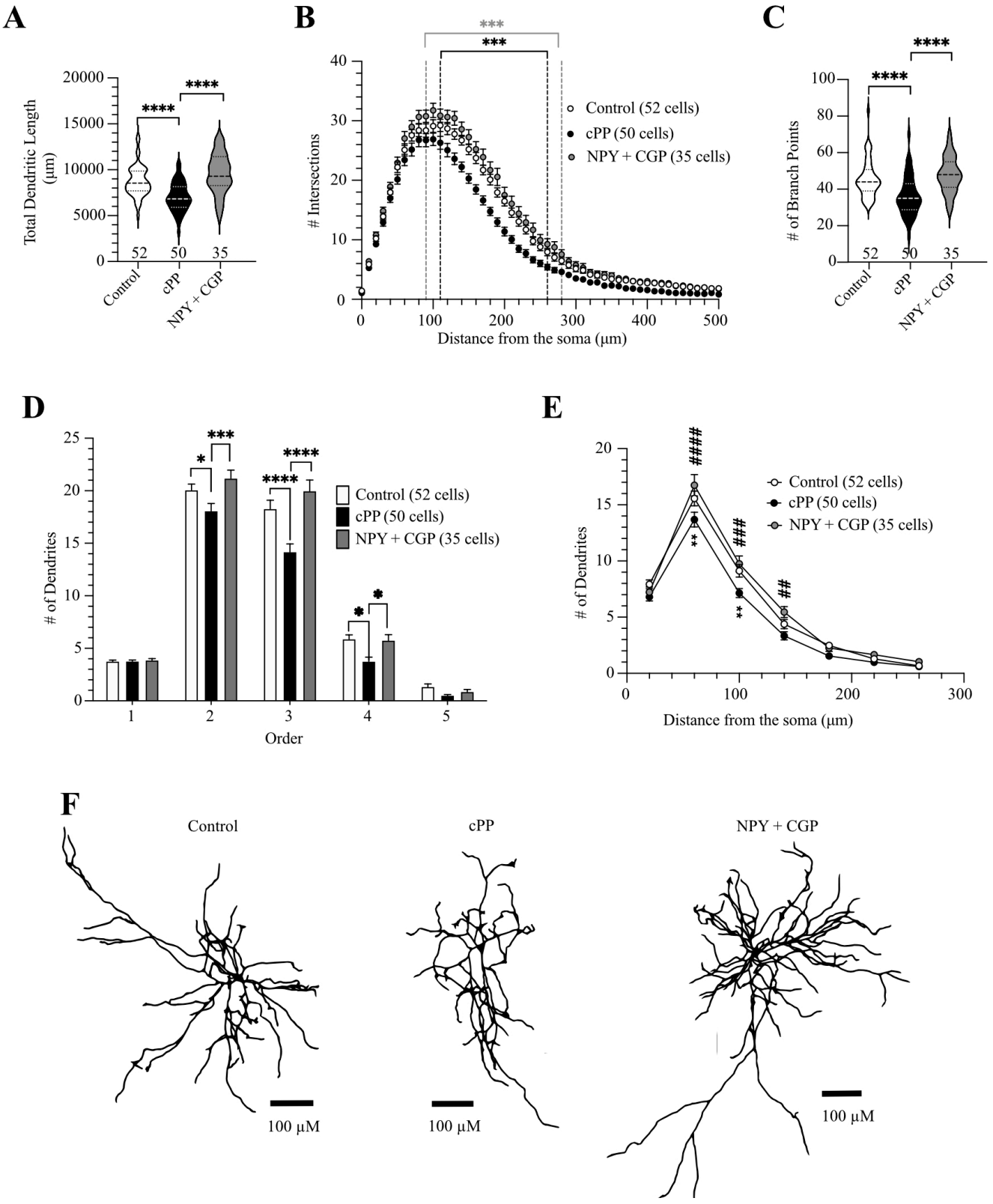
A
Total Dendritic Length (µm)
20000
15000
10000
5000
0
****
****
52
50
35
Control
cPP
NPY + CGP
B
Intersections
40
30
20
10
0
***
***
Control (52 cells)
cPP (50 cells)
NPY + CGP (35 cells)
0
100
200
300
400
500
Distance from the soma (µm)
C
# of Branch Points
100
80
60
40
20
0
****
****
52
50
35
Control
cPP
NPY + CGP
D
# of Dendrites
25
20
15
10
5
0
*
***
****
****
*
*
Control (52 cells)
cPP (50 cells)
NPY + CGP (35 cells)
1
2
3
4
5
Order
E
# of Dendrites
20
15
10
5
0
####
**
###
**
##
Control (52 cells)
cPP (50 cells)
NPY + CGP (35 cells)
0
100
200
300
Distance from the soma (µm)
F
Control
cPP
NPY + CGP
100 µM
100 µM
100 µM

Figure 14: Morphometric analysis of BLA neurons from animals treated with the Y_5R agonist cPP, NPY + the Y_5R antagonist CGP. A-E. Total dendritic length (A), sholl analysis (B), number of branch points (C), number of 1^{st}, 2^{nd}, 3^{rd}, 4^{th} and 5^{th} order dendrites (D) and number of branch points as a function of distance from the soma (E). F. Representative traces of BLA pyramidal neurons from control, cPP and NPY + CGP. Data on B, D and E represent the Mean ± SEM. Violin plots on A and C show the 1st and 3rd quartile in lower and upper dotted lines, respectively, and the median in a dashed line. Violin plot shapes indicate the density of the data at different values smoothed by a Kerner density *p<0.05, **p<0.01, ***p<0.001 cPP. #p<0.05, ##p<0.01, ###p<0.001 cPP compared to NPY + CGP.

3.7 NPY acute effects on BLA neurons *in vitro* are specific to BNST-projecting BLA neurons

The BLA projects widely throughout the brain (Fig 3,4). To better understand the role of the BLA and the circuitry underlying anxiety, fear and NPY-induced stress resilience a more comprehensive analysis of the projections made by NPY-sensitive BLA neurons; do these neurons project widely or do they have specific downstream targets? The BLA projects heavily to both regions of the medial prefrontal cortex (mPFC), the prelimbic (PL) and infralimbic (IL) mPFC (Fig 3,4) (Hoover and Vertes, 2007). The PL mPFC is required for fear expression (Dilgen et al., 2013). Inactivation of BLA decreases PL mPFC neurons activity (Sotres-Bayon et al., 2012b) and fear conditioning increases Fos expression in BLA neurons that project to the PL mPFC while the extinction of fear induces Fos expression in BLA neurons that project to the IL mPFC (Senn et al., 2014). Moreover, optogenetic inhibition of BLA neurons that project to PL mPFC promotes the extinction of fear. BLA neurons also project Bed nucleus of the stria terminalis (BNST) to modulate behavioral, autonomic and endocrine response to stress. Pharmacological inactivation of the BNST abolishes anxiety behaviors (Walker and Davis, 1997) and BNST disinhibition increases anxiety (Sajdyk et al., 2008a). Additionally, photoinhibition and photostimulation of the BNST decreases and increases, respectively, anxiety-like behaviors in mice (Kim et al., 2013a).

Thus, by using fluorescent retrobeads we studied the acute effects of NPY on BLA neurons that project to the PL and IL regions of the mPFC and to the bed nucleus of the stria terminalis (BNST). We hypothesize that NPY will hyperpolarize and reduce the excitability of BLA pyramidal neurons that project to both, the PL mPFC and BNST as these regions are activated in high states of fear and anxiety. We do not expect to NPY exert any effects on BLA neurons projecting to the IL mPFC as this brain region is involved in the extinction of fear.

To evaluate the neuronal properties and the NPY sensitivity of BLA neurons projecting to PL, IL and BNST, we prepared acute BLA slices from animals that were injected, into each region, targeted fluorescently labeled neurons and compared neuronal properties and NPY sensitivity based on projection pattern.

We begin asking whether neurons that project to both regions of the mPFC and BNST differ on their basic properties. We found that BLA pyramidal neurons that project to the BNST (BNST-projecting) and PL mPFC (PL-projecting) have smaller I_h amplitude than neurons that project to the IL mPFC (Fig. 15A. PL-projecting: -294.3 ± 15.8 pA, n = 21 p=0.02; BNST-projecting: -292.6 ± 16.4 pA, n = 26 p=0.01; IL-projecting: -344.3 ± 26.2 pA, n = 19). Inward rectifying currents (I_{IR})of BNST-projecting and PL-projecting BLA pyramidal neurons were also smaller than IL-projecting BLA neurons (Fig. 15B. PL-projecting -125 mV: -680.5 ± 41.3 pA p=0.01; -135 mV: -894.2 ± 51.9 pA, p=0.0005, n = 21. BNST-projecting -125 mV: -676.4 ± 36.4 pA p=0.005; -135 mV: -880.5 ± 45.8 pA p<0.0001, n = 26. IL-projecting: -1055.2 ± 64.6 pA, n = 18. Two-way ANOVA. Tukey's multiple comparisons test). Resting membrane potential from PL-projecting BLA pyramidal neurons was more hyperpolarized than resting membrane potential from IL-projecting BLA pyramidal neurons (Fig. 15C. PL-projecting: -80.8 ± 0.7 mV p=0.04 vs IL, n = 21; BNST-projecting: -79.9 ± 0.5 mV, n = 26; IL-projecting: -78.5 ± 0.7 mV, n = 19. One-way ANOVA. Tukey's multiple comparisons test). Rheobase from BNST-projecting BLA pyramidal neurons was lower than rheobase from PL-projecting and IL-projecting BLA neurons (Fig. 15D. PL-projecting: 305.8 ± 68.26 pA, n = 21; BNST-projecting: 221.2 ± 67.78 pA, n = 26 p<0.0001 vs IL, p=0.004 vs PL; IL-projecting: 356.6 ± 27.0 pA, n = 19. One-way ANOVA. Tukey's multiple

comparisons test). BNST-projecting BLA pyramidal neurons showed more depolarized holding current, measured at -75 mV, compared to PL-projecting and IL-projecting BLA pyramidal neurons (Fig. 15E. PL-projecting: 106.0 ± 8.7 pA, n = 17; BNST-projecting: 68.8 ± 7.5 pA p=0.007 vs PL p=0.0002 vs IL, n = 26; IL-projecting: 139.1 ± 13.7 pA, n = 7. One-way ANOVA. Tukey's multiple comparisons test). Input resistance was similar across the three groups (Fig. 15F. PL-projecting: 75.74 ± 16.63 MΩ, n = 21; BNST-projecting: 82.06 ± 23.5 MΩ, n = 26; IL-projecting: 68.05 ± 23.63 MΩ, n = 14. One-way ANOVA. Tukey's multiple comparisons test) Capacitance was also similar between PL= BNST- and IL-projecting BLA neurons (Fig, 15G. PL-projecting: 206.7 ± 6.49 pF, n = 21; BNST-projecting: 205.5 ± 5.96 pF, n = 26; IL-projecting: 209.2 ± 8.4 pF, n = 14. One-way ANOVA. Tukey's multiple comparisons test).

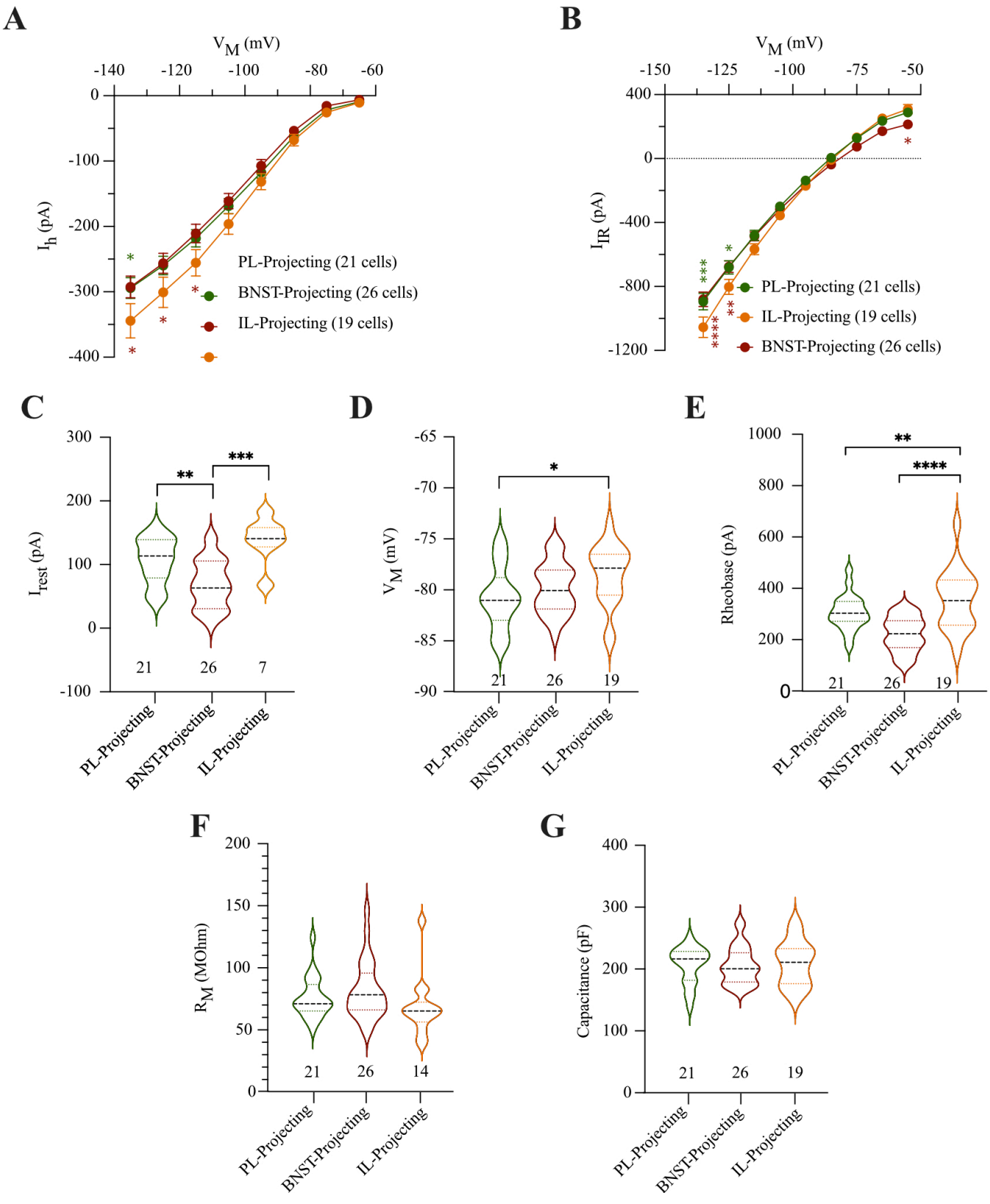
A
V_M (mV)
-140
-120
-100
-80
-60
0
-100
-200
-300
-400
I_h (pA)
PL-Projecting (21 cells)
BNST-Projecting (26 cells)
IL-Projecting (19 cells)
B
V_M (mV)
-150
-125
-100
-75
-50
400
0
-400
-800
-1200
I_{IR} (pA)
PL-Projecting (21 cells)
IL-Projecting (19 cells)
BNST-Projecting (26 cells)
C
I_{rest} (pA)
300
200
100
0
-100
**
***
21
26
7
PL-Projecting
BNST-Projecting
IL-Projecting
D
V_M (mV)
-65
-70
-75
-80
-85
-90
*
21
26
19
PL-Projecting
BNST-Projecting
IL-Projecting
E
Rheobase (pA)
1000
800
600
400
200
0
**
****
21
26
19
PL-Projecting
BNST-Projecting
IL-Projecting
F
R_M (MOhm)
200
150
100
50
0
21
26
14
PL-Projecting
BNST-Projecting
IL-Projecting
G
Capacitance (pF)
400
300
200
100
0
21
26
19
PL-Projecting
BNST-Projecting
IL-Projecting

Figure 15: Passive resting properties of BLA pyramidal neurons that project to PL mPFC, IL mPFC and BNST. A-G. I_h amplitude (A), inward rectifying current (B), resting membrane potential (C), rheobase (D), resting current at -75 mV (E), input resistance (F) and capacitance (G) of BLA neurons that project to PL mPFC (green), IL mPFC (orange) and BNST (red). Data on A and B represent the Mean ± SEM. Violin plots on C – G show the 1st and 3rd quartile in lower and upper dotted lines, respectively, and the median in a dashed line. Violin plot shapes indicate the density of the data at different values smoothed by a Kerner density**.** *p<0.05, **p<0.01, ****p<0.0001.

Then, we asked if neurons from PL and IL mPFC are sensitive to the inhibitory actions of NPY. We found that bath application of NPY (1 μM) acutely reduced max I_h amplitude in all BLA neurons regardless of projection (Fig. 16A, H. PL-projecting Control: -298.2 ± 18.5 pA; +NPY: -237.9 ± 15.1, n = 15, $p < 0.01$; IL-projecting Control: -354.5 ± 32.9 pA, + NPY: -284.8 ± 26.8, n = 14, $p < 0.01$; BNST-projecting , Fig. 17A, C. Control -292.6 ± 16.6; + NPY: -232.7 ±15.0 pA, n = 26, $p < 0.001$). The inwardly rectifying current was suppressed by NPY in PL- (Fig. 16. B) and BNST-projecting (Fig. 17. B, C), but not IL-projecting BLA neurons (PL-projecting Control: -910.9 ± 62.8 pA; + NPY: -816.2 ± 55.5 pA, n = 15, $p < 0.0001$. BNST-projecting Control: -880.5 ± 45.8 pA; + NPY: -756.9 ± 37.2 pA, n = 26, $p < 0.001$).

Bath application of NPY had no other effects on PL- and IL-projecting BLA neurons (Fig. 16). However, NPY hyperpolarized (Fig. 17D. Control: -79.8 ± 0.5 mV; + NPY: -83.5 ± 0.5 mV, n = 26, $p < 0.001$) increased holding current at -75 mV (Fig. 17E. Control: 68.8 ± 7.5 pA; + NPY: 105.9 ± 6.1 pA, n = 26, $p < 0.001$), decreased rheobase (Fig. 17F. Control: 221.2 ± 13.3 pA; + NPY: 271.2 ± 15.2 pA, n = 26, $p < 0.001$) of BNST-projecting neurons. NPY had not effect on input resistance (Fig. 17G. Control: 84.6 ± 5.1 MΩ; + NPY: 89.8 ± 3.9 MΩ, n = 22). Taken together, these data suggest that the acute actions of NPY are predominantly on BLA pyramidal neurons that project to the BNST.

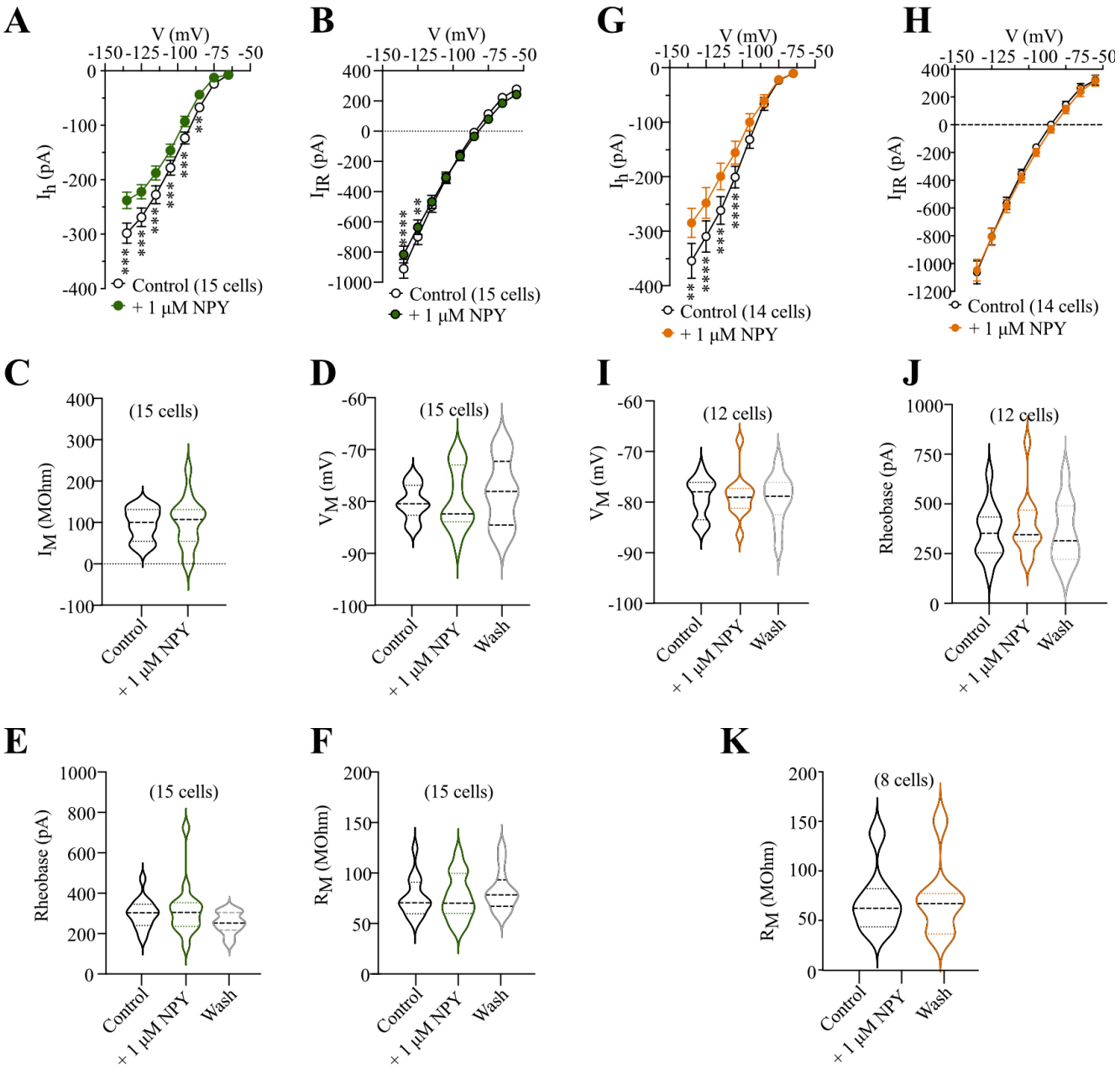
A
V (mV)
-150 -125 -100 -75 -50
I_h (pA)
Control (15 cells)
+ 1 µM NPY
B
V (mV)
-150 -125 -100 -75 -50
I_{IR} (pA)
Control (15 cells)
+ 1 µM NPY
G
V (mV)
-150 -125 -100 -75 -50
I_h (pA)
Control (14 cells)
+ 1 µM NPY
H
V (mV)
-150 -125 -100 -75 -50
I_{IR} (pA)
Control (14 cells)
+ 1 µM NPY
C
(15 cells)
I_M (MOhm)
Control
+ 1 µM NPY
D
(15 cells)
V_M (mV)
Control
+ 1 µM NPY
Wash
I
(12 cells)
V_M (mV)
Control
+ 1 µM NPY
Wash
J
(12 cells)
Rheobase (pA)
Control
+ 1 µM NPY
Wash
E
(15 cells)
Rheobase (pA)
Control
+ 1 µM NPY
Wash
F
(15 cells)
R_M (MOhm)
Control
+ 1 µM NPY
Wash
K
(8 cells)
R_M (MOhm)
Control
+ 1 µM NPY
Wash

Figure 16: Acute effects of NPY on BLA neurons that project to PL or IL regions of the mPFC. A-G. Effect of bath applications of NPY on I_h amplitude (A), inward rectifying current (B), resting current (C), resting membrane potential (D), rheobase (E) and input resistance (F) of BLA neurons that project to PL region of the mPFC. G-K. Effect of bath applications of NPY on I_h amplitude (G), inward rectifying current (H), resting membrane potential (I), rheobase (J) and input resistance (K) of BLA neurons that project to IL region of the mPFC. Data on A, B, G and H represent the Mean ± SEM. Violin plots on C – F and I – K show the 1st and 3rd quartile in lower and upper dotted lines, respectively, and the median in a dashed line. Violin plot shapes indicate the density of the data at different values smoothed by a Kerner density. **p<0.01, ***p<0.001

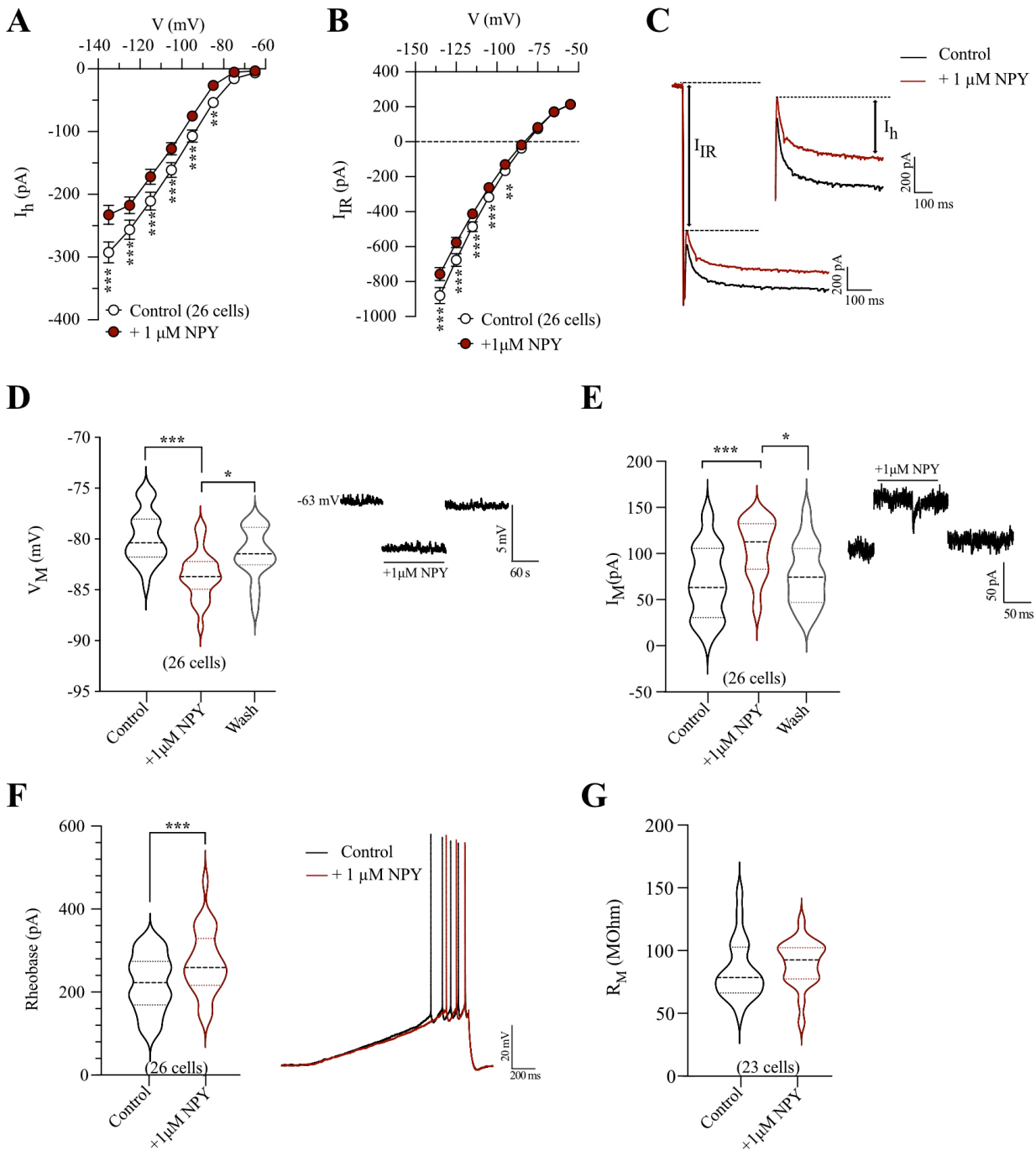
A
V (mV)
-140 -120 -100 -80 -60
0
-100
-200
-300
-400
I_h (pA)
Control (26 cells)
+ 1 µM NPY
B
V (mV)
-150 -125 -100 -75 -50
400
200
0
-200
-400
-600
-800
-1000
I_{IR} (pA)
Control (26 cells)
+1µM NPY
C
Control
+ 1 µM NPY
I_{IR}
I_h
200 pA
100 ms
200 pA
100 ms
D
-70
-75
-80
-85
-90
-95
V_M (mV)
(26 cells)
Control
+1µM NPY
Wash
-63 mV
+1µM NPY
5 mV
60 s
E
200
150
100
50
0
-50
I_M(pA)
(26 cells)
Control
+1µM NPY
Wash
+1µM NPY
50 pA
50 ms
F
600
400
200
0
Rheobase (pA)
(26 cells)
Control
+1µM NPY
Control
+ 1 µM NPY
20 mV
200 ms
G
200
150
100
50
0
R_M (MOhm)
(23 cells)
Control
+1µM NPY

Figure 17: Acute effects of NPY on BLA neurons that project to the BNST. A-J. Effect of NPY on I_h amplitude (A, C), inward rectifying current (B, C), RMP (D), membrane current at a -75 mV holding potential (E), rheobase (F) and input resistance (G) of BLA neurons that project to BNST. D right: representative trace of RMP from a BNST-projecting neuron before, during and after bath application of NPY. E right: representative trace of the membrane current at a -75 mV holding potential from a BNST-projecting neuron before, during and after bath application of NPY. F right: representative trace of the effect of bath application NPY on rheobase. Data on A and B represent the Mean ± SEM. Violin plots on D – G show the 1st and 3rd quartile in lower and upper dotted lines, respectively, and the median in a dashed line. Violin plot shapes indicate the density of the data at different values smoothed by a Kerner density. *$p<0.05$, **$p<0.01$, ***$p<0.001$.

3.8 Long-term effects of NPY administered *in vivo* are predominantly on BNST-projecting BLA neurons

Because the acute effects of NPY are predominantly on BNST-projecting BLA neurons we compared the effects of 5 days of NPY, or vehicle, injections into the BLA on BLA neurons that project to the BNST (BNST-NPY, BNST-control) and BLA neurons that do not project to the BNST (nonBNST-NPY, nonBNST-control) 4 weeks after the treatment. We hypothesize that NPY treatment will produce a long-term reduction in the excitability and hypotrophy only in BNST-projecting BLA neurons.

Intra-BLA injections of NPY reduced whole-cell capacitance on BLA pyramidal neurons that project to the BNST (BNST-NPY) compared to neurons that project to the BNST from the control (BNST Control) group; ($p = 0.0015$) and compared to BLA pyramidal neurons that do not project to the BNST ($p = 0.0001$ vs nonBNST-NPY and $p=0.001$ vs nonBNST-Control), suggesting that the effect of NPY on capacitance occurs predominantly on BLA neurons that project to the BNST. (Fig. 18A. BNST-NPY: 178.3 ± 5.5 pF, n = 30; BNST-Control: 206.9 ± 4.5 pF, n = 36; nonBNST-NPY: 218.3 ± 8.4 pF, n = 19).

Intriguingly, NPY had no effect on max I_h amplitude (Fig. 18B. BNST-Control: -314.7 ± 12.3 pA, n = 20; BNST-NPY: -305.8 ± 15.3 pA $p=0.9$ vs BNST-Control, $p=0.7$ vs nonBNST-NPY, $p=0.3$ vs nonBNST-Control, n = 31; nonBNST-Control: -336.5 ± 21.9 pA, n = 9; nonBNST-NPY: -322.3 ± 20.0 pA, n = 16). NPY did, however, decreased the IIR current in BNST-projecting BLA neurons compared to BNST-projecting neurons from controls ($p=0.004$) and nonBNST neurons from the NPY-treated group ($p<0.0001$)(Fig. 18C. BNST-Control: -994.1 ± 42.0 pA, n = 28; BNST-NPY:

-876.6 ± 40.6 pA, n = 30; nonBNST-Control: -1011.5 ± 83.9 pA, n = 9; nonBNST-NPY: -1147.2 ± 68.8 pA, n = 16).

Membrane current, at a holding potential of -75 mV (Fig. 15D. BNST-Control: 125.3± 12.42 pA, n = 28; BNST-NPY: 107.7 ± 8.6 pA, n = 30; nonBNST-Control: -131.3 ± 22.9 pA, n = 9; nonBNST-NPY: -142.3 ± 17.3 pA, n = 16) and resting membrane potential (Fig. 18E. BNST-Control: -81.6 ± 0.75 mV, n = 29; BNST-NPY: -80.8 ± 0.4 nM, n = 30; nonBNST-Control: -82.2 ± 1.8 mV, n = 9; nonBNST-NPY: -82.5 ± 0.8 mV, n = 16) were similar in all groups of BLA neurons.

Rheobase from nonBNST-projecting BLA pyramidal neurons from the NPY-treated group (nonBNST-NPY) was increased compared to BNST-projecting neurons from the control group (BNST-Control, p=-0.48) and BNST-projecting neurons from the NPY-treated group (nonBNST-NPY, p=0.44) (Fig. 18F. BNST-Control: 334.5 ± 15.2 pA, n = 28; BNST-NPY: 318.4 ± 18.3 pA, n = 30; nonBNST-Control: 355.2 ± 32.2 pA, n = 9; nonBNST-NPY: 418.8 ± 34.3 pA, n = 16). NPY also decreased input resistance in BLA neurons that do not project to the BNST (nonBNST-NPY, p=0.04) compared to BLA neurons that project to the BNST (BNST-NPY) (Fig. 18G. BNST-Control: 67.2 ± 2.8 MΩ, n = 28; BNST-NPY: 73.6 ± 3.27 MΩ, n = 29; nonBNST-Control: 62.6 ± 3.5 MΩ, n = 9; nonBNST-NPY: 60.5 ± 3.6 pA, n = 16, $p < 0.05$).

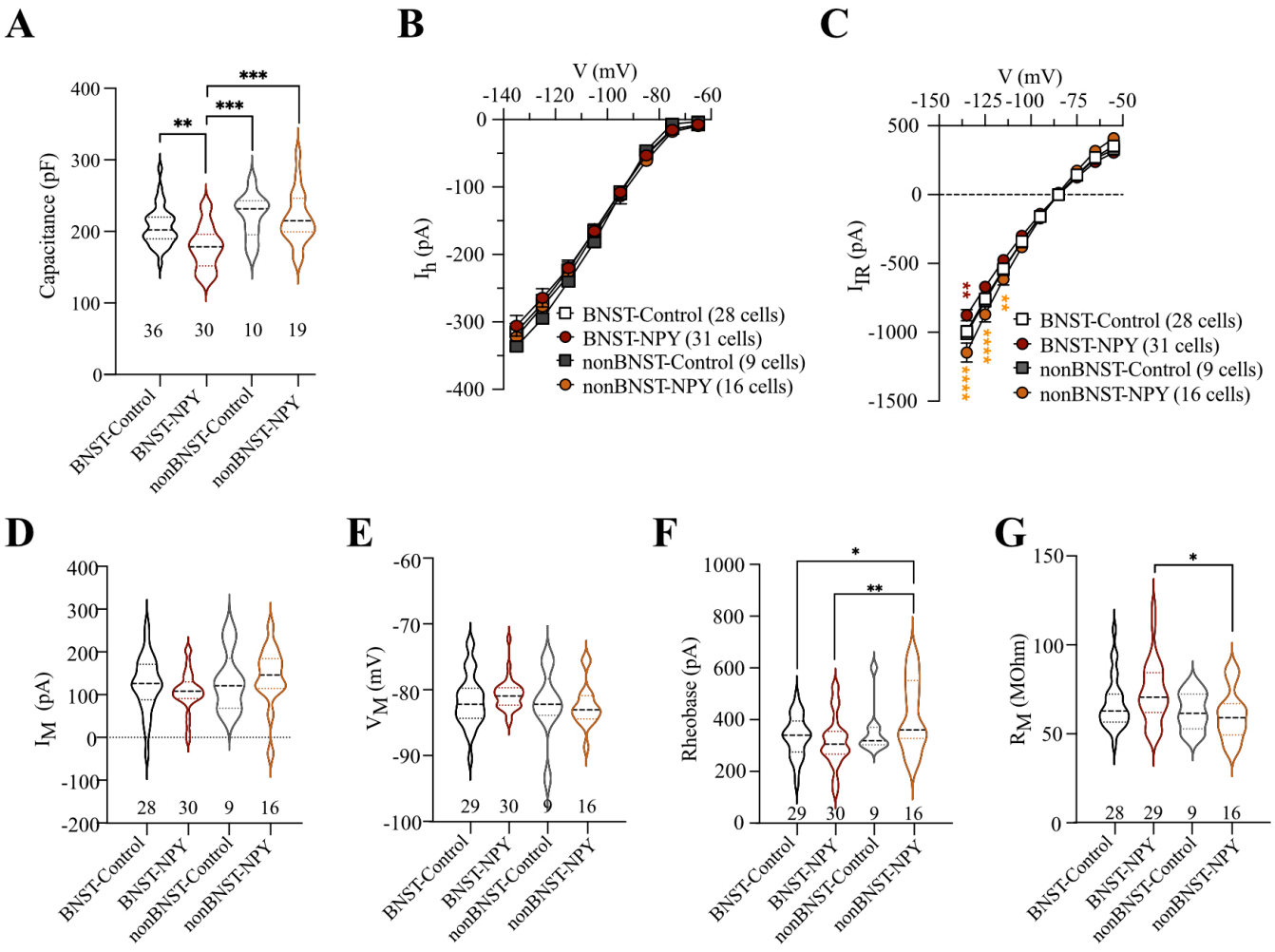

Figure 18: Effects injections of NPY into the BLA on resting properties of BLA neurons that project to BNST. A-G. Effect of intra-BLA NPY administration on capacitance (A), I_h amplitude (B), inward rectifying current (C), resting current (D), resting membrane potential (E), rheobase (F) and input resistance (G). Data on B and C represent the Mean ± SEM. Violin plots on A, D – G show the 1st and 3rd quartile in lower and upper dotted lines, respectively, and the median in a dashed line. Violin plot shapes indicate the density of the data at different values smoothed by a Kerner density*p<0.05, **p<0.01, ***p<0.001, ***p<0.0001.

The NPY-induced decrease capacitance (Fig. 18A) was accompanied by a reduction in total dendritic length of BNST-projecting BLA neurons (Fig. 19A. BNST-Control: 9140 ± 402 μm, n = 11; BNST-NPY: 7551 ± 331 μm, p=0.01, n = 20) compared with control. Sholl analysis (Fig. 19B) revealed that the decrease in dendritic arborization was between 200 – 220 μm from the soma ($p < 0.01$). There was a non-significant trend towards a decrease in the number of bran points (Fig. 19C. BNST-Control: 43.2 ± 2.4, n = 11; BNST-NPY: 39.2 ± 1.8 μm, p=0.3, n = 19) but no change on the number of dendrites as a function of order (Fig. 19. D). Together, these results suggest that NPY reduces excitability and possibly induces hypotrophy on BLA neurons that project to the bed nucleus of the stria terminalis (BNST).

In summary, in this thesis I have provided evidence showing that NPY, via Y_5R, induces a prolonged state of anxiolysis by reducing excitability and hypotrophy of BLA. I also provided evidence indicating that NPY act on a specific subset of BLA neurons that project to the BNST.

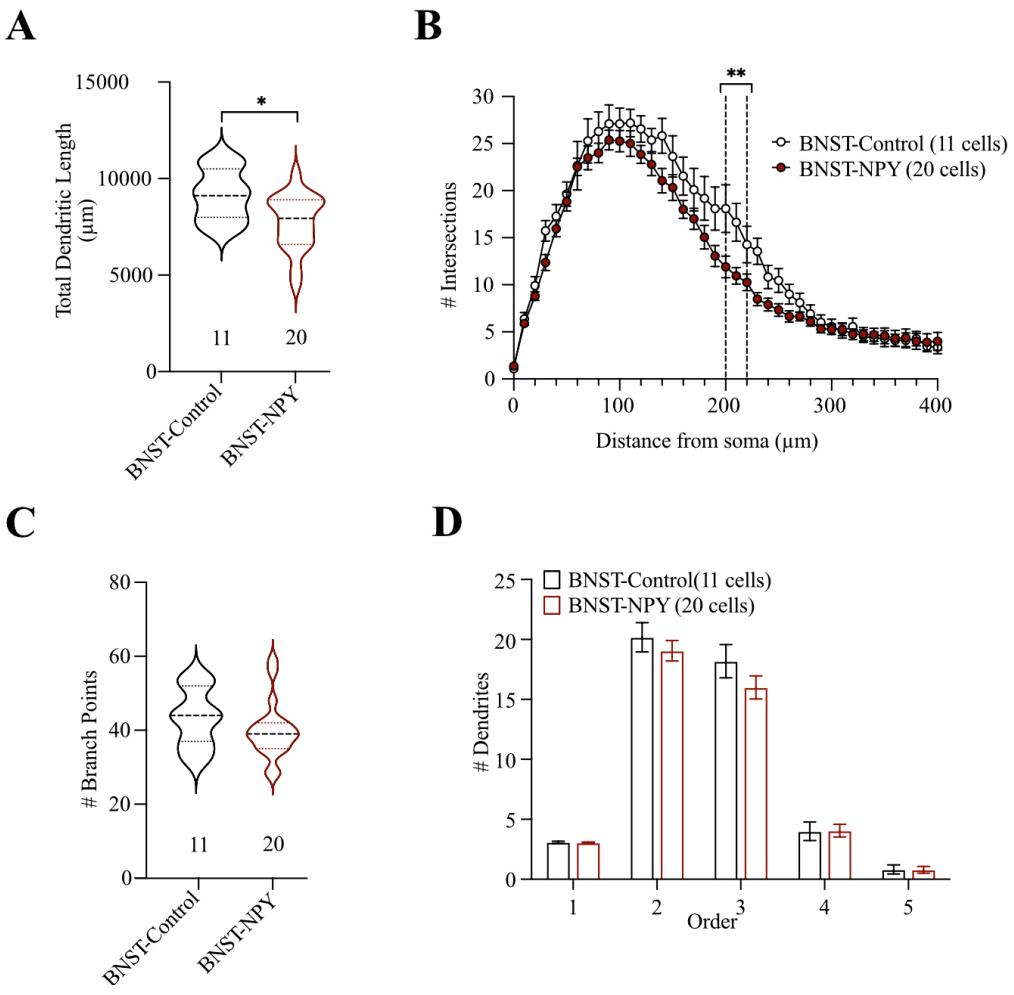

Figure 19: Morphometric analysis of BLA neurons that project to BNST. A-G. Effect of NPY administration into the BLA on total dendritic length (A), dendritic arborization (B), number of branch points (C), and number of dendrites as a function of order (D). Data on B represent the Mean ± SEM. Violin plots on A, C and D show the 1st and 3rd quartile in lower and upper dotted lines, respectively, and the median in a dashed line. Violin plot shapes indicate the density of the data at different values smoothed by a Kerner density. *p<0.5, **p<0.01.

4. Discussion

It is well stablished that NPY is a potent anxiolytic that can promote a prolonged state of behavioral anxiolysis, or stress resilience (Sajdyk et al., 1999; 2008b; Giesbrecht et al., 2010a; Silveira Villarroel et al., 2018; Michaelson et al., 2020) that long outlasts the duration of NPY administration. The purpose of this component of the thesis was to advance mechanistic understanding of this long-term, NPY-mediated anxiolysis. The first objective was to identify the underlying NPYR subtype. The second objective was to establish whether the population of NPY-sensitive BLA neurons that underlies the anxiolysis are those that project to the PL mPFC or to the BNST.

4.1 Contribution of NPY Y_1 and Y_5 receptors to NPY-induced stress resilience.

The acute anxiolytic actions of NPY are mediated by the activation of Y_1Rs in PNs of the basolateral amygdala (Sajdyk et al., 1999; 2002a; Giesbrecht et al., 2010), where NPY acutely hyperpolarized and reduced I_h in a subset of BLA PNs (Giesbrecht et al., 2010). Repeated administration of NPY into the BLA promotes hyperpolarization of pyramidal neurons with reduced I_h amplitude and inward rectifying currents and stress resilience (Silveira Villarroel et al., 2018). However, the cellular and molecular mechanisms underlying long-term NPY-mediated stress resilience are unknown. Here we show that NPY acting through Y_5Rs, but not Y_1Rs, is responsible for the development of a less anxious phenotype and that this less anxious phenotype is associated with dendritic hypotrophy of BLA PNs and that Y_5R activation is associated with decreased excitatory and increased inhibitory synaptic drive onto BLA pyramidal neurons.

Repeated administration of NPY into the BLA for five days promotes a long-lasting decrease in anxiety behavior that can be seen up-to eight weeks after the treatment has ended (Sajdyk et al., 2008b; Silveira Villarroel et al., 2018; Michaelson et al., 2020). The acute anxiolytic effects of NPY are Y_1R-mediated (Sajdyk et al., 1999). Thus, it was a surprise when intra-BLA administration of a selective Y_1R agonist failed to reproduce the full complement of NPY-mediated effects on anxiety behaviors. Most surprising, the Y_1R-mediated decrease in anxiety was only evident while the drug was being delivered, from day 1 to day 5. This effect quicky vanished once the treatment was withdrawn with anxiety levels returning back to the pre-treatment baseline. This is consistent with evidence showing that Y_1Rs are responsible for the acute anxiolytic actions of NPY (Sajdyk et al., 1999; Giesbrecht et al., 2010a; Michaelson et al., 2020). While our data confirm that Y_1Rs mediate the acute anxiolysis, they also strongly suggest that NPY-induced stress resilience does not involve the activation of Y_1Rs. Y_1Rs are predominantly expressed on PNs of the BLA (Sajdyk et al., 2002a) where they hyperpolarize membrane potential and downregulate I_h to decrease BLA excitability (Giesbrecht et al., 2010a), which is believed to underlie acute reductions in anxiety. Additionally, a 5 days treatment with NPY result on BLA neurons with smaller I_h compared to controls (Silveira Villarroel et al., 2018). Here we show that the peak I_h amplitude was not affected after a 5 days treatment with an Y_1R-agonist, which is consistent with our behavioral data suggesting that Y_1Rs are not involved in the development of stress resilience. Surprisingly, resting membrane potential of pyramidal neurons from the Y_1R agonist-treated animals was more hyperpolarized and neurons were less excitable, which are also characteristic features of neurons after long-term exposure to NPY, but neither I_h or CM were altered by long term Y_1R agonists, suggesting that the effects of NPY on I_h or Cm may be more important in resiliency.-Whether the rapid internalization of Y_1Rs (Berglund et al., 2003; Holliday et al., 2005)

and resulting desensitization to NPY is a factor in Y_1Rs mediating acute but not long-term effects is not clear. It seems unlikely, however, because the acute, Y_1R-mediated effects of NPY to reduce anxiety last as long as the agonist is applied. If Y_1R desensitization was a factor in any of these behaviours, I would expect that the anxiolytic effects of Y_1R agonist administration would diminish over the course of the 5 day exposure.

Y_2Rs are unlikely to underlie the NPY-mediated anxiolysis and resiliency because selective activation of Y_2Rs in the BLA promotes anxiety (Sajdyk et al., 2002b), possibly through reductions in the $GABA_B$R-mediated tonic inhibition of BLA PNs and a resultant increase in their excitability (Mackay et al., 2019). Y_2R activation also promotes hypertrophy of BLA neurons *in vitro* (Michaelson et al., 2020). Our interest in Y_5Rs as a possible mediator of the NPY anxiolysis was based on the observation that Y_2Rs are anxiogenic (Sajdyk et al., 2002b), the finding that a Y_2R/Y_5R non-selective agonist decreases anxiety and that the anxiolytic effect of the Y_2R/Y_5R agonist can be blocked by a Y_5R antagonist (Sajdyk et al., 2002a). Thus, we studied the acute effects of Y_5R activation on the passive and active properties of BLA pyramidal neurons *in vitro* as well as the longer term effects of Y_5R activation in vivo on membrane properties and on anxiety related behaviours *in vivo*.

Administration of a selective Y_5R agonist, surprisingly, had no effect on I_h, RMP, IR or rheobase of BLAOTC pyramidal neurons. The Y_5R agonist, did however, decrease whole-cell capacitance. Importantly, NPY-induced anxiolysis and resilience are associated with reduced dendritic arborization of BLA pyramidal neurons *in vitro* and *in vivo* (Michaelson et al., 2020). Additional evidence that Y_5R activation may inhibit BLA neuron growth is that BLA OTC neurons grown in

culture in the presence of the Y_5R agonist are smaller and have less complex dendritic trees comparted to control BLA OTC neurons. Finally, a selective Y_5R antagonist not only blocked the NPY-induced decrease in whole-cell capacitance and hypotrophy of BLA OTC, it increased capacitance and caused hypertrophy. This increase in cell size after a treatment with NPY + Y_5R antagonist is consistent with a Y_2R-mediated growth effect that is unmasked by antagonizing Y_5Rs (Michaelson et al., 2020). In addition, activation of Y_5Rs decreases excitatory and increases inhibitory drive into BLAOTC. One limitation of experiments on BLA OTCs is that cytoarchitecture, biochemistry and signaling pathways of culture neurons may not be completely mature at the time of culture preparation and may not develop into a fully mature system. Our BLA OTC neurons seem to represent an intermediate stage between the age of preparation (p14) and a mature 12 week stage (Michaelson et al., 2020). This could give account for differences on the effect of Y_5R agonist on I_h between BLA OTCs and BLA PNs. However, it is possible that this reduction on I_h is an effect of the reduction on capacitance rather that an effect of Y_5R on HCN channels, and this effect is more evident on BLA PNs than BLA OTCs since the former are considerably bigger and more have complex dendritic trees (Michaelson et al., 2020). Another limitation is that in our experimental design we did not included a group treated with only NPY as a positive control, as this data was previously produced by Dr. Michaelson (Michaelson, 2016).

At the behavioural level, repeated administration of a selective Y_5R agonist into the BLA *in vivo* had a potent anxiolytic effect and induced dendritic hypotrophy of BLA pyramidal neurons. Most importantly, a Y_5R antagonist completely blocked the NPY-mediated stress resilience and dendritic hypotrophy. Considered together, these data suggest that NPY acts through Y_5Rs to induce hypotrophy of BLA OTC pyramidal neurons, which somehow contributes to the NPY-

induced stress resilience *in vivo*. One shortcoming of our *in vivo* data is that we evaluated anxiety based on one single test. Social interaction is a widely used very robust test to measure anxiety but it only accounts for sociability. Additional tests, such as novelty-induced hyperphagia, elevated plus maze and acoustic potentiated startle, would be useful to understand if NPY-induced anxiolysis and the underlying circuits are recruited on specific features of anxiety (ie. only recruited by social anxiety) or conform a general mechanism. The biggest limitation of our *in vitro* and *in vivo* studies is that it was only done on male rats. It is now known that repeated stress, and CRF, produces dendritic hypertrophy of BLA neurons from male rats (Vyas et al., 2002; Michaelson et al., 2020). However, in female rats, stress does not induces hypertrophy of BLA neurons (Blume et al., 2019). Thus, it is possible that NPY effects are sex specific so it will be crucial to study the effect of NPY on BLA neurons and behavior on female rats across the estrous cycle.

The mechanisms by which Y_5Rs mediate stress resilience and dendritic remodeling are unknown. Repeated exposure to stress causes dendritic hypertrophy of BLA PNs (Padival et al., 2013) and CRF increases excitatory drive onto BLA pyramidal neurons (Rainnie et al., 2004) which promotes anxiety. Y_5R activation has the opposite effect on neuronal morphology and synaptic input, which likely accounts for the anxiolytic effects of Y_5R activation. This does not, however, provide great mechanistic insight. BLA pyramidal neurons co-express Y_1Rs and the protein phosphatase calcineurin (Sajdyk et al., 2008b; Leitermann et al., 2012), a phosphatase involved in the development of LTD in the BLA and fear extinction (Lin et al., 2003a; 2003b). Calcineurin activity is also required for the NPY-induced stress resilience (Sajdyk et al., 2008b) and it was recently demonstrated that the actions of Y_5Rs on BLA dendritic remodeling *in vitro* require the activation

of calcineurin (Michaelson et al., 2020), suggesting that Y_5R act through a calcineurin-dependent signalling pathway to promote stress resilience. Previous data from the Colmers laboratory has reported that NPY, via Y_1Rs reduced calcium influx on the distal dendrites of layer V pyramidal neurons (Hamilton et al., 2013). It was also reported that NPY inhibits calcium elevations induced by depolarization and inhibits a N-type calcium current on rat dentate granule cells via Y_1Rs. (McQuiston et al., 1996). More recently, preliminary data from the Colmers laboratory showed that NPY reduces calcium currents on BLA pyramidal neurons, but the type of calcium current is yet to be determined (Mackay, 2016). This was accompanied by a decrease on afterhyperpolarization currents which was an effect of the NPY-mediated inhibition of VGCC (Mackay, 2016). This effect was not mediated by Y_1Rs. In fact, preliminary data showed that Y_5Rs seem to mediate the NPY effects on VGCC (Mackay, 2016). Thus, Y_5R could inhibit VGCC, limiting calcium entry to promote the activation of calcineurin to finally induce dendritic remodeling and stress resilience. Why in one neurons calcium current seem to be mediated by different NPY receptors is unclear but it is possible that this difference is due to the type of VGCC co-expressed with NPY receptors.

4.2 Neural pathway involved on NPY-induced stress resilience

Anxiety states are mediated by neural circuits comprised of local and wide range projections between brain regions (Fig.4). Cortical and thalamic networks detect information regarding the environment and transmit this information to the BLA. The interpretation of the threatening or non-threatening nature of a stimulus depends on an interaction between the BLA and additional brain structures. Events that promote anxiety recruit neural pathways involving excitatory projections from the BLA to the BNST (Davis et al., 2010; Calhoon and Tye, 2015). Threatening

events that elicit fear recruit projections from the BLA to the PL mPFC. On the other hand, stimuli that act as safety signals after a threat recruit projections from the BLA to the IL mPFC, that dampen both fear and anxiety responses (Calhoon and Tye, 2015). Once the information is interpreted, it is further evaluated, and an appropriate response is initiated (Fig. 4). We targeted neuros from the BLA that project to the mPFC BNST and studied their sensitivity to acute administration of NPY. Our findings that NPY acts principally on BLA neurons that project to the BNST but not on BLA neurons that project to the mPFC suggest some degree of specificity in the neural pathways that mediate NPY-induced anxiolysis and that the BLA to BNST is most important. At present, we cannot exclude the possibility that the stress resilience associated with NPY activation of the BLA results from activation of BLA projections that were not examined here. The BLA projects to multiple areas. including the hippocampus and CeA, that could contribute to anxiolysis and resilience.

During fear conditioning, neurons of the BA that project to the PL mPFC increased their activity. This activation of BLA neurons promotes the increase of firing rate of PL mPFC neurons which elicit freezing, a typical response to fear (Burgos-Robles et al., 2009). If BLA neurons that project to the PL mPFC are recruited and activated during fear learning, stimulating the activity of mPFC neurons to elicit fear, we thought possible that NPY could act on BLA neurons that are active during fear and project to the mPFC to reduce fear. This was not the case. We found that BLA neurons that project to the PL mPFC only responded to acute NPY applications with a decrease in I_h. RM or rheobase were not affected by acute NPY, suggesting perhaps that NPY as minimal effects, if any, on neurons that project to the PL mPFC. On the other hand, during the extinction of fear, another subpopulation of BLA are activated, known as extinction neurons, and they were

found to project to the IL mPFC (Herry et al., 2008; Senn et al., 2014). If BLA neurons that project to the IL mPFC are needed to extinguish fear, then NPY actions (ie. overall decrease on activity) on these neurons would be counterproductive, and it would limit the ability to extinguish fear memories. In line with this we were not expecting NPY to act on BLA neurons that project to the IL mPFC. Similar to BLA neurons that project to the PL mPFC neurons, in neurons that target IL mPFC NPY only decreases I_h. This reduction on I_h without the reduction of excitability or hyperpolarization that are well known to be induced by NPY could suggest that NPY might contribute, to some extent, to decrease the activity of mPFC under states of fear or extinction. The role of NPY in fear and extinction is supported by a study showing that the administration of NPY into the BLA reduces the expression of fear expression, after fear learning is stablished (Gutman et al., 2008). In line with this, is possible that NPY, act on BLA neurons thar project to the mPFC only during high states of fear, when BLA and PL mPFC activity is increased, and not on basal low fear states such as in our conditions. This reduction on I_h could also be explained by a time-dependent run down of I_h in all cells that did not reflect an action of NPY, especially if this effect was not accompanied by hyperpolarization and decrease on excitability. One the limitation in our study is that we did not evaluated the effect of NPY on BLA neurons from animals exposed to a fear-inducing stimulus. Neither we studied the effect of injections into the BLA on fear conditioning. These types of studies would be key to determine if NPY acts on BLA neurons that project to mPFC. Further experiments testing the effect of NPY administrated into the BLA on the activity (ie. firing rate) of mPFC neurons would also help to clarify if NPY modulates the activity of BLA neurons that project to the cortex.

The BNST is a mayor target of the BLA and has long been hypothesized to mediate anxiety. When an anxiety-evoking stimulus is presented, BLA activity increases and excites neurons of the BNST to evoke an appropriated anxiety response. Pharmacological studies showed that when the BLA is activated but the BNST is inhibited, anxiety responses are abolished (Davis et al., 2010). Suggesting that the projections form the BLA to the BNST recruited by anxiogenic circumstances. We thought that it is possible that NPY acts on BLA neurons that target the BNST to reduce the activity of BNST neurons and terminate the response to anxiogenic stimuli. We found that the acute actions of NPY, i.e reduction of I_h, hyperpolarization and decrease on excitability, were predominantly on BLA neurons that project to the BNST. We also found that NPY causes a long-term decrease on capacitance and dendritic hypotrophy of BLA neurons thar project to the BNST. This suggest that NPY acts preferentially on the BLA-BNST pathway to decrease anxiety. Recently, Kim et al (2013) reported opposite roles of different subregions of the BNST in modulating anxiety. Using optogenetic approaches, when authors inhibited the cell bodies of BNST neurons anxiety was reduced. Strikingly, when they stimulated BLA terminals in the anterodorsal region of the BNST (adBNST), anxiety was decreased. Consistent with this, optogenetic inhibition of BLA terminals in the adBNST potentiated anxiety (Kim et al., 2013a). At first glance, these data appear to contradict our findings. If BLA projections to the BNST are excitatory and their activation promotes anxiety by increasing BNST activity, then NPY should decrease excitability of BLA neurons that target the BNST, thereby limiting BNST activity to finally dampen anxiety. However, the BNST is a complex area and it is possible that NPY-sensitive BLA neurons project to a different region of the BNST. Kim et al. (2013) reported that selective optical inhibition of another region of the BNST, the oval BNST (ovBNST), reduced anxiety (Kim et al., 2013a). Thus, it is possible that NPY-sensitive neurons from the BLA target the ovBNST

and reduce anxiety through this pathway. Another study reported that stress impaired SI in rodents and pharmacological inhibition of the ventrolateral BNST (vBNST, which is located ventral to the adBNST) during stress prevents the SI impairment induced by stress (Christianson et al., 2011). It is possible that BLA neurons sensitive to the anxiolytic actions of NPY target the vBNST. Based on our experiments we cannot definitively conclude which BNST subregion is involved in anxiolysis (or resiliency) since we targeted the majority of the BNST. Further experiments that specifically explore the different subregions of the BNST that receive NPY-sensitive BLA projections are needed to unravel the neural pathways underlying the modulation of stress resilience and anxiety by NPY. We were unable to stablish which receptor is expressed on BLA neurons that project to the BNST, however, based on the data reported here, we expect that the acute actions of NPY on BNST-projecting BLA neurons are Y_1R-mediated and the long-term actions of NPY on BNST-projecting BLA neurons are Y_5R-mediated.

5. Summary

Compelling evidence propose a role of NPY on resilience to stress. Works from the Colmers laboratory has shown that NPY induced downregulation Ih, hyperpolarization, reduced excitability and dendritic hypotrophy of a subpopulation of BLA PNs and a state of behavioral anxiolysis (Giesbrecht et al., 2010; Silveira Villarroel et al., 2018; Michaelson et al). In summary, the main contributions of these experiments are two-fold, First, we have demonstrated that NPY acts through Y_5R to reduce anxiety and promote stress resilience and that these behavioural changes are associated with dendritic remodeling and reduced excitatory drive to BLA pyramidal neurons. Second, we have demonstrated that the acute actions of NPY (Giesbrecht et al., 2010), as well as the long term plastic changes induced by NPY (Silveira Villarroel et al., 2018; Michaelson et al.,

2020), are mediated through activation of BLA neurons that project to the BNST. These findings help us deepen our knowledge of the mechanism by which NPY elicits stress resilience and contributes to a more comprehensive understanding of the neural circuits of anxiety and the modulation of NPY. Additional experiments aimed to determine the NPY sensitivity of BLA neurons that project to other brain regions associated with anxiety such as the hippocampus and CeA would give us a more complete map of the NPY circuitry that underlies stress resilience. Finally, if stress induces a non-reversible hypertrophy of BLA PNs, could a treatment with NPY prevent, or more importantly, reverse stress-induced dendritic hypertrophy *in vivo?* Experiments aimed to test the effect of NPY on BLA neurons on a rodent model of stress will be key in assessing the potential anti-anxiety or stress-protective properties and mechanisms of NPY

6. References

Adamec R, Hebert M, Blundell J, Mervis RF (2012) Dendritic morphology of amygdala and hippocampal neurons in more and less predator stress responsive rats and more and less spontaneously anxious handled controls. Behavioural Brain Research 226:133–146.

Adrian TE, Allen JM, Bloom SR, Ghatei MA, Rossor MN, Roberts GW, Crwo TJ, Tatemoto K, Polak JM (1983) Neuropeptide Y distribution in human brain. 306:584–586.

Adolphs R, Tranel D, Damasio H, Damasio A (1994) Impaired recognition of emotion in facial expressions following bilateral damage to the human amygdala. Nature 372:669–672.

Amano T, Duvarci S, Popa D, Pare D (2011) The Fear Circuit Revisited: Contributions of the Basal Amygdala Nuclei to Conditioned Fear. J Neurosci 31:15481–15489.

Amano T, Unal CT, Pare D (2010) Synaptic correlates of fear extinction in the amygdala. Nat Neurosci 13:489–494.

Berglund MM, Schober DA, Statnick MA, McDonald PH, Gehlert DR (2003) The Use of Bioluminescence Resonance Energy Transfer 2 to Study Neuropeptide Y Receptor Agonist-Induced β-Arrestin 2 Interaction. J Pharmacol Exp Ther 306:147–156.

Bissière S, Humeau Y, Lüthi A (2003) Dopamine gates LTP induction in lateral amygdala by suppressing feedforward inhibition. Nat Neurosci 6:587–592.

Blair HT, Schafe GE, Bauer EP, Rodrigues SM, LeDoux JE (2001) Synaptic plasticity in the lateral amygdala: a cellular hypothesis of fear conditioning. Learning & Memory 8:229–242.

Blanchard DC, Blanchard RJ (1972) Innate and conditioned reactions to threat in rats with amygdaloid lesions. J Comp Physiol Psychol 81:281–290.

Blomqvist AG, Söderberg C, Lundell I (1992) Strong evolutionary conservation of neuropeptide Y: sequences of chicken, goldfish, and Torpedo marmorata DNA clones.

Blume SR, Padival M, Urban JH, Rosenkranz JA (2019) Disruptive effects of repeated stress on basolateral amygdala neurons and fear behavior across the estrous cycle in rats. Sci Rep 9:12292.

Boehme S, Ritter V, Tefikow S, Stangier U, Strauss B, Miltner WHR, Straube T (2014) Brain activation during anticipatory anxiety in social anxiety disorder. Soc Cogn Affect Neurosci 9:1413–1418.

Burgos-Robles A, Vidal-Gonzalez I, Quirk GJ (2009) Sustained conditioned responses in prelimbic prefrontal neurons are correlated with fear expression and extinction failure. Journal of Neuroscience 29:8474–8482.

Butler RK, White LC, Frederick-Duus D, Kaigler KF, Fadel JR, Wilson MA (2012) Comparison of the activation of somatostatin- and neuropeptide Y-containing neuronal populations of the rat amygdala following two different anxiogenic stressors. Exp Neurol 238:52–63.

Calhoon GG, Tye KM (2015) Resolving the neural circuits of anxiety. Nat Neurosci 18:1394–1404.

Chee MJS, Myers MG, Price CJ, Colmers WF (2010) Neuropeptide Y Suppresses Anorexigenic Output from the Ventromedial Nucleus of the Hypothalamus. Journal of Neuroscience 30:3380–3390.

Christianson JP, Jennings JH, Ragole T, Flyer JGN, Benison AM, Barth DS, Watkins LR, Maier SF (2011) Safety signals mitigate the consequences of uncontrollable stress via a circuit involving the sensory insular cortex and bed nucleus of the stria terminalis. Biological Psychiatry 70:458–464.

Chrousos GP (2009) Stress and disorders of the stress system. Nat Rev Endocrinol 5:374–381.

Ciocchi S, Herry C, Grenier F, Wolff SBE, Letzkus JJ, Vlachos I, Ehrlich I, Sprengel R, Deisseroth K, Stadler MB, Müller C, Lüthi A (2010) Encoding of conditioned fear in central amygdala inhibitory circuits. Nature 468:277–282.

Davis M, Walker DL, Miles L, Grillon C (2010) Phasic vs Sustained Fear in Rats and Humans: Role of the Extended Amygdala in Fear vs Anxiety. Neuropsychopharmacology 35:105–135.

Davis M, Walker DL, MYERS KM (2003) Role of the Amygdala in Fear Extinction Measured with Potentiated Startle. Annals of the New York Academy of Sciences 985:218–232.

Daviu N, Bruchas MR, Moghaddam B, Sandi C, Beyeler A (2019) Neurobiological links between stress and anxiety. Neurobiology of Stress 11:100191.

De Quidt ME, Emson PC (1986a) Distribution of neuropeptide Y-like immunoreactivity in the rat central nervous system—II. Immunohistochemical analysis. Neuroscience 18:545–618.

De Quidt ME, Emson PC (1986b) Distribution of neuropeptide Y-like immunoreactivity in the rat central nervous system—I. Radioimmunoassay and chromatographic characterisation. Neuroscience 18:527–543.

Dilgen J, Tejeda HA, O'Donnell P (2013) Amygdala inputs drive feedforward inhibition in the medial prefrontal cortex. Journal of Neurophysiology 110:221–229.

Etkin A, Prater KE, Schatzberg AF, Menon V, Greicius MD (2009) Disrupted Amygdalar Subregion Functional Connectivity and Evidence of a Compensatory Network in Generalized Anxiety Disorder. Arch Gen Psychiatry 66:1361–1372.

Felix-Ortiz AC, Tye KM (2014) Amygdala Inputs to the Ventral Hippocampus Bidirectionally Modulate Social Behavior. Journal of Neuroscience 34:586–595.

File SE, Seth P (2003) A review of 25 years of the social interaction test. European Journal of Pharmacology 463:35–53.

Garcia R, Vouimba R-M, Baudry M, Thompson RF (1999) The amygdala modulates prefrontal cortex activity relative to conditioned fear. Nature 402:294–296.

Garrett JE, Wellman CL (2009) Chronic stress effects on dendritic morphology in medial prefrontal cortex: sex differences and estrogen dependence. Neuroscience 162:195–207.

Giesbrecht CJ, Mackay JP, Silveira HB, Urban JH, Colmers WF (2010) Countervailing modulation of Ih by neuropeptide Y and corticotrophin-releasing factor in basolateral amygdala as a possible mechanism for their effects on stress-related behaviors. Journal of Neuroscience 30:16970–16982.

Govindarajan A, Rao BSS, Nair D, Trinh M, Mawjee N, Tonegawa S, Chattarji S (2006) Transgenic brain-derived neurotrophic factor expression causes both anxiogenic and antidepressant effects. Proceedings of the National Academy of Sciences 103:13208–13213.

Grupe DW, Nitschke JB (2013) Uncertainty and anticipation in anxiety: an integrated neurobiological and psychological perspective. Nat Rev Neurosci 14:488–501.

Gutman AR, Yang Y, Ressler KJ, Davis M (2008) The role of neuropeptide Y in the expression and extinction of fear-potentiated startle. Journal of Neuroscience 28:12682–12690.

Hamilton TJ, Xapelli S, Michaelson SD, Larkum ME, Colmers WF (2013) Modulation of distal calcium electrogenesis by neuropeptide Y_1 receptors inhibits neocortical long-term depression. Journal of Neuroscience 33:11184–11193.

Haubensak W, Kunwar PS, Cai H, Ciocchi S, Wall NR, Ponnusamy R, Biag J, Dong H-W, Deisseroth K, Callaway EM, Fanselow MS, Lüthi A, Anderson DJ (2010) Genetic dissection of an amygdala microcircuit that gates conditioned fear. Nature 468:270–276.

Heilig M (1995) Antisense inhibition of neuropeptide Y (NPY)-Y1 receptor expression blocks the anxiolytic-like action of NPY in amygdala and paradoxically increases feeding. Regulatory Peptides 59:201–205.

Heilig M, McLeod S, Brot M, Heinrichs SC, Menzaghi F, Koob GF, Britton KT (1993) Anxiolytic-like action of neuropeptide Y: mediation by Y1 receptors in amygdala, and dissociation from food intake effects. Neuropsychopharmacology 8:357–363.

Heilig M, Söderpalm B, Engel JA, Psychopharmacology EW, (1989) Centrally administered neuropeptide Y (NPY) produces anxiolytic-like effects in animal anxiety models. Springer

.

Heilig M, Zachrisson O, Thorsell A, Ehnvall A, Mottagui-Tabar S, Sjögren M, Åsberg M, Ekman R, Wahlestedt C, Ågren H (2004) Decreased cerebrospinal fluid neuropeptide Y (NPY) in patients with treatment refractory unipolar major depression: preliminary evidence for association with preproNPY gene polymorphism. Journal of Psychiatric Research 38:113–121.

Herry C, Ciocchi S, Senn V, Demmou L, Müller C, Lüthi A (2008) Switching on and off fear by distinct neuronal circuits. Nature 454:600–606.

Holliday ND, Lam C-W, Tough IR, Cox HM (2005) Role of the C terminus in neuropeptide Y Y1 receptor desensitization and internalization. Molecular Pharmacology 67:655–664.

Hoover WB, Vertes RP (2007) Anatomical analysis of afferent projections to the medial prefrontal cortex in the rat. Brain Struct Funct 212:149–179.

Irle E, Ruhleder M, Lange C, Seidler-Brandler U, Salzer S, Dechent P, Weniger G, Leibing E, Leichsenring F (2010) Reduced amygdalar and hippocampal size in adults with generalized social phobia. J Psychiatry Neurosci 35:126–131.

Janak PH, Tye KM (2015) From circuits to behaviour in the amygdala. Nature 517:284–292.

Jarvis ED et al. (2005) Avian brains and a new understanding of vertebrate brain evolution. Nat Rev Neurosci 6:151–159.

Jimenez-Vasquez PA, Mathé AA, Thomas JD, Riley EP, Ehlers CL (2001) Early maternal separation alters neuropeptide Y concentrations in selected brain regions in adult rats. Developmental Brain Research 131:149–152.

Johansen JP, Diaz-Mataix L, Hamanaka H, Ozawa T, Ycu E, Koivumaa J, Kumar A, Hou M, Deisseroth K, Boyden ES, LeDoux JE (2014) Hebbian and neuromodulatory mechanisms interact to trigger associative memory formation. Proceedings of the National Academy of Sciences 111:E5584–E5592.

Johansen JP, Hamanaka H, Monfils MH, Behnia R, Deisseroth K, Blair HT, LeDoux JE (2010) Optical activation of lateral amygdala pyramidal cells instructs associative fear learning. Proceedings of the National Academy of Sciences 107:12692–12697.

Johnston JB (1923) Further contributions to the study of the evolution of the forebrain. Journal of Comparative Neurology.

Kim M, Campeau S, Falls WA, Davis M (1993) Infusion of the non-NMDA receptor antagonist CNQX into the amygdala blocks the expression of fear-potentiated startle. Behavioral and Neural Biology 59:5–8.

Kim S-Y, Adhikari A, Lee SY, Marshel JH, Kim CK, Mallory CS, Lo M, Pak S, Mattis J, Lim BK, Malenka RC, Warden MR, Neve R, Tye KM, Deisseroth K (2013a) Diverging neural pathways assemble a behavioural state from separable features in anxiety. Nature 496:219–223.

Kim S-Y, Adhikari A, Lee SY, Marshel JH, Kim CK, Mallory CS, Lo M, Pak S, Mattis J, Lim BK, Malenka RC, Warden MR, Neve R, Tye KM, Deisseroth K (2013b) Diverging neural pathways assemble a behavioural state from separable features in anxiety. Nature 496:219–223.

Kwon J-T, Nakajima R, Kim H-S, Jeong Y, Augustine GJ, Han J-H (2014) Optogenetic activation of presynaptic inputs in lateral amygdala forms associative fear memory. Learning & Memory 21:627–633.

LaBar KS, Gatenby JC, Gore JC, LeDoux JE, Phelps EA (1998) Human amygdala activation during conditioned fear acquisition and extinction: a mixed-trial fMRI study. Neuron 20:937–945.

Lakshminarasimhan H, Chattarji S (2012) Stress Leads to Contrasting Effects on the Levels of Brain Derived Neurotrophic Factor in the Hippocampus and.

Lanuza E, Belekhova M, Martínez-Marcos A, Font C, Martínez-García F (1998) Identification of the reptilian basolateral amygdala: an anatomical investigation of the afferents to the

posterior dorsal ventricular ridge of the lizard Podarcis hispanica. Eur J Neurosci 10:3517–3534.

LeDoux JE (2000) Emotion circuits in the brain. Annu Rev Neurosci 23:155–184.

LeDoux JE, Cicchetti P, Xagoraris A, Romanski LM (1990) The lateral amygdaloid nucleus: sensory interface of the amygdala in fear conditioning. J Neurosci 10:1062–1069.

Lee Y, Fitz S, Johnson PL, Shekhar A (2008) Repeated Stimulation of CRF Receptors in the BNST of Rats Selectively Induces Social but not Panic-Like Anxiety. Neuropsychopharmacology 33:2586–2594.

Leitermann RJ, Rostkowski AB, Urban JH (2016) Neuropeptide Y input to the rat basolateral amygdala complex and modulation by conditioned fear. Journal of Comparative Neurology 524:2418–2439.

Leitermann RJ, Sajdyk TJ, Urban JH (2012) Cell-specific expression of calcineurin immunoreactivity within the rat basolateral amygdala complex and colocalization with the neuropeptide Y Y1 receptor. Journal of Chemical Neuroanatomy 45:50–56.

Leuner B, Shors TJ (2013) Axiety, and dendritic spoines: what are the connections? Neuroscience 251:108–119.

Li F, Jia C-H, Huang J, Bi G-Q, Lau P-M (2020) High frequency optogenetic activation of inputs to the lateral amygdala forms distant association with foot-shock. Mol Brain 13:44.

Li H, Penzo MA, Taniguchi H, Kopec CD, Huang ZJ, Li B (2013) Experience-dependent modification of a central amygdala fear circuit. Nat Neurosci 16:332–339.

Li XF, Armony JL, LeDoux JE (1996) GABAA and GABAB receptors differentially regulate synaptic transmission in the auditory thalamo-amygdala pathway: An in vivo microiontophoretic study and a model. Synapse 24:115–124.

Lin C-H, Lee C-C, Gean P-W (2003a) Involvement of a Calcineurin Cascade in Amygdala Depotentiation and Quenching of Fear Memory. Molecular Pharmacology 63:44–52.

Lin C-H, Yeh S-H, Leu T-H, Chang W-C, Wang S-T, Gean P-W (2003b) Identification of Calcineurin as a Key Signal in the Extinction of Fear Memory. J Neurosci 23:1574–1579.

Little JP, Carter AG (2013) Synaptic mechanisms underlying strong reciprocal connectivity between the medial prefrontal cortex and basolateral amygdala. Journal of Neuroscience 33:15333–15342.

Machado-de-Sousa JP, de Lima Osório F, Jackowski AP, Bressan RA, Chagas MHN, Torro-Alves N, DePaula ALD, Crippa JAS, Hallak JEC (2014) Increased Amygdalar and Hippocampal Volumes in Young Adults with Social Anxiety Chen H, ed. PLoS ONE 9:e88523.

Mackay JP (2016) Mechanisms of NPY Y2 Receptor-Mediated Anxiogenesis in the Basolateral Amygdala.

Mackay JP, Bompolaki M, DeJoseph MR, Michaelson SD, Urban JH, Colmers WF (2019) NPY2 Receptors Reduce Tonic Action Potential-Independent GABAB Currents in the Basolateral Amygdala. Journal of Neuroscience 39:4909–4930.

Maren S, Holmes A (2015) Stress and Fear Extinction. Neuropsychopharmacology.

Maren S, Quirk GJ (2004) Neuronal signalling of fear memory. Nat Rev Neurosci 5:844–852.

Mascagni F, McDonald AJ (2003) Immunohistochemical characterization of cholecystokinin containing neurons in the rat basolateral amygdala. Brain Research 976:171–184.

Mathé AA, Rudorfer MV, Stenfors C, Manji HK, Potter WZ, Theodorsson E (1995) Effects of electroconvulsive treatment on somatostatin, neuropeptide Y, endothelin, and neurokinin a concentrations in cerebrospinal fluid of depressed patients: A pilot study. Depression 3:250–256.

McDonald AJ (1982) Neurons of the lateral and basolateral amygdaloid nuclei: a Golgi study in the rat. J Comp Neurol 212:293–312.

McDonald AJ (1984) Neuronal organization of the lateral and basolateral amygdaloid nuclei in the rat. Journal of Comparative Neurology 222:589–606.

McDonald AJ (1985) Immunohistochemical identification of gamma-aminobutyric acid-containing neurons in the rat basolateral amygdala. Neuroscience Letters 53:203–207.

McDonald AJ (1989) Coexistence of somatostatin with neuropeptide Y, but not with cholecystokinin or vasoactive intestinal peptide, in neurons of the rat amygdala. Brain Research 500:37–45.

McDonald AJ (1996) Glutamate and aspartate immunoreactive neurons of the rat basolateral amygdala: colocalization of excitatory amino acids and projections to the limbic circuit. J Comp Neurol 365:367–379.

McDonald AJ, Mascagni F (2001) Colocalization of calcium-binding proteins and GABA in neurons of the rat basolateral amygdala. NSC 105:681–693.

McDonald AJ, Muller JF, Mascagni F (2002) GABAergic innervation of alpha type II calcium/calmodulin-dependent protein kinase immunoreactive pyramidal neurons in the rat basolateral amygdala. J Comp Neurol 446:199–218.

McDonald AJ, Pearson JC (1989) Coexistence of GABA and peptide immunoreactivity in non-pyramidal neurons of the basolateral amygdala. Neuroscience Letters 100:53–58.

McEwen BS, Eiland L, Hunter RG, Miller MM (2012) Neuropharmacology. Neuropharmacology 62:3–12.

McEwen BS, Gianaros PJ (2011) Stress- and Allostasis-Induced Brain Plasticity. Annu Rev Med 62:431–445.

McQuiston AR, Petrozzino JJ, Connor JA, Colmers WF (1996) Neuropeptide Y1 receptors inhibit N-type calcium currents and reduce transient calcium increases in rat dentate granule cells. J Neurosci 16:1422–1429.

Michaelson SD (2016) Organotypic Basolateral Amygdala Slice Cultures: A Model for Stress-related Circuitry. University of Alberta.

Michaelson SD, Miranda Tapia AP, McKinty A, Silveira Villarroel H, Mackay JP, Urban JH, Colmers WF (2020) Contribution of NPY Y5 Receptors to the Reversible Structural Remodeling of Basolateral Amygdala Dendrites in Male Rats Associated with NPY-Mediated Stress Resilience. Journal of Neuroscience 40:3231–3249.

Miserendino MJ, Sananes CB, Melia KR, Davis M (1990) Blocking of acquisition but not expression of conditioned fear-potentiated startle by NMDA antagonists in the amygdala. Nature 345:716–718.

Mitra R, Ferguson D, Sapolsky RM (2009) SK2 potassium channel overexpression in basolateral amygdala reduces anxiety, stress-induced corticosterone secretion and dendritic arborization. Molecular Psychiatry 14:847–855.

Mitra R, Jadhav S, McEwen BS, Vyas A, Chattarji S (2005) Stress duration modulates the spatiotemporal patterns of spine formation in the basolateral amygdala. Proceedings of the National Academy of Sciences 102:9371–9376.

Morgan CA III, Rasmusson AM, Wang S, Hoyt G, Hauger RL, Hazlett G (2002) Neuropeptide-Y, cortisol, and subjective distress in humans exposed to acute stress: replication and extension of previous report. Biological Psychiatry 52:136–142.

Morgan CA III, Wang S, Rasmusson A, Hazlett G, Anderson G, Charney DS (2001) Relationship Among Plasma Cortisol, Catecholamines, Neuropeptide Y, and Human Performance During Exposure to Uncontrollable Stress. Psychosomatic Medicine 63:412–422.

Morgan CA III, Wang S, Southwick SM, Rasmusson A (2000) Plasma neuropeptide-Y in humans exposed to acute uncontrollable stress. Biological Psychiatry.

MYERS KM, Davis M (2002) Behavioral and Neural Analysis of Extinction. Neuron 36:567–584.

Nabavi S, Fox R, Proulx CD, Lin JY, Tsien RY, Malinow R (2014) Engineering a memory with LTD and LTP. Nature 511:348–352.

Nader K, Majidishad P, Amorapanth P, LeDoux JE (2001) Damage to the lateral and central, but not other, amygdaloid nuclei prevents the acquisition of auditory fear conditioning. Learning & Memory 8:156–163.

Nakajima M, Inui A, Asakawa A, Momose K, Ueno N, Teranishi A, Baba S, Kasuga M (1998) Neuropeptide Y produces anxiety via Y2-type receptors. Peptides 19:359–363.

Namburi P, Beyeler A, Yorozu S, Calhoon GG, Halbert SA, Wichmann R, Holden SS, Mertens KL, Anahtar M, Felix-Ortiz AC, Wickersham IR, Gray JM, Tye KM (2015) A circuit mechanism for differentiating positive and negative associations. Nature 520:675–678.

Nesse RM (1990) Evolutionary explanations of emotions. Human nature.

Nesse RM (1994) Fear and fitness: An evolutionary analysis of anxiety disorders. Ethology and sociobiology 15:247–261.

Nieh EH, Kim S-Y, Namburi P, Tye KM (2013) Optogenetic dissection of neural circuits underlying emotional valence and motivated behaviors. Brain Research 1511:73–92.

Nikisch G, Ågren H, Eap CB, Czernik A, Baumann P, Mathé AA (2005) Neuropeptide Y and corticotropin-releasing hormone in CSF mark response to antidepressive treatment with citalopram. Int J Neuropsychopharmacol 8:403–410.

Padival M, Quinette D, Rosenkranz JA (2013) Effects of Repeated Stress on Excitatory Drive of Basal Amygdala Neurons In Vivo. Neuropsychopharmacology 38:1748–1762.

Patel D, Anilkumar S, Chattarji S, Buwalda B (2018) Repeated social stress leads to contrasting patterns of structural plasticity in the amygdala and hippocampus. Behavioural Brain Research 347:314–324.

Polepalli JS, Gooch H, Sah P (2020) Diversity of interneurons in the lateral and basal amygdala. NPJ Sci Learn 5:10–19.

Quirk GJ, Armony JL, LeDoux JE (1997) Fear Conditioning Enhances Different Temporal Components of Tone-Evoked Spike Trains in Auditory Cortex and Lateral Amygdala. Neuron 19:613–624.

Rainnie DG, Bergeron R, Sajdyk TJ, Patil M, Gehlert DR, Shekhar A (2004) Corticotrophin releasing factor-induced synaptic plasticity in the amygdala translates stress into emotional disorders. Journal of Neuroscience 24:3471–3479.

Rainnie DG, of EAJ, 1993 (1993) Intracellular recordings from morphologically identified neurons of the basolateral amygdala. Journal of Neurophys. 69:1350–1362.

Rasmusson AM, Hauger RL, Morgan III CA, Bremner JD, Charney DS, Southwick SM (2000) Low baseline and yohimbine-stimulated plasma neuropeptide Y (NPY) levels in combat-related PTSD. BPS 47:526–539.

Robinson RB, Siegelbaum SA (2003) Hyperpolarization-activated cation currents: from molecules to physiological function. Annu Rev Physiol 65:453–480.

Rogan MT, Stäubli UV, LeDoux JE (1997) Fear conditioning induces associative long-term potentiation in the amygdala. Nature 390:604–607.

Roozendaal B, McEwen BS, Chattarji S (2009) Stress, memory and the amygdala. Nat Rev Neurosci 10:423–433.

Rose M, Devine J (2014) Assessment of patient-reported symptoms of anxiety. Dialogues Clin Neurosci 16:197–211.

Rosenkranz JA, Grace AA (1999) Modulation of basolateral amygdala neuronal firing and afferent drive by dopamine receptor activation in vivo. Journal of Neuroscience 19:11027–11039.

Rosenkranz JA, Venheim ER, Padival M (2010) Chronic Stress Causes Amygdala Hyperexcitability in Rodents. Biological Psychiatry 67:1128–1136.

Rostkowski AB, Leitermann RJ, Urban JH (2013) Differential activation of neuronal cell types in the basolateral amygdala by corticotropin releasing factor. Neuropeptides 47:273–280.

Rostkowski AB, Teppen TL, Peterson DA, Urban JH (2009) Cell-specific expression of neuropeptide Y Y1 receptor immunoreactivity in the rat basolateral amygdala. J Comp Neurol 517:166–176.

Rovira-Esteban L, Gunduz-Cinar O, Bukalo O, Limoges A, Brockway E, Müller K, Fenno L, Kim YS, Ramakrishnan C, Andrási T, Deisseroth K, Holmes A, Hájos N (2019) Excitation of Diverse Classes of Cholecystokinin Interneurons in the Basal Amygdala Facilitates Fear Extinction. eNeuro 6:ENEURO.0220–19.2019.

Ryan SJ, Ehrlich DE, Rainnie DG (2016) Morphology and dendritic maturation of developing principal neurons in the rat basolateral amygdala. Brain Struct Funct 221:839–854.

Sah P, Faber ESL, Lopez De Armentia M, Power J (2003) The amygdaloid complex: anatomy and physiology. Physiological Reviews 83:803–834.

Sah R, Ekhator NN, Strawn JR, Sallee FR, Baker DG, Horn PS, Geracioti TD Jr. (2009) Low Cerebrospinal Fluid Neuropeptide Y Concentrations in Posttraumatic Stress Disorder. Biological Psychiatry 66:705–707.

Sajdyk T, Johnson P, Fitz S, Shekhar A (2008a) Chronic inhibition of GABA synthesis in the bed nucleus of the stria terminalis elicits anxiety-like behavior. Journal of Psychopharmacology 22:633–641.

Sajdyk TJ, Fitz SD, Shekhar A (2006) The role of neuropeptide Y in the amygdala on corticotropin-releasing factor receptor-mediated behavioral stress responses in the rat. Stress 9:21–28.

Sajdyk TJ, Johnson PL, Leitermann RJ, Fitz SD, Dietrich A, Morin M, Gehlert DR, Urban JH, Shekhar A (2008b) Neuropeptide Y in the amygdala induces long-term resilience to stress-induced reductions in social responses but not hypothalamic-adrenal-pituitary axis activity or hyperthermia. Journal of Neuroscience 28:893–903.

Sajdyk TJ, Schober DA, Gehlert DR (2002a) Neuropeptide Y receptor subtypes in the basolateral nucleus of the amygdala modulate anxiogenic responses in rats. Neuropharmacology 43:1165–1172.

Sajdyk TJ, Schober DA, Smiley DL, Gehlert DR (2002b) Neuropeptide Y-Y2 receptors mediate anxiety in the amygdala. Pharmacology, Biochemistry and Behavior 71:419–423.

Sajdyk TJ, Vandergriff MG, Gehlert DR (1999) Amygdalar neuropeptide Y Y1 receptors mediate the anxiolytic-like actions of neuropeptide Y in the social interaction test. European Journal of Pharmacology 368:143–147.

Sanders SK, Shekhar A (1995) Regulation of anxiety by GABAA receptors in the rat amygdala. Pharmacology, Biochemistry and Behavior 52:701–706.

Selye H (1936) A Syndrome produced by Diverse Nocuous Agents. Nature 138:32–32.

Senn V, Wolff SBE, Herry C, Grenier F, Ehrlich I, Gründemann J, Fadok JP, Müller C, Letzkus JJ, Lüthi A (2014) Long-range connectivity defines behavioral specificity of amygdala neurons. Neuron 81:428–437.

Sergeyev V, Fetissov S, Mathé AA, Jimenez PA, Bartfai T, Mortas P, Gaudet L, Moreau J-L, Hökfelt T (2005) Neuropeptide expression in rats exposed to chronic mild stresses. Psychopharmacology 178:115–124.

Shaban H, Humeau Y, Herry C, Cassasus G, Shigemoto R, Ciocchi S, Barbieri S, van der Putten H, Kaupmann K, Bettler B, Lüthi A (2006) Generalization of amygdala LTP and conditioned fear in the absence of presynaptic inhibition. Nat Neurosci 9:1028–1035.

Shekhar A, Sajdyk TJ, Gehlert DR, Rainnie DG (2003) The Amygdala, Panic Disorder, and Cardiovascular Responses. Annals of the New York Academy of Sciences 985:308–325.

SHOLL DA (1953) Dendritic organization in the neurons of the visual and motor cortices of the cat. J Anat 87:387–406.

Silveira Villarroel H, Bompolaki M, Mackay JP, Miranda Tapia AP, Michaelson SD, Leitermann RJ, Marr RA, Urban JH, Colmers WF (2018) NPY Induces Stress Resilience via Downregulation of Ih in Principal Neurons of Rat Basolateral Amygdala. Journal of Neuroscience 38:4505–4520.

Sotres-Bayon F, Sierra-Mercado D, Pardilla-Delgado E, Quirk GJ (2012a) Gating of fear in prelimbic cortex by hippocampal and amygdala inputs. Neuron 76:804–812.

Sotres-Bayon F, Sierra-Mercado D, Pardilla-Delgado E, Quirk GJ (2012b) Gating of fear in prelimbic cortex by hippocampal and amygdala inputs. Neuron 76:804–812.

Spampanato J, Polepalli J, Sah P (2011) Interneurons in the basolateral amygdala. Neuropharmacology 60:765–773.

Stoppini L, Buchs PA, Muller D (1991) A simple method for organotypic cultures of nervous tissue. Journal of Neuroscience Methods 37:173–182.

Sun N, Cassell MD (1993) Intrinsic GABAergic neurons in the rat central extended amygdala. Journal of Comparative Neurology 330:381–404.

Swanson LW, Petrovich GD (1998) What is the amygdala? Trends in Neurosciences 21:323–331.

Tatemoto K, Carlquist M, Mutt V (1982) Neuropeptide Y—a novel brain peptide with structural similarities to peptide YY and pancreatic polypeptide. Nature.

Tazumi T, Okaichi H (2002) Effect of lesions in the lateral nucleus of the amygdala on fear conditioning using auditory and visual conditioned stimuli in rats. Neurosci Res 43:163–170.

Thorsell A, Michalkiewicz M, Dumont Y, Quirion R, Caberlotto L, Rimondini R, Mathé AA, Heilig M (2000) Behavioral insensitivity to restraint stress, absent fear suppression of behavior and impaired spatial learning in transgenic rats with hippocampal neuropeptide Y overexpression. Proceedings of the National Academy of Sciences 97:12852–12857.

Thorsell A, Svensson P, Wiklund L, Sommer W, Ekman R, Heilig M (1998) Suppressed neuropeptide Y (NPY) mRNA in rat amygdala following restraint stress. Regulatory Peptides 75-76:247–254.

Tipps M, Marron Fernandez de Velasco E, Schaeffer A, Wickman K (2018) Inhibition of Pyramidal Neurons in the Basal Amygdala Promotes Fear Learning. eNeuro 5:ENEURO.0272–18.2018.

Tovote P, Fadok JP, Lüthi A (2015) Neuronal circuits for fear and anxiety. Nat Rev Neurosci 16:317–331.

Tye KM, Prakash R, Kim S-Y, Fenno LE, Grosenick L, Zarabi H, Thompson KR, Gradinaru V, Ramakrishnan C, Deisseroth K (2011) Amygdala circuitry mediating reversible and bidirectional control of anxiety. Nature 471:358–362.

Uliana DL, Gomes FV, Grace AA (2020) Stress impacts corticoamygdalar connectivity in an age-dependent manner. Neuropsychopharmacology:1–11.

Urban KR, Valentino RJ (2016) Age- and Sex-Dependent Impact of Repeated Social Stress on Intrinsic and Synaptic Excitability of the Rat Prefrontal Cortex. Cerebral Cortex 15:96.

van den Pol AN (2012) Neuropeptide Transmission in Brain Circuits. Neuron 76:98–115.

Vyas A, Bernal S, Chattarji S (2003) Effects of chronic stress on dendritic arborization in the central and extended amygdala. Brain Research 965:290–294.

Vyas A, Jadhav S, Chattarji S (2006) Prolonged behavioral stress enhances synaptic connectivity in the basolateral amygdala. NSC 143:387–393.

Vyas A, Mitra R, Shankaranarayana Rao BS, Chattarji S (2002) Chronic stress induces contrasting patterns of dendritic remodeling in hippocampal and amygdaloid neurons. Journal of Neuroscience 22:6810–6818.

Walker DL, Davis M (1997) Double Dissociation between the Involvement of the Bed Nucleus of the Stria Terminalis and the Central Nucleus of the Amygdala in Startle Increases Produced by Conditioned versus Unconditioned Fear. J Neurosci 17:9375–9383.

Walker DL, Davis M (2008) Role of the extended amygdala in short-duration versus sustained fear: a tribute to Dr. Lennart Heimer. Brain Struct Funct 213:29–42.

Walker DL, Miles LA, Davis M (2009) Progress in Neuro-Psychopharmacology & BiologicalPsychiatry. Progress in Neuropsychopharmacology & Biological Psychiatry 33:1291–1308.

Washburn MS, Moises HC (1992) Electrophysiological and morphological properties of rat basolateral amygdaloid neurons in vitro. J Neurosci 12:4066–4079.

Weiskrantz L (1956) Behavioral changes associated with ablation of the amygdaloid complex in monkeys. J Comp Physiol Psychol 49:381–391.

Widerlöv E, Lindström LH, Wahlestedt C, Ekman R (1988) Neuropeptide Y and peptide YY as possible cerebrospinal fluid markers for major depression and schizophrenia, respectively. Journal of Psychiatric Research 22:69–79.

Wolff SBE, Gründemann J, Tovote P, Krabbe S, Jacobson GA, Müller C, Herry C, Ehrlich I, Friedrich RW, Letzkus JJ, Lüthi A (2014) Amygdala interneuron subtypes control fear learning through disinhibition. Nature 509:453–458.

Yehuda R, Brand S, Yang R-K (2006) Plasma neuropeptide Y concentrations in combat exposed veterans: relationship to trauma exposure, recovery from PTSD, and coping. Biological Psychiatry 59:660–663.

Zhou Z et al. (2008) Genetic variation in human NPY expression affects stress response and emotion. Nature 452:997–1001.

III. List of references

Abbott SBG, Stornetta RL, Coates MB, Guyenet PG (2011) Phox2b-expressing neurons of the parafacial region regulate breathing rate, inspiration, and expiration in conscious rats. Journal of Neuroscience 31:16410–16422.

Abbracchio MP, Burnstock G, Boeynaems J-M, Barnard EA, Boyer JL, Kennedy C, Knight GE, Fumagalli M, Gachet C, Jacobson KA, Weisman GA (2006) International Union of Pharmacology LVIII: Update on the P2Y G Protein-Coupled Nucleotide Receptors: From Molecular Mechanisms and Pathophysiology to Therapy. Pharmacol Rev 58:281–341.

Abbracchio MP, Burnstock G, Verkhratsky A, Zimmermann H (2009) Purinergic signalling in the nervous system: an overview. Trends in Neurosciences 32:19–29.

Abdel-Hady H (2015) Caffeine therapy in preterm infants. WJCP 4:81.

Adamec R, Hebert M, Blundell J, Mervis RF (2012) Dendritic morphology of amygdala and hippocampal neurons in more and less predator stress responsive rats and more and less spontaneously anxious handled controls. Behavioural Brain Research 226:133–146.

Adrian TE, Allen JM, Bloom SR, Ghatei MA, Rossor MN, Roberts GW, Crwo TJ, Tatemoto K, Polak JM (1983) Neuropeptide Y distribution in human brain. 306:584–586.

Adolphs R, Tranel D, Damasio H, Damasio A (1994) Impaired recognition of emotion in facial expressions following bilateral damage to the human amygdala. Nature 372:669–672.

Amadio S, Vacca F, Martorana A, Sancesario G, Volonté C (2007) P2Y1 receptor switches to neurons from glia in juvenile versus neonatal rat cerebellar cortex. BMC Dev Biol 7:1–17.

Amano T, Duvarci S, Popa D, Pare D (2011) The Fear Circuit Revisited: Contributions of the Basal Amygdala Nuclei to Conditioned Fear. J Neurosci 31:15481–15489.

Amano T, Unal CT, Pare D (2010) Synaptic correlates of fear extinction in the amygdala. Nat Neurosci 13:489–494.

Anderson TM, Garcia AJ, Baertsch NA, Pollak J, Bloom JC, Wei AD, Rai KG, Ramirez J-M (2016) A novel excitatory network for the control of breathing. Nature 536:76–80.

Anderson TM, Ramirez J-M (2017) Respiratory rhythm generation: triple oscillator hypothesis. F1000Res 6:139.

Angelova PR, Kasymov V, Christie I, SheikhBahaei S, Turovsky E, Marina N, Korsak A, Zwicker J, Teschemacher AG, Ackland GL, Funk GD, Kasparov S, Abramov AY, Gourine AV (2015) Functional Oxygen Sensitivity of Astrocytes. J Neurosci 35:10460–10473.

Aoki Y, Yamada E, Endoh T, Suzuki T (2004) Multiple actions of extracellular ATP and adenosine on calcium currents mediated by various purinoceptors in neurons of nucleus tractus solitarius. Neurosci Res 50:245–255.

Aranda JV, Turmen T, Davis J, Trippenbach T, Grondin D, Zinman R, Watters G (1983) Effect of caffeine on control of breathing in infantile apnea. The Journal of Pediatrics 103:975–978.

Baertsch NA, Baertsch HC, Ramirez J-M (2018) The interdependence of excitation and inhibition for the control of dynamic breathing rhythms. Nat Commun 9:843–17.

Baertsch NA, Ramirez J-M (2019) Insights into the dynamic control of breathing revealed through cell-type-specific responses to substance P. Elife 8:76.

Bansal V, Fisher TE (2017) Osmotic activation of a Ca2+-dependent phospholipase C pathway that regulates ΔN TRPV1-mediated currents in rat supraoptic neurons. Physiol Rep 5:8 e13259.

Bayliss DA, Barhanin J, Gestreau C, Guyenet PG (2015) The role of pH-sensitive TASK channels in central respiratory chemoreception. Pflugers Arch 467:917–929.

Benemei S, Patacchini R, Trevisani M, Geppetti P (2015) TRP channels. Curr Opin Pharmacol 22:18–23.

Berglund MM, Schober DA, Statnick MA, McDonald PH, Gehlert DR (2003) The Use of Bioluminescence Resonance Energy Transfer 2 to Study Neuropeptide Y Receptor Agonist-Induced β-Arrestin 2 Interaction. J Pharmacol Exp Ther 306:147–156.

Berridge MJ, Bootman MD, Roderick HL (2003) Calcium: Calcium signalling: dynamics, homeostasis and remodelling. Nat Rev Mol Cell Biol 4:517–529.

Biancardi V, Saini J, Pageni A, Prashaad M H, Funk GD, Pagliardini S (2020) Mapping of the excitatory, inhibitory, and modulatory afferent projections to the anatomically defined active expiratory oscillator in adult male rats. Journal of Comparative Neurology 29:5806.

Bilmen JG, Wootton LL, Michelangeli F (2002) The mechanism of inhibition of the sarco/endoplasmic reticulum Ca2+ ATPase by paxilline. Arch Biochem Biophys 406:55–64.

Bissière S, Humeau Y, Lüthi A (2003) Dopamine gates LTP induction in lateral amygdala by suppressing feedforward inhibition. Nat Neurosci 6:587–592.

Bissonnette JM, Hohimer RA, Chao CR, Knopp SJ, Notoroberto NF (1990) Theophylline Stimulates Fetal Breathing Movements during Hypoxia. Pediatr Res 28:83–86.

Blair HT, Schafe GE, Bauer EP, Rodrigues SM, LeDoux JE (2001) Synaptic plasticity in the lateral amygdala: a cellular hypothesis of fear conditioning. Learning & Memory 8:229–242.

Blanchard DC, Blanchard RJ (1972) Innate and conditioned reactions to threat in rats with amygdaloid lesions. J Comp Physiol Psychol 81:281–290.

Bloodgood BL, Sabatini BL (2007) Nonlinear regulation of unitary synaptic signals by CaV(2.3) voltage-sensitive calcium channels located in dendritic spines. Neuron 53:249–260.

Blomqvist AG, Söderberg C, Lundell I (1992) Strong evolutionary conservation of neuropeptide Y: sequences of chicken, goldfish, and Torpedo marmorata DNA clones.

Blume SR, Padival M, Urban JH, Rosenkranz JA (2019) Disruptive effects of repeated stress on basolateral amygdala neurons and fear behavior across the estrous cycle in rats. Sci Rep 9:12292.

Bochorishvili G, Stornetta RL, Coates MB, Guyenet PG (2012) Pre-Bötzinger complex receives glutamatergic innervation from galaninergic and other retrotrapezoid nucleus neurons. Journal of Comparative Neurology 520:1047–1061.

Boehme S, Ritter V, Tefikow S, Stangier U, Strauss B, Miltner WHR, Straube T (2014) Brain activation during anticipatory anxiety in social anxiety disorder. Soc Cogn Affect Neurosci 9:1413–1418.

Bolser DC, Davenport PW (2002) Functional organization of the central cough generation mechanism. Pulm Pharmacol Ther 15:221–225.

Borvendeg SJ, Gerevich Z, Gillen C, Illes P (2003) P2Y receptor-mediated inhibition of voltage-dependent Ca2+ channels in rat dorsal root ganglion neurons. Synapse 47:159–161.

Bouvier J, Thoby-Brisson M, Renier N, Dubreuil V, Ericson J, Champagnat J, Pierani A, Chédotal A, Fortin G (2010) Hindbrain interneurons and axon guidance signaling critical for breathing. Nat Neurosci 13:1066–1074.

Brockhaus J, Ballanyi K (2001) Synaptic inhibition in the isolated respiratory network of neonatal rats. Eur J Neurosci 10:3823–3839.

Brown DA, Filippov AK, Barnard EA (2000) Inhibition of potassium and calcium currents in neurones by molecularly-defined P2Y receptors. J Auton Nerv Syst 81:31–36.

Brown TG (1914) On the nature of the fundamental activity of the nervous centres; together with an analysis of the conditioning of rhythmic activity in progression, and a theory of the evolution of function in the nervous system. The Journal of Physiology 48:18–46.

Burgos-Robles A, Vidal-Gonzalez I, Quirk GJ (2009) Sustained conditioned responses in prelimbic prefrontal neurons are correlated with fear expression and extinction failure. Journal of Neuroscience 29:8474–8482.

Burnstock G (2018) Purine and purinergic receptors. Brain Neurosci Adv 2:1–10

Burr D, Sinclair JD (1988) The effect of adenosine on respiratory chemosenstivity in the awake rat. Respiration Physiology 72:47–57.

Butler RK, White LC, Frederick-Duus D, Kaigler KF, Fadel JR, Wilson MA (2012) Comparison of the activation of somatostatin- and neuropeptide Y-containing neuronal populations of the rat amygdala following two different anxiogenic stressors. Exp Neurol 238:52–63.

Büsselberg D, Bischoff AM, Richter DW (2003) A combined blockade of glycine and calcium-dependent potassium channels abolishes the respiratory rhythm. NSC 122:831–841.

Calhoon GG, Tye KM (2015) Resolving the neural circuits of anxiety. Nat Neurosci 18:1394–1404.

Chandaka GK, Salzer I, Drobny H, Boehm S, Schicker KW (2011) Facilitation of transmitter release from rat sympathetic neurons via presynaptic P2Y1 receptors. British Journal of Pharmacology 164:1522–1533.

Chee MJS, Myers MG, Price CJ, Colmers WF (2010) Neuropeptide Y Suppresses Anorexigenic Output from the Ventromedial Nucleus of the Hypothalamus. Journal of Neuroscience 30:3380–3390.

Chen X, Kovalchuk Y, Adelsberger H, Henning HA, Sausbier M, Wietzorrek G, Ruth P, Yarom Y, Konnerth A (2010) Disruption of the olivo-cerebellar circuit by Purkinje neuron-specific ablation of BK channels. Proceedings of the National Academy of Sciences 107:12323–12328.

Christianson JP, Jennings JH, Ragole T, Flyer JGN, Benison AM, Barth DS, Watkins LR, Maier SF (2011) Safety signals mitigate the consequences of uncontrollable stress via a circuit involving the sensory insular cortex and bed nucleus of the stria terminalis. Biological Psychiatry 70:458–464.

Chrousos GP (2009) Stress and disorders of the stress system. Nat Rev Endocrinol 5:374–381.

Ciocchi S, Herry C, Grenier F, Wolff SBE, Letzkus JJ, Vlachos I, Ehrlich I, Sprengel R, Deisseroth K, Stadler MB, Müller C, Lüthi A (2010) Encoding of conditioned fear in central amygdala inhibitory circuits. Nature 468:277–282.

Contet C, Goulding SP, Kuljis DA, Barth AL (2016) BK Channels in the Central Nervous System. Int Rev Neurobiol 128:281–342.

Coppi E, Pedata F, Gibb AJ (2012) P2Y 1receptor modulation of Ca 2+-activated K +currents in medium-sized neurons from neonatal rat striatal slices. Journal of Neurophysiology 107:1009–1021.

Cui Y, Kam K, Sherman D, Janczewski WA, Zheng Y, Feldman JL (2016) Defining preBötzinger Complex Rhythm- and Pattern-Generating Neural Microcircuits In Vivo. Neuron 91:602–614.

Davis M, Walker DL, Miles L, Grillon C (2010) Phasic vs Sustained Fear in Rats and Humans: Role of the Extended Amygdala in Fear vs Anxiety. Neuropsychopharmacology 35:105–135.

Davis M, Walker DL, MYERS KM (2003) Role of the Amygdala in Fear Extinction Measured with Potentiated Startle. Annals of the New York Academy of Sciences 985:218–232.

Daviu N, Bruchas MR, Moghaddam B, Sandi C, Beyeler A (2019) Neurobiological links between stress and anxiety. Neurobiology of Stress 11:100191.

De Quidt ME, Emson PC (1986a) Distribution of neuropeptide Y-like immunoreactivity in the rat central nervous system—II. Immunohistochemical analysis. Neuroscience 18:545–618.

De Quidt ME, Emson PC (1986b) Distribution of neuropeptide Y-like immunoreactivity in the rat central nervous system—I. Radioimmunoassay and chromatographic characterisation. Neuroscience 18:527–543.

Del Negro CA, Funk GD, Feldman JL (2018) Breathing matters. Nat Rev Neurosci 19:351–367.

Del Negro CA, Koshiya N, Robert J Butera J, Smith JC (2002) Persistent Sodium Current, Membrane Properties and Bursting Behavior of Pre-Bötzinger Complex Inspiratory Neurons In Vitro. Journal of Neurophysiology 88:2242–2250.

Del Negro CA, Morgado-Valle C, Hayes JA, Mackay DD, Pace RW, Crowder EA, Feldman JL (2005) Sodium and calcium current-mediated pacemaker neurons and respiratory rhythm generation. Journal of Neuroscience 25:446–453.

del Puerto A, Díaz-Hernández J-I, Tapia M, Gómez-Villafuertes R, Benitez MJ, Zhang J, Miras-Portugal MT, Wandosell F, Díaz-Hernández M, Garrido JJ (2012) Adenylate cyclase 5 coordinates the action of ADP, P2Y1, P2Y13 and ATP-gated P2X7 receptors on axonal elongation. J Cell Sci 125:176–188.

Deng P, Pang Z-P, Lei Z, Shikano S, Xiong Q, Harvey BK, London B, Wang Y, Li M, Xu ZC (2011) Up-Regulation of A-Type Potassium Currents Protects Neurons Against Cerebral Ischemia. J Cereb Blood Flow Metab 31:1823–1835.

DePuy SD, Kanbar R, Coates MB, Stornetta RL, Guyenet PG (2011) Control of Breathing by Raphe Obscurus Serotonergic Neurons in Mice. J Neurosci 31:1981–1990.

Dilgen J, Tejeda HA, O'Donnell P (2013) Amygdala inputs drive feedforward inhibition in the medial prefrontal cortex. Journal of Neurophysiology 110:221–229.

Doble A (1996) The pharmacology and mechanism of action of riluzole. Neurology 47:233S–241S.

Eldridge FL, Millhorn DE, Kiley JP (1984) Respiratory effects of a long-acting analog of adenosine. Brain Research 301:273–280.

Eldridge FL, Millhorn DE, Kiley JP (1985) Antagonism by theophylline of respiratory inhibition induced by adenosine. Journal of Applied Physiology 59:1428–1433.

Elnazir B, Marshall JM, Kumar P (1996) Postnatal development of the pattern of respiratory and cardiovascular response to systemic hypoxia in the piglet: the roles of adenosine. The Journal of Physiology 492:573–585.

Etkin A, Prater KE, Schatzberg AF, Menon V, Greicius MD (2009) Disrupted Amygdalar Subregion Functional Connectivity and Evidence of a Compensatory Network in Generalized Anxiety Disorder. Arch Gen Psychiatry 66:1361–1372.

Faber ESL, Delaney AJ, Sah P (2005) SK channels regulate excitatory synaptic transmission and plasticity in the lateral amygdala. Nat Neurosci 8:635–641.

Feldman JL, Del Negro CA (2006) Looking for inspiration: new perspectives on respiratory rhythm. Nat Rev Neurosci 7:232–241.

Feldman JL, Del Negro CA, Gray PA (2013) Understanding the Rhythm of Breathing: So Near, Yet So Far. http://dxdoiorgloginezproxylibraryualbertaca/101146/annurev-physiol-040510-130049 75:423–452.

Feldman JL, Smith JC (1989) Cellular mechanisms underlying modulation of breathing pattern in mammals. Annals of the New York Academy of Sciences 563:114–130.

Felix-Ortiz AC, Tye KM (2014) Amygdala Inputs to the Ventral Hippocampus Bidirectionally Modulate Social Behavior. Journal of Neuroscience 34:586–595.

Ferreira-Neto HC, Biancardi VC, Stern JE (2017) A reduction in SK channels contributes to increased activity of hypothalamic magnocellular neurons during heart failure. The Journal of Physiology 595:6429–6442.

File SE, Seth P (2003) A review of 25 years of the social interaction test. European Journal of Pharmacology 463:35–53.

Filippov AK, Brown DA, Barnard EA (2000) The P2Y1 receptor closes the N-type Ca2+ channel in neurones, with both adenosine triphosphates and diphosphates as potent agonists. British Journal of Pharmacology 129:1063–1066.

Filippov AK, Choi RCY, Simon J, Barnard EA, Brown DA (2006) Activation of P2Y1 nucleotide receptors induces inhibition of the M-type K+ current in rat hippocampal pyramidal neurons. Journal of Neuroscience 26:9340–9348.

Filippov AK, Fernández-Fernández JM, Marsh SJ, Simon J, Barnard EA, Brown DA (2004) Activation and inhibition of neuronal G protein-gated inwardly rectifying K(+) channels by P2Y nucleotide receptors. Molecular Pharmacology 66:468–477.

Fortuna MG, West GH, Stornetta RL, Guyenet PG (2008) Bötzinger Expiratory-Augmenting Neurons and the Parafacial Respiratory Group. J Neurosci 28:2506–2515.

Funk GD (2013) Neuromodulation: purinergic signaling in respiratory control. Compr Physiol 3:331–363.

Funk GD, Smith JC, Feldman JL (1993) Generation and transmission of respiratory oscillations in medullary slices: role of excitatory amino acids. Journal of Neurophysiology.

Gallego D, Hernández P, Clavé P, Jiménez M (2006) P2Y1 receptors mediate inhibitory purinergic neuromuscular transmission in the human colon. American Journal of Physiology-Gastrointestinal and Liver Physiology 291:G584–G594.

Garcia R, Vouimba R-M, Baudry M, Thompson RF (1999) The amygdala modulates prefrontal cortex activity relative to conditioned fear. Nature 402:294–296.

Garrett JE, Wellman CL (2009) Chronic stress effects on dendritic morphology in medial prefrontal cortex: sex differences and estrogen dependence. Neuroscience 162:195–207.

Gerevich Z, Borvendeg SJ, Schröder W, Franke H, Wirkner K, Nörenberg W, Fürst S, Gillen C, Illes P (2004) Inhibition of N-type voltage-activated calcium channels in rat dorsal root ganglion neurons by P2Y receptors is a possible mechanism of ADP-induced analgesia. Journal of Neuroscience 24:797–807.

Gestreau C, Heitzmann D, Thomas J, Dubreuil V, Bandulik S, Reichold M, Bendahhou S, Pierson P, Sterner C, Peyronnet-Roux J, Benfriha C, Tegtmeier I, Ehnes H, Georgieff M, Lesage F, Brunet J-F, Goridis C, Warth R, Barhanin J (2010) Task2 potassium channels set central respiratory CO2 and O2 sensitivity. Proc Natl Acad Sci USA 107:2325–2330.

Giesbrecht CJ, Mackay JP, Silveira HB, Urban JH, Colmers WF (2010a) Countervailing modulation of Ih by neuropeptide Y and corticotrophin-releasing factor in basolateral amygdala as a possible mechanism for their effects on stress-related behaviors. Journal of Neuroscience 30:16970–16982.

Gonçalves J, Queiroz G (2008) Presynaptic adenosine and P2Y receptors. Handb Exp Pharmacol:339–372.

Gourine AV, Atkinson L, Deuchars J, Spyer KM (2003) Purinergic Signalling in the Medullary Mechanisms of Respiratory Control in the Rat: Respiratory Neurones Express the P2X2 Receptor Subunit. The Journal of Physiology 552:197–211.

Gourine AV, Kasymov V, Marina N, Tang F, Figueiredo MF, Lane S, Teschemacher AG, Spyer KM, Deisseroth K, Kasparov S (2010) Astrocytes Control Breathing Through pH-Dependent Release of ATP. Science 329:571–575.

Gourine AV, Llaudet E, Dale N, Spyer KM (2005a) ATP is a mediator of chemosensory transduction in the central nervous system. Nature 436:108–111.

Gourine AV, Llaudet E, Dale N, Spyer KM (2005b) Release of ATP in the Ventral Medulla during Hypoxia in Rats: Role in Hypoxic Ventilatory Response. J Neurosci 25:1211–1218.

Govindarajan A, Rao BSS, Nair D, Trinh M, Mawjee N, Tonegawa S, Chattarji S (2006) Transgenic brain-derived neurotrophic factor expression causes both anxiogenic and antidepressant effects. Proceedings of the National Academy of Sciences 103:13208–13213.

Gray PA, Hayes JA, Ling GY, Llona I, Tupal S, Picardo MCD, Ross SE, Hirata T, Corbin JG, Eugenín J, Del Negro CA (2010) Developmental Origin of PreBötzinger Complex Respiratory Neurons. J Neurosci 30:14883–14895.

Gray PA, Janczewski WA, Mellen N, McCrimmon DR, Feldman JL (2001) Normal breathing requires preBötzinger complex neurokinin-1 receptor-expressing neurons. Nat Neurosci 4:927–930.

Gray PA, Rekling JC, Bocchiaro CM, Feldman JL (1999a) Modulation of Respiratory Frequency by Peptidergic Input to Rhythmogenic Neurons in the PreBötzinger Complex. Science 286:1566–1568.

Greer JJ, Smith JC, Feldman JL (1991) Role of excitatory amino acids in the generation and transmission of respiratory drive in neonatal rat. The Journal of Physiology 437:727–749.

Grupe DW, Nitschke JB (2013) Uncertainty and anticipation in anxiety: an integrated neurobiological and psychological perspective. Nat Rev Neurosci 14:488–501.

Gu QD, Joe DS, Gilbert CA (2017) Activation of bitter taste receptors in pulmonary nociceptors sensitizes TRPV1 channels through the PLC and PKC signaling pathway. Am J Physiol Lung Cell Mol Physiol 312:L326–L333.

Guinamard R, Simard C, Del Negro C (2013) Flufenamic acid as an ion channel modulator. Pharmacology and Therapeutics 138:272–284.

Gutman AR, Yang Y, Ressler KJ, Davis M (2008) The role of neuropeptide Y in the expression and extinction of fear-potentiated startle. Journal of Neuroscience 28:12682–12690.

Guyenet PG, Bayliss DA (2015) Neural Control of Breathing and CO2 Homeostasis. Neuron 87:946–961.

Guyenet PG, Bayliss DA, Stornetta RL, Kanbar R, Shi Y, Holloway BB, Souza GMPR, Basting TM, Abbott SBG, Wenker IC (2018) Interdependent feedback regulation of breathing by the carotid bodies and the retrotrapezoid nucleus. The Journal of Physiology 596:3029–3042.

Guyenet PG, Mulkey DK, Stornetta RL, Bayliss DA (2005) Regulation of ventral surface chemoreceptors by the central respiratory pattern generator. Journal of Neuroscience 25:8938–8947.

Guyenet PG, Stornetta RL, Bayliss DA (2010) Central respiratory chemoreception. Journal of Comparative Neurology 518:3883–3906.

Guyenet PG, Stornetta RL, Souza GMPR, Abbott SBG, Shi Y, Bayliss DA (2019) The Retrotrapezoid Nucleus: Central Chemoreceptor and Regulator of Breathing Automaticity. Trends in Neurosciences 42:807–824.

Guzman SJ, Gerevich Z, Hengstler JG, Illes P, Kleemann W (2005) P2Y1 receptors inhibit both strength and plasticity of glutamatergic synaptic neurotransmission in the rat prefrontal cortex. Synapse 57:235–238.

Hamilton TJ, Xapelli S, Michaelson SD, Larkum ME, Colmers WF (2013) Modulation of distal calcium electrogenesis by neuropeptide Y_1 receptors inhibits neocortical long-term depression. Journal of Neuroscience 33:11184–11193.

Haubensak W, Kunwar PS, Cai H, Ciocchi S, Wall NR, Ponnusamy R, Biag J, Dong H-W, Deisseroth K, Callaway EM, Fanselow MS, Lüthi A, Anderson DJ (2010) Genetic dissection of an amygdala microcircuit that gates conditioned fear. Nature 468:270–276.

Hawryluk JM, Moreira TS, Takakura AC, Wenker IC, Tzingounis AV, Mulkey DK (2012) KCNQ Channels Determine Serotonergic Modulation of Ventral Surface Chemoreceptors and Respiratory Drive. J Neurosci 32:16943–16952.

Heilig M (1995) Antisense inhibition of neuropeptide Y (NPY)-Y1 receptor expression blocks the anxiolytic-like action of NPY in amygdala and paradoxically increases feeding. Regulatory Peptides 59:201–205.

Heilig M, McLeod S, Brot M, Heinrichs SC, Menzaghi F, Koob GF, Britton KT (1993) Anxiolytic-like action of neuropeptide Y: mediation by Y1 receptors in amygdala, and dissociation from food intake effects. Neuropsychopharmacology 8:357–363.

Heilig M, Söderpalm B, Engel JA, Psychopharmacology EW, 1989 (n.d.) Centrally administered neuropeptide Y (NPY) produces anxiolytic-like effects in animal anxiety models. Springer.

Heilig M, Zachrisson O, Thorsell A, Ehnvall A, Mottagui-Tabar S, Sjögren M, Åsberg M, Ekman R, Wahlestedt C, Ågren H (2004) Decreased cerebrospinal fluid neuropeptide Y (NPY) in patients with treatment refractory unipolar major depression: preliminary evidence for association with preproNPY gene polymorphism. Journal of Psychiatric Research 38:113–121.

Herlenius E, Lagercrantz H, Yamamoto Y (1997) Adenosine Modulates Inspiratory Neurons and the Respiratory Pattern in the Brainstem of Neonatal Rats. Pediatr Res 42:46–53.

Herry C, Ciocchi S, Senn V, Demmou L, Müller C, Lüthi A (2008) Switching on and off fear by distinct neuronal circuits. Nature 454:600–606.

Holliday ND, Lam C-W, Tough IR, Cox HM (2005) Role of the C terminus in neuropeptide Y Y1 receptor desensitization and internalization. Molecular Pharmacology 67:655–664.

Hoover WB, Vertes RP (2007) Anatomical analysis of afferent projections to the medial prefrontal cortex in the rat. Brain Struct Funct 212:149–179.

Hu B, Boyle CA, Lei S (2020) Oxytocin receptors excite lateral nucleus of central amygdala by phospholipase Cβ- and protein kinase C-dependent depression of inwardly rectifying K+ channels. The Journal of Physiology 598:3501–3520.

Huckstepp RT, Henderson LE, Cardoza KP, Feldman JL (2016) Interactions between respiratory oscillators in adult rats. Elife 5:5613.

Huckstepp RTR, Bihi RI, Eason R, Spyer KM, Dicke N, Willecke K, Marina N, Gourine AV, Dale N (2010) Connexin hemichannel-mediated CO2-dependent release of ATP in the medulla oblongata contributes to central respiratory chemosensitivity. The Journal of Physiology 588:3901–3920.

Huckstepp RTR, Cardoza KP, Henderson LE, Feldman JL (2015) Role of Parafacial Nuclei in Control of Breathing in Adult Rats. J Neurosci 35:1052–1067.

Huxtable AG, Zwicker JD, Alvares TS, Ruangkittisakul A, Fang X, Hahn LB, de Chaves EP, Baker GB, Ballanyi K, Funk GD (2010) Glia Contribute to the Purinergic Modulation of Inspiratory Rhythm-Generating Networks. J Neurosci 30:3947–3958.

Huxtable AG, Zwicker JD, Poon BY, Pagliardini S, Vrouwe SQ, Greer JJ, Funk GD (2009) Tripartite purinergic modulation of central respiratory networks during perinatal development: the influence of ATP, ectonucleotidases, and ATP metabolites. Journal of Neuroscience 29:14713–14725.

Irle E, Ruhleder M, Lange C, Seidler-Brandler U, Salzer S, Dechent P, Weniger G, Leibing E, Leichsenring F (2010) Reduced amygdalar and hippocampal size in adults with generalized social phobia. J Psychiatry Neurosci 35:126–131.

Janak PH, Tye KM (2015) From circuits to behaviour in the amygdala. Nature 517:284–292.

Janczewski WA, Feldman JL (2006) Distinct rhythm generators for inspiration and expiration in the juvenile rat. The Journal of Physiology 570:407–420.

Janczewski WA, Tashima A, Hsu P, Cui Y, Feldman JL (2013) Role of inhibition in respiratory pattern generation. Journal of Neuroscience 33:5454–5465.

Jarvis ED et al. (2005) Avian brains and a new understanding of vertebrate brain evolution. Nat Rev Neurosci 6:151–159.

Jimenez-Vasquez PA, Mathé AA, Thomas JD, Riley EP, Ehlers CL (2001) Early maternal separation alters neuropeptide Y concentrations in selected brain regions in adult rats. Developmental Brain Research 131:149–152.

Johansen JP, Diaz-Mataix L, Hamanaka H, Ozawa T, Ycu E, Koivumaa J, Kumar A, Hou M, Deisseroth K, Boyden ES, LeDoux JE (2014) Hebbian and neuromodulatory mechanisms interact to trigger associative memory formation. Proceedings of the National Academy of Sciences 111:E5584–E5592.

Johansen JP, Hamanaka H, Monfils MH, Behnia R, Deisseroth K, Blair HT, LeDoux JE (2010) Optical activation of lateral amygdala pyramidal cells instructs associative fear learning. Proceedings of the National Academy of Sciences 107:12692–12697.

Johnson SM, Smith JC, Funk GD, Feldman JL (1994) Pacemaker behavior of respiratory neurons in medullary slices from neonatal rat. Journal of Neurophysiology 72:2598–2608.

Johnston JB (1923) Further contributions to the study of the evolution of the forebrain. Journal of Comparative Neurology.

Kawai A, Okada Y, Mückenhoff K, Scheid P (1995) Theophylline and hypoxic ventilatory response in the rat isolated brainstem-spinal cord. Respiration Physiology 100:25–32.

Kim M, Campeau S, Falls WA, Davis M (1993) Infusion of the non-NMDA receptor antagonist CNQX into the amygdala blocks the expression of fear-potentiated startle. Behavioral and Neural Biology 59:5–8.

Kim S-Y, Adhikari A, Lee SY, Marshel JH, Kim CK, Mallory CS, Lo M, Pak S, Mattis J, Lim BK, Malenka RC, Warden MR, Neve R, Tye KM, Deisseroth K (2013a) Diverging neural pathways assemble a behavioural state from separable features in anxiety. Nature 496:219–223.

Kim S-Y, Adhikari A, Lee SY, Marshel JH, Kim CK, Mallory CS, Lo M, Pak S, Mattis J, Lim BK, Malenka RC, Warden MR, Neve R, Tye KM, Deisseroth K (2013b) Diverging neural pathways assemble a behavioural state from separable features in anxiety. Nature 496:219–223.

King AE, Ackley MA, Cass CE, Young JD, Baldwin SA (2006) Nucleoside transporters: from scavengers to novel therapeutic targets. Trends in Pharmacological Sciences 27:416–425.

Koizumi H, Koshiya N, Chia JX, Cao F, Nugent J, Zhang R, Smith JC (2013) Structural-functional properties of identified excitatory and inhibitory interneurons within pre-Botzinger complex respiratory microcircuits. Journal of Neuroscience 33:2994–3009.

Koizumi H, Mosher B, Tariq MF, Zhang R, Koshiya N, Smith JC (2016) Voltage-Dependent Rhythmogenic Property of Respiratory Pre-Bötzinger Complex Glutamatergic, Dbx1-Derived, and Somatostatin-Expressing Neuron Populations Revealed by Graded Optogenetic Inhibition. eNeuro 3(3)0081–16.2016.

Koos BJ, Kawasaki Y, Kim Y-H, Bohorquez F (2005) Adenosine A2A-receptor blockade abolishes the roll-off respiratory response to hypoxia in awake lambs. American Journal of Physiology - Regulatory, Integrative and Comparative Physiology 288:R1185–R1194.

Koos BJ, Mason BA, Punla O, Adinolfi AM (1994) Hypoxic inhibition of breathing in fetal sheep: relationship to brain adenosine concentrations. Journal of Applied Physiology. 77:2734–2739

Koos BJ, Matsuda K (1990) Fetal breathing, sleep state, and cardiovascular responses to adenosine in sheep. Journal of Applied Physiology 68:489–495.

Koshiya N, Smith JC (1999) Neuronal pacemaker for breathing visualized in vitro. Nature 400:360–363.

Kshatri AS, Gonzalez-Hernandez A, Giraldez T (2018) Physiological Roles and Therapeutic Potential of Ca2+ Activated Potassium Channels in the Nervous System. Front Mol Neurosci 11.

Kumar NN et al. (2015) Regulation of breathing by CO2 requires the proton-activated receptor GPR4 in retrotrapezoid nucleus neurons. Science 348:1255–1260.

Kuwana S-I, Tsunekawa N, Yanagawa Y, Okada Y, Kuribayashi J, Obata K (2006) Electrophysiological and morphological characteristics of GABAergic respiratory neurons in the mouse pre-Bötzinger complex. Eur J Neurosci 23:667–674.

Kwon J-T, Nakajima R, Kim H-S, Jeong Y, Augustine GJ, Han J-H (2014) Optogenetic activation of presynaptic inputs in lateral amygdala forms associative fear memory. Learning & Memory 21:627–633.

LaBar KS, Gatenby JC, Gore JC, LeDoux JE, Phelps EA (1998) Human amygdala activation during conditioned fear acquisition and extinction: a mixed-trial fMRI study. Neuron 20:937–945.

Lagercrantz H, Yamamoto Y, Fredholm BB, Prabhakar NR, Euler von C (1984) Adenosine Analogues Depress Ventilation in Rabbit Neonates. Theophylline Stimulation of Respiration via Adenosine Receptors? Pediatr Res 18:387–390.

Lakshminarasimhan H, Chattarji S (2012) Stress Leads to Contrasting Effects on the Levels of Brain Derived Neurotrophic Factor in the Hippocampus and.

Lanuza E, Belekhova M, Martínez-Marcos A, Font C, Martínez-García F (1998) Identification of the reptilian basolateral amygdala: an anatomical investigation of the afferents to the posterior dorsal ventricular ridge of the lizard Podarcis hispanica. Eur J Neurosci 10:3517–3534.

LeDoux JE (2000) Emotion circuits in the brain. Annu Rev Neurosci 23:155–184.

LeDoux JE, Cicchetti P, Xagoraris A, Romanski LM (1990) The lateral amygdaloid nucleus: sensory interface of the amygdala in fear conditioning. J Neurosci 10:1062–1069.

Lee Y, Fitz S, Johnson PL, Shekhar A (2008) Repeated Stimulation of CRF Receptors in the BNST of Rats Selectively Induces Social but not Panic-Like Anxiety. Neuropsychopharmacology 33:2586–2594.

Leitermann RJ, Rostkowski AB, Urban JH (2016) Neuropeptide Y input to the rat basolateral amygdala complex and modulation by conditioned fear. Journal of Comparative Neurology 524:2418–2439.

Leitermann RJ, Sajdyk TJ, Urban JH (2012) Cell-specific expression of calcineurin immunoreactivity within the rat basolateral amygdala complex and colocalization with the neuropeptide Y Y1 receptor. Journal of Chemical Neuroanatomy 45:50–56.

Leonard EM, Salman S, Nurse CA (2018) Sensory Processing and Integration at the Carotid Body Tripartite Synapse: Neurotransmitter Functions and Effects of Chronic Hypoxia. Front Physiol 9:225.

Leuner B, Shors TJ (2013) ANXIETY, AND DENDRITIC SPINES: WHAT ARE THE CONNECTIONS? Neuroscience 251:108–119.

Li F, Jia C-H, Huang J, Bi G-Q, Lau P-M (2020) High frequency optogenetic activation of inputs to the lateral amygdala forms distant association with foot-shock. Mol Brain 13:44.

Li H, Penzo MA, Taniguchi H, Kopec CD, Huang ZJ, Li B (2013) Experience-dependent modification of a central amygdala fear circuit. Nat Neurosci 16:332–339.

Li H-S, Xu X-ZS, Montell C (1999) Activation of a TRPC3-Dependent Cation Current through the Neurotrophin BDNF. Neuron 24:261–273.

Li P, Janczewski WA, Yackle K, Kam K, Pagliardini S, Krasnow MA, Feldman JL (2016) The peptidergic control circuit for sighing. Nature 530:293–297.

Li XF, Armony JL, LeDoux JE (1996) GABAA and GABAB receptors differentially regulate synaptic transmission in the auditory thalamo-amygdala pathway: An in vivo microiontophoretic study and a model. Synapse 24:115–124.

Lieske SP, Ramirez J-M (2006) Pattern-specific synaptic mechanisms in a multifunctional network. I. Effects of alterations in synapse strength. Journal of Neurophysiology 95:1323–1333.

Lin C-H, Lee C-C, Gean P-W (2003a) Involvement of a Calcineurin Cascade in Amygdala Depotentiation and Quenching of Fear Memory. Molecular Pharmacology 63:44–52.

Lin C-H, Yeh S-H, Leu T-H, Chang W-C, Wang S-T, Gean P-W (2003b) Identification of Calcineurin as a Key Signal in the Extinction of Fear Memory. J Neurosci 23:1574–1579.

Little JP, Carter AG (2013) Synaptic mechanisms underlying strong reciprocal connectivity between the medial prefrontal cortex and basolateral amygdala. Journal of Neuroscience 33:15333–15342.

Long WQ, Anthonisen NR (1994) Aminophylline partially blocks ventilatory depression with hypoxia in the awake cat. Can J Physiol Pharmacol 72:673–678.

Lopes JM, Davis GM, Mullahoo K, Aranda JV (1994) Role of adenosine in the hypoxic ventilatory response of the newborn piglet. Pediatr Pulmonol 17:50–55.

Lorier AR, Huxtable AG, Robinson DM, Lipski J, Housley GD, Funk GD (2007) P2Y1 Receptor Modulation of the Pre-Bötzinger Complex Inspiratory Rhythm Generating Network In Vitro. J Neurosci 27:993–1005.

Lorier AR, Lipski J, Housley GD, Greer JJ, Funk GD (2008) ATP sensitivity of preBötzinger complex neurones in neonatal rat in vitro: mechanism underlying a P2 receptor-mediated increase in inspiratory frequency. The Journal of Physiology 586:1429–1446.

Luthardt J, Borvendeg SJ, Sperlágh B, Poelchen W, Wirkner K, Illes P (2003) P2Y(1) receptor activation inhibits NMDA receptor-channels in layer V pyramidal neurons of the rat prefrontal and parietal cortex. Neurochem Int 42:161–172.

Machado-de-Sousa JP, de Lima Osório F, Jackowski AP, Bressan RA, Chagas MHN, Torro-Alves N, DePaula ALD, Crippa JAS, Hallak JEC (2014) Increased Amygdalar and

Hippocampal Volumes in Young Adults with Social Anxiety Chen H, ed. PLoS ONE 9:e88523.

Mackay JP (2016) Mechanisms of NPY Y2 Receptor-Mediated Anxiogenesis in the Basolateral Amygdala.

Mackay JP, Bompolaki M, DeJoseph MR, Michaelson SD, Urban JH, Colmers WF (2019) NPY2 Receptors Reduce Tonic Action Potential-Independent GABAB Currents in the Basolateral Amygdala. Journal of Neuroscience 39:4909–4930.

Mader F, Krause L, Tokay T, Hakenberg OW, Köhling R, Kirschstein T (2016) P2Y receptor-mediated transient relaxation of rat longitudinal ileum preparations involves phospholipase C activation, intracellular Ca 2+ release and SK channel activation. Acta Pharmacol Sin 37:617–628.

Marchenko V, Koizumi H, Mosher B, Koshiya N, Tariq MF, Bezdudnaya TG, Zhang R, Molkov YI, Rybak IA, Smith JC (2016) Perturbations of Respiratory Rhythm and Pattern by Disrupting Synaptic Inhibition within Pre-Bötzinger and Bötzinger Complexes. eNeuro 3:ENEURO.0011–16.

Maren S, Holmes A (2015) Stress and Fear Extinction. Neuropsychopharmacology.

Maren S, Quirk GJ (2004) Neuronal signalling of fear memory. Nat Rev Neurosci 5:844–852.

Martin RJ, Abu-Shaweesh JM, (2005) Control of breathing and neonatal apnea. Biol. Neonate 87:288–295.

Mascagni F, McDonald AJ (2003) Immunohistochemical characterization of cholecystokinin containing neurons in the rat basolateral amygdala. Brain Research 976:171–184.

Mathé AA, Rudorfer MV, Stenfors C, Manji HK, Potter WZ, Theodorsson E (1995) Effects of electroconvulsive treatment on somatostatin, neuropeptide Y, endothelin, and neurokinin a concentrations in cerebrospinal fluid of depressed patients: A pilot study. Depression 3:250–256.

Matschke LA, Rinné S, Snutch TP, Oertel WH, Dolga AM, Decher N (2018) Calcium-activated SK potassium channels are key modulators of the pacemaker frequency in locus coeruleus neurons. Molecular and Cellular Neuroscience 88:330–341.

McDonald AJ (1982) Neurons of the lateral and basolateral amygdaloid nuclei: a Golgi study in the rat. J Comp Neurol 212:293–312.

McDonald AJ (1984) Neuronal organization of the lateral and basolateral amygdaloid nuclei in the rat. Journal of Comparative Neurology 222:589–606.

McDonald AJ (1985) Immunohistochemical identification of gamma-aminobutyric acid-containing neurons in the rat basolateral amygdala. Neuroscience Letters 53:203–207.

McDonald AJ (1989) Coexistence of somatostatin with neuropeptide Y, but not with cholecystokinin or vasoactive intestinal peptide, in neurons of the rat amygdala. Brain Research 500:37–45.

McDonald AJ (1996) Glutamate and aspartate immunoreactive neurons of the rat basolateral amygdala: colocalization of excitatory amino acids and projections to the limbic circuit. J Comp Neurol 365:367–379.

McDonald AJ, Mascagni F (2001) Colocalization of calcium-binding proteins and GABA in neurons of the rat basolateral amygdala. NSC 105:681–693.

McDonald AJ, Muller JF, Mascagni F (2002) GABAergic innervation of alpha type II calcium/calmodulin-dependent protein kinase immunoreactive pyramidal neurons in the rat basolateral amygdala. J Comp Neurol 446:199–218.

McDonald AJ, Pearson JC (1989) Coexistence of GABA and peptide immunoreactivity in non-pyramidal neurons of the basolateral amygdala. Neuroscience Letters 100:53–58.

McEwen BS, Eiland L, Hunter RG, Miller MM (2012) Neuropharmacology. Neuropharmacology 62:3–12.

McEwen BS, Gianaros PJ (2011) Stress- and Allostasis-Induced Brain Plasticity. Annu Rev Med 62:431–445.

McQuiston AR, Petrozzino JJ, Connor JA, Colmers WF (1996) Neuropeptide Y1 receptors inhibit N-type calcium currents and reduce transient calcium increases in rat dentate granule cells. J Neurosci 16:1422–1429.

Meredith AL, Wiler SW, Miller BH, Takahashi JS, Fodor AA, Ruby NF, Aldrich RW (2006) BK calcium-activated potassium channels regulate circadian behavioral rhythms and pacemaker output. Nat Neurosci 9:1041–1049.

Michaelson SD (2016) Organotypic Basolateral Amygdala Slice Cultures: A Model for Stress-related Circuitry. University of Alberta.

Michaelson SD, Miranda Tapia AP, McKinty A, Silveira Villarroel H, Mackay JP, Urban JH, Colmers WF (2020) Contribution of NPY Y5 Receptors to the Reversible Structural Remodeling of Basolateral Amygdala Dendrites in Male Rats Associated with NPY-Mediated Stress Resilience. Journal of Neuroscience 40:3231–3249.

Mironov SL, Richter DW (2000) Hypoxic modulation of L-type Ca2+ channels in inspiratory brainstem neurones: Intracellular signalling pathways and metabotropic glutamate receptors. Brain Research 869:166–177.

Miserendino MJ, Sananes CB, Melia KR, Davis M (1990) Blocking of acquisition but not expression of conditioned fear-potentiated startle by NMDA antagonists in the amygdala. Nature 345:716–718.

Mitra R, Ferguson D, Sapolsky RM (2009) SK2 potassium channel overexpression in basolateral amygdala reduces anxiety, stress-induced corticosterone secretion and dendritic arborization. Molecular Psychiatry 14:847–855.

Mitra R, Jadhav S, McEwen BS, Vyas A, Chattarji S (2005) Stress duration modulates the spatiotemporal patterns of spine formation in the basolateral amygdala. Proceedings of the National Academy of Sciences 102:9371–9376.

Montandon G, Liu H, Horner RL (2016a) Contribution of the respiratory network to rhythm and motor output revealed by modulation of GIRK channels, somatostatin and neurokinin-1 receptors. Sci Rep 6:1–15.

Montandon G, Qin W, Liu H, Ren J, Greer JJ, Horner RL (2011) PreBotzinger complex neurokinin-1 receptor-expressing neurons mediate opioid-induced respiratory depression. Journal of Neuroscience 31:1292–1301.

Montandon G, Ren J, Victoria NC, Liu H, Wickman K, Greer JJ, Horner RL (2016b) G-protein-gated Inwardly Rectifying Potassium Channels Modulate Respiratory Depression by Opioids. Anesthesiology 124:641–650.

Morgado-Valle C, Baca SM, Feldman JL (2010) Glycinergic Pacemaker Neurons in PreBötzinger Complex of Neonatal Mouse. J Neurosci 30:3634–3639.

Morgan CA III, Rasmusson AM, Wang S, Hoyt G, Hauger RL, Hazlett G (2002) Neuropeptide-Y, cortisol, and subjective distress in humans exposed to acute stress: replication and extension of previous report. Biological Psychiatry 52:136–142.

Morgan CA III, Wang S, Rasmusson A, Hazlett G, Anderson G, Charney DS (2001) Relationship Among Plasma Cortisol, Catecholamines, Neuropeptide Y, and Human Performance During Exposure to Uncontrollable Stress. Psychosomatic Medicine 63:412–422.

Morgan CA III, Wang S, Southwick SM, Rasmusson A (2000) Plasma neuropeptide-Y in humans exposed to acute uncontrollable stress. Biological Psychiatry.

Moss IR (2000) Respiratory responses to single and episodic hypoxia during development: mechanisms of adaptation. Respiration Physiology 121:185–197.

Mulkey DK, Stornetta RL, Weston MC, Simmons JR, Parker A, Bayliss DA, Guyenet PG (2004a) Respiratory control by ventral surface chemoreceptor neurons in rats. Nat Neurosci 7:1360–1369.

Mulkey DK, Stornetta RL, Weston MC, Simmons JR, Parker A, Bayliss DA, Guyenet PG (2004b) Respiratory control by ventral surface chemoreceptor neurons in rats. Nat Neurosci 7:1360–1369.

Mulkey DK, Talley EM, Stornetta RL, Siegel AR, West GH, Chen X, Sen N, Mistry AM, Guyenet PG, Bayliss DA (2007) TASK Channels Determine pH Sensitivity in Select Respiratory Neurons But Do Not Contribute to Central Respiratory Chemosensitivity. J Neurosci 27:14049–14058.

Myers KM, Davis M (2002) Behavioral and Neural Analysis of Extinction. Neuron 36:567–584.

Nabavi S, Fox R, Proulx CD, Lin JY, Tsien RY, Malinow R (2014) Engineering a memory with LTD and LTP. Nature 511:348–352.

Nader K, Majidishad P, Amorapanth P, LeDoux JE (2001) Damage to the lateral and central, but not other, amygdaloid nuclei prevents the acquisition of auditory fear conditioning. Learning & Memory 8:156–163.

Nakajima M, Inui A, Asakawa A, Momose K, Ueno N, Teranishi A, Baba S, Kasuga M (1998) Neuropeptide Y produces anxiety via Y2-type receptors. Peptides 19:359–363.

Namburi P, Beyeler A, Yorozu S, Calhoon GG, Halbert SA, Wichmann R, Holden SS, Mertens KL, Anahtar M, Felix-Ortiz AC, Wickersham IR, Gray JM, Tye KM (2015) A circuit mechanism for differentiating positive and negative associations. Nature 520:675–678.

Nattie E, Li A (2009) Central chemoreception is a complex system function that involves multiple brain stem sites. Journal of Applied Physiology 106:1464–1466.

Nesse RM (1990) Evolutionary explanations of emotions. Human nature.

Nesse RM (1994) Fear and fitness: An evolutionary analysis of anxiety disorders. Ethology and sociobiology 15:247–261.

Neylon CB, Nurgali K, Hunne B, Robbins HL, Moore S, Chen MX, Furness JB (2004) Intermediate-conductance calcium-activated potassium channels in enteric neurones of the

mouse: pharmacological, molecular and immunochemical evidence for their role in mediating the slow afterhyperpolarization. J Neurochem 90:1414–1422.

Ngo-Anh TJ, Bloodgood BL, Lin M, Sabatini BL, Maylie J, Adelman JP (2005) SK channels and NMDA receptors form a Ca 2+ -mediated feedback loop in dendritic spines. Nat Neurosci 8:642–649.

Nieh EH, Kim S-Y, Namburi P, Tye KM (2013) Optogenetic dissection of neural circuits underlying emotional valence and motivated behaviors. Brain Research 1511:73–92.

Nikisch G, Ågren H, Eap CB, Czernik A, Baumann P, Mathé AA (2005) Neuropeptide Y and corticotropin-releasing hormone in CSF mark response to antidepressive treatment with citalopram. Int J Neuropsychopharmacol 8:403–410.

Onimaru H, Ballanyi K, Homma I (2003) Contribution of Ca2+-dependent conductances to membrane potential fluctuations of medullary respiratory neurons of newborn rats in vitro. The Journal of Physiology 552:727–741.

Onimaru H, Homma I (2003) A Novel Functional Neuron Group for Respiratory Rhythm Generation in the Ventral Medulla. J Neurosci 23:1478–1486.

Onimaru H, Ikeda K, Kawakami K (2008) CO2-Sensitive Preinspiratory Neurons of the Parafacial Respiratory Group Express Phox2b in the Neonatal Rat. J Neurosci 28:12845–12850.

Padival M, Quinette D, Rosenkranz JA (2013) Effects of Repeated Stress on Excitatory Drive of Basal Amygdala Neurons In Vivo. Neuropsychopharmacology 38:1748–1762.

Pagliardini S, Adachi T, Ren J, Funk GD, Greer JJ (2005) Fluorescent Tagging of Rhythmically Active Respiratory Neurons within the Pre-Bötzinger Complex of Rat Medullary Slice Preparations. J Neurosci 25:2591–2596.

Pagliardini S, Janczewski WA, Tan W, Dickson CT, Deisseroth K, Feldman JL (2011) Active expiration induced by excitation of ventral medulla in adult anesthetized rats. Journal of Neuroscience 31:2895–2905.

Pankratov Y, Lalo U, Krishtal OA, Verkhratsky A (2009) P2X receptors and synaptic plasticity. NSC 158:137–148.

Patel D, Anilkumar S, Chattarji S, Buwalda B (2018) Repeated social stress leads to contrasting patterns of structural plasticity in the amygdala and hippocampus. Behavioural Brain Research 347:314–324.

Pankratov Y, Lalo U, Krishtal OA, Verkhratsky A (2009) P2X receptors and synaptic plasticity. NSC 158:137–148.

Peng Y-J, Makarenko VV, Gridina A, Chupikova I, Zhang X, Kumar GK, Fox AP, Prabhakar NR (2019) H2S mediates carotid body response to hypoxia but not anoxia. Respiratory Physiology & Neurobiology 259:75–85.

Peng Y-J, Nanduri J, Raghuraman G, Souvannakitti D, Gadalla MM, Kumar GK, Snyder SH, Prabhakar NR (2010) H2S mediates O2 sensing in the carotid body. Proceedings of the National Academy of Sciences 107:10719–10724.

Picardo MCD, Weragalaarachchi KTH, Akins VT, Del Negro CA (2013) Physiological and morphological properties of Dbx1-derived respiratory neurons in the pre-Bötzinger complex of neonatal mice. The Journal of Physiology 591:2687–2703.

Pisanski A, Ding X, Koch NA, Pagliardini S (2020) Chemogenetic modulation of the parafacial respiratory group influences the recruitment of abdominal activity during REM sleep. Sleep 43:351.

Piskuric NA, Nurse CA (2012) Effects of chemostimuli on [Ca2+]i responses of rat aortic body type I cells and endogenous local neurons: comparison with carotid body cells. The Journal of Physiology 590:2121–2135.

Pitts T (2014) Airway protective mechanisms. Lung 192:27–31.

Pitts T, Morris K, Lindsey B, Davenport P, Poliacek I, Bolser D (2012) Co-ordination of cough and swallow in vivo and in silico. Exp Physiol 97:469–473.

Polepalli JS, Gooch H, Sah P (2020) Diversity of interneurons in the lateral and basal amygdala. NPJ Sci Learn 5:10–19.

Prabhakar NR (2013) Sensing hypoxia: physiology, genetics and epigenetics. The Journal of Physiology 591:2245–2257.

Prabhakar NR (2016) O2 and CO2 Detection by the Carotid and Aortic Bodies. In: Chemosensory Transduction, pp 321–338. Academic Press.

Pusch M, Neher E (1988) Rates of diffusional exchange between small cells and a measuring patch pipette. Pflugers Arch 411:204-211.

Quirk GJ, Armony JL, LeDoux JE (1997) Fear Conditioning Enhances Different Temporal Components of Tone-Evoked Spike Trains in Auditory Cortex and Lateral Amygdala. Neuron 19:613–624.

Rainnie DG, Bergeron R, Sajdyk TJ, Patil M, Gehlert DR, Shekhar A (2004) Corticotrophin releasing factor-induced synaptic plasticity in the amygdala translates stress into emotional disorders. Journal of Neuroscience 24:3471–3479.

Rainnie DG, of EAJ, 1993 (1993) Intracellular recordings from morphologically identified neurons of the basolateral amygdala. Journal of Neurophys. 69:1350–1362.

Rajani V, Zhang Y, Revill AL, Funk GD (2016) The role of P2Y1 receptor signaling in central respiratory control. Respiratory Physiology & Neurobiology 226:3–10.

Ramirez J-M, Baertsch NA (2018) The Dynamic Basis of Respiratory Rhythm Generation: One Breath at a Time. Annu Rev Neurosci 41:475–499.

Ramirez JM, Quellmalz UJA, Wilken B, Richter DW (1998) The hypoxic response of neurones within the in vitro mammalian respiratory network. The Journal of Physiology 507:571–582.

Rasmusson AM, Hauger RL, Morgan III CA, Bremner JD, Charney DS, Southwick SM (2000) Low baseline and yohimbine-stimulated plasma neuropeptide Y (NPY) levels in combat-related PTSD. BPS 47:526–539.

Reklow RJ, Alvares TS, Zhang Y, Miranda Tapia AP, Biancardi V, Katzell AK, Frangos SM, Hansen MA, Toohey AW, Cass CE, Young JD, Pagliardini S, Boison D, Funk GD (2019) The Purinome and the preBötzinger Complex - A Ménage of Unexplored Mechanisms That May Modulate/Shape the Hypoxic Ventilatory Response. Front Cell Neurosci 13:365.

Richter DW (1982) Generation and maintenance of the respiratory rhythm. Journal of Experimental Biology 100:93–107.

Richter DW, Ballantyne D, Remmers JE (1986) How Is the Respiratory Rhythm Generated? A Model. Physiology 1:109–112.

Richter DW, Heyde F, Gabriel M (1975) Intracellular recordings from different types of medullary respiratory neurons of the cat. Journal of Neurophysiology 38:1162–1171.

Richter DW, Schmidt-Garcon P, Pierrefiche O, Bischoff AM, Lalley PM (1999) Neurotransmitters and neuromodulators controlling the hypoxic respiratory response in anaesthetized cats. The Journal of Physiology 514:567–578.

Robert J Butera J, Rinzel J, Smith JC (1999) Models of Respiratory Rhythm Generation in the Pre-Bötzinger Complex. I. Bursting Pacemaker Neurons. Journal of Neurophysiology 82:382–397.

Robinson RB, Siegelbaum SA (2003) Hyperpolarization-activated cation currents: from molecules to physiological function. Annu Rev Physiol 65:453–480.

Rogan MT, Stäubli UV, LeDoux JE (1997) Fear conditioning induces associative long-term potentiation in the amygdala. Nature 390:604–607.

Rong W, Gourine AV, Cockayne DA, Xiang Z, Ford APDW, Spyer KM, Burnstock G (2003) Pivotal role of nucleotide P2X2 receptor subunit of the ATP-gated ion channel mediating ventilatory responses to hypoxia. Journal of Neuroscience 23:11315–11321.

Roozendaal B, McEwen BS, Chattarji S (2009) Stress, memory and the amygdala. Nat Rev Neurosci 10:423–433.

Rose M, Devine J (2014) Assessment of patient-reported symptoms of anxiety. Dialogues Clin Neurosci 16:197–211.

Rosenkranz JA, Grace AA (1999) Modulation of basolateral amygdala neuronal firing and afferent drive by dopamine receptor activation in vivo. Journal of Neuroscience 19:11027–11039.

Rosenkranz JA, Venheim ER, Padival M (2010) Chronic Stress Causes Amygdala Hyperexcitability in Rodents. Biological Psychiatry 67:1128–1136.

Rostkowski AB, Leitermann RJ, Urban JH (2013) Differential activation of neuronal cell types in the basolateral amygdala by corticotropin releasing factor. Neuropeptides 47:273–280.

Rostkowski AB, Teppen TL, Peterson DA, Urban JH (2009) Cell-specific expression of neuropeptide Y Y1 receptor immunoreactivity in the rat basolateral amygdala. J Comp Neurol 517:166–176.

Rovira-Esteban L, Gunduz-Cinar O, Bukalo O, Limoges A, Brockway E, Müller K, Fenno L, Kim YS, Ramakrishnan C, Andrási T, Deisseroth K, Holmes A, Hájos N (2019) Excitation of Diverse Classes of Cholecystokinin Interneurons in the Basal Amygdala Facilitates Fear Extinction. eNeuro 6:ENEURO.0220–19.2019.

Ruangkittisakul A, Schwarzacher SW, Secchia L, Poon BY, Ma Y, Funk GD, Ballanyi K (2006) High Sensitivity to Neuromodulator-Activated Signaling Pathways at Physiological [K+] of Confocally Imaged Respiratory Center Neurons in On-Line-Calibrated Newborn Rat Brainstem Slices. J Neurosci 26:11870–11880.

Ruffault P-L, D'Autréaux F, Hayes JA, Nomaksteinsky M, Autran S, Fujiyama T, Hoshino M, Hägglund M, Kiehn O, Brunet J-F, Fortin G, Goridis C (2015) The retrotrapezoid nucleus neurons expressing Atoh1 and Phox2b are essential for the respiratory response to CO_2. Elife 4:16410.

Runold M, Lagercrantz H, Prabhakar NR, Fredholm BB (1989) Role of adenosine in hypoxic ventilatory depression. Journal of Applied Physiology 67:541–546.

Ryan SJ, Ehrlich DE, Rainnie DG (2016) Morphology and dendritic maturation of developing principal neurons in the rat basolateral amygdala. Brain Struct Funct 221:839–854.

Sah P, Faber ESL, Lopez De Armentia M, Power J (2003) The amygdaloid complex: anatomy and physiology. Physiological Reviews 83:803–834.

Sah R, Ekhator NN, Strawn JR, Sallee FR, Baker DG, Horn PS, Geracioti TD Jr. (2009) Low Cerebrospinal Fluid Neuropeptide Y Concentrations in Posttraumatic Stress Disorder. Biological Psychiatry 66:705–707.

Saitow F, Murakoshi T, Suzuki H, Konishi S (2005) Metabotropic P2Y Purinoceptor-Mediated Presynaptic and Postsynaptic Enhancement of Cerebellar GABAergic Transmission. J Neurosci 25:2108–2116.

Sajdyk T, Johnson P, Fitz S, Shekhar A (2008a) Chronic inhibition of GABA synthesis in the bed nucleus of the stria terminalis elicits anxiety-like behavior. Journal of Psychopharmacology 22:633–641.

Sajdyk TJ, Fitz SD, Shekhar A (2006) The role of neuropeptide Y in the amygdala on corticotropin-releasing factor receptor-mediated behavioral stress responses in the rat. Stress 9:21–28.

Sajdyk TJ, Johnson PL, Leitermann RJ, Fitz SD, Dietrich A, Morin M, Gehlert DR, Urban JH, Shekhar A (2008b) Neuropeptide Y in the amygdala induces long-term resilience to stress-induced reductions in social responses but not hypothalamic-adrenal-pituitary axis activity or hyperthermia. Journal of Neuroscience 28:893–903.

Sajdyk TJ, Schober DA, Gehlert DR (2002a) Neuropeptide Y receptor subtypes in the basolateral nucleus of the amygdala modulate anxiogenic responses in rats. Neuropharmacology 43:1165–1172.

Sajdyk TJ, Schober DA, Smiley DL, Gehlert DR (2002b) Neuropeptide Y-Y2 receptors mediate anxiety in the amygdala. Pharmacology, Biochemistry and Behavior 71:419–423.

Sajdyk TJ, Vandergriff MG, Gehlert DR (1999) Amygdalar neuropeptide Y Y1 receptors mediate the anxiolytic-like actions of neuropeptide Y in the social interaction test. European Journal of Pharmacology 368:143–147.

Sanchez M, McManus OB (1996) Paxilline inhibition of the alpha-subunit of the high-conductance calcium-activated potassium channel. Neuropharmacology 35:963–968.

Sanders SK, Shekhar A (1995) Regulation of anxiety by GABAA receptors in the rat amygdala. Pharmacology, Biochemistry and Behavior 52:701–706.

Sausbier M, Hu H, Arntz C, Feil S, Kamm S, Adelsberger H, Sausbier U, Sailer CA, Feil R, Hofmann F, Korth M, Shipston MJ, Knaus HG, Wolfer DP, Pedroarena CM, Storm JF, Ruth P (2004) Cerebellar ataxia and Purkinje cell dysfunction caused by Ca2+-activated K+ channel deficiency. Proceedings of the National Academy of Sciences 101:9474–9478.

Schmid K, Foutz AS, Denavit-Saubié M (1996) Inhibitions mediated by glycine and GABAA receptors shape the discharge pattern of bulbar respiratory neurons. Brain Research 710:150–160.

Schicker KW, Chandaka GK, Geier P, Kubista H, Boehm S (2010) P2Y1 receptors mediate an activation of neuronal calcium-dependent K+ channels. The Journal of Physiology 588:3713–3725.

Schmidt B, Anderson PJ, Doyle LW, Dewey D, Grunau RE, Asztalos EV, Davis PG, Tin W, Moddemann D, Solimano A, Ohlsson A, Barrington KJ, Roberts RS, Caffeine for Apnea of Prematurity (CAP) Trial Investigators (2012) Survival without disability to age 5 years after neonatal caffeine therapy for apnea of prematurity. JAMA 307:275–282.

Schmidt B, Roberts RS, Davis P, Doyle LW, Barrington KJ, Ohlsson A, Solimano A, Tin W (2009) Long-Term Effects of Caffeine Therapy for Apnea of Prematurity. http://dxdoiorgloginezproxylibraryualbertaca/101056/NEJMoa073679 357:1893–1902.

Schmidt B, Roberts RS, of PDEJ (2006) Caffeine therapy for apnea of prematurity. Mass Medical Soc. 3454:2112–2121.

Schmidt C, Bellingham MC, Richter DW (1995) Adenosinergic modulation of respiratory neurones and hypoxic responses in the anaesthetized cat. The Journal of Physiology 483:769–781.

Schulz R, Kirschstein T, Brehme H, Porath K, Mikkat U, Köhling R (2012) Network excitability in a model of chronic temporal lobe epilepsy critically depends on SK channel-mediated AHP currents. Neurobiology of Disease 45:337–347.

Selye H (1936) A Syndrome produced by Diverse Nocuous Agents. Nature 138:32–32.

Senn V, Wolff SBE, Herry C, Grenier F, Ehrlich I, Gründemann J, Fadok JP, Müller C, Letzkus JJ, Lüthi A (2014) Long-range connectivity defines behavioral specificity of amygdala neurons. Neuron 81:428–437.

Sergeyev V, Fetissov S, Mathé AA, Jimenez PA, Bartfai T, Mortas P, Gaudet L, Moreau J-L, Hökfelt T (2005) Neuropeptide expression in rats exposed to chronic mild stresses. Psychopharmacology 178:115–124.

Shaban H, Humeau Y, Herry C, Cassasus G, Shigemoto R, Ciocchi S, Barbieri S, van der Putten H, Kaupmann K, Bettler B, Lüthi A (2006) Generalization of amygdala LTP and conditioned fear in the absence of presynaptic inhibition. Nat Neurosci 9:1028–1035.

Shao XM, Feldman JL (1997) Respiratory Rhythm Generation and Synaptic Inhibition of Expiratory Neurons in Pre-Bötzinger Complex: Differential Roles of Glycinergic and GABAergic Neural Transmission. Journal of Neurophysiology 77:1853–1860.

SheikhBahaei S, Turovsky EA, Hosford PS, Hadjihambi A, Theparambil SM, Liu B, Marina N, Teschemacher AG, Kasparov S, Smith JC, Gourine AV (2018) Astrocytes modulate brainstem respiratory rhythm-generating circuits and determine exercise capacity. Nat Commun 9:1–10.

Shekhar A, Sajdyk TJ, Gehlert DR, Rainnie DG (2003) The Amygdala, Panic Disorder, and Cardiovascular Responses. Annals of the New York Academy of Sciences 985:308–325.

Sherman D, Worrell JW, Cui Y, Feldman JL (2015) Optogenetic perturbation of preBötzinger complex inhibitory neurons modulates respiratory pattern. Nat Neurosci 18:408–414.

Shipston MJ (2018) Control of anterior pituitary cell excitability by calcium-activated potassium channels. Molecular and Cellular Endocrinology 463:37–48.

Sholl DA (1953) Dendritic organization in the neurons of the visual and motor cortices of the cat. J Anat 87:387–406.

Sickmann T, Klose A, Huth T, Alzheimer C (2008) Unexpected suppression of neuronal G protein-activated, inwardly rectifying K+ current by common phospholipase C inhibitor. Neuroscience Letters 436:102–106.

Silveira Villarroel H, Bompolaki M, Mackay JP, Miranda Tapia AP, Michaelson SD, Leitermann RJ, Marr RA, Urban JH, Colmers WF (2018) NPY Induces Stress Resilience via Downregulation of Ih in Principal Neurons of Rat Basolateral Amygdala. Journal of Neuroscience 38:4505–4520.

Smith JC, Abdala APL, Borgmann A, Rybak IA, Paton JFR (2013) Brainstem respiratory networks: building blocks and microcircuits. Trends in Neurosciences 36:152–162.

Smith JC, Ellenberger HH, Ballanyi K, Richter DW, Feldman JL (1991) Pre-Botzinger complex: a brainstem region that may generate respiratory rhythm in mammals. Science 254:726–729.

Smith JC, Feldman JL (1987) In vitro brainstem-spinal cord preparations for study of motor systems for mammalian respiration and locomotion. Journal of Neuroscience Methods 21:321–333.

Sobrinho CR, Wenker IC, Poss EM, Takakura AC, Moreira TS, Mulkey DK (2014) Purinergic signalling contributes to chemoreception in the retrotrapezoid nucleus but not the nucleus of the solitary tract or medullary raphe. The Journal of Physiology 592:1309–1323.

Solomon IC (2005) Glutamate Neurotransmission Is Not Required for, But May Modulate, Hypoxic Sensitivity of Pre-Bötzinger Complex In Vivo. Journal of Neurophysiology 93:1278–1284.

Solomon IC, Edelman NH, Neubauer JA (2000) Pre-Bötzinger Complex Functions as a Central Hypoxia Chemosensor for Respiration In Vivo. Journal of Neurophysiology 83:2854–2868.

Sotres-Bayon F, Sierra-Mercado D, Pardilla-Delgado E, Quirk GJ (2012a) Gating of fear in prelimbic cortex by hippocampal and amygdala inputs. Neuron 76:804–812.

Sotres-Bayon F, Sierra-Mercado D, Pardilla-Delgado E, Quirk GJ (2012b) Gating of fear in prelimbic cortex by hippocampal and amygdala inputs. Neuron 76:804–812.

Spampanato J, Polepalli J, Sah P (2011) Interneurons in the basolateral amygdala. Neuropharmacology 60:765–773.

Stemkowski PL, Tse FW, Peuckmann V, Ford CP, Colmers WF, Smith PA (2002) ATP-Inhibition of M Current in Frog Sympathetic Neurons Involves Phospholipase C But Not Ins P(3), Ca(2+), PKC, or Ras. J Neurophysiol 88:277-288.

Stocker M, Pedarzani P (2000) Differential Distribution of Three Ca2+-Activated K+ Channel Subunits, SK1, SK2, and SK3, in the Adult Rat Central Nervous System. Molecular and Cellular Neuroscience 15:476–493.

Stoppini L, Buchs PA, Muller D (1991) A simple method for organotypic cultures of nervous tissue. Journal of Neuroscience Methods 37:173–182.

Stornetta RL, Moreira TS, Takakura AC, Kang BJ, Chang DA, West GH, Brunet J-F, Mulkey DK, Bayliss DA, Guyenet PG (2006) Expression of Phox2b by Brainstem Neurons Involved in Chemosensory Integration in the Adult Rat. J Neurosci 26:10305–10314.

Stornetta RL, Rosin DL, Wang H, Sevigny CP, Weston MC, Guyenet PG (2003) A group of glutamatergic interneurons expressing high levels of both neurokinin-1 receptors and somatostatin identifies the region of the pre-Bötzinger complex. J Comp Neurol 455:499–512.

Sun N, Cassell MD (1993) Intrinsic GABAergic neurons in the rat central extended amygdala. Journal of Comparative Neurology 330:381–404.

Suzue T (1984) Respiratory rhythm generation in the in vitro brain stem-spinal cord preparation of the neonatal rat. The Journal of Physiology 354:173–183.

Swanson LW, Petrovich GD (1998) What is the amygdala? Trends in Neurosciences 21:323–331.

Tan W, Janczewski WA, Yang P, Shao XM, Callaway EM, Feldman JL (2008) Silencing preBötzinger Complex somatostatin-expressing neurons induces persistent apnea in awake rat. Nat Neurosci 11:538–540.

Tan Z, Liu Y, Xi W, Lou H-F, Zhu L, Guo Z, Mei L, Duan S (2017) Glia-derived ATP inversely regulates excitability of pyramidal and CCK-positive neurons. Nat Commun 8:1–14.

Tatemoto K, Carlquist M, Mutt V (1982) Neuropeptide Y—a novel brain peptide with structural similarities to peptide YY and pancreatic polypeptide. Nature.

Tazumi T, Okaichi H (2002) Effect of lesions in the lateral nucleus of the amygdala on fear conditioning using auditory and visual conditioned stimuli in rats. Neurosci Res 43:163–170.

Thoby-Brisson M, Karlén M, Wu N, Charnay P, Champagnat J, Fortin G (2009) Genetic identification of an embryonic parafacial oscillator coupling to the preBötzinger complex. 12:1028–1035

Thoby-Brisson M, Ramirez J-M (2000) Role of Inspiratory Pacemaker Neurons in Mediating the Hypoxic Response of the Respiratory Network In Vitro. J Neurosci 20:5858–5866.

Thorsell A, Michalkiewicz M, Dumont Y, Quirion R, Caberlotto L, Rimondini R, Mathé AA, Heilig M (2000) Behavioral insensitivity to restraint stress, absent fear suppression of behavior and impaired spatial learning in transgenic rats with hippocampal neuropeptide Y overexpression. Proceedings of the National Academy of Sciences 97:12852–12857.

Thorsell A, Svensson P, Wiklund L, Sommer W, Ekman R, Heilig M (1998) Suppressed neuropeptide Y (NPY) mRNA in rat amygdala following restraint stress. Regulatory Peptides 75-76:247–254.

Tipps M, Marron Fernandez de Velasco E, Schaeffer A, Wickman K (2018) Inhibition of Pyramidal Neurons in the Basal Amygdala Promotes Fear Learning. eNeuro 5:ENEURO.0272–18.2018.

Tovote P, Fadok JP, Lüthi A (2015) Neuronal circuits for fear and anxiety. Nat Rev Neurosci 16:317–331.

Tse A, Yan L, Lee AK, Tse FW (2012) Autocrine and paracrine actions of ATP in rat carotid body. Can J Physiol Pharmacol 90:705–711.

Tye KM, Prakash R, Kim S-Y, Fenno LE, Grosenick L, Zarabi H, Thompson KR, Gradinaru V, Ramakrishnan C, Deisseroth K (2011) Amygdala circuitry mediating reversible and bidirectional control of anxiety. Nature 471:358–362.

Uliana DL, Gomes FV, Grace AA (2020) Stress impacts corticoamygdalar connectivity in an age-dependent manner. Neuropsychopharmacology:1–11.

Urban KR, Valentino RJ (2016) Age- and Sex-Dependent Impact of Repeated Social Stress on Intrinsic and Synaptic Excitability of the Rat Prefrontal Cortex. Cerebral Cortex 15:96.

Van den Pol AN (2012) Neuropeptide Transmission in Brain Circuits. Neuron 76:98–115.

Vann NC, Pham FD, Dorst KE, Del Negro CA (2018) Dbx1 Pre-Bötzinger Complex Interneurons Comprise the Core Inspiratory Oscillator for Breathing in Unanesthetized Adult Mice. eNeuro 5(3) e0130-18.2018.

Vigil FA, Carver CM, Shapiro MS (2020) Pharmacological Manipulation of Kv7 Channels as a New Therapeutic Tool for Multiple Brain Disorders. Front Physiol 11:688.

Vyas A, Bernal S, Chattarji S (2003) Effects of chronic stress on dendritic arborization in the central and extended amygdala. Brain Research 965:290–294.

Vyas A, Jadhav S, Chattarji S (2006) Prolonged behavioral stress enhances synaptic connectivity in the basolateral amygdala. NSC 143:387–393.

Vyas A, Mitra R, Shankaranarayana Rao BS, Chattarji S (2002) Chronic stress induces contrasting patterns of dendritic remodeling in hippocampal and amygdaloid neurons. Journal of Neuroscience 22:6810–6818.

Walker DL, Davis M (1997) Double Dissociation between the Involvement of the Bed Nucleus of the Stria Terminalis and the Central Nucleus of the Amygdala in Startle Increases Produced by Conditioned versus Unconditioned Fear. J Neurosci 17:9375–9383.

Walker DL, Davis M (2008) Role of the extended amygdala in short-duration versus sustained fear: a tribute to Dr. Lennart Heimer. Brain Struct Funct 213:29–42.

Walker DL, Miles LA, Davis M (2009) Progress in Neuro-Psychopharmacology & BiologicalPsychiatry. Progress in Neuropsychopharmacology & Biological Psychiatry 33:1291–1308.

Wallén-Mackenzie Å, Gezelius H, Thoby-Brisson M, Nygård A, Enjin A, Fujiyama F, Fortin G, Kullander K (2006) Vesicular Glutamate Transporter 2 Is Required for Central Respiratory Rhythm Generation But Not for Locomotor Central Pattern Generation. J Neurosci 26:12294–12307.

Wang H, Stornetta RL, Rosin DL, Guyenet PG (2001) Neurokinin-1 receptor-immunoreactive neurons of the ventral respiratory group in the rat. J Comp Neurol 434:128–146.

Wang S, Benamer N, Zanella S, Kumar NN, Shi Y, Bévengut M, Penton D, Guyenet PG, Lesage F, Gestreau C, Barhanin J, Bayliss DA (2013) TASK-2 Channels Contribute to pH Sensitivity of Retrotrapezoid Nucleus Chemoreceptor Neurons. J Neurosci 33:16033–16044.

Wang X, Hayes JA, Revill AL, Song H, Kottick A, Vann NC, LaMar MD, Picardo MCD, Akins VT, Funk GD, Del Negro CA (2014) Laser ablation of Dbx1 neurons in the pre-Bötzinger complex stops inspiratory rhythm and impairs output in neonatal mice. Elife 3:e03427.

Washburn MS, Moises HC (1992) Electrophysiological and morphological properties of rat basolateral amygdaloid neurons in vitro. J Neurosci 12:4066–4079.

Weese-Mayer DE, Berry-Kravis EM, Ceccherini I, Keens TG, Loghmanee DA, Trang H (2010) An Official ATS Clinical Policy Statement: Congenital Central Hypoventilation Syndrome. Am J Respir Crit Care Med 181:626–644.

Wei AD, Ramirez J-M (2019) Presynaptic Mechanisms and KCNQ Potassium Channels Modulate Opioid Depression of Respiratory Drive. Front Physiol 10:1407.

Weiskrantz L (1956) Behavioral changes associated with ablation of the amygdaloid complex in monkeys. J Comp Physiol Psychol 49:381–391.

Widerlöv E, Lindström LH, Wahlestedt C, Ekman R (1988) Neuropeptide Y and peptide YY as possible cerebrospinal fluid markers for major depression and schizophrenia, respectively. Journal of Psychiatric Research 22:69–79.

Wilson CG, Martin RJ, Jaber M, Abu-Shaweesh J, Jafri A, Haxhiu MA, Zaidi S (2004) Adenosine A2A receptors interact with GABAergic pathways to modulate respiration in neonatal piglets. Respiratory Physiology & Neurobiology 141:201–211.

Winter SM, Fresemann J, Schnell C, Oku Y, Hirrlinger J, Hülsmann S (2009) Glycinergic interneurons are functionally integrated into the inspiratory network of mouse medullary slices. Pflugers Arch 458:459–469.

Wolff SBE, Gründemann J, Tovote P, Krabbe S, Jacobson GA, Müller C, Herry C, Ehrlich I, Friedrich RW, Letzkus JJ, Lüthi A (2014) Amygdala interneuron subtypes control fear learning through disinhibition. Nature 509:453–458.

Wu J, Capelli P, Bouvier J, Goulding M, Arber S, Fortin G (2017) A V0 core neuronal circuit for inspiration. Nat Commun 8:544–12.

Wu J, Ding W-G, Matsuura H, Horie M (2012) Regulatory mechanisms underlying the modulation of GIRK1/GIRK4 heteromeric channels by P2Y receptors. Pflugers Arch 463:625–633.

Xu J, Tse FW, Tse A (2003) ATP triggers intracellular Ca2+ release in type II cells of the rat carotid body. The Journal of Physiology 549:739–747.

Xu J, Xu F, Tse FW, Tse A (2005) ATP inhibits the hypoxia response in type I cells of rat carotid bodies. J Neurochem 92:1419–1430.

Yamamoto M, Nishimura M, Kobayashi S, Akiyama Y, Miyamoto K, Kawakami Y (1994) Role of endogenous adenosine in hypoxic ventilatory response in humans: a study with dipyridamole. Journal of Applied Physiology 76:196–203.

Yan S, Laferriere A, Zhang C, Moss IR (1995) Microdialyzed adenosine in nucleus tractus solitarii and ventilatory response to hypoxia in piglets. Journal of Applied Physiology 79:405–410.

Yang CF, Feldman JL (2018) Efferent projections of excitatory and inhibitory preBötzinger Complex neurons. Journal of Comparative Neurology 526:1389–1402.

Yang H, Zhang G, Cui J (2015) BK channels: multiple sensors, one activation gate. Front Physiol 6:29.

Yehuda R, Brand S, Yang R-K (2006) Plasma neuropeptide Y concentrations in combat exposed veterans: relationship to trauma exposure, recovery from PTSD, and coping. Biological Psychiatry 59:660–663.

Yoshioka K, Hosoda R, Kuroda Y, Nakata H (2002) Hetero-oligomerization of adenosine A1 receptors with P2Y1 receptors in rat brains. FEBS Lett 531:299–303.

Zaika O, Tolstykh GP, JAFFE DB, Shapiro MS (2007) Inositol triphosphate-mediated Ca2+ signals direct purinergic P2Y receptor regulation of neuronal ion channels. Journal of Neuroscience 27:8914–8926.

Zavala-Tecuapetla C, Aguileta MA, Lopez-Guerrero JJ, González-Marín MC, Peña F (2008) Calcium-activated potassium currents differentially modulate respiratory rhythm generation. Eur J Neurosci 27:2871–2884.

Zhang J, Chen L, He Y, Ding Y, Zhou H, Hu H, Tang Y, Zheng Y (2010) Large-conductance calcium-activated potassium channels in the neurons of pre-Bötzinger complex and their participation in the regulation of central respiratory activity in neonatal rats. Neuroscience Letters 481:159–163.

Zhang Y, Gourine A, Kasparov S, Alvares T, Funk GD (2016a) ATP Excitation of the PreBötzinger Complex and Inspiratory Neurons in vitro is Mediated in Part via a PLC/IP3-mediated increase In [Ca2+]i. FASEB. Online.

Zhang Y, Gourine AV, Kasparov S, Alvares T, Funk GD (2016b) ATP excites the preBötzinger Complex network in vitro via activation of a Gαq-signaling pathway. SFN. San Diego. Online.

Zhang Y, Jaib AT, Gourine A, Kasparov S, Alvares T, Funk GD (2018) cAMP-dependent modulation of Ih underlies the P2Y1 receptor-mediated excitation of the preBötzinger Complex inspiratory network in vitro. SFN. San Diego. Online.

Zhao MG, Hülsmann S, Winter SM, Dutschmann M, Richter DW (2006) Calcium-regulated potassium currents secure respiratory rhythm generation after loss of glycinergic inhibition. Eur J Neurosci 24:145–154.

Zhou Y, Lingle CJ (2014) Paxilline inhibits BK channels by an almost exclusively closed-channel block mechanism. J Gen Physiol 144:415–440.

Zhou Z et al. (2008) Genetic variation in human NPY expression affects stress response and emotion. Nature 452:997–1001.

Zoccal DB, Silva JN, Barnett WH, Lemes EV, Falquetto B, Colombari E, Molkov YI, Moreira TS, Takakura AC (2018) Interaction between the retrotrapezoid nucleus and the parafacial respiratory group to regulate active expiration and sympathetic activity in rats. Am J Physiol Lung Cell Mol Physiol 315:L891–L909.

Zwicker JD, Rajani V, Hahn LB, Funk GD (2011) Purinergic modulation of preBötzinger complex inspiratory rhythm in rodents: the interaction between ATP and adenosine. The Journal of Physiology 589:4583–4600.